Investigation into the role of sirtuins in vascular calcification

F Bartoli-Leonard

PhD 2019

Investigation into the role of sirtuins in vascular calcification

Francesca Bartoli-Leonard

A thesis submitted in partial fulfilment of the requirements of Manchester Metropolitan University for the degree of Doctor of Philosophy

Department of Life Sciences
Manchester Metropolitan University

2019

Abstract

Vascular calcification is a major health risk throughout the world and has long been associated with the development of type II diabetes. Previously thought to be a result of passive degeneration it is now understood to involve a host of complex signalling pathways, which regulate the promotors and inhibitors of osteogenesis within vascular smooth muscle cells (vSMCs). With 1 in 4 of the British population suggested to have diabetes, unpicking the molecular mechanism behind the development of this crippling pathology is required to develop further treatment of vascular calcification.

Sirtuin 1 (SIRT1), an NAD+ dependent deacetylase has shown a beneficial role in insulin sensitivity and glucose homeostasis, as well as a known protective effect on inhibiting oxidative stress and inflammation within the vessel wall and therefore may be a promising candidate for regulation of vascular calcification within diabetic vessels.

This study determined that SIRT1 is reduced within the diabetic patient ubiquitously, both within the vSMCs and serum when compared to non-diabetic controls. Furthermore, it confirms that vSMCs explanted from a diabetic vessel exhibit increased migratory and adhesive properties, presenting with extensive DNA damage and have an increased capacity to adopt a senescence associated secretory phenotype, in which osteogenic master transcription factor Runx2 is switched on, increasing trans-differentiation to an osteogenic phenotype. Additionally, the utilisation of a high glucose, phosphate and calcium vSMC tissue culture model demonstrates the induction of an osteogenic phenotype can be inhibited via the activation of SIRT1 using small molecular activator SRT1720 and conversely exacerbated by its inhibition using Sirtinol or siRNA. Furthermore, SIRT1 activation inhibits proliferative and migratory factors ERK and AKT activity within vSMCs, whilst increasing activation of DNA repair complex MRN and associated kinase ATM.

These findings suggest that activation of SIRT1 within a diabetic vSMC model may reduce their migratory capacity, therefore reducing their development of a senescent phenotype through increasing repair of DNA damage, thus overall reducing the cells ability to promote calcification.

Contents Pages

List of figures……...1

List of tables……....4

Declaration…….....5

Presentations……...6

Prizes and Awards……..8

Publications…….....9

Abbreviations…….....10

1. Introduction

1.1. Cardiovascular disease as a growing global non-communicable epidemic……13

1.2. Cardiovascular risk factors……..15

1.3. Prevalence of type II diabetes and current treatment strategies…....17

1.4. Arterial vessel structure……20

1.5. Vascular calcification……21

1.6. Clinical significance of vascular calcification……22

1.7. Current therapies for cardiovascular disease……....23

1.8. Pathological development of vascular mineralisation……..24

1.9. Inducers of calcification……26

1.9.1. Cellular senescence……26

1.9.2. Loss of osteogenic inhibitors……...26

1.9.3. Oxidative stress……27

1.10. Microvesicle formation and their role in vascular calcification……....27

1.11. Extracellular matrix deposition……28

1.12. Vascular smooth muscle cell phenotypic switching and plasticity.…29

1.13. Origins of calcifying vascular smooth muscle cells……..……32

1.14. Molecular aspects attributing to vascular calcification.……32

1.14.1. Hyperglycaemia……...32

1.14.2. Runx2 Pathway……33

1.14.3. DNA Damage……...37

1.14.4. Wnt Signalling pathway……..40

1.15. Models of vascular calcification……43

1.16. Sirtuins……44

1.16.1. Molecular structure and localisation of SIRT1..……44

1.16.2. SIRT1 Activity……..……47

1.16.3. Regulation of SIRT1……..……..48
1.16.4. Post-translational modifications…….51
1.16.5. Effects of SIRT1 in the cardiovascular system and disease...55
1.16.6. Role of SIRT1 in diabetes……...58
1.16.7. Small molecular activators of SIRT1……..58
1.16.8. Clinical outcomes of SIRT1 activators……...61
1.17. Aims……....63

2. Material and Methods

2.1. Chemicals and Reagents…….....….....64
2.2. Tissue culture.....65
2.2.1. Primary smooth muscle cells.....65
2.2.2. Extraction of primary diabetic vascular smooth muscle cells..65
2.2.3. Human vascular smooth muscle cell maintenance and passage.....65
2.2.4. Induction of calcification.....66
2.2.5. siRNA transfection.....66
2.3. Histology.....67
2.3.1. Sample preparation.....67
2.3.2. Haematoxylin and Eosin staining.....67
2.3.3. Alizarin red staining.....67
2.3.4. Von Kossa staining.....68
2.3.5. Sudan Black B (Lipofuscin Stain).....68
2.3.6. Immunohistochemistry.....68
2.3.7. Immunocytochemistry.....69
2.4. DNA Integrity assays.....70
2.4.1. Comet assay.....70
2.4.2. Relative telomere length quantification.....70
2.4.3. TUNEL assay.....71
2.5. RNA Assays.....72
2.5.1. RNA Isolation.....72
2.5.2. Reverse transcription and cDNA generation.....72
2.5.3. Polymerase chain reaction.....73
2.5.4. Agarose gel electrophoresis.....73
2.5.5. Quantitative polymerase chain reaction.....73

2.6. Protein analysis....75
2.6.1. Protein isolation....75
2.6.2. Nuclear fractionation....75
2.6.3. Protein determination....75
2.6.4. Sodium Dodecyl Sulphate / Polyacrylamide Gel Electrophoresis(SDS/PAGE)....76
2.6.5. Western blotting....76
2.6.6. ELISA....77
2.7. Migration and Adhesion assays....78
2.7.1. Modified Boyden chamber assay....78
2.7.2. Adhesion assay....78
2.8. Survival assays....79
2.8.1. Cellular viability (Alamar blue)....79
2.8.2. Cellular cytotoxicity....79
2.8.3. β-galactosidase assay....79
2.9. Calcification assays....80
2.9.1. Alkaline phosphatase assay....80
2.9.2. Quantification of calcium deposition....80
2.9.3. Alizarin red staining and elution....81
2.10. Griess assay....82
2.11. Chromatin Immunoprecipitation....83
2.12. Cell cycle analysis....85
2.13. Statistics....86

3. SIRT1 activation reduces the osteogenic differentiation of vascular smooth muscle cells *in vitro* through a senescence and Runx2 dependent pathway

3.1. Introduction....87
3.1.1. Clinical problem of vascular calcification....87
3.1.2. Vascular calcification induced senescence....87
3.1.3. Runx2 pathway in the process of cellular mineralisation....88
3.1.4. SIRT1 as a regulator of vascular calcification....89
3.2. Aim and Objectives....90
3.3. Results....91
3.3.1. Hyperglycaemic conditions reduce SIRT1 expression....91

3.3.2. Hyperglycaemic conditions induce smooth muscle cell mineralisation.....93
3.3.3. Hyperglycaemic conditions induce Runx2 activation.....95
3.3.4. Diabetic patient vessels exhibit calcification markers.....99
3.3.5. Hyperglycaemic conditions induce cellular senescence and increase smooth muscle cell plasticity.....101
3.3.6. SIRT1 expression can be modulated via chemical and genetic approaches.....106
3.3.7. Modulation of SIRT1 modifies smooth muscle cell mineralisation.....109
3.3.8. SIRT1 activation negatively regulates proteins downstream in the Runx2 pathway.....115
3.3.9. SIRT1 inhibition increases cellular senescence under hyperglycaemic conditions.....119
3.3.10. SIRT1 inhibition reduces smooth muscle cell proliferation and cell cycle progression.....123
3.4. Discussion.....127
3.4.1. Marker expression correlates with reduction in SIRT1 expression.....127
3.4.2. SIRT1 activation promotes negative regulation of the Runx2 pathway.....128
3.4.3. Hyperglycaemia reduces expression of SIRT1.....130
3.4.4. SIRT1 activation inhibits hyperglycaemia promoted loss of smooth muscle markers.....131
3.4.5. SIRT1 activation inhibits development of a senescence associated secretory phenotype.....132
3.5. Limitations.....136
3.6. Conclusion.....136
4. Diabetic vascular smooth muscle cells exhibit increased migration and proliferation through activation of focal adhesion kinase and associated proteins via the ERK pathway, which can be attenuated via the activation of SIRT1
4.1 Introduction.....137
4.1.1. The pathological impact of diabetes on the vasculature.....137

4.1.2. Role of cellular cytoskeletal reorganisation and focal adhesion formation in diabetic vessels.....138
4.1.3. SIRT1 as a possible treatment for reduction of smooth muscle cell migration in diabetes.....139
4.2. Aim and Objectives.....140
4.3. Results.....141
4.3.1. Diabetic patients exhibit decreased SIRT1 levels.....141
4.3.2. Morphological differences between diabetic and non-diabetic vascular smooth muscle cells.....144
4.3.3. Diabetic vascular smooth muscle cells exhibit increased proliferative capacity.....146
4.3.4. Diabetic induced migration and adhesion within smooth muscle cells is reduced under SIRT1 activation following hyperglycaemic treatment.....148
4.3.5. Focal adhesion formation is reduced following SIRT1 activation.....150
4.3.6. Activation of the ERK and AKT pathways is upregulated in diabetic vascular smooth muscle cells.....159
4.4. Discussion.....162
4.4.1. Distinct changes in morphology are present between diabetic and non-diabetic vascular smooth muscle cells.....162
4.4.2. High glucose conditions reduce actin organisation and increase proliferation.....163
4.4.3. Reduction of SIRT1 within the diabetic patient correlates with increased vessel calcification.....166
4.4.4. SIRT1 reduces diabetic induced migration and adhesion under hyperglycaemic conditions.....167
4.4.5. Focal adhesion formation is increased within diabetic vascular smooth muscle cells.....169
4.4.6. SIRT1 activation reduces the occurrence of focal adhesion formation.....171
4.5 Limitations.....174
4.6. Conclusion.....174

5. Loss of SIRT1 in diabetes accelerates DNA damaged induced smooth muscle mineralisation *in vitro* and reduces activation of the DNA repair MRN complex

5.1. Introduction.....175

5.1.1. The prevalence of diabetic induced calcification.....175

5.1.2. DNA damage response pathways.....175

5.1.3. The role of SIRT1 in DNA damage sensing.....176

5.2. Aim and Objectives.....177

5.3. Results.....178

5.3.1. Diabetic patients exhibit DNA damage and decreased SIRT1 expression.....178

5.3.2. Cells harvested from diabetic patients exhibit low SIRT1 expression and increased DNA damage.....182

5.3.3. Hyperglycaemic conditions induce DNA damage.....185

5.3.4. SIRT1 attenuates DNA damage induced osteogenic differentiation.....188

5.3.5. SIRT1 translocation increased following DNA damage.....192

5.3.6. SIRT1 activation protects against DNA damage.....195

5.3.7. SIRT1 activation reduces chromatin acetylation and increases MRN activation.....203

5.4. Discussion.....208

5.4.1. DNA damage is prevalent within the diabetic patient.....208

5.4.2. An increase in cellular SIRT1 levels following DNA damage increases DNA repair.....209

5.4.3. DNA repair through the MRN complex is not fully activated in a reduced SIRT1 environment.....210

5.5. Limitations.....212

5.6. Conclusions.....212

6. Conclusions and Future Works

6.1. General Discussion.....214

6.2. Future Work.....219

6.3. Conclusion.....222

7. Appendix.....223

8. Bibliography.....227

List of figures

Figure. 1.1. Pathologies associated with endothelial dysfunction and smooth muscle calcification....14
Figure. 1.2. Vessel structure....20
Figure. 1.3. Localisation of vascular calcification....21
Figure. 1.4. Vessel wall during osteogenic differentiation....25
Figure. 1.5. TNAP induction of smooth muscle cell calcification....28
Figure 1.6 Smooth muscle cell differentiation....31
Figure. 1.7. Table of major Runx2 regulated genes....34
Figure. 1.8. Runx2 signalling pathway....36
Figure. 1.9. MRN Pathway....39
Figure. 1.10. Canonical Wnt pathway....42
Figure. 1.11. Role of Calorific Restriction on SIRT1 expression....49
Figure. 1.12. Regulation of SIRT1 through p53 activation....50
Figure. 1.13. Known post-translational modifications of SIRT1....53
Figure 1.14 Table of major SIRT1 regulated genes....57
Figure. 1.15. Structure of SIRT1 in both open and closed states....60
Figure. 3.1. SIRT1 expression decreased under hyperglycaemic conditions....92
Figure. 3.2. Hyperglycaemic conditions induce smooth muscle cell mineralisation....94
Figure. 3.3. Hyperglycaemic conditions increase Runx2 promotor acetylation and protein expression....96
Figure. 3.4. Hyperglycaemic conditions increase protein expression of downstream markers of the Runx2 pathway *in vitro*....98
Figure. 3.5. Osteogenic marker expression is increased in diabetic patients....100
Figure. 3.6. Hyperglycaemic conditions increased cellular senescence and associated markers....102
Figure. 3.7. Hyperglycaemic conditions modify cellular phenotype....104
Figure. 3.8. SIRT1 modulation via chemical approaches....107
Figure. 3.9. SIRT1 knockdown via a genetic approach....108
Figure. 3.10. Modulation of SIRT1 modifies smooth muscle cell mineralisation...110
Figure. 3.11. Modulation of SIRT1 modifies smooth muscle cell alkaline phosphatase activity....111
Figure. 3.12. Activation of SIRT1 modulates the Runx2 pathway....113

Figure. 3.13. Genetic knockdown of SIRT1 modulates the Runx2 pathway.....114
Figure. 3.14. SIRT1 modulates OCN expression downstream of the Runx2 pathway.....116
Figure. 3.15. SIRT1 modulates Runx2 downstream gene expression.....117
Figure. 3.16. SIRT1 siRNA increases downstream Runx2 marker expression.....118
Figure. 3.17. SIRT1 modulation effects cellular senescence.....121
Figure. 3.18. SIRT1 modulation effects cellular senescence marker expression.....122
Figure. 3.19. SIRT1 modulation effects smooth muscle cell marker Expression.....125
Figure. 3.20. SIRT1 modulation effects cellular proliferation and cell cycle progression.....126
Figure. 3.21. Suggested model for the role of SIRT1 in the Runx2 calcification pathway.....135
Figure. 4.1. Diabetic patients exhibit a decreased level of SIRT1.....141
Figure. 4.2. Diabetic patient vSMCs exhibit a decreased level of SIRT1.....143
Figure. 4.3. Photomicrographs of diabetic and non-diabetic vSMCs.....145
Figure. 4.4. Diabetic vSMCs exhibit increased proliferation and decrease nitric oxide availability.....147
Figure. 4.5. Adhesion and migration of diabetic vSMCs was reduced with SIRT1 activation.....149
Figure. 4.6. SIRT1 activation reduced diabetic vSMC vinculin expression.....151
Figure. 4.7. SIRT1 activation reduced diabetic vSMC paxillin expression.....154
Figure. 4.8. SIRT1 activation reduced diabetic vSMC focal adhesion kinase activation.....157
Figure. 4.9. MAPK and AKT activation are increased in diabetic vSMCs.....160
Figure. 4.10. ERK and AKT activation is reduced in diabetic vSMCs with the addition of SIRT1 activator SRT1720.....161
Figure. 4.11. Suggested mechanism for the role of SIRT1 in glucose activated focal adhesion formation.....173
Figure. 5.1. Diabetic patient vessels exhibit increased DNA damage and senescence marker expression.....179
Figure. 5.2. Diabetic patient vSMCs exhibit DNA damage and low SIRT1 expression.....183

Figure. 5.3. Diabetic patient vSMCs exhibit decreased telomere length and increase senescence and DNA marker gene expression.....184
Figure. 5.4. Hyperglycaemic conditions increase DNA damage marker γH2AX expression.....186
Figure. 5.5. Hyperglycaemic conditions increase DNA damage marker expression.....187
Figure. 5.6. SIRT1 activation inhibits DNA damage induced smooth muscle cell calcification.....189
Figure. 5.7. SIRT1 activation inhibits DNA damage induced smooth muscle calcification.....191
Figure. 5.8. SIRT1 expression is increased following DNA damage but reduced in the nucleus.....193
Figure. 5.9. SIRT1 activation decreases DNA damage marker γH2AX expression….....196
Figure. 5.10. SIRT1 activation protects against DBS formation.....200
Figure. 5.11. SIRT1 activation reduces promotor acetylation of the MRN complex.....204
Figure. 5.12. SIRT1 activation reduces MRN complex activation.....207
Figure. 5.13. Suggested mechanism for the role of SIRT1 in DNA damage induced calcification.....213
Figure 6.1. Suggested mechanism of diabetic induced vascular calcification...215

List of Tables

Table. 1.1. Risk factors of cardiovascular disease.....16
Table. 1.2. Comorbidities of Type II diabetes.....19
Table. 1.3 List of SIRTs within Sirtuin family and their role and location.....46
Table. 1.4. List of SIRT1 activating and inhibiting compounds.....62
Table. 7.1. Antibodies used throughout thesis.....223
Table. 7.2. DNA oligonucleotide primers used for quantitative real-time PCR.....224
Table. 7.3. DNA oligonucleotide primers used for chromatin Immunoprecipitation quantitative PCR.....225

Declaration

I hereby declare that I have personally undertaken all the work described in this thesis.

Presentations

Oral presentation **at the MMU Science and Engineering Research Symposium, Manchester Metropolitan University, 2018**

Title: The loss of SIRT1 stimulates increased proliferation in diabetic vascular smooth muscle cells via the ERK pathway

Poster **presented at the British Atherosclerosis Society / British Society for Cardiovascular Research Conference, Manchester, UK, 2019**

Title: Loss of SIRT1 in diabetes enhances DNA damage and reduces MRN complex activation resulting in increased vascular calcification

Poster **presented at the Asian Pacific Vascular Biology Organisation Conference, Guangzhou, China, 2019**

Title: SIRT1 attenuates hyperglycaemic induced calcification in vascular smooth muscle cells

Poster **presented at the European Society of Microcirculation / European Vascular Biology Organisation Conference, Maastricht, The Netherlands, 2019**

Title: SIRT1 deacetylation of p53 inhibits hyperglycaemia induced senescence in vascular smooth muscle cells

Poster **presented at the Northern Vascular Biology Forum, University of Bradford, 2018**

Title: Diabetes induced DNA damage is ameliorated with SIRT1 activation

Moderated Poster **presented at the British Atherosclerosis Society / British Society for cardiovascular Research, Manchester, UK, 2018**

Title: SIRT1 attenuates hyperglycaemic induced calcification and associated senescence in vascular smooth muscle cells

Poster **presented at the Frontiers for Vascular Biology Conference, Vienna, Austria, 2018**

Title: Novel Small molecule SIRT1 activators attenuate vascular calcification in an *in vitro* diabetic model

Poster **presented at the Northern Vascular Biology Forum, Liverpool John Moores, 2017**

Title: Novel small molecular SIRT1 activators attenuates vascular smooth muscle cell calcification

Prizes and Awards

British Society for Cardiovascular Research - Best Poster Abstract Prize, Winner, 2019

British Society for Cardiovascular Research - Travel Grant Award, 2019

Manchester Metropolitan University - Conference Funding Grant Award, 2019

Vector Labs Image Competition - Winner, 2018

Frontiers in Cardiovascular Biology / European Vascular Biology Organisation - Travel Grant Award, 2018

British Atherosclerosis Society / British Society for Cardiovascular Research - Best Moderated Poster, Runner Up, 2018

Publications

Bartoli-Leonard, F., Wilkinson, F., Schiro, A., Serracino-Inglott, F., Alexander, MY., Weston, R., (2019), 'SIRT1 attenuates diabetes induced adhesion and migration in vascular smooth muscle cells through inhibition of focal adhesion formation', in preparation

Bartoli-Leonard, F., Wilkinson, F., Schiro, A., Serracino-Inglott, F., Alexander, MY., Weston, R., (2019), 'Loss of SIRT1 in diabetes enhances DNA damage induced vascular calcification via reduction of the MRN complex activation', in review.

Bartoli-Leonard, F., Alexander, MY., Weston, R., (2019), 'Loss of SIRT1 in diabetes enhances DNA damage and reduces MRN complex activation resulting in increased vascular calcification', Heart, 105, S6, BS59 (Conference abstract)

Bartoli-Leonard, F., Alexander, MY., Weston, R., (2019), 'SIRT1 deacetylation of p53 inhibits hyperglycaemia induced senescence in vascular smooth muscle cells', Journal of Vascular Research, 56, S1, S23 (Conference abstract)

Bartoli-Leonard, F., Wilkinson, F., Schiro, A., Serracino-Inglott, F., Alexander, MY., Weston, R., (2019), 'Suppression of SIRT1 in diabetic conditions induces osteogenic differentiation of human vascular smooth muscle cells via Runx2 signalling', Scientific reports, https://doi.org/10.1038/s41598-018-37027-2

Bartoli-Leonard, F., Wilkinson, F., Langford-Smith A., Alexander, MY., Weston., R., (2018), 'The interplay of SIRT1 and Wnt signalling in vascular calcification', Frontiers in Cardiovascular Medicine, https://doi.org/10.3389/fcvm.2018.00183

Bartoli-Leonard, F., Alexander, MY., Weston., R., (2018), 'Novel small molecule SIRT1 activators attenuate vascular calcification in an *in vitro* diabetic model', Cardiovascular Research, 114, S1 S91 (Conference abstract)

Bartoli-Leonard, F., Alexander, MY., Weston., R., 2018), 'SIRT1 attenuates hyperglycaemic induced calcification and associated senescence in vascular smooth muscle cells', Heart, 104: A92 (Conference abstract)

List of Abbreviations

A-NHEJ	Alternative non-homologous end joining
AGE	Advanced glycated end-product
ALP	Alkaline phosphatase
ANOVA	Analysis of variance
ATM	Ataxia telangiectasia mutated
BCA	Bicinchoninic acid assay
BMP	Bone morphogenic protein
BrDu	Bromodeoxyuridine
CA SMC	Coronary artery smooth muscle cell
CABG	Coronary artery bypass graft
CBPs	CREB binding proteins
cDNA	Complementary DNA
ChIP	Chromatin immunoprecipitation
CR	Calorific restriction
CVC	Calcifying vascular cell
CVD	Cardiovascular disease
DAB	3,3'-Diaminobenzidine
DAPI	4,6'-diamidino-2-phenylindole
DDR	DNA damage response
DEPC	Diethyl pyrocarbonate
DM	Diabetes mellitus
DM SMC	Diabetes mellitus smooth muscle cell
DMEM	Dulbecco's modified eagle's medium
DMSO	Dimethyl sulfoxide
DNA	Deoxyribonucleic acid
dNTP	deoxyribonucleotide triphosphae
DSBs	Double stranded breaks
DTT	Dithlothreltol
dUTP	Deoxyuridine triphosphate
ECL	Enhanced chemiluminescence
ECM	Extracellular matrix
EDTA	Ethylenediaminetetraactic acid
ELISA	Enzyme-linked immunosorbent assay
eNOS	Endothelial nitric oxide
ERK	Extracellular signal related kinases
FACS	Fluorescence-activated cell sorting
FAK	Focal adhesion kinase
FCS	Foetal calm serum
FGFs	Fibroblast growth factor
FRZs	Frizzled protein
H2AX	Histone H2A variant
hEGF	Human endothelial growth factor
HG	High glucose
HR	Homologous recombination
HUVEC	Human umbilical vein endothelial cells
IMA	Internal mammary artery
LEF	Lymphoid enhancer-binding factor
LDL	Low density lipoprotein

LDS	Lithium dodecyl sulphate
MGP	Matrix gla protein
MMP	Matrix metalloproteinase
MRN	MRE11-RAD50-NBS1
mRNA	Messenger RNA
Msx2	Msh homoebox 2
NAD	Nicotinamide adenine dinucleotide
NADH	Nicotinamide adenine dinucleotide oxidised
NADP	Nicotinamide adenine dinucleotide phosphate
NADPH	Dihydronicotinamide-adenine dinucleotide phosphate
NHEJ	Non-homologous end joining
NO	Nitric oxide
OCN	Osteocalcin
OPG	Osteoprotegerin
OPN	Osteopontin
oxLDL	Oxidised LDL
PA	Popliteal artery
PBS	Phosphate buffered solution
PBST	PBS-Tween (0.01%)
PCR	Polymerase chain reaction
PDGF	Platelet-derived growth factor
PFA	Paraformaldehyde
PIC	Protease inhibitor cocktail
pNPP	Para-Nitrophenylphosphate
PVDF	Polyvinylidee difluoride
qPCR	Quantitative PCR
RAGE	Receptor of advanced glycated end-product
RNA	**R**ibonucleic acid
ROS	Reactive oxygen species
Runx2	Runt related transcription factor 2
ScOPE-MS	Single cell proteomics by mass spectrometry
scRNA	Scrambled RNA
SC RNA-Seq	Single cell RNA-sequencing
SDS	Sodium dodecyl sulphate
siRNA	Small interfering RNA
SIRT1	Sirtuin 1
SMAD	Mothers against decapentaplegic homologue
SMC	Smooth muscle cell
SNPs	Single nucleotide polymorphisms
SRT	SRT1720
STAC	Sirtuin activating compound
TBE	Tris-borate-EDTA
TCF	T cell factor
TEMED	Tetramethylethylenediamine
TMB	3,3’,5,5’-tetramethylbenzidine
VC	Vascular calcification
VSMC	Vascular smooth muscle cell
WHO	World health organisation
BGP	Beta-glycerophosphate

1. Introduction

1.1. Cardiovascular disease as a growing global non-communicable epidemic

Cardiovascular disease (CVD) is the leading cause of death worldwide and is an umbrella term for all heart and circulatory disorders, including coronary artery disease, myocardial infarction, hypertension and stroke (1). The concept of CVD being a disease of affluence is no longer correct, as the prevalence of CVD in developing countries is increasing exponentially, and thus is fast becoming a universal epidemic. Globally CVD accounts for 31% of all mortality, with the majority of this ascribed to coronary artery disease and stroke (2, 3). Once believed to have distinct differences in development, coronary artery disease, myocardial infarction (4) and stroke can all be attributed to the build-up of atherosclerotic plaques (5, 6), restricting the blood flow through the artery and if left untreated, causing long term damage and possible occlusion, resulting in the need for amputation or the loss of blood flow to the heart or brain (7, 8). Underpinning CVD is the breakdown in communication between endothelial cells and vascular smooth muscle cells (vSMCs) and the subsequent phenotypic changes which occur within the vessels under disease conditions (Fig. 1.1) and it is this phenotypic switch within the smooth muscle layer that this thesis sought to examine.

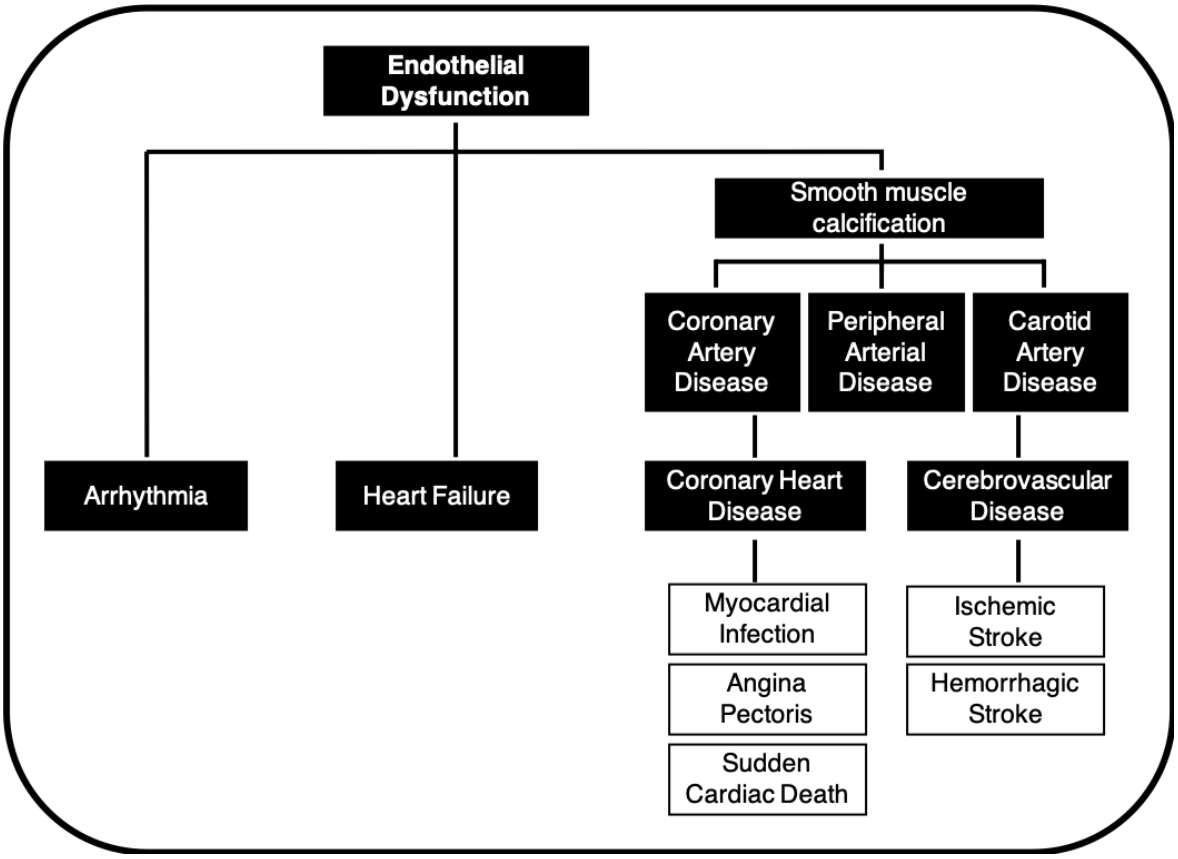

Fig. 1.1 Pathologies associated with endothelial dysfunction and smooth muscle calcification. Endothelial dysfunction can be directly correlated with the increase in development of heart failure and arrhythmias. Increased smooth muscle calcification following on from endothelial dysfunction can result in the development of both coronary artery disease and peripheral artery disease, leading to a range of downstream pathologies.

1.2. Cardiovascular risk factors

Risk factors for cardiovascular disease or events are currently divided into two major classes; non-modifiable and modifiable risks (Table 1.1).

Non-modifiable: These risk factors are those which are uncontrollable, and include; age, gender, ethnicity and family history. Within an aging population the susceptibility to the development of CVD increases, due to age-associated functional and structural changes within the heart and vessels and accumulation of damage from modifiable risk factors over the years (9, 10). Men are at higher risk for CVD then pre-menopausal women due to the protective effect of oestrogen on regulating cholesterol levels, however this disparity is decreased following the menopause (11, 12). Ethnic background also affects the risk of heart disease, with over double the mortality rates from CVD found in those from an Asian ethnicity compared to white Caucasian within the United States of America (13). Finally, family history of incidence is also a key risk factor, but with many genes contributing to the development of CVD, this remains arguably the least well understood (14). Moreover, rare genetic diseases such as pseudoxanthoma elasticum and Keutel syndrome caused by abnormalities in ABCC6 and MGP gene expression respectively (70), also lead to increased vascular calcification, however with diagnosis and treatment plans hard to develop, patients with rare disease are often undiagnosed (94).

Modifiable: These risk factors are controllable, and include a sedentary lifestyle, which is currently a leading cause in the development of CVD, with the world health organisation (WHO) suggesting only 40% of the global population are sufficiently active in their day to day lives (15). Whist physical activity not only reduces the risk of obesity and type II diabetes (T2DM), it also improves both blood lipid and glycaemic control, both of which, when dysregulated, contribute significantly to endothelial and smooth muscle dysfunction (16). Unsurprisingly, tobacco is also linked to the development of CVD, with 1 in 10 cardiovascular deaths attributed directly to smoking (17). Smoking also appears to have multiple interactions with other major cardiovascular risk factors such as high lipid serum levels, hypertension and diabetes, and has been linked to the development of aneurysms (18) and a variety of cancers (19). Tobacco smoke reduces flow mediated dilation in systemic

arteries in a dose dependent manor, leading to endothelial dysfunction and potentially hypertension (20). Within the blood serum cholesterol, low density lipoproteins (LDL) are found to be significantly upregulated in smokers, with a correlation apparent between the decrease in high density lipoproteins and apolipoprotein A1, leading to a proatherogenic environment for the development of atherosclerosis. Apart from lipid modulation, smoking also increases free radical and oxidants production, leading to a pro-oxidative environment which ultimately results in the oxidation of LDL and increased DNA damage (21, 22). Oxidised LDL (oxLDL) is well known to be recognised by macrophage scavenger receptors, causing macrophages to transform into foam cells (23), an essential element of lipid deposition and plaque formation (24). The activation of endothelial cells from cigarette smoke leads to the increased production and subsequent activation of both Matrix Metalloproteinase 9 (MMP9) and STAT3, leading to significant changes in matrix deposition as well as the activation of macrophages, again contributing to a proinflammatory pro-calcification environment (25).

Risk Factors	
Non-modifiable	Modifiable
Age	Hypertension
Sex	Diabetes mellitus
Family history of CVD	Obesity
Metabolic syndrome	Cigarette smoking
Lipid disorders	Physical inactivity
Ethnicity & Race	Dyslipidemia
Menopause	High cholesterol

Table 1.1. Risk factors for cardiovascular disease; divided into non-modifiable and modifiable risks. Adapted from British Heart Foundation. Modifiable and non-modifiable risk factors, 2016.

1.3. Prevalence of type II diabetes and current treatment strategies

With diabetes mellitus (DM) widely regarded as the oldest known disease to mankind and the prevalence of DM continuously increasing worldwide, it is unsurprising that the annual cost of diabetes has risen to more than $827 billion worldwide, tripling in the last 10 years (26, 27). 90% of those with diabetes have Type II, in which blood glucose obtained from ingested carbohydrates converts to glucose and triggers the pancreas to produce insulin. Due to the constant high levels of blood glucose, the pancreas reduces the amount of insulin made or the cellular mechanisms to produce insulin break down and the body begins to resist it, leading to sustained hyperglycaemia in the patient (28). Constant hyperglycaemia reduces the bioavailability of vasodilator nitric oxide (NO) within the vasculature (29), increasing blood pressure, whilst also damaging the endothelial layer (30, 31), resulting in inflammatory cell infiltration (32), the accumulation of macrophages within the medial layer and eventually the development of atherosclerotic plaque and calcification along the vessel wall (33). With T2DM patients, many of whom are obese and have high cholesterol and hypertriglyceridemia, diabetes manifests as a comorbidity, increasing multiple risk factors of cardiovascular disease, consequently, diabetic patients are four times more likely to die from CVD than a non-diabetic person (34).

Following the development of T2DM, patients often suffer from a range of comorbidities, which can be as debilitating as diabetes itself. Studies such as the Maastricht Study; which aimed to study the aetiology and pathophysiology of T2DM in an extensive phenotyping approach have highlighted a range of classic and emerging comorbidities (35, 36). Classic comorbidities, such as diabetic neuropathy (DN) occur due to sustained systemic hyperglycaemia and accounts for more than 50% if non-traumatic amputations (37). Defined as a symmetric length dependent sensorimotor polyneuropathy attributable to metabolic and microvascular alterations as a result of chronic exposure to hyperglycaemia DN often presents as immense pain followed by fibre dysfunction and loss of motor control, and with no treatment beyond pain management it should be considered as debilitating a condition as T2DM itself (38). Moreover, peripheral vascular disease (PVD), a manifestation of atherosclerosis and characterised as an occlusive disease of the lower extremities effects more than 200 million people worldwide (39) with 20-30%

having DM. With strong evidence suggesting significant abnormalities in vSMC and endothelial function during PAD development (40), it is clear that the molecular mechanism behind the development needs to be addressed before full manifestation occurs in order to circumnavigate these crippling comorbidities. More recently, diseases within the digestive system such as non-alcoholic fatty liver disease have been associated with T2DM, which is considered to be the manifestation of the clinical tetrad of hyperinsulinemia with insulin resistance, visceral obesity, dyslipidaemia and hypertension, associated with up to 55% of DM patients (41). As the breadth of comorbidities associated with T2DM is ever expanding (Table 1.2) this further highlights the current need for treatment in the control of hyperglycaemia within the diabetic patients.

Whilst an increase in physical activity and an improvement in overall diet are recommended for those patients with T2DM, metformin is widely prescribed for this patient group, preventing the production of glucose in the liver, thus improving both basal and postprandial plasma glucose levels (42). Metformin has also been demonstrated to protect against coronary artery calcification within diabetic patients (43, 44), possibly through a Sirtuin 1 (SIRT1) - p53 - p21 pathway (45, 46). However, whilst this further suggests an exciting relationship between SIRT1, T2DM and vessel calcification, further elucidation of this mechanism is required.

Comorbidity	Prevalence	Study
Hypertension	60%	(47)
Ischemic heart disease	20%	(48)
Cardiomyopathies	40%	(49)
Arrhythmias	43%	(50)
Heart failure	31%	(51)
Coronary artery disease	26%	(50)
Peripheral vascular disease	25%	(52)
Myocardial infarction	10%	(53)
Pulmonary embolism	1%	(54)
Diabetic retinopathy	35%	(55)
Diabetic neuropathy	50%	(56)
Diabetic nephropathy	40%	(57)
Alzheimer's / Dementia Disease	2%	(58)
Cataracts	66%	(59)
Chronic obstructive pulmonary disease	19%	(60)
Gout	11%	(61)
Non-alcoholic hepatitis, non-alcoholic fatty liver disease	70%	(62)

Table 1.2. Comorbidities of Type II Diabetes. Taken from the findings of the Maastricht Study, adapted from Schram, et al. 2014.

1.4. Arterial vessel structure

In terms of histopathological examination, a large arterial wall is a structure composed of three layers, tunica intima, tunica media and adventitia (Fig. 1.2). The tunica intima is the thinnest layer, comprised of a single continuous endothelial layer, supported by a subendothelial layer of connective tissue. The tunica intima is surrounded by an internal elastic lamina which runs parallel to the vessel, which separates it from the tunica media. Secondly, the tunica media is comprised of vascular smooth muscle cells (vSMCs) and elastic fibres; which are in greater abundance in arteries compared to veins. Finally, the adventitia is the outermost layer of the vessel, composed entirely of external elastic lamina; which functions to anchor the vessel within the surrounding tissue, smaller blood vessels and nerves. The integrity of the vessel wall is compromised in patients with diabetes and cardiovascular risk and it is this process of cellular phenotypic change under diabetic conditions which is the stimuli for the development of calcification (63).

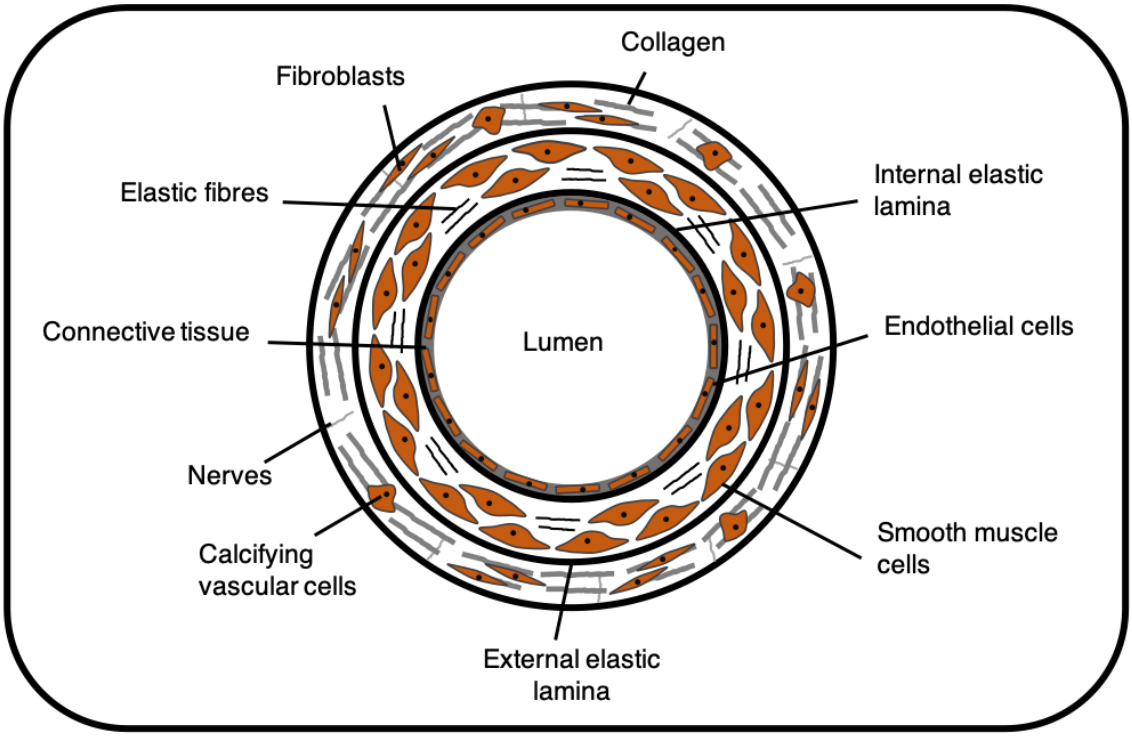

Fig. 1.2. Vessel structure. The vessel is structured into three main sections. The adventitia; comprised of adventitial fibroblasts and stem-cell like progenitor cells; known as calcifying vascular cells, perivascular nerves, connective tissue and fibroblasts, suggested to be a gateway for immune cell migration into the vessel. The media layer; mainly comprised of vSMCs, responsible for contraction and relaxation of the vessel and may contain calcifying vascular cells. The intimal layer; comprised of a thin layer of endothelial cells, responsible for the release and absorption of molecules from the blood to the vessel.

1.5. Vascular calcification

Vascular calcification (VC); once thought to result from passive degeneration of vSMCs to a calcified mass, is now known to involve a complex regulated process of biomineralisation resembling bone osteogenesis (64, 65). VC is considered an important part of the development of atherosclerosis and it is often associated with poor prognosis within different disease conditions, where its extent is a strong indicator of the overall burden of atherosclerotic disease and risk of mortality (66, 67). VC occurs within two distinct areas of the vessel wall, the tunica intima and media, and may be categorised as such (Fig. 1.3).

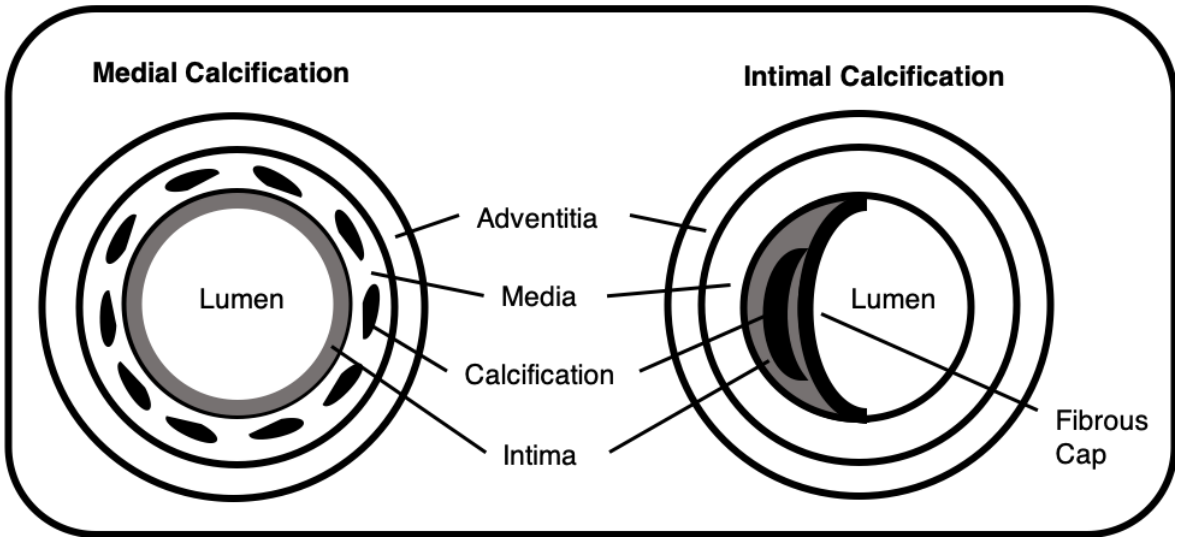

Fig. 1.3. Localisation of vascular calcification. Medial calcification; found mainly in aging, diabetes and renal disease occurs concentrically around the vessel within the muscular medial layer often due to high levels of calcium, phosphate or both. Intimal calcification; found within inflammatory atherosclerotic vessels presents as a large cholesterol filled plaque covered with a fibrous cap which when removed can lead to occlusion of the vessel.

Firstly, Intimal calcification occurs within an atherosclerotic plaque; associated with inflammation, lipid accumulation, macrophage aggregation and vSMCs. Morphologically, Intimal calcification occurs at the base and within the centre of the plaque and is associated with advanced atherosclerosis, contributing to occlusion or stenosis (68, 69).

In contrast, medial calcification is generally associated with vSMCs alone, can occur in the presence and absence of atherosclerosis and is often found in a concentric and symmetrical formation within the medial layer of the vessel, commonly in aging populations and those with diabetes (70). Medial calcification contributes significantly to increased mortality associated with diabetes, due to an increase in arterial stiffness, loss of arterial elasticity and vascular dysfunction (71). Whilst the theory of intimal and medial calcification remains distinct, in practice the close proximity of both types of calcification within the vessel make it difficult to distinguish between the two and their occurrence may often overlap (72).

1.6. Clinical significance of vascular calcification

Clinically, extensive calcification is associated with significant stenosis, with radiographically detected vascular calcification generally accepted as a sensitive marker for atherosclerosis (73). The first imaging of calcification was achieved using chest radiographs (74), however these only gave a positive reading when calcification was extensive. More recently, electron beam and multidetector computed tomography has been used to generate a more sensitive high-resolution scan, thus being able to provide a total calcium score dependent on the calcium mass observed (75). In general, a higher calcium score correlates with an overall increased atherosclerotic plaque burden and can be used to determine the following course of treatment. Whilst calcification is noted as a marker for cardiovascular risk, controversy surrounding the prognostic significance remains. Identification of VC increases the risk of myocardial infarction and lower limb amputation, even when adjusted for traditional risk factors such as age, hypertension, diabetes, smoking and dyslipidaemia, with lower limb vessel calcification correlated to both cardiac and renal events (76).

1.7. Current therapies for cardiovascular disease

In recent decades, a wide range of therapies have been developed for the treatment of atherosclerosis and CVD, however more recent evidence shows a growing rise in CVD related deaths (77). This provides the impetus for a greater understanding of related pathologies and the development of novel, more personalised drug treatments. Whilst lifestyle changes are always recommended first to minimise the modifiable CVD risk factors, many patients including those with co-morbidities such as diabetes, are often placed on statins alongside medication to lower blood sugar and increase insulin sensitivity to reduce the risk of developing VC (78). Whilst the mechanism of statins is multifaceted (78), recent studies have demonstrated the effect of statins in upregulating a family of histone deacetylases within endothelial cells, which in turn, lowers stress-induced senescence, reducing their dysfunction and resulting in the maintenance of vessel homeostasis (79).

However, if both lifestyle and drug treatments are ineffective in patients for the treatment of atherosclerosis, surgery is often then required. Coronary artery bypass grafting (CABG) surgery is often the next option, which involves the removal of plaque build-up from inside the vessel before it ruptures and causes a complete blockage, often resulting in a myocardial infarction. During CABG surgery a healthy artery or vein; often from the internal mammary vessels are grafted to the coronary artery to bypass the blocked portion of the vessel, creating a new path for oxygen rich blood to flow to the heart (80). Offcuts of the mammary vessels are often used as negative controls in histological studies, due to the proven resistance to the development of calcification (81). However, in recent years a more minimally invasive angioplasty and stent procedure (percutaneous coronary intervention) in which a metal stent is inserted through a distal vessel and threaded to the site of atherosclerosis alongside a small balloon, which is then inflated to flatten the stent against the lipid plaque along the vessel, before the balloon catheter is removed and the stent is left in place. More recently stents have been preferred to CABGs due to its reduced recovery time and ability to be drug eluting, which reduces the prevalence of the blockage reoccurring (82), although it is not always advised for the more serious blockages or if multiple grafts are needed. However, these surgical procedures still carry significant risk, driving the need to understand the molecular components within the development of CVD, to determine if a more stratified and

personalised drug treatment can be administered before the need for surgical intervention, and thus this is the foundation for this thesis.

1.8. Pathological development of vascular mineralisation

Under normal physiological conditions there is sufficient concentrations of both calcium and phosphate to initiate the calcification process (83), however a range of mechanisms control and regulate its formation, only allowing calcification in places where it is required; such as during bone development and repair. Once the balance between inhibitory and pro-calcification mechanisms is lost, then pathological calcification may occur (84). Previously thought to be a passive, degenerative, end-stage process it is now known to be a tightly regulated, slowly progressive course, in which vesicle-like structures are exuded from vSMCs and bind to the matrix, depositing hydroxyapatite crystals (85, 86). These crystals are then used as a nucleation sites for further calcification, either in large plaques, or concentrically spreading around the vessel (Fig. 1.4).

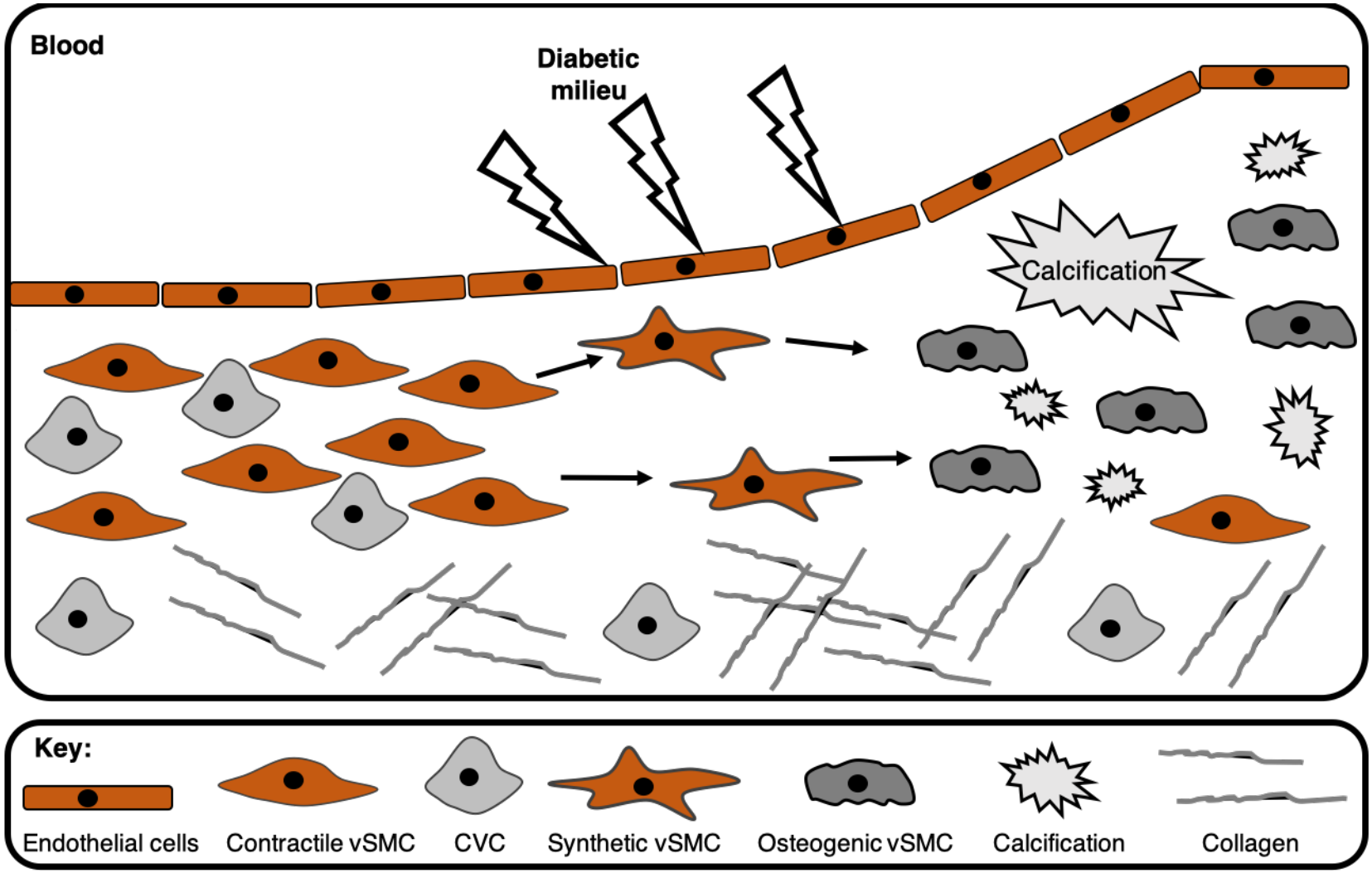

Fig. 1.4. Vessel wall during osteogenic differentiation. During diabetes a hyperglycaemic, inflammatory microenvironment with mineral ion imbalances leads to endothelial dysfunction and damage. The medial layer then triggers a repair response which often perpetuates further vascular dysfunction via the activation of calcifying vascular cells (CVCs) and contractile vascular smooth muscle cells (vSMCs), the layer of which differentiate into synthetic vSMCs and then subsequently osteogenic vSMCs, depositing a calcified matrix within the vessel.

1.9. Inducers of calcification

1.9.1. Cellular senescence

The development of calcification is associated with a deviation from the homeostatic norm, in which quiescent vSMCs undergo a complex process of differentiation, followed by the development of senescence (87). vSMC senescence involves the reduction of proliferative marker expression and an increase in cytokine and protease production; termed the senescence associated secretory phenotype, in which the vSMC induces a more inflammatory, osteogenic environment to allow further trans-differentiation and the subsequent development of calcification (88). Development of this unique phenotype has been associated with the overexpression of cell cycle inhibitors and an increase in DNA damage (89), leading to chromatin instability, however the precise mechanism in which osteogenic differentiation is triggered via senescence remains unclear.

1.9.2. Loss of osteogenic inhibitors

As calcification is now understood to be an active process, the dynamic between both activators and inducers in calcification is considered to be a careful balancing act, in which too much of either can have detrimental effects (84, 90). vSMC are able to effectively modulate a range of these proteins, by altering their transcriptional programme as needed, however in the event of calcification, a loss of inhibitors is often the cause (84). Osteogenic inhibitors such as fetuin A, osteopotegrin and matrix Gla protein (MGP) are shown to be decreased in both diabetic and chronic kidney disease (CKD) patients and positively associated with an increased risk of mortality (91, 92). Fetuin A sequesters calcium and when contained within extracellular vesicles, inhibits calciums' ability to form calcium-phosphate molecules, further stabilising the vesicle membrane and preventing its deposition (93-95). This reduction in calcium phosphate deposition not only reduces extracellular matrix (ECM) mineralisation, but reduces macrophage apoptosis and their differentiation to foam cells, slowing atheroma formation and the development of plaque (93). Secondly, MGP is produced within vSMCs and acts as an inhibitor of pro-osteogenic bone morphogenic proteins (BMPs) and thus with its loss, an upregulation of BMP2 has been reported (96), contributing to the drive in osteogenic differentiation and subsequent calcification. However, studies have questioned the direct relationship between MGP and the development of calcification, with the level

of γ-carboxylation on the MGP molecule shown to control plaque development rather than the actual expression of MGP (97). With carboxylation attributed to vitamin K-dependent enzyme γ-carboxylase, a deficiency in vitamin K rather than levels of MGP itself may be responsible for the development of these plaques (98), however a greater understanding is still required within this field (99).

1.9.3. Oxidative stress

Both oxidative and endoplasmic stress has been implicated in the development of osteogenic differentiation and subsequent VC (100). Within the vessel, the presence of hyperglycaemia and reactive oxygen species leads to increased NADPH oxidase activity, producing elevated levels of hydrogenic peroxide (101). Following this, hydrogen peroxide then induces differentiation via activation of the Runt related transcription factor 2 (Runx2) pathway and contributes to vSMC osteogenic differentiation (102). Similarly, in an inflammatory diabetic vascular environment, advanced glycated end products (AGEs) contribute to the activation of pro-inflammatory receptor for advanced glycated end products (RAGE). This in turn induces an increase in NADPH oxidase activity, again leading to an activation of Runx2 and alkaline phosphatase (ALP) activity, with an inhibition of both AGEs and RAGE shown to reduce calcification in animal models (103, 104).

1.10. Microvesicle formation and their role in vascular calcification

During osteogenesis within bone, the formation of vesicles is a normal feature, by which to spread and advance bone development (105). The vesicles are rich in ALP (106), which catalyses the breakdown of pyrophosphate; a key inhibitor of calcification. These vesicles are enclosed in a tri-lamellar membrane equipped with a sodium-dependent phosphate pump, through which phosphate ions are actively transported. The pumping of phosphate ions into vesicles is potentiated by an increase in phosphate within the extracellular fluid, which occurs during chronic diabetes or kidney failure (107, 108). Once the vesicle membrane disintegrates calcium phosphate is released into the extracellular fluid and comes into contact with the ECM, triggering the formation of hydroxyapatite crystals; leading to a hardening and loss of matrix function (109) (Fig. 1.5).

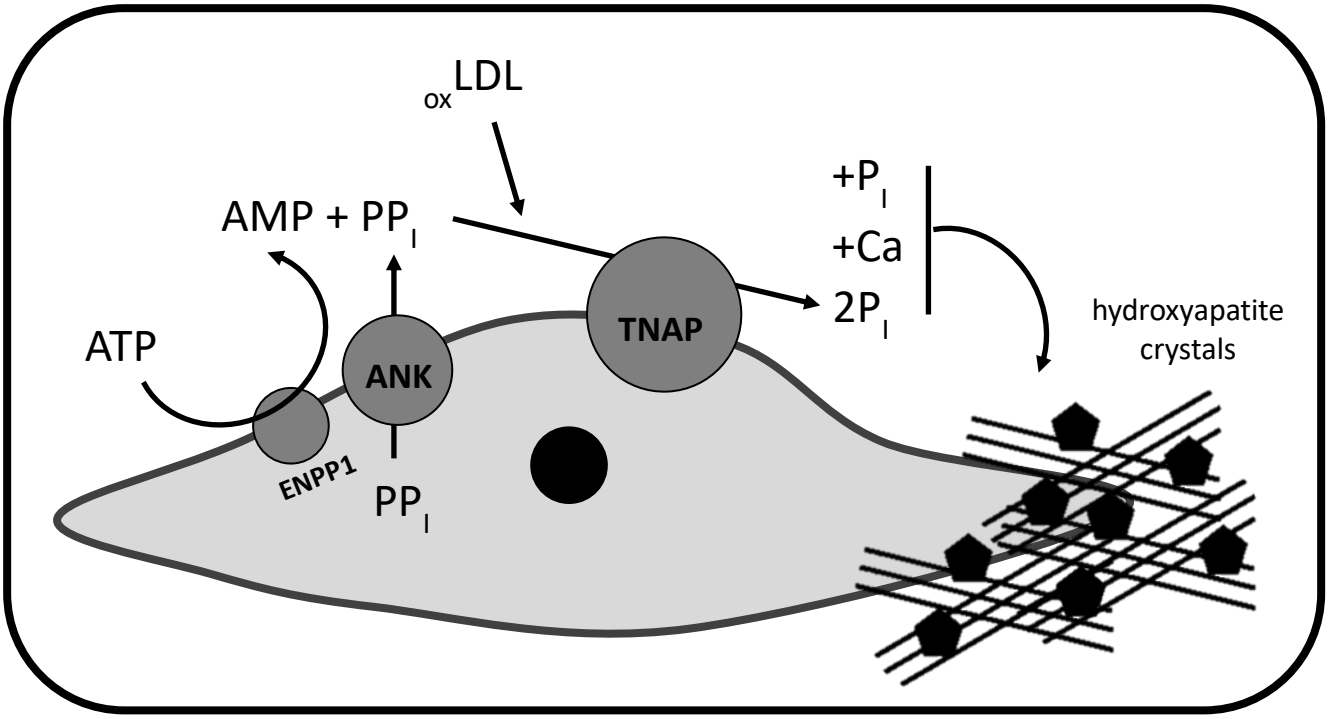

Figure 1.5. TNAP induction of smooth muscle cell calcification. vSMCs exposed to increased oxidized LDL, phosphate and calcium, form hydroxyapatite crystals on their matrix, leading to vascular calcification. ENPP1 converts ATP to AMP, which binds with pyrophosphate (PP_I) shuttled out the cell by ANK. TNAP catalyses the breakdown of calcification inhibitor pyrophosphate to phosphate, further propagating the development of matrix calcification.

1.11. Extracellular matrix deposition

Whilst the majority of calcification research has focused on the vSMC phenotype switching, a growing importance on the ECM in which the vSMCs are embedded has emerged. Modulation of vSMCs via their relationship with the ECM, through focal adhesions and integrin receptors may contribute to their ability to maintain their contractile phenotype and slow down proliferation (110). Whilst the expression of most ECM proteins in their native form such as; laminin, perlecan, fibronectin collagen I and collagen VI appear to help maintain a contractile anti-proliferative phenotype, manipulation or breakdown of these; such as monomeric collagen I, increases proliferation, migration and cellular adhesion, suggesting a change in ECM may induce the trans-differentiation of vSMCs, leading to calcification (111). Recent studies have suggested that the ECM could be considered a reservoir of cytokines and growth factors which can modulate the vSMC phenotype (112), and that modulation of the ECM via stress or change to the composition of the vessel

may increase the bioavailability of these, thus inducing the changes observed within the smooth muscle.

1.12. Vascular smooth muscle cell phenotypic switching and plasticity

vSMCs are usually confined to the tunica media of the vessel where they exhibit a contractile tone, which functions to maintain normal vascular tone. Under healthy conditions, vSMCs are non-voluntary, contractile cells, found in the intimal layer of vessels and responsible for the optimal function of blood vessels, primarily controlling blood pressure through contraction and relaxation. Within the vessel, contractile vSMCs respond to signals such as acetylcholine and adrenaline signals to contact and express a range of contractile proteins, such as SMAα SM22a SM-MHC (113). Morphologically the contractile phenotype exhibits an elongated spindle-like shape, with a low level and size of organelles present, as instead these are replaced via contractile filaments, attributing to vessel elasticity and the quiescent state of the cells (112).

Historically vSMCs were believed to maintain a contractile phenotype except when under stress, were they were thought to differentiate in a linear manner, in which contractile and synthetic vSMCs represented two ends off a spectrum and which coincided with significant changes in morphology. A synthetic phenotype exhibits a greater number of organelles and a faster proliferative rate than a contractile vSMC, with a higher energy turn-over than contractile cells (65). Morphologically, synthetic SMCs resemble a more rhomboid shape, with cobblestone morphology and are often more disorganised within the intima layer of the vessels, with a reduction in contractile filaments found, which correlates with a decrease in arterial compliance (114, 115).

However, with mounting research demonstrating the differentiation from contractile phenotype to at least four distinct phenotypes apparent (116), the field is widening rapidly, with more research needed to fully characterise them (117). Moreover, unlike other cell types, mature vSMCs do not terminally differentiate, and retain remarkable plasticity, depending on the environmental and extracellular signals to which they are exposed (118). This plasticity is required for vascular remodelling

and adaptation, and vSMCs can display features of osteoblasts, chondrocytes, adipocytes and macrophages (119, 120).

The most common differentiation process of a vSMC during calcification is osteogenic differentiation, in which vSMCs will switch to the synthetic phenotype, exhibiting an increased rate of proliferation, which accounts for the development of restenosis or atherosclerosis (121). Additionally, migration of the vSMC into the tunica intima can be correlated with the upregulation of focal adhesions and activation of major proliferation pathways such as ERK (122-124). This leads to the subsequent increase in MMP and collagen deposition and the cells lay down new matrix and begin to calcify (123, 125). Once vSMCs have laid down a matrix and calcification becomes apparent, the cells switch again from a synthetic phenotype to an osteogenic phenotype, in which proliferation is significantly reduced and the production of Runx2 and Msx2 is upregulated and ALP is activated, resulting in the production and release of calcifying vesicles to further propagate mineralisation (65). Furthermore, it has become apparent that whilst vSMCs undergo osteogenic differentiation in response to elevated calcium and phosphate, the damage to the vessel due to hyperglycaemia or oxidative stress resulting in DNA damage (126, 127) may induce senescence within the vessel through cyclin-dependent kinase inhibitors p16 and p21, contributing to the inability of the cell to repair itself and further perpetuating vascular dysfunction and calcification (128, 129) (Fig. 1.6). Interestingly whilst Runx2 activation allows osteogenic differentiation, Msx2; which is also found to be upregulated during this process, leads the cells down a chondrocyte differentiation pathway and it is the fine balance between these two major transcription factors which determines the differentiation pathway, however fluctuations in their relevant expression allows plasticity between the two osteoblastic and chondrocytic phenotype (130).

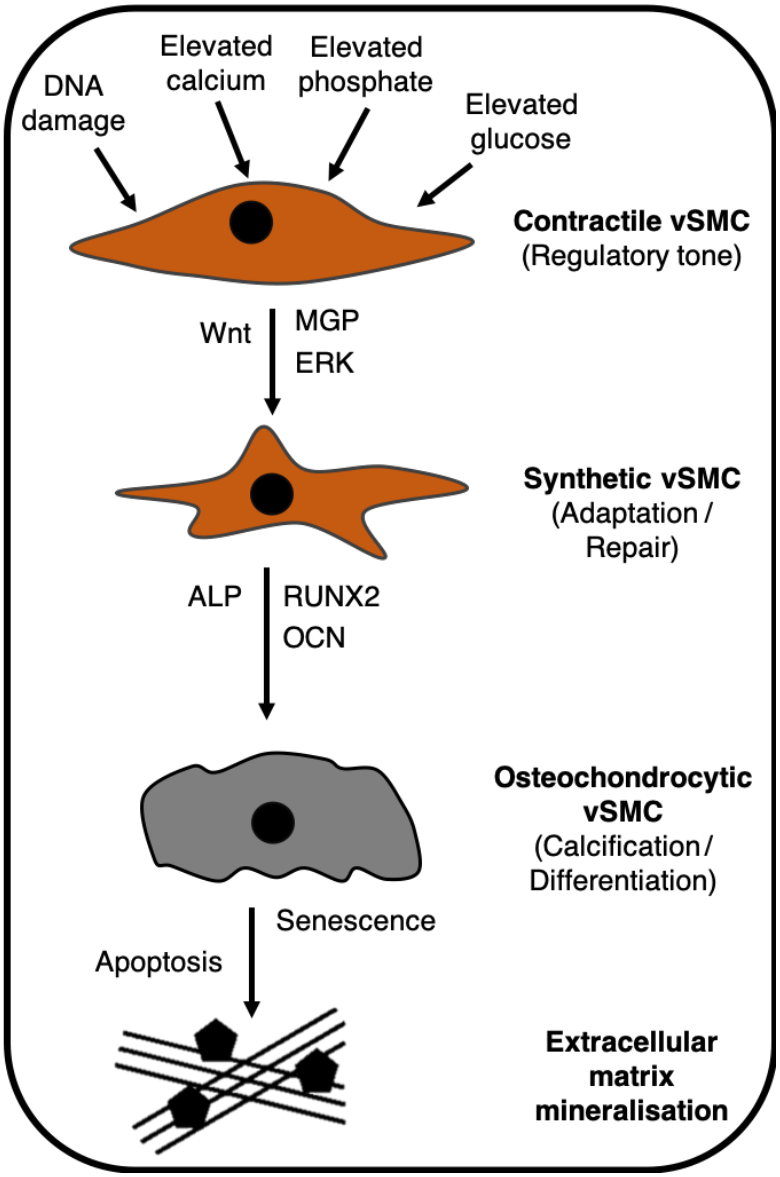

Fig. 1.6. Smooth muscle cell differentiation. Regulatory contractile smooth muscle cells (vSMCs) are exposed to increased phosphate, calcium, glucose and DNA damage, resulting in the activation of multiple pathways; including ERK, Wnt, and the loss of endogenous calcification inhibitors. Recently differentiated synthetic vSMCs begin to express alkaline phosphatase (ALP) Runx2 and Osteocalcin (OCN) which furthers their differentiation to osteogenic vSMCs, leading to cellular senescence and the increased deposition of a calcified extracellular matrix.

1.13. Origins of calcifying vascular smooth muscle cells

The origins of vSMCs are complicated, due to the conflicting beliefs that exist regarding whether SMCs in the vessel wall are heterogenous or derived from multipotent vascular stem cells lineage which are linked to the development of calcification. Embryonic development research has given critical insight into the formation of *de novo* vasculature from the embryonic splanchnic mesoderm via vasculogenesis, resulting in the production of both smooth muscle and endothelial precursor cells (131). Embryonic differentiating vSMCs exhibit high rates of proliferation and migration, producing and laying down a large amount of ECM associated proteins in order to form the vascular system. Following the development of large vessels, angiogenesis occurs to refine the pattern of the vessels and determine whether they develop to be an artery or a vein, with PDGF-BB and TGF-β signalling playing an important role in their development (132). However, an alternative view suggests that calcifying vascular cells (CVCs) are solely responsible for the development of the calcified plaques within the vessels, which arise from a resident subpopulation of neural crest derived progenitor cells from within the arterial wall, as opposed to those resulting in mesoderm lineage (133). With atherosclerosis believed to have clonal origins, there is accumulating evidence that this permanent resident subpopulation may be responsible. CVCs have been shown to exhibit all normal vSMC markers; such as SM22A and SMAα, however under culture they spontaneously differentiate to an osteogenic phenotype and produce calcified nodules within the matrix. Whilst CVCs share many similar properties to bone, they also share several pericyte phenotypic markers, including αActin, β-Actin and 3G5 epitope. With Pericytes long suspected to be from mesenchymal origin, the suggestion that CVCs may be of mesenchymal origin gains more traction (134, 135).

1.14. Molecular aspects attributing to vascular calcification

1.14.1. Hyperglycaemia

Long term hyperglycaemia generates metabolic, osmotic and oxidative stress within the vessels, all of which contribute to the development of vascular calcification (127). The presence of hyperglycaemic stress has been shown to remain even after glucose normalisation, defined as ‘hyperglycaemic memory’ (136). Originally described in streptozotocin-induced diabetic rats in which return to normoglycemia

did not reduce fibronectin expression in the kidney cortex (137) the mechanism was then fully described in human endothelial cells as a sustained response to hyperglycaemia with continuing damage (138). Hyperglycaemia increases reactive oxygen species (ROS) production within in the mitochondria, activating the polypol and hexosamine pathway, increasing production of AGEs and protein kinase C (PKC) activation, all of which increase vascular dysfunction and the upregulation of pro-oxidant enzymes and inflammatory markers, even after the return of normoglycemia (139, 140). Pathways such as NAD(P)H and PKC become persistent, leading to vasoconstriction of the vessels, which results in high blood pressure and may lead to hypertension or vascular dysfunction (141). Additionally, persistent PKC signalling has been demonstrated to increase Runx2 and BMP protein expression which forms a positive feedback loop alongside other osteogenic markers such as ALP and Msx2, resulting in dyslipidaemia and increased calcification (142). Prolonged hyperglycaemia also increases BMP2/Wnt axis expression, leading to an osteogenic phenotype switch of myofibroblasts, increasing BMP2 expression and arterial calcification and has been linked to the osteogenic switch within the vascular smooth muscle layer as well (143, 144).

1.14.2. Runx2 Pathway

Runx2 (or Cbfa1) is a bone related transcription factor which is essential for the differentiation of osteoblasts from mesenchymal precursors, causing ECM deposition and an increase in bone density (145). Activation of Runx2 directly upregulates a range of osteogenic downstream targets such as BMPs, Collagen I, Collagen III and OCN via binding to their promotor regions at a core enhancer sequence (PuCCPuCA), allowing for an increase in osteogenesis and bone development (142) (Fig. 1.7). However, when activated in tissues within the vasculature this increase in matrix deposition and mineralisation can cause significant problems, and a wide variety of pathways converge on this axis to both perpetuate and inhibit this process.

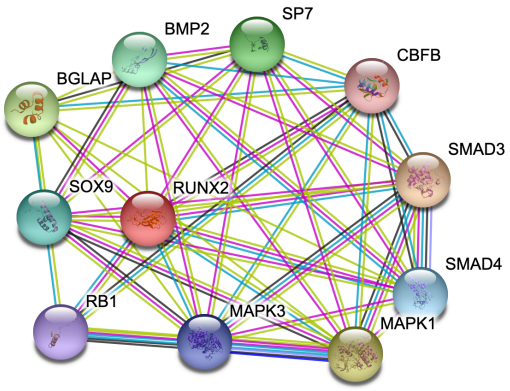

Major Runx2 Regulation Genes	
Gene	Function
BGLAP	Non-collagenous calcium binding protein hormone.
BMP2	Member of the TGF-beta family. Induces cartilage and bone formation. Stimulates osteoblast differentiation.
CBFB	DNA binding factor for RUNX2.
MAPK1	Serine/threonine kinase within the MAP kinase signal transduction pathway. Heterodimerises with MAPK3.
MAPK3	Serine/threonine kinase within the MAP kinase signal transduction pathway. Heterodimerizes with MAPK1.
RB1	Tumour suppressor and key regulator of entry into cell division, suppressing E2F1 transcription leading to cell cycle arrest. When phosphorylated promotes G0-G1 transition.
SMAD3	R-SMAD, intracellular signal transducer and transcriptional modulator activated by TGF-beta. Forms heterodimer with SMAD4, activating transcription.
SMAD4	Interacts with SMAD1/5 following BMP2 activation to interact with Runx2 increasing downstream transcription. Acts within the BMP2-Smad-Runx2 feed forward loop.
SOX9	Physically interacts with Runx2 to inhibit the transactivation of Runx2 and subsequent phosphorylation-dependent degradation of Runx2, regulating osteochondrogenesis.
OSX	Required for bone formation. Transcription factor essential for osteoblast differentiation. Binds downstream of Runx2 at response elements and is responsible for osteoblast-specific Col1a1 production.

Fig. 1.7. List of major Runx2 regulated genes. Adapted from STRING biological database. search term ‘RUNX2’.

Differentiation of both osteoblasts and smooth muscle requires secretion of an ECM as previously described, which subsequently allows for the induction of osteoblast-related genes such as those encoding OCN, bone sialoprotein (BSP) and ALP, all of which contribute to the development of matrix calcification (146). ECM activation further increases the binding of Runx2 to the OCN promotor region, again increasing the deposition of a calcified matrix (147). Integrin signalling, induced via ECM binding, activates the MEK/ERK signalling pathway (MAPK) which quickly becomes phosphorylated, allowing for further induction of OCN and Runx2 expression (148, 149), with MAPK pathway inhibitors demonstrated to limit the induction of ECM dependent osteoblastic differentiation in both stromal cells (150) and vSMCs (151). Likewise, overexpression or constitutive activation of MEK1 induces both endogenous OCN mRNA production as well as an increase in the phosphorylation of Runx2 (124, 149, 152). Whilst other post-translational modifications of Runx2 may affect its activation, phosphorylation is currently the best described for Runx2. Phosphorylation of Runx2 by MAPK has been shown to be vital in the process of maintaining bone homeostasis (152, 153), however this increased phosphorylation in regions such as the vasculature may lead to aberrant Runx2 signalling, resulting in calcification.

Furthermore, the BMP family of proteins; a member of the TGF-β superfamily, are best described as inducers of osteoblast and chondrocyte differentiation, operating in conjunction with Runx2 (154, 155). BMP signalling uses receptor regulated Smads 1,5 and 8 (R-Smads) and Smad 4 to propagate the signalling pathway. Once activated the Smads then translocate to the nucleus complexing with enhancer sequences on target genes; such as Runx2, leading to their production (156). BMP overexpression has been directly linked to the activation of Runx2 in mesenchymal cells, either via direct Smad signalling or by alternative pathways, with BMP and Runx2 shown to synergistically increase OCN expression (157) (Fig. 1.8).

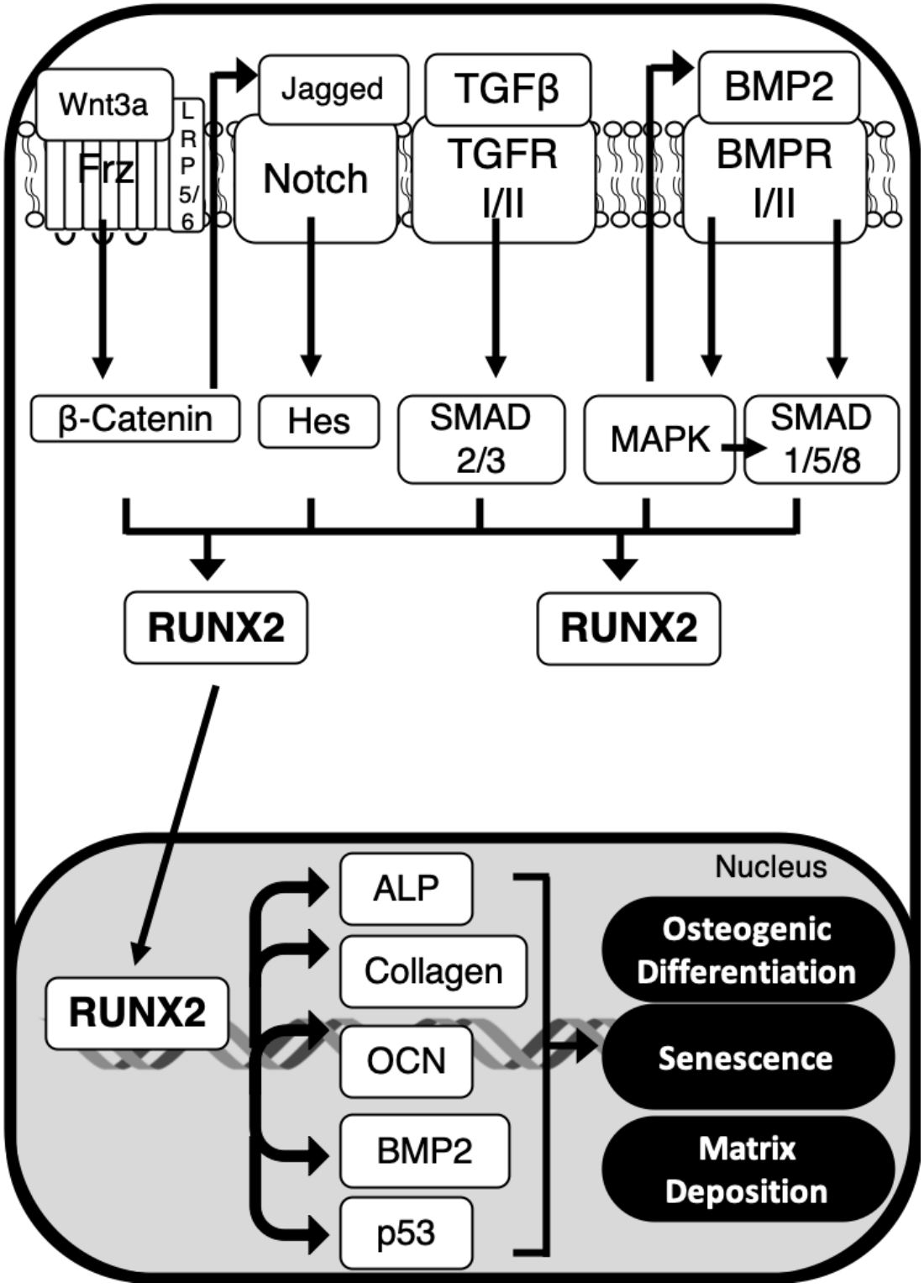

Fig. 1.8. Runx2 Signalling Pathway. Multiple extracellular signals, including osteogenic Wnts, TGFβ and bone morphogenic proteins (BMPs) activate cell membrane receptors, leading in activation of multiple signal transduction pathways; such as SMAD, β-Catenin and MAPK. In turn these pathways activate Runx2, increasing its expression and translocation to the nucleus. Runx2 acts as a transcription factor for multiple osteogenic proteins, allowing for osteogenic differentiation, cellular senescence and an increase in calcified matrix deposition.

1.14.3. DNA Damage

Vascular dysregulation and calcification can be attributed to the increase in DNA damage within the vessels (121, 158). DNA damage can be detected early on in the development of atherosclerotic calcification and its prominence increases with the severity of plaque formation and vascular dysfunction (159). DNA damage includes single (SSB) and double stranded breaks (DSB), nucleotide modifications, micronuclei development and deletion of DNA segments. The mechanism of repair following a DSB depends on the phase of the cell cycle, with error free homologous repair (HR) being favoured during the S/G2 phase of the cycle, when sister chromatids are available as homologous templates. Whereas non-homologous end joining (NHEJ) is more error prone and favoured during G1 and G2, where the cell is dormant and recently described alternative non-homologous end-joining (A-NHEJ) occurs during the cells entry to S phase (160).

Homologous recombination can be divided into four steps. Initial processing of the break involves the MRN complex; composed of scaffolding proteins; MRE11, RAD50 and NBS1, and the Ataxia Telanglectasia Mutated (ATM) kinase which are recruited to the site of damage (161, 162). ATM then phosphorylates both the MRN complex and H2AX, activating the downstream cascade of proteins which signal the start of DNA repair (163), in which the cell will either repair and return to its phenotype before damage occurred, or undergo apoptosis.

If the cell is within G1 to G2 phase within the cycle, NHEJ is favoured. Firstly, a heterodimer of Ku70 and Ku80 recognises the DNA ends and complexes with DNA-dependent protein kinase (DNA-PK), auto-phosphorylating and forming a stable complex which remains tethered to the end preventing further access by other proteins. This results in a conformational change within the DNA-binding catalytic subunit, allowing terminal end processing, in which a DNA polymerase allows the trimming of the overhangs, thus producing two blunt ends ready for ligation. Finally, ligation occurs via XRCC4 and DNA ligase IV complex, which stabilises the DNA, resulting in repair (164, 165).

Finally, A-NHEJ occurs in a similar mechanism to NHEJ in the absence of key NHEJ cofactors. In the absence of Ku proteins, PARP1 binds to the DSB and is

subsequently activated and auto-poly(ADP-ribosyl)ated (158), resulting in decreased affinity for nucleosomes in a relaxed chromatin structure, facilitating chromatin remodelling which is needed for DNA repair. Following recognition, DNA end processing occurs via the PARP1-PAR synthesis (166), triggering recruitment of the MRN complex to initiate incompatible end resection. Finally, ligation of the DNA ends occurs when the MRN complex interacts with the DNA ligase IIIa/XRCC1 complex, stimulating the joining of the end.

Within a prolonged inflammatory pro-calcification environment, DNA repair by whichever method is often reduced and the cells often undergo apoptosis when overwhelmed by stress. Prelamin A, a precursor of Lamin A induces vSMC senescence and DNA damage via the inhibition of mitosis (129). Once accumulated in senescent cells it downregulates ATM, which inhibits activation of the MRN complex and thus DNA repair. DNA damage response signalling has been demonstrated to induce differentiation of vSMCs following senescence with an increase in p16 and ALP activity reported in damaged cells (167) (Fig. 1.9).

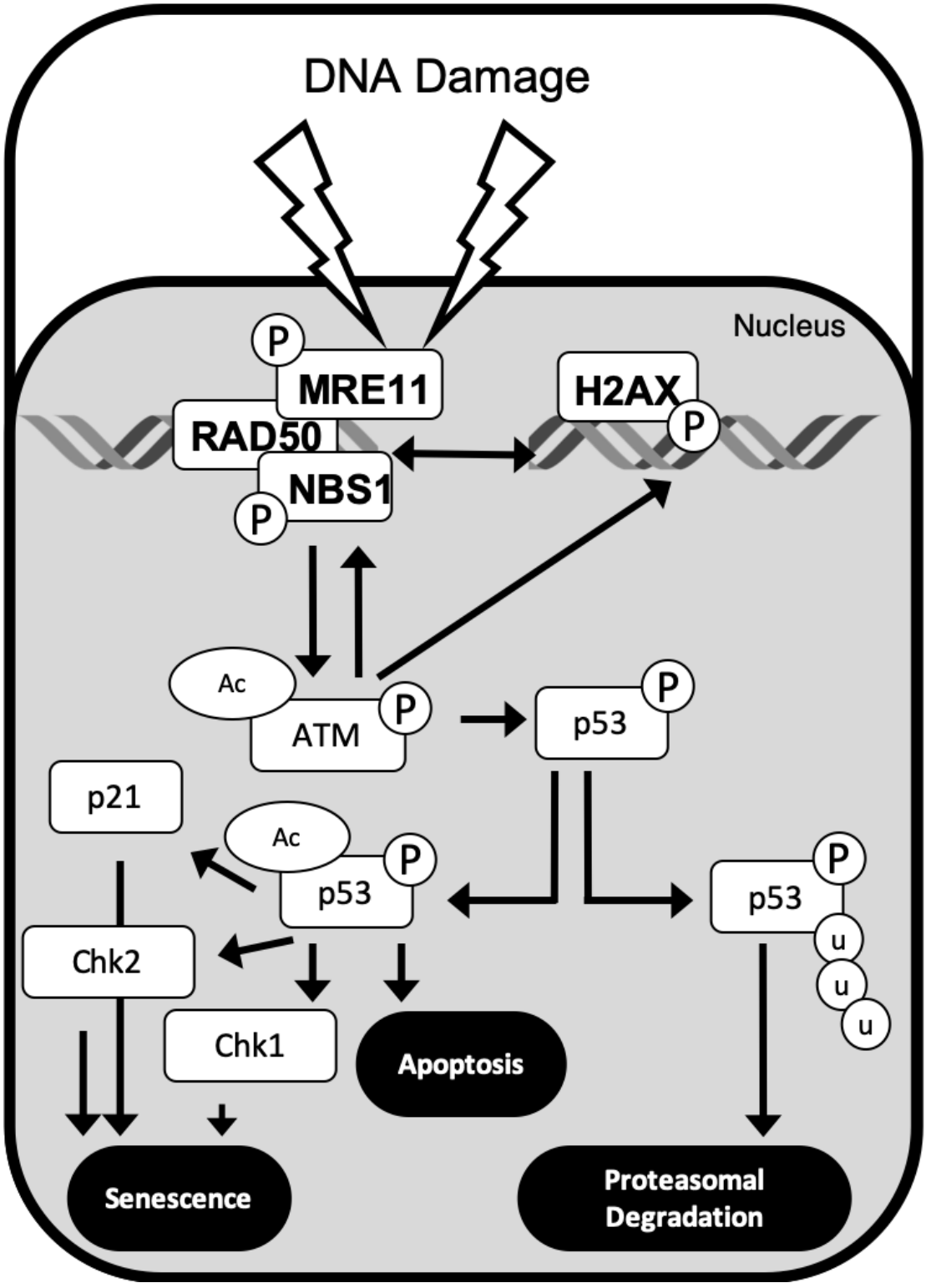

Fig. 1.9. MRN Pathway. DNA damage induces phosphorylation of the H2AX protein via ATM, leading to the accumulation of the MRN complex to the site of the DNA break. Activation of ATM then either phosphorylates p53, targeting it for ubiquitination, or p53 becomes acetylated, increasing p21 expression and a range of checkpoint inhibitors, resulting in cellular senescence or subsequent apoptosis.

1.14.4. Wnt Signalling pathway

Wnt signalling and its downstream mediators affects a range of biological processes ranging from embryonic development to insulin secretion and vascular calcification (168-170). A highly conserved group of 19 genes encoding for cysteine-rich-secreted glycoproteins, the Wnt family was first identified in *Drodophilia melanogaster* as a mutant wingless gene Wnt (171). Whilst highly conserved and well-studied in eukaryotes, *Wnt* signalling was believed to be essential for embryonic development, regulating cellular proliferation, polarity and apoptosis, yet significantly decreased in adults, with recent studies suggesting Wnt signalling is reactivated in cardiovascular pathologies (172). Whilst Runx2 is noted to play a key role in osteogenesis and bone remodelling, the Wnt pathway is now known to be necessary for the commencement of osteoblast differentiation. Wnt signalling is commonly divided into three main pathways, all dependent firstly on the Wnt protein firstly becoming palmitoylated on conserved serine residues before becoming glycosylated and binding to a receptor on the cellular membrane (173). The most well observed being the canonical pathway, involving Wnt and the β-Catenin protein with the strongest links to calcification and vascular dysfunction.

The Canonical pathway, the most well understood of the three Wnt pathways is β-Catenin dependent, characterised by the accumulation of β-Catenin in the cytoplasm and subsequent translocation to the nucleus. Secreted osteogenic Wnt ligands, classically Wnt3a, Wnt5a and Wnt7a (174), bind to the transmembrane Frz co-receptor and competitively interacts with co-receptors LRP5 and LRP6, propagating canonical Wnt signalling. This binding evokes the downstream Wnt signalling cascade, resulting in the dephosphorylation and stabilisation of β-Catenin (175), leading to the translation of β-Catenin into the nucleus where it interacts with its DNA binding partner T cell factor (TCF) / lymphoid enhancer-binding factor (LEF) to initiate the transcription of Wnt target genes such as Runx2 (176). Furthermore, phosphorylation of β-Catenin at Ser675 via p21 activated kinase 1 increases its activation, which highlights the intertwined nature of senescence and the induction of calcification (177). Additionally, β-Catenin activation regulates the expression of ECM components, including versican, MMPs, focal adhesin proteins and fibronectin which when upregulated can increase vessel stiffness and vascular calcification (178).

Within the nucleus, Runx2 expression is controlled by Wnt signalling via the direct binding of TCF / LCF co-transcription factors. Direct β-Catenin binding to TCF7 / LEF1 at Runx2 promotor sites or indirect DNA binding of SMADs and TCF7L2 via protein-protein enhances Runx2 expression (176). Furthermore FHL2, from the LIM protein superfamily interacts with β-Catenin, increasing its nuclear translocation and increased TCF/LEF binding, resulting in increased Runx2 expression (179). Conversely non-canonical Wnt activation through the PI3K-Atk pathway allows Runx2 to complex with LEF1, interacting with Runx2 and repressing Runx2 induced osteocalcin activation (102) (Fig. 1.10).

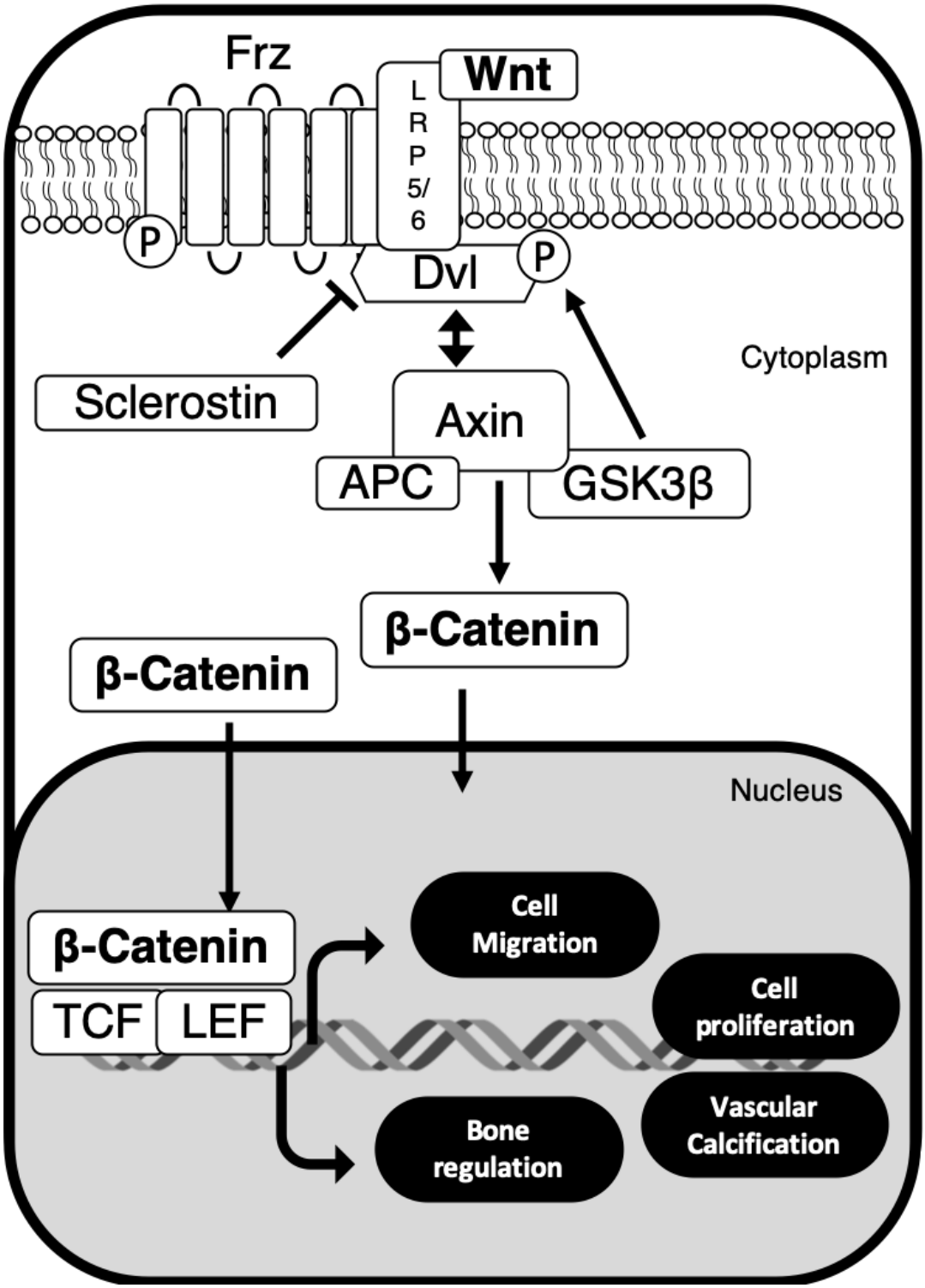

Fig. 1.10. Canonical Wnt Pathway. Activation of the Frizzled receptors (Frz) and LRP5/6 co-receptor via a Wnt ligand leads to the GSK3β which phosphorylates the receptors. Subsequent recruitment of the Dishevelled (Dvl) protein to the membrane allows its polymerisation and further recruitment of Axin and APC, releasing β-catenin from its inactive state. β-Catenin then accumulates within the cytoplasm before translocating into the nucleus. There, β-Catenin forms an active complex with LEF and TEF transcription factors, leading to a production of a range of proteins resulting to a change in multiple cellular processes.

1.15. Models of vascular calcification

A range of both *in vivo* and *in vitro* models have been developed to study the development of vascular calcification. *In vivo* CKD rodent models such as glomerular injury and nephrectomy models developed severe and rapid widespread calcification, with high levels of serum calcium and creatinine and are useful models for severe calcification (57, 228). Isolated vitamin D is widely used *in vivo* to study calcification, with potentially toxic amounts used, resulting in acute hypercalcemia and phosphoremia within a short frame time. Chronic and long-term vitamin D exposure results in metastatic calcification with a reduction in renal function. Additionally, vitamin D exposure results in a loss of arterial wall elastin and collagen fibres, causing arterial stiffness and a decrease in vascular compliance (180, 181). Transgenic mice have also been a useful source of VC models, with many current models obese, either through genetic manipulation or feeding of a western diet. Monogenic obesity models; such as defective leptin signalling; either deficient in leptin or the receptor, causes hyperphagia, hyperinsulinemia, hyperglycaemia and subsequent obesity (182). Additionally, a range of atherosclerotic mice models have been produced, predominately through mutations in LDL receptor (LDLR) and Apolipoprotein E (APOE) genes; leading to hyperlipidaemic disorders. Both ApoE $^{(-/-)}$ and Ldlr $^{(-/-)}$ mice show elevated plasma cholesterol levels and develop diet-dependent calcification in under 14 weeks (183), (184). Whilst mice models are useful in the understanding of the overall disease, there are some distinct differences between the development of human and mouse calcification. In humans, calcification often develops in the coronary arteries, something not observed in mice models, with mice exhibiting extremely high levels of blood lipids and a different metabolism pathway, which contribute to a faster and more aggressive plaque development than found in humans (185). Additionally, mice models do not manifest an unstable atherosclerotic plaque with overlying thrombosis; the lesion most associated with clinical cardiovascular events, and are lacking vasa vasorum surrounding the vessel which are key for the migration of inflammatory cells within a human vessel (186, 187).

In vitro models have been established as an alternative to murine models, utilising human vSMCs grown in culture to deposit a mineralised matrix. vSMCs grown in the presence of 5 mM β-Glycerophosphate (βGP) and 2.6 mM calcium chloride will

induce vSMC mineralisation (87). Deposition of the calcification matrix and osteogenic differentiation has been demonstrated to corelate with a loss of vSMC markers such as ACTA1 and ACTA2 and an upregulation of osteogenic markers such as ALP, Runx2, OCN, indicating the hyperphosphatemia and hypercalcemia environment induces mineralisation (90). Within this study, a model utilising both 5 mM βGP and 2.6 mM calcium chloride will be used in both physiologically relevant high (25 mM) glucose conditions; reflective to that of a type II diabetic in hyperglycaemic emergency and within low (5 mM) glucose conditions which is considered a healthy fasting level (188), with the relevant markers used to confirm the trans-differentiation of the vSMCs. Whilst both conditions are expected to induce calcification relative to the control without the addition of osteogenic conditions, this study will determine the effect of osteogenic conditions of VC alone, compared to a hyperglycaemic osteogenic model.

1.16. Sirtuins

1.16.1. Molecular structure and localisation of SIRT1

Sirtuins are NAD+ dependent deacetylases from a large family of deacetylases, which deacetylate a range of histone and protein targets. Highly conserved from bacteria, silent information regulator 2 (Sir2) was first identified through *Saccharomyces cervisiae* used to silence mating type information locus *HM* (189). So far, seven isoforms in humans have been identified, via their intracellular distribution and various roles within cellular processes; such as apoptosis, senescence, glucose homeostasis and aging (190) (Table 1.3). SIRT1, the most well studied Sirtuin is known to have a range of calcification related targets, and therefore will be the focus of this thesis.

The SIRT1 gene is located at chromosome 10q21.3 and contains 11 exons. There are two isoforms of SIRT1 as a result of alternative splicing. SIRT1FL is the canonical SIRT1, composed of 747 amino acids with a predicated weight of 80kDa, however it is normally observed at 120kDa, most likely attributed to a result of posttranslational modifications (191). SIRT1FL is constitutively expressed and demonstrates robust deacetylase activity compared to isoform 2; Δexon 8 which is composed of 561 amino acids and stress inducible. Δexon 8 isoform however exhibits increased RNA/protein stability and protein-protein interactions and is able

to regulate p53 in an auto-regulatory loop, whilst p53 also influences SIRT1 splicing (192).

SIRT1 contains four domains, an NAD+ binding domain (catalytic domain), zinc binding domain, helical module and a c-terminal regulatory segment (CTR). The CTR site is located upon the outside of the SIRT1 molecule next to the catalytic domain and is composed of 25-residues. Divided into two parts, the larger N-terminal region forms a hairpin that complements the central parallel β-sheet within the NAD+ binding domain. The smaller of the two halves; the C-terminal extension, forms contacts with the helical module whilst in closed formation and engages the extended tail region of the catalytic domain during open formation, allowing for a 25° rotation, disrupting all interactions between the subdomains and allowing the exposure of the hydrophobic tunnel in which the substrate may enter. The active site is located between the zinc binding domain and the helical module, where upon substrate and NAD+ binding the site undergoes a conformational change, forming a hydrophobic tunnel. During substrate and NAD+ binding the peptide binds within the border between the NAD+ binding domain, the Zn^{2+} module and the helical module, following which the hydrophobic acetylated lysine substrate residue can reach the active site through the hydrophobic tunnel and deacetylation will occur (193).

SIRT1 was originally suggested to be a nuclear protein, believed to have been involved in embryogenesis and differentiation, however under different environmental cues and tissue type, it can dynamically shuttle between the nucleus and the cytoplasm (194). Within *in vivo* and *in vitro* studies, the localisation of SIRT1 has differed, with some cells expressing SIRT1 in the cytoplasm alone or within both the nucleus and the cytoplasm (195, 196). Subcellular localisation of SIRT1 is regulated via two evolutionally conserved nuclear localisation sequences and nuclear export signals within its amino acid sequence, suggested to be dependent on the PI3K signal cascade (197), however the exact mechanism for this remains unclear.

Sirtuins				
Gene name	Cellular location	Function	Enzymatic activity	Chromosomal location
SIRT1	Nucleus and Cytoplasm	Glucose metabolism, fatty acid & cholesterol metabolism, insulin secretion and neuroprotection	Deacetylase	10q21.3
SIRT2	Cytoplasm	Cell cycle control, tubulin deacetylation	Deacetylase	19q13.3
SIRT3	Mitochondria	ATP production, regulation of mitochondrial protein deacetylation, fatty acid oxidation	Deacetylase	11p15.5
SIRT4	Mitochondria	Insulin secretion	ADP-ribosyl transferase	12q
SIRT5	Mitochondria	Urea cycle	Deacetylase	6p23
SIRT6	Nucleus	Telomeres and telomeric functions, DNA repair	Deacetylase and ADP-ribosyl transferase	19p13.1
SIRT7	Nucleus	RNA polymerase I transcription	Deacetylase	17q25

Table 1.3. **List of SIRTs within the Sirtuin family and their role and location.** Adapted from McGuinness, et al 2011.

1.16.2. SIRT1 Activity

Reduction of NAD+ to NADH is known for its role in energy homeostasis and metabolism, with SIRT1 requiring NAD+ as a cofactor to deacetylate a range of targets. Within diabetes, the balance between NADH and NAD is severely perturbed (198), with NADH overproduced due to the increased influx of glucose into the glycolytic and Krebs cycle pathways due to hyperglycaemia and the activation of the polyol pathway as previously discussed. This impairment of the NAD balance results in changes within the enzymatic activity of SIRT1 during the deacetylation reaction, in which the glyosidic bond between 2'-O-acetyl-adenosine disphosphoribose (OAADPr) in NAD and nicotinamide being cleaved, releasing the molecules into the environment (199). However, with the lack of NAD present, there is little to no release of nicotinamide into the environment, thus the negative feedback loop is not activated which would reduce SIRT1s activation, so SIRT1 is still present, however unable to deacetylate its targets.

Moreover, as no cleavage occurs in a diabetic environment, the OAADPr which would act as an independent agent to reduce endogenous ROS and diverts glucose preventing oxidative damage is not produced, therefore increasing damage within the cell and perpetuating an oxidative environment. Recent studies also suggest a role for OAADPr in gene silencing, by facilitating the assembly and loading of SIRTs into nucleosomes (200, 201).

SIRT1 has a variety of targets within the nucleus, mainly concerned with the regulation of cell survival and metabolism; p53, Ku70, p300, stress response control; FOXO, NF-kB, PPARy, ROS scavenging and apoptosis (202). Moreover, SIRT1 has been linked to multiple cell and developmental mechanism, through both gene modulation expression via histone deacetylation at targeted loci and deacetylation of non-histone proteins involved in protein differentiation. During embryogenesis, global histone acetylation dynamics have been observed, however these are predominantly linked to HDAC1, however knockdown of HDAC1 in mice does not result in a change to global transcription rate (203, 204), suggesting the role may be shared by other histone deacetylases; such as SIRT1. Within embryonic stem cells derived from the blastocyst, levels of histone acetylation appear to be higher than lineage restricted stem cells, and thus histone deacetylation plays an

important role in tissue specific gene silencing; demonstrated by the SIRT1$^{(-/-)}$ knockout mutation leading to be embryonic lethal or showing severe developmental defects in mice (205, 206).

1.16.3. Regulation of SIRT1

Regulation of SIRT1 via calorific restriction (CR) has been suggested to increase lifespan and act as a tumour suppressor in both animal models and humans (207) and is often the first line of treatment for a pre-diabetic patient (208). During CR, cells increase resistance to oxidative stress and undergo metabolic reprogramming to an oxidative metabolism; to increase energy intake from food consumed, however the exact mechanism of regulation remains a source of debate (209, 210). The initial hypothesis suggests that the metabolic shift increases intracellular NAD+ levels and decreases NADH; an inhibitor of SIRT1 deacetylase activity, thus giving SIRT1 more substrate and therefore an increase in activity (211). However, this hypothesis suggests that in cells unable to undergo a shift to oxidative metabolism there should be no benefit in CR, yet in yeast deficient of undergoing oxidative respiration CR still increased lifespan, suggesting there may be an alternative mechanism.

An alternative hypothesis was proposed that CR increases SIRT1 activity via the decrease of intracellular nicotinamide; a product of the SIRT1 deacetylation reaction which inhibits its activity. It is suggested that CR increases Nampt expression; a nicotinamidase enzyme which catalyses the initial reaction of NAD+ from nicotinamide; known as the nicotinamide salvage pathway, thus maintaining NAD+ levels and therefore allowing greater SIRT1 activity (212, 213). Consistent with this second hypothesis, the effects of CR are inhibited in yeast devoid of PNC1; a Nampt homolog were significantly blunted, suggesting there indeed may be a role for CR in SIRT1 regulation (214) (Fig. 1.11).

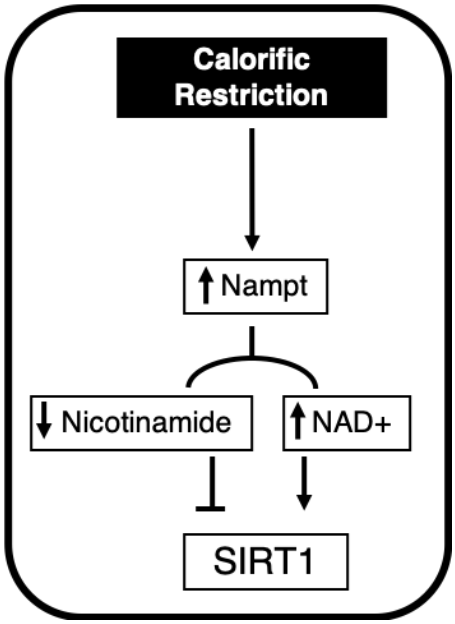

Fig. 1.11. Role of Calorific Restriction on SIRT1 expression. When Calorific Restriction is activated, an increase in nicotinamide phosphoribosyltransferase (Nampt) leads to a shift in NAD+ production; the substrate SIRT1 is dependent on, and a decrease in Nicotinamide, a known SIRT1 inhibitor.

Furthermore, the interplay between SIRT1 and PARP1 has been shown to regulate SIRT1 activation as both require NAD+ as a substrate. PARP1 is a nuclear protein involved in DNA repair and chromatin remodelling and has similar mechanisms to SIRT1 through the sharing of cofactor NAD, demonstrating a duel role in cell survival and ATP depletion, with PARP1 activation directly inhibiting SIRT1 through competitive inhibition (215, 216). SIRT1 inhibition through PARP1 activation and subsequent NAD+ depletion has been demonstrated to increase H_2O_2 induced cell senescence. With SIRT1 deacetylation inhibiting activation of PARP1 and its ability to utilise NAD+, this suggests a negative feedback loop exists between SIRT1 and PARP1 in regulating cell function (217).

Additionally, under DNA damage and cellular stress SIRT1 is positively regulated by the cell cycle and apoptosis regulator E2F1. E2F1 binds to the SIRT1 promotor via a consensus site at -65bp and induces transcription, however upregulation of SIRT1 then inhibits E2F1 via deacetylation, inhibiting cell cycle progression until DNA damage is repaired. As PARP1 binds E2F1 and co-activates the re-entry of quiescent cells into S phase, it suggests the regulation of SIRT1 is key to cell cycle progression following DNA damage and stress (218).

SIRT1 is also regulated via p53, with research suggesting that SIRT1 inhibition leads to the stabilisation of p53 due to its hyperacetylation, whereas the upregulation of SIRT1 deacetylates p53 at Lys 382 resulting in its inhibition. Once p53 is stable,

it binds to -158bp and -182bp within the SIRT1 promotor, negatively regulating its transcription (Fig. 1.12). Interestingly in p53 deficient mice SIRT1 levels did not increase, suggesting further regulation by alternative pathways may also regulate SIRT1 expression (219).

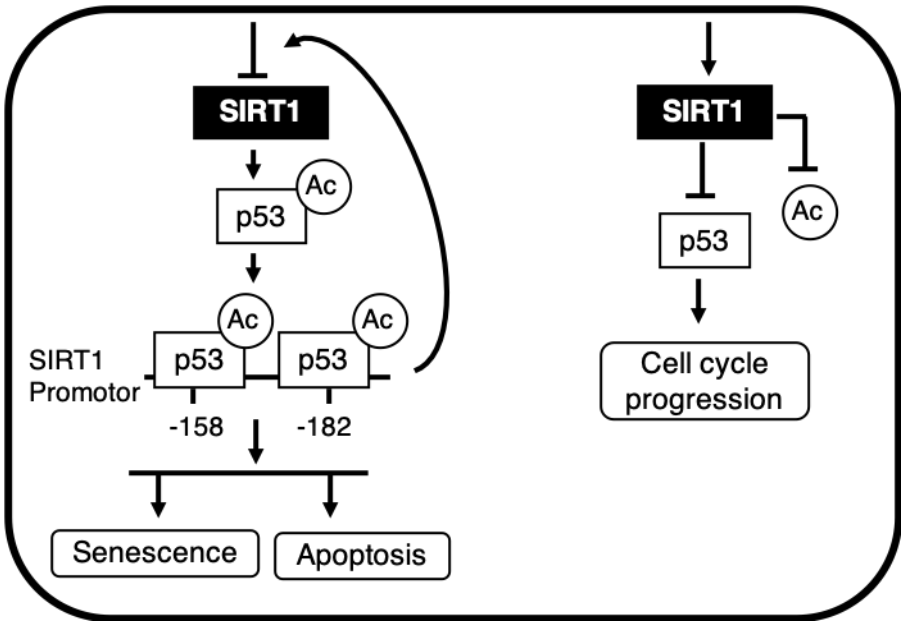

Fig. 1.12. Regulation of SIRT1 through p53 activation. Reduction of SIRT1 leads to hyperacetylation of p53. p53 then binds to the SIRT1 promotor region, inhibiting SIRT1 production and increasing cellular senescence and apoptosis in diseases such as diabetes. When SIRT1 is present, it inhibits acetylation of p53, resulting in a p53 molecule which is unstable and quickly degraded, allowing for cell cycle progression.

1.16.4. Post-translational modifications

Alongside regulation via transcription factors, SIRT1 can also be regulated via a range of post-translational modifications (Fig. 1.13). Firstly, phosphorylation is the most common biological approach to protein regulation involving the covalent addition of a phosphate group to a serine, threonine, tyrosine or histidine residue by a kinase. So far 15 sites of phosphorylation have been suggested for SIRT1, both in the C-terminus and N-terminus however it is likely many more exist (220). JNK1 phosphorylates SIRT1 at Ser27 and 47 and Thr 530 during cellular stress and increases protection from oxidative stress within the cardiovascular system, which appear to decrease the deacetylase activity of SIRT1 towards histone H3, however exhibits no effect on p53 (221), suggesting phosphorylation may alter SIRT1 in a substrate specific manner. Additionally, Casein Kinase II (CK2) phosphorylates Ser 659 and 661 within human SIRT1, increasing substrate affinity and thus total activity of SIRT1 towards acetylated p53 and p65, the latter reducing NF-kB activation when deacetylated, contributing to increased cellular survival (222, 223). Furthermore, CDK1 complex phosphorylates SIRT1 at Thr 530 and Ser 540. Whilst the repercussions of this phosphorylation are not fully understood, mutation of these residues disrupts cell cycle progression and slows proliferation, suggesting the phosphorylation impacts downstream targets of SIRT1 as well (220). Finally, cyclin AMP/Protein Kinase A (cAMP/PKA) phosphorylates SIRT1 within the highly conserved core of the protein at Ser 434 (224). This phosphorylation rapidly increases intrinsic deacetylase activity of SIRT1 independent of NAD+ levels, increasing stimulation of fatty acid oxidation and energy expenditure in response to cellular stress and other stimuli.

Besides phosphorylation, methylation of SIRT1 at lysine and arginine residues has also been shown to regulate the biological activity of SIRT1. SIRT1 is methylated at Lys 233, 235, 236 and 238 via lysine methyltransferase SET domain containing 7 (Setd7 or Set7/9). Whilst the exact effect of methylation remains unclear, the interaction between Setd7 and SIRT1 prevents SIRT1 binding to p53, suggesting that methylation reduces SIRT1 ability to bind to protein substrates (225).

SUMOylation; the reversible addition of small ubiquitin like modifiers (-12kDa) to lysine residues has also been demonstrated to modify SIRT1 activity. SIRT1 is

SUMOylated at Lys 734, inhibiting its deacetylase activity towards p53 and possibly other targets. The deSUMOylation enzyme Sentrin-specific protease (SENP) removes SUMOylation from SIRT1 and has been shown to increase stress induced apoptosis, whereas SUMOylated SIRT1 increases cellular resistance to apoptosis (226).

Nitrosylation; the covalent incorporation of a NO moiety into thiol groups via S-nitrosylated glyceraldehyde-3-phosphate dehydrogenase (SNO-GAPDH) is suggested to nitrosylate SIRT1 at Cys 387 and 390. As both these residues are located within the catalytic core of SIRT1, SIRT1 nitrosylation reduces the deacetylase activity of SIRT1, increasing acetylation of PGC1a, which in turn reduces mitochondrial biogenesis an activity, such as in times of calorie restriction or cellular starvation (227).

Finally, ubiquitylation; the binding of a ubiquitin protein molecule which present in all eukaryotic cells and associated with protein degradation can control SIRT1 expression. Once a protein is covalently bound to one ubiquitin molecule (mono-ubiquitylated) multiple ubiquitin molecules are subsequently added to create a large ubiquitin chain which is then rapidly degraded along with the protein via the proteasome. Following phosphorylation at Ser 47 SIRT1 activity is briefly increased before it is rapidly poly-ubiquitylated and degraded. Interestingly, within obese patients, SIRT1 expression is reduced and persistent activation of JNK1 is increased, suggesting a possible mechanism for SIRT1 reduction in vascular calcification associated with obesity (228-230).

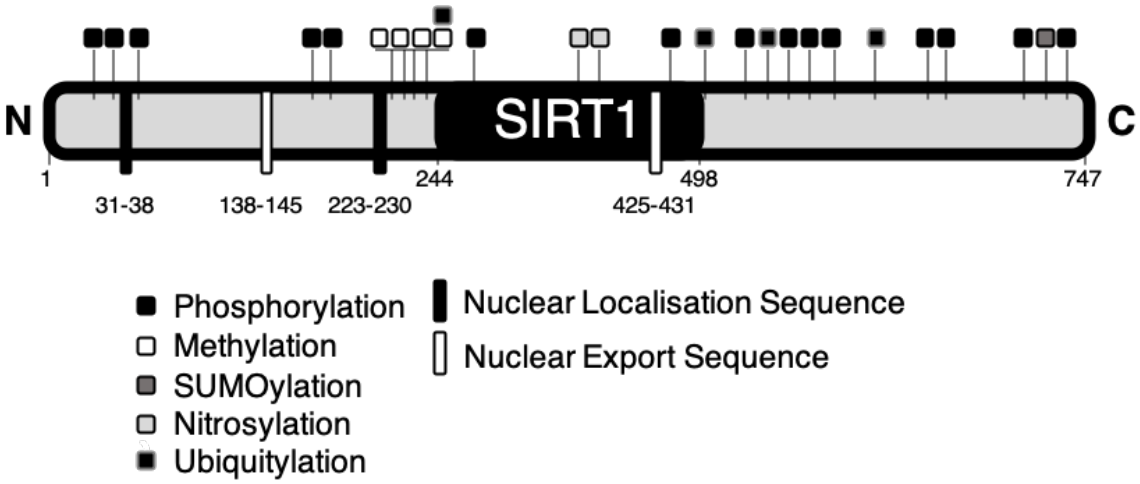

Fig. 1.13. Known post-translational modifications of SIRT1. Adapted from PhosphoSitePlus biological database. search term 'SIRT1'. Table shown on next page.

Post Translational Modifications of SIRT1		
Target site	Modification	Change in activity
Ser14	Phos	No known effect
Ser26	Phos	No known effect
Ser27	Phos	Reduces deacetylase activity. Intracellular localisation
Ser47	Phos	Reduces deacetylase activity. Intracellular localisation
Ser172	Phos	Inhibits nuclear localisation. Reduces deacetylase activity
Ser173	Phos	Inhibits nuclear localisation. Reduces deacetylase activity
Lys233	Me	Reduces ability to bind substrates
Lys235	Me	No known effect
Lys236	Me	No known effect
Lys238	Me / Ub	No known effect / Degradation
Tyr280	Phos	Regulates protein association. Inhibits transcription
Tyr301	Phos	Regulates protein association. Inhibits transcription
Lys314	Ub	Degradation
Cys387	NO	Reduces deacetylase activity
Cys390	NO	Reduces deacetylase activity
Ser434	Phos	Increases deacetylase activity independent of NAD+
Lys499	Ub	Degradation
Thr530	Phos	Reduces deacetylase activity. Intracellular localization. Regulates protein association.
Ser540	Phos	Increases acetylation. Increases enzymatic activity
Lys601	Ub	Degradation
Ser659	Phos	Increases substrate affinity. Essential for SIRT1 activity
Ser661	Phos	Increases substrate affinity. Essential for SIRT1 activity
Ser682	Phos	Intracellular localisation
Lys734	Sumo	Reduces deacetylase activity
Ser747	Phos	No known effect

1.16.5. Effects of SIRT1 in the cardiovascular system and in disease

SIRT1 has been demonstrated to have a function in a variety of vascular and cardiac cells suggesting it has a key role in cardiovascular pathologies, through a range of molecular pathways (Fig. 1.14). SIRT1 is highly expressed in endothelial cells, maintaining normal endothelial function and angiogenic potential (231). Under pathological conditions SIRT1 shuttles between the nucleus and the cytoplasm modulating signalling within the oxidative stress protection pathway. Specifically, SIRT1 prevents H_2O_2 induced senescence in ECs via deacetylation of p53 and inhibits the induction of functional abnormalities (232, 233).

Additionally, SIRT1 has been demonstrated to protect against hyperglycaemic induced endothelial dysfunction through the downregulation of P66Shc expression and eNOS regulation (234). SIRT1 mRNA and protein levels progressively decline during endothelial senescence, which is associated with CVD risk factors, with overexpression of SIRT1 increasing the deacetylation of stress responsive serine/threonine kinase BI, again preventing endothelial senescence. SIRT1 has also been shown to stimulate NO production through deacetylation at Lys 496 and 506 of eNOS in endothelial cells (232, 233), increasing the prevention of endothelial dysfunction. Since NO synthesised by the endothelial layer is a gas, it diffuses across the endothelium in to the adjacent vSMCs (235, 236), maintaining GTP controlled muscle tension, homeostasis (237) and ultimately inhibiting atherosclerotic lesion formation. Additionally, SIRT1 activation has been shown to blunt oxLDL induced apoptosis within the endothelium in $ApoE^{(-/-)}$ mice, whilst also reducing aortic plaque development in those fed a western diet (238).

Within macrophages, SIRT1 downregulation was concurrent with the production of foam cells (239), with activation of SIRT1 via SRT1720 blocking the formation of foam cells *in vitro*. SIRT1 deacetylates RelA/p65 and suppresses the expression of Lox-1, a scavenger receptor for oxLDL, and thereby prevents the intake of LDL and the subsequent foam cell formation (240). SIRT1 has been shown to contribute to a mechanism regulating monocyte adhesion to endothelial cells via miR-34a; a known repressor of SIRT1 which is critically involved in endothelial inflammation and downregulated via shear stress (241). Moreover, treatment with resveratrol has been shown to reduce ICAM-1, VCAM-1 and monocyte chemoattract protein-1

(MCP-1) through a SIRT1 dependent mechanism, suggesting an interesting effect of SIRT1 activation on the inflammatory pathways associated with T2DM (242).

Coronary heart disease, often resulting from a high fat diet and the elevation of fatty acid and lipoprotein lipase products (243) may be attenuated via the activation of endothelial SIRT1 (195, 244, 245). The dysregulation of the endothelium provides the foundation of plaque development via platelet activation and vessel thrombosis, whereas the hypertrophy of vSMCs results in the deposition of the calcified matrix in which the foam cells can adhere. The application of resveratrol leads to a reduction of ERK activation, resulting in a decrease in oxidative stress induced proliferation, often considered to be the first step in plaque formation (246).

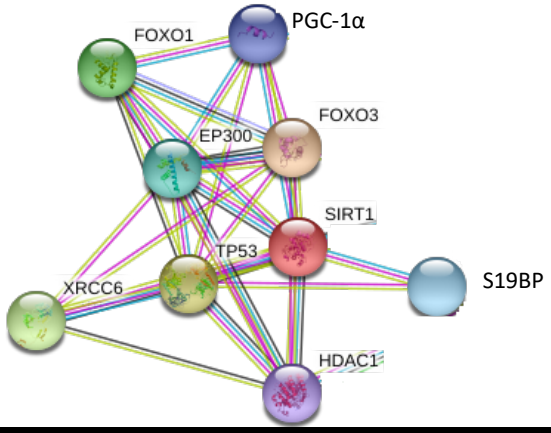

Major SIRT1 Regulation Genes	
Gene	**Function**
EP300	Histone acetyltransferase. Regulates transcription via chromatin remodelling.
PGC-1α	Transcriptional coactivator for steroid receptors and nuclear receptors. Regulates key mitochondrial genes.
TP53	Tumour suppressor, inducing growth arrest or apoptosis depending on the physiological circumstances and post-translational modifications.
S19BP	Active regulator of SIRT1. Enhances SIRT1-mediated deacetylation of p53.
FOXO3	Forkhead box protein 3. Transcriptional activator triggers apoptosis in the absence of survival factors.
Ku70	X-ray repair cross complementing protein. Single stranded DNA-dependent ATP-dependent helicase.
HDAC1	Histone deacetylase 1. Has roles in epigenetic repression in transcriptional regulation, cell cycle progression and developmental events.
FOXO1	Forkhead box protein 1. Transcriptional factor that targets insulin signalling and regulates metabolic homeostasis in response to oxidative stress.

Figure 1.14. Table of major SIRT1 regulated genes. Adapted from STRING biological database. search term ‘SIRT1’.

1.16.6. Role of SIRT1 in diabetes

With the role of SIRT1 well described within the context of cardiovascular disease, the impact of its activation on vascular calcification specifically will be the focus of this thesis. Administration of Resveratrol, a natural SIRT1 activator has been demonstrated to reduce arterial calcification both in non-human primates and in uremic rats, suggesting SIRT1 may be a good candidate for sustained control of VC. (247, 248) In hyperphosphatemia induced calcification, SIRT1 activation was shown to inhibit the development of matrix mineralisation *in vitro* via the reduction of senescence associated calcification, through the blunting of a phosphate cotransporter NPC (249). However, whilst this model mimics part of the diabetic environment through elevated phosphate, no increase in calcium and glucose was used, raising the question of SIRT1s ability to exhibit control of mineralisation within a complete diabetic model.

1.16.7. Small molecule activators of SIRT1

Since Sirtuins have been suggested to mediate a range of pathologies associated with both cardiovascular disease and cancer, there has been considerable interest in producing drugs to target their mechanisms. Competitive inhibitors such as nicotinamide, or more potent Sirtuin inhibitors such as Sirtinol, Splitomycin and Suramin have shown promise in some cancer models (250), via a decrease in the *in vivo* and *in vitro* binding of the substrate with the catalytic domain, reversing the first catalytic step of SIRT1 activation.

A range of natural and synthetic SIRT1 activating compounds (STACs) have been developed predominantly through high-throughput screening using recombinant SIRT1. Most activators identified were polyphenolic with a structure activity relationship characterised by planar multi-phenyl rings bearing hydroxyl groups (251). Resveratrol; probably the most well-known activator enhances SIRT1 deacetylation activity 8-fold and has since been documented to be present in a wide range of victuals, such as red wine, dark chocolate and berries (252). Since natural STACs proved the concept and benefit of SIRT1 activation, a range of second generation STACs (SRT1720, SRT1460, SRT2183) were produced with greater bioavailability, solubility and potency. These STACs are derivatives of

imidazothiazole scaffolds and chemically distinct form resveratrol, with a much lower EC_{50} required to elicit a response (253).

Mechanistically, STACs increase the activity of SIRT1 via one of two suggested models. Firstly, allosteric activation of SIRT1 through the lowering of the K_m; and thus an increase affinity to its substrate, or secondly through an indirect activation resulting from off-target effects (251, 253-255). Whilst the first model has been more widely accepted, the interaction between SIRT1 and STACs may be either direct between the compound and the SIRT1 bound substrate, or as a result of assisted allosteric activation, in which the STAC binds to a substrate induced exosite on SIRT1, which stabilises the substrate binding and subsequent deacetylation (256). However, whilst the precise mechanism of action remains elusive, STACs have been increasingly trialled in a range of models pertaining to cancer, cardiovascular, inflammation, neurodegeneration and metabolism and the outcomes will be eagerly observed by many (Fig. 1.15).

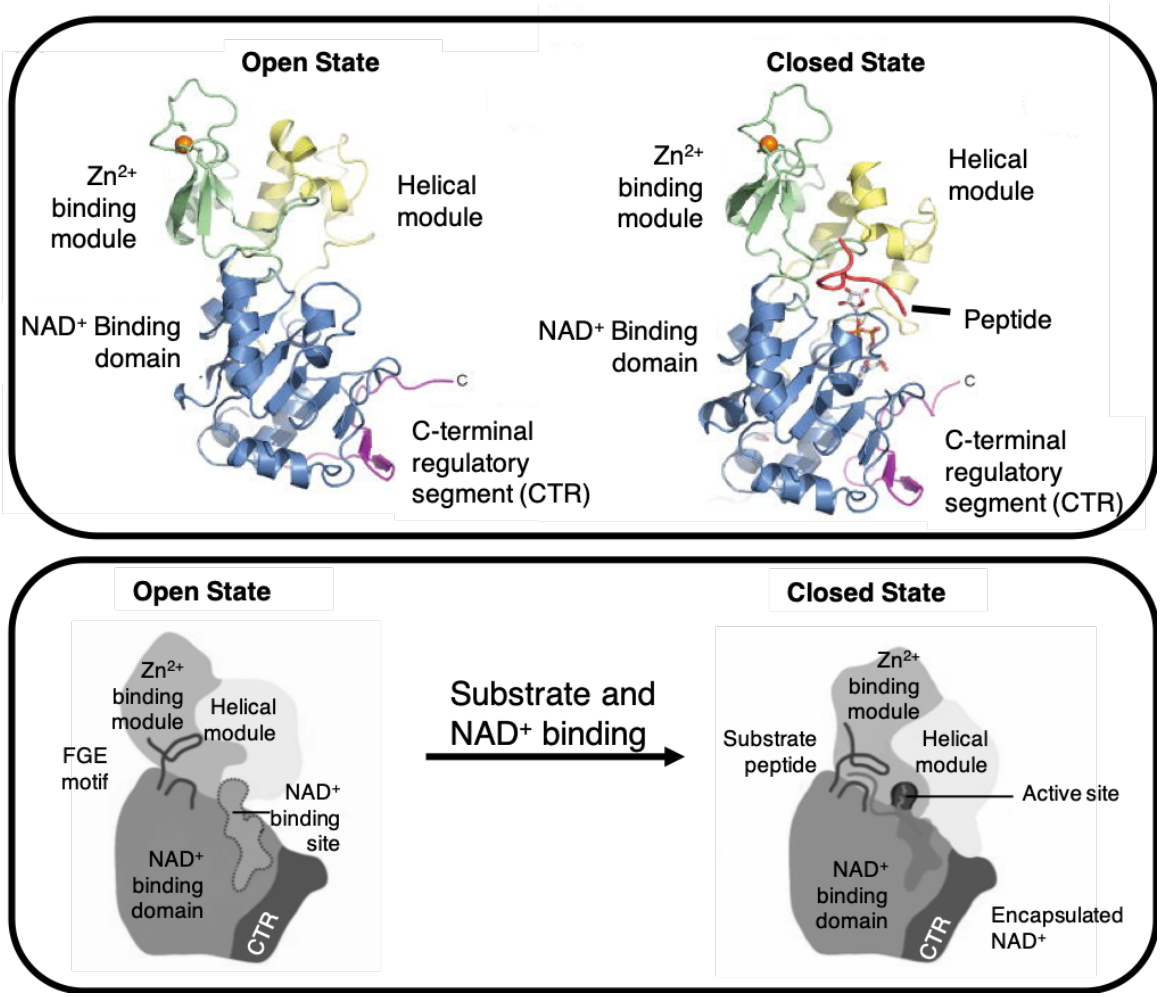

Fig. 1.15. Structure of SIRT1 in both open and closed states. When inactivated SIRT1 presents as an open state with an NAD+ binding domain on the outside. Following substrate and NAD+ binding the Zn2+ binding motif rotates and closes around the substrate, deacetylating it within the active site. Adapted from Davenport *et al.* 2014

1.16.8. Clinical outcomes of SIRT1 activators

Since SIRT1 has been demonstrated to play a role in a wide range of human pathologies, over 24 clinical trials have been conducted to evaluate the safety and efficacy of SIRT1 activation (Table 1.4). Preliminary phase 2 clinical trials have been conducted by GSK for the tolerance of SRT2104 (NCT00937326), a second generation SIRT1 activator. Up to 2 grams of SRT2104 per day were well tolerated, with no significant primary or secondary negative outcomes up to 28 days treatment with a 58 day follow up. No significant improvement in glucose or insulin control was observed, likely to be due to the observed pharmacokinetics which were not dose dependent on the participant (257). Interestingly, a follow on trial looking at the effects of SRT2104 on arterial stiffness in type II diabetic patients and smokers (NCT01031108) found that 2g/day reduced augmentation pressure and may improve measures of arterial stiffness, however a larger sample size was recommended to increase statistical relevance (258, 259).

In addition to SRT2104, SRT2379; another small molecule SIRT1 specific activator was trialled for the reduction of endotoxin induced inflammation (NCT01416376). 1000 mg of SRT2379 was administered 4 hours before IV LPS (4 ng/kg) and demonstrated a dose-dependent reduction in IL-17, IL-6 and Tumour necrosis factor alpha (TNFα) when compared with placebo. Moreover, a significant reduction in both glucose response and increased vascular endothelium activation was found, which may suggest a possible role within vascular disease or glucose homeostasis. A Phase 1 clinical trial (NCT01018628) aimed to evaluate the effect of SRT2379 on plasma fibroblast growth factor 21 (FGF21) a biomarker for T2DM. SRT2379 dose-dependently reduced FGF21 expression and reduced C-reactive protein expression, possibly suggesting future clinical use as part of a T2DM treatment.

SIRT1 Modulators		
Drug name	Activator / Inhibitor	Clinical Trial
Resveratrol	Activator	NCT01150955, NCT03384329, NCT01668836, NCT03819517, NCT00654667, NCT02549924, NCT02433925, NCT02123121, NCT01938521
SRT1720	Activator	No
SRT1460	Activator	No
SRT3025	Activator	NCT01340911
SRT2183	Activator	No
SRT2104	Activator	NCT01014117, NCT01031108, NCT01018017, NCT00938275, NCT00937326, NCT00933530, NCT00933062
SRT2379	Activator	NCT01018628, NCT01262911, NCT01416376
STAC5	Activator	No
STAC9	Activator	No
STAC10	Activator	No
Nicotinamide	Inhibitor	NCT02961829, NCT02558595
Sirtinol	Inhibitor	No
Splitomicin	Inhibitor	No
Suramin	Inhibitor	No
EX-527	Inhibitor	No
MC2141	Inhibitor	No

Table 1.4. List of SIRT1 activating and inhibiting compounds. Adapted from clinicaltrials.gov NIH national library of Medicine, search term 'SIRT1'.

1.17. Aims

Vascular calcification is now recognised as a clinically important component of cardiovascular disease (260) and further insight into the mechanisms which control its development may result in novel strategies to better manage and control it. The overarching aim of this study was to examine the role of SIRT1 in vascular calcification and diabetes and investigate the effects of hyperglycaemia on the development of calcification. The aim was achieved by the following objectives:

1. To determine the effect of hyperglycaemia *in vitro* using two concentrations of glucose. Additionally, the effect of this model on a key osteogenic pathway; Runx2 was also examined.

2. To elucidate the role of SIRT1 within this established tissue culture model calcification process via the use of small molecule activators and inhibitors, and siRNA.

3. To identify the inherent differences in adhesion and cytoskeleton formation between diabetic and non-diabetic vascular smooth muscle cells.

4. To determine the effect of SIRT1 on DNA damage induced calcification, through the MRN DNA repair pathway. With previous studies demonstrating hyperglycaemic conditions induce DNA damage related calcification the effect of SIRT1 on this mechanistic pathway was investigated.

2. Materials and Methods

2.1. Chemicals and Reagents

All chemicals were analytical grade and purchased from Sigma, unless stated otherwise. All glassware, plasticware, media and reagents were either supplied sterile or, where necessary, were sterilised by autoclaving at 121°C for 15 minutes, or via filtering using a 0.22 μm filter (Millipore). All cell culture medium, serum and supplements were acquired from Lonza, unless otherwise stated. Cell culture consumables were supplied by Nunc. Thermo Fisher. Specific chemicals and reagents used in individual methods are referred to within the descriptions. Details of all primary, secondary and conjugated antibodies are provided within the appendix, as are all primers used within this thesis.

2.2. Tissue culture

2.2.1. Primary smooth muscle cells

Commercially available primary human coronary artery vascular smooth muscle cells (CA vSMCs) were used for the majority of these experiments, with diabetic mellitus patient popliteal artery vascular smooth muscle cells (DM vSMCs) extracted for validation of a different vascular bed. CA vSMCs were acquired from Caltag at passage 3 and used up to passage 9. Primary popliteal artery vSMCs were harvested from diabetic patients undergoing amputation, as described below, under ethics approval number REC Ref: 14/MW/1062; IRAS Project ID 142332 and cultured for a maximum of 6 passages.

2.2.2. Extraction of primary diabetic vascular smooth muscle cells

Human samples were received and immediately processed to release SMCs from the arterial sample (87). The sample was washed in smooth muscle cell media (PromoCell, UK) and the outer layers of tissue removed to expose the vessel wall. The vessel was then sliced open longitudinally and the endothelial layer was removed, and the remaining tissue was washed again. The tissue was sliced finely into 1-2 mm sections and placed internal side down into 6-well plates and 0.5 mL of culture medium as described below was added to each well containing the tissue biopsy and incubated overnight at 37°C as to not move or rotate the sections. After 24 hours, the media was topped up (1 - 1.5 mL) and incubated until cells appeared to proliferate outward from the tissue.

2.2.3. Human vascular smooth muscle cell maintenance and passage

vSMCs were cultured in smooth muscle cell basal medium 2 (PromoCell, UK) supplemented with Foetal Calf Serum (FCS) (0.5 mg/mL), hFGF (2 ng/mL), hEGF (0.5 ng/mL) and insulin (2.5 μg/mL). Cells were grown until 80% confluent in T75 flasks with the media changed every three days, and then passaged 1:2 via trypsinisation. Cells were washed once with PBS, and trypsin EDTA was added and returned to the incubator for 2 minutes. The flask was then lightly tapped until the cells were dislodged and viewed as mobile under a light microscope. Trypsin was subsequently neutralised with culture medium and the cell suspension was transferred to Falcon tubes and centrifuged at 300*g* for 5 minutes. The supernatant

was removed, and the cells were resuspended in an appropriate volume before being seeded at a density of 10 x 10^5 cells/cm^2 into the appropriate number of culture flasks.

2.2.4. Induction of calcification

Mineralisation of vSMCs was induced using an osteogenic media. vSMCs were seeded into 6 well plates at 80% confluence at a density of 1 x 10^6 per well and the media changed from smooth muscle cell basal medium 2 (5.5mM glucose) (PromoCell, UK) to low (5 mM) or high (25 mM) Glucose DMEM accordingly, supplemented with 10% FBS, 5% Penicillin-Streptomycin, 5% L-Glutamine, to reflect a normal or diabetic milieu respectively. Both low and high glucose DMEM possess the same osmolarity as each other. Cells were left for 24 hours to adhere after which the media was switched to osteogenic media containing 5 mM β-glycerophosphate (BGP) and 2.6 mM $CaCl_2$ for 21 days or until mineralisation was apparent (87). Negative controls used only low glucose DMEM without $CaCl_2$ and BGP.

2.2.5. siRNA Transfection

Cells were plated in 6-well plates at 1 x 10^6 per well and left to adhere overnight. Media was changed to serum and antibiotic-free media for 2 hours before siRNA was added. 1.5 μg of siRNA was dissolved in TE buffer; [10 mM Tris-HCl, 1 mM EDTA pH 8 in dH_20] with 100 μL of serum and antibiotic-free media and mixed. 10 μL of PolyFect (Qiagen) was then added and mixed via vortex and left for 10 minutes at room temperature to allow complex formation. Media was subsequently aspirated from the plate and 100 μL of siRNA solution was added to each well drop-wise, along with 600 μL of serum and antibiotic-free media. Plates were gently swirled for uniform distribution of the complexes and incubated for 6 hours. Media was then replaced with either low or high DMEM complete media and cells harvested to check for gene expression for up to seven days.

2.3. Histology

2.3.1. Sample preparation

Human popliteal arteries were obtained from diabetic patients in the Manchester Royal Infirmary during lower limb amputation (Ethics Reference 14/NW/1062). Human internal mammary arterial sections were used from the archived Alexander/Wilkinson repository of human embedded tissues (obtained during coronary artery bypass surgery and surplus to surgical requirements). Vessels obtained from the diabetic patients were washed in PBS and cut into two pieces; the first being processed for embedding to be cut into 7 μm wax sections, while the second part of the vessel retained for smooth muscle cell extraction. Tissues for histology were fixed in 4% paraformaldehyde (PFA) overnight at 4°C. Following this, tissues were washed, and placed into a tissue processor (Shandon), in which they were dehydrated in ascending ethanol concentrations (40%, 50%, 70%, 85%, 100%) followed by two changes in 100% xylene. Tissues were then immersed in liquid paraffin and left to set on a cold plate until solidified. Wax-embedded tissue was then cut into 7 μm sections on a microtome (Lecia) and transferred to super-frost-plus slides and allowed to dry overnight at 37°C before use (90).

2.3.2. Haematoxylin and Eosin staining

Paraffin sections were rehydrated by placing first in xylene for 2 x 3 minutes, followed by decreasing ethanol concentrations (100%, 100%, 90%, 70%, 50%) and washed in distilled water, then PBS. Sections were then stained with Mayer's haematoxylin for 5 minutes and washed under running water for 5 minutes. Sections were then immersed in eosin for 5 minutes and washed in running water for a further 3 minutes (261). The samples were then dehydrated in increasing ethanol concentrations as before and cleared in xylene before mounting with DPX and left to dry overnight. Slides were imaged via the Axio Imager M1 brightfield microscope.

2.3.3. Alizarin red staining

Paraffin sections were rehydrated as before, then stained with 4% Alizarin red solution (pH 4.2) for 5 minutes to detect the extent of calcium mineral deposition (261). The slides were then washed in distilled water to remove excess dye. Sections were dehydrated in acetone for 30 seconds, followed by acetone-xylene

(1:1) solution, followed by xylene for 30 seconds each, then mounted with DPX and left to dry overnight. Slides were imaged via the Axio Imager M1 brightfield microscope (Zeiss).

2.3.4. Von Kossa staining

Von Kossa staining was used to determine phosphate ion presence (262). Paraffin sections were rehydrated as before and rinsed twice in distilled water. Sections were then incubated in 1% aqueous silver nitrate solution in a clear glass copulin jar placed under a 60w lightbulb for 1 hour. Slides were rinsed twice in distilled water and placed in 5% sodium thiosulfate for 5 minutes to remove any unreacted silver. Sections were then rinsed in distilled water and counterstained with nuclear fast red for five minutes. The slides were dehydrated in ascending concentrations of ethanol as before, for 3 minutes each and following 2 x 5 minutes of xylene, coverslips were mounted using DPX and left to dry overnight. Slides were imaged via the Axio Imager M1 brightfield microscope.

2.3.5. Sudan Black B (Lipofuscin Stain)

Sudan black B staining was used as a stain to visualise lipofuscin accumulation as a senescence associated marker, to determine the presence of senescent cells in paraffin fixed sections (263). Paraffin sections were rehydrated as before and rinsed twice in distilled water. Sudan black was dissolved in 70% ethanol and filtered through filer paper and used immediately. Single drops of Sudan black B were placed onto coverslips with the section slides placed flat on top. Staining was observed under a microscope before 5 minutes until stain became apparent. Cells were then washed in 50% ethanol and transferred and washed in distilled water before counter staining with nuclear fast red for five minutes. Slides were then washed again in distilled water, dehydrated as before and coverslips were mounted using DPX and left to dry overnight. Slides were imaged via the Axio Imager M1 brightfield microscope.

2.3.6. Immunohistochemistry

Paraffin sections were rehydrated as before and placed in 95°C citrate buffer (10 mM citric acid, pH 6) and left until cool (264). Slides were then incubated in 3% H_2O_2 in methanol for 5 minutes to block endogenous peroxide activity. Slides were

washed with PBS and incubated with 4% goat serum in PBS for 1 hour, then washed in PBS and incubated in 2% goat serum with the appropriate primary antibody (Table 7.1) for 2 hours at room temperature. Slides were rinsed three times in PBS and then incubated with a secondary HRP-conjugated antibody (Table 7.1) for 1 hour. Slides were then washed and incubated with diaminobenzidine (DAB) (Vector Labs) with nickel for 2-10 minutes, until black stain appeared. The sections were counterstained with nuclear fast red for 5 minutes before washing in distilled water, then dehydrated in ascending concentrations of ethanol then xylene as before and coverslips were mounted using DPX and left to dry overnight. Slides were imaged via the Axio Imager M1 brightfield microscope.

2.3.7. Immunocytochemistry

vSMCs were seeded into 8-well chamber slides at a density of 1 x 10^5 per well (87). Cells were treated for 4 days as previously described, then washed with PBS and fixed with 4% PFA for 10 minutes. Fixed cells were then washed in PBS and incubated for 1 hour in 4% goat serum in PBS. Following this, the cells were incubated with a primary antibody at the appropriate concentration (Table 7.1) in 2% goat serum in PBS for 2 hours. Negative controls were performed by replacing the primary antibody with normal IgG at the same concentration. Cells were then incubated for 1 hour in 2% goat serum in PBS with the appropriate Alexa Fluor secondary antibody (Table 7.1) diluted at 1:1000. Where phalloidin (Fluka) was used, it was added at this stage at 1:5000 dilution in 2% goat serum. After three washes in PBS, cells were mounted with DAPI antifade gold (Vector Labs) and left to dry overnight in the dark at room temperature. Slides were imaged via florescence the Leica SP5 confocal microscope or the Zeiss Axioimager Z1.

2.4. DNA Integrity assays

2.4.1. Comet assay

The comet assay has a specific advantage over other sensitive methods for detecting DNA damage in that it is a single-cell assay and can detect variation in the extent of damage between both cells of the same type and between different types of cells in mixed populations (265). Cells were pre-treated for four days in assay-dependent media before moving to serum-free media supplemented with 200 μM H_2O_2 for 1 hour, or 2 mM H_2O_2 for positive control. Cells were then washed and either harvested immediately or placed back in conditioned media and left to recover for up to 3 hours. Cells were counted via a haemocytometer and were concentrated at 1 x 10^6/mL, diluted 1 in 7 in PBS and 30 μL was mixed with 1 mL of 0.7% low melting agarose. The cell suspension was plated on top of 1% agarose on microscope slides, and a cover slip placed on top, all of which was then placed on ice for 5 minutes. Coverslips were then removed, and slides were placed in Comet lysis buffer [2.5 M NaCl, 100 mM EDTA, 0.3 M NaOH. 5.5% DMSO, 1.1% Triton X-100 pH 10] for 100 minutes at 4°C. Slides were washed in dH_20 for five minutes, before transferring to an opaque electrophoresis tank containing Comet electrophoresis buffer (3M anhydrous sodium acetate, 10M Tris, pH 9) and allowed to equilibrate for twenty minutes. Following this, electrophoresis was carried out at 25V, 300mA for 25 minutes. Slides were then transferred to Comet neutralisation buffer [0.4M Tris Base pH 7.5, diluted to 30% in dH_2O] for 10 minutes, before drying overnight at room temperature. The following day, slides were rehydrated for 30 minutes in dH_20 and dried briefly. SYBR Gold (Thermo Fisher) was then diluted 1:10,000 and added to each gel for 30 minutes before washing in dH_20 for 10 minutes and drying. Slides were imaged on a Zeiss Axio1 fluorescent microscope at x100. Subsequent images were quantified using ImageJ software. Comet assay data was presented as tail percentage of entire comet, head percentage of entire comet and tail moment; an index of induced DNA damage taking into consideration both migration and relative amount of DNA in the tail.

2.4.2. Relative telomere length quantification

Cells were cultured in 6-well plates and RNA isolated via TriZol, as described in section 2.5.1 and reversed transcribed. Quantitative real-time polymerase chain

reaction (qPCR) was used to determine relative telomere length (266). Briefly, qPCR was conducted in 96 well plates. Each reaction contained 20 μL in total, 10 μL of SYBR Green master mix (BioLine), 400 nM of each forward and reverse primers and 6 μL of cDNA (10 ng/μL). All reactions were completed in triplicate, with relevant no cDNA and no primer controls used and cycled on a StepOnePlus cycler (Thermo, UK). Initial denaturation was carried out at 95°C for 10 minutes, followed by 40 cycles of 95°C for 60 seconds, annealing at 58°C for 30 seconds, and extension at 72°C for 30 seconds. Primers were designed to amplify either a single copy gene (Col6a and Col3a) or Telo1; a CG rich segment of the telomere sequence. The relative telomere length was calculated via the ratio of the telomere amplification production to that of a single copy gene, using the $2^{-\Delta\Delta Cq}$ method.

2.4.3. TUNEL assay

The terminal deoxynucleotidyl transferase dUTP nick end labelling (TUNEL) assay assesses DNA damage via labelling the 3'-hydroxyl termini within double stranded breaks. A TUNEL colorimetric kit was purchased from Promega (G7360). Briefly, slides were washed twice in xylene for 5 minutes before being immersed in 100% ethanol for 5 minutes. Slides were then rehydrated in decreasing concentrations of ethanol (100%, 95%, 85%, 70%, 50%) for 3 minutes each. Finally, slides were then washed in 0.85% NaCl for 5 minutes followed by 5 minutes in PBS. Slides were then immersed in 4% PFA for 15 minutes, before washing in PBS. Cells were then permeabilised with 20 μg/mL of proteinase K for 30 minutes at room temperature before washing twice in PBS. Slides were then fixed in 4% PFA again for 5 minutes, before washing with PBS and equilibrating slides with equilibration buffer for 10 minutes. 100 μL of TdT reaction mix was then added and incubated for 60 minutes at 37°C in a humidified chamber. Slides were then washed in 2x SSC for 15 minutes, following 3 washes in PBS. Slides were then blocked in 0.3% H_2O_2 for 5 minutes, before rewashing and adding 100 μL of Streptavidin HRP (1:500) for 30 minutes at room temperature. Slides were then washed in PBS and 100 μL of DAB salutation was added. Slides were all developed for the same time and then washed in deionized water before mounting coverslips using DPX and left to dry overnight. Finally, slides were imaged via the Axio Imager M1 brightfield microscope.

2.5. RNA Assays

2.5.1. RNA Isolation

Cells were grown in relevant media to 80% confluence on 6-well plates for four days before direct lysis with 1 mL TRIzol reagent per well, according to manufacturer's instruction. Cells were then incubated for 15 minutes at room temperature for complete dissociation of nucleoprotein complexes, before all cell lysate was transferred into pre-chilled RNase-free Eppendorf tubes. 200 μL of chloroform per 1 mL of TRIzol was added and vigorously mixed for 30 seconds, before another 10 minute incubation at room temperature. Samples were then centrifuged at 12000*g* for 15 minutes at 4°C until phase separation was observed. Supernatant containing RNA was removed and precipitated from the aqueous phase via mixing an equal volume of chilled isopropanol and vortexing. The sample was then incubated for 10 minutes at room temperature before centrifugation at 12000*g* for 10 minutes at 4°C. The RNA pellet was washed in 1 mL of chilled 75% ethanol and centrifuged at 7500*g* for 5 minutes at 4°C and air-dried for 5-10 minutes. The RNA was resuspended in DEPC-treated water and the concentration of the RNA measured using a spectrophotometer (Nanodrop, UK).

RNA quality was assessed using agarose gel electrophoresis. 1 μg of RNA was loaded on a 1.5% agarose gel prepared with fresh 1X TBE buffer [45 mM Tris Base, 44.5 mM Boric Acid, 1 mM EDTA, pH 8] and electrophoresis was conducted using RNase-free tank and 1 X TBE buffer. If both the 18S and 28S ribosomal RNA bands are observed, it could be concluded that no degradation occurred, and the RNA preparation would be suitable for further PCR analysis. The RNA sample was aliquoted and stored at -80°C in DEPC-treated water for use within a month. For long term usage RNA was stored in ethanol and precipitated for use.

2.5.2. Reverse transcription and cDNA generation

500 ng of total RNA was reverse-transcribed into complementary DNA (cDNA) via a Tetro cDNA synthesis kit (BioLine), all samples were vortexed before use and prepared on ice. 1 μL of random hexamers, 1 μL of 10 mM dNTP mix, 4 μL 2x RT Buffer, 1 μL Ribosafe RNase Inhibitor and 1 μL of tetro reverse transcriptase (200 ug/μL) were mixed with total RNA in a pre-chilled Eppendorf and made up to 20 μL

with DPEC-treated water. Samples were then incubated at 25°C for 10 minutes followed by 45°C for 30 minutes. The reaction was terminated by incubating at 85°C for 5 minutes, then chilled on ice and used immediately or stored at -20°C.

2.5.3. Polymerase chain reaction

PCR experiments were prepared on ice using MyTaq Mix (BioLine). 5 ng of template was added to 2 μL of forward and reverse primers (20 μM), 25uL of MyTaq Mix (BioLine), and dH_20 to make the solution up to 50 μL. Samples were vortexed and subjected to an initial denaturisation step of 1 minute at 95°C, followed by 30 cycles of: denaturation for 15 seconds at 95°C, annealing for 15 seconds at 65°C and extension for 10 seconds at 75°C. Followed by a final elongation step of 5 minutes at 75°C. PCR products were subjected to electrophoresis on agarose gel.

2.5.4. Agarose gel electrophoresis

RNA quality was assessed using agarose gel electrophoresis. A 1.5% agarose gel was dissolved with heat in TBE buffer, then 1.5 μL of Midori Green (Fisher) was added for DNA visualisation, and the mixture swirled to ensure an even mix. 1 μg of RNA was loaded using Blue Loading Dye (BioLine) and a 1kb HyperLadder (BioLine) was used to identify the size of the DNA bands. All samples were loaded, and electrophoresis was conducted at 100V until loading dye front had reached the end of the gel, using an RNase-free tank and TBE buffer.

2.5.5. Quantitative polymerase chain reaction

qPCR was conducted in 96 well plates. Each reaction contained a final volume of 10 μL in total, 5 μL of SYBR Green master mix (BioLine), 400 nM of each forward and reverse primer, and 3 μL cDNA (50 ng/μL). A no cDNA template and no primer control were used, with DPEC-treated water replacing the relevant component. The qPCR was cycled on a StepOnePlus thermocycler (Thermo, UK). Initial denaturation was carried out at 95°C for 5 minutes, followed by 40 cycles of 95°C for 30 seconds, 58°C for 30 seconds and 72°C for 30 seconds, each sample was used to generate technical triplicates with each experiment being performed a minimum of four times to generate biological repeats. Primers were designed to span an exon in order to avoid amplifying genomic DNA. Relative expression of the analysed genes was compared to housekeeping genes GAPDH and ß-Actin and

calculated via the $2^{-\Delta\Delta Ct}$ method. Primer efficiency was confirmed via serial dilution of both the cDNA and the primers, at a range of Tm's from 60-65°C. Data was then plotted on a standard curve, and the amplification efficiency over 90% was used in further experiments. All primers used had efficiency checked and was determined to be between 90-95%.

2.6. Protein analysis

2.6.1. Protein isolation

Total protein was extracted from cells cultured in 6-well plates. Media was removed and cells were washed once with PBS. 30 μL of cold lysis buffer [1.5 μL of 50 mM Tris pH 8.0, 0.9 μL 150 mM NaCl, 0.3 μL 1% Triton X-100, 0.03 μL 1 M DTT, 0.3 μL 1X Protease inhibitor Cocktail, 0.3 μL 1X Phosphatase inhibitor Cocktail and 26.67 μL DPEC-Treated water]; was added to each well and a cell scraper was used to remove all cells and transfer to a pre-chilled Eppendorf tube. Cell suspensions were incubated for 20 minutes on ice and vortexed every 2 minutes to increase lysis efficiency, then centrifuged at 14,000*g* at 4°C for 5 minutes. Supernatant containing protein was then collected in a pre-chilled Eppendorf tube and the debris within the pellet discarded. The supernatant was used immediately for downstream application or stored at - 80°C for further analysis.

2.6.2. Nuclear fractionation

Total protein was extracted from cells cultured in 6 well plates and a nuclear extraction kit (ab113474) was used to fractionate the protein. Media was removed and cells washed once with PBS. Cells were then detached with Trypsin, centrifuged at 300*g* for 5 minutes and counted. 2.5 x 10^6 cells were then resuspended in 200 μL of 1x pre-extraction buffer (completed with DTT and phosphatase inhibitor) and incubated on ice for 10 minutes before vortexing and centrifuging for at 12,000*g* at 4°C for 1 minute. Cytoplasmic extract contained within the supernatant was removed and used immediately for downstream application or stored at - 80°C for further analysis. 20 μL of extraction buffer was then added to the remaining pellet and incubated on ice for 15 minutes and vortexed every three minutes. Samples were then centrifuged at 14,000*g* at 4°C for 10 minutes. The supernatant was then collected in a pre-chilled Eppendorf tube and the pellet discarded. The supernatant was used immediately for downstream application or stored at -80°C for further analysis.

2.6.3. Protein determination

Protein concentration was determined using a bicinchoninic acid (BCA) assay kit (Pierce, Thermofisher). Standards were made from bovine serum albumin (2 mg/mL

to 0.2 mg/mL) diluted in lysis buffer. 10 μL of all samples (diluted where required) and standards were added to individual wells on a 96 well plate and run in triplicate. 190 μL of master mix [50 parts buffer A to 1 part buffer B] was added to both samples and standards, mixing well. The plate was incubated at 37°C for 30 minutes before being read at 562nm on a Synergy HTX Multi-mode plate reader (BioTek).

2.6.4. Sodium Dodecyl Sulphate / Polyacrylamide Gel Electrophoresis (SDS/PAGE)

Proteins were separated on a 10% resolving mini gel [10% (v/v) 50% Acrylaminde/BIS (29:1).] Resolving gel [(10% (v/v) Acrylamide/Bisacrylaminde (37:1), 0.373 M Tris-HCl pH 8.8, 0.1 % (w/v) 1% SDS, 2.5%(w/v) Ammonium persulphate, 0.025M (v/v) TEMED] made up to 15 mL final volume with dH_2O. 10% SDS polyacrylamide resolving gel was poured into a preassembled cassette (Invitrogen), overlaid with water and allowed to set. A 4% stacking gel was prepared; [4% (v/v) 50% acrylamide/BIS (29:1), 0.125M Tris-HCl pH 6.8, 1% SDS, 0.075% ammonium persulphate, 0.15 (v/v) TEMED]. The water was removed from the resolving gel and the stacking gel poured, the comb promptly inserted to form wells and the gel was allowed to set. 20 μg of protein sample was mixed with 3x LDS Loading buffer (Invtrogen) containing 1:4 1M DTT and denatured for 5 minutes at 100°C, before being chilled on ice and loaded onto the gel alongside 10 μL of pre-stained protein ladder (Cleaver Scientific). The gel was electrophoresed at 200V for 45 minutes, until the loading dye reached the bottom.

2.6.5. Western blotting

Proteins were separated on a 4-12% Bis-Tris Gel (Invitrogen) or 10% self-cast gels, using X Cell surelock Mini-Cell kit (Invitrogen) and transferred onto an Amersham Hybond-P PVDF membrane (GE Healthcare) using a X Cell II Blot module (Invitrogen), equilibrated in NuPage transfer buffer (Invitrogen). The gel was sandwiched between sponges, absorbent filter papers and PVDF membrane and transferred using 35V for 90 minutes.

Non-specific binding sites were blocked by incubating the membrane in 10 mL of blocking buffer (PBS Tween (0.1%) containing 5% (w/v) non-fat powdered milk) for 1 hour at room temperature on a rocker. Primary antibodies (Table 7.1) were diluted

according to manufacturer's instructions and incubated overnight at 4°C on rocker. Following this, the membrane was washed three times in PBS with 0.2% Tween (PBST) for 10 minutes each, then incubated in HRP-conjugated secondary antibody diluted in blocking buffer as per manufacturer's instructions for 1 hour. The blot was washed as before, and immunoreactivity was detected using ECL reagent (Pierce) and visualised immediately via chemiluminescence on a ChemiDoc, (BioRad). The membrane was stripped between each staining of primary antibodies, using Restore western blot stripping buffer (ThermoFisher) for 10 minutes at room temperature, and washed in PBST. α-Tubulin (Table 7.1) was used as a loading control for all blots.

2.6.6. ELISA

A SIRT1 ELISA SimpleStep kit (AbCam) was used to determine SIRT1 serum concentration (87). All materials were equilibrated to room temperature prior to use. A standard curve was produced using reconstituted human SIRT1 protein within a 40-0 ng/mL range just before use. 50 μL of both standards and serum samples (diluted 1:2 in dilution buffer) were added to microplate strips in duplicate, alongside 50 μL of the antibody cocktail solution. The plate was then incubated for 1 hour at room temperature shaking at 400 rpm. Each well was washed three times with wash buffer PT before adding 100 μL of TMB substrate to each well and incubating for 10 minutes at room temperature in the dark shaking at 400 rpm. 100 μL of stop solution was added to each well and shaken for 1 minute to mix. Endpoint readings were then taken at 450nm on a Synergy HTX Multi-mode plate reader.

2.7. Migration and Adhesion assays

2.7.1. Modified Boyden chamber assay

Cells were seeded at 80% confluence and treated for four days as previously described (267). A modified Boyden chamber was set up utilising 8μm pore sizes, with serum-free media completed with 20 ng/mL of Platelet Derived Growth Factor (PDGF) BB used as a chemoattractant. The top chamber was filled with serum-free media as before, containing no PDGF. In drug-treated wells, the drug was added equally to both the top and the bottom chamber. The cells were counted and seeded into the top of the chamber at 1 x 10^5 cells per well and incubated for 6 hours. The media was then removed, and cells were fixed with 4% PFA for 10 minutes before staining with DAPI in PBS and counted using the Lecia live cell imager AF6000.

2.7.2. Adhesion assay

Cells were seeded at 80% confluence in a 24-well plate and treated for four days as previously described (268). The cells were then counted and seeded at 1 x 10^5 cells per well and incubated for either 45 minutes or 3 hours. Cells were then washed three times with PBS to remove non-adhered cells before fixing with 4% PFA for 10 minutes. Cells were finally stained with nuclear fast red and imaged on the Zeiss Primovert microscope.

2.8. Survival assays

2.8.1. Cellular viability (Alamar blue)

Cells were harvested from confluent wells on 6-well plates at day 14 and day 21 after calcification induction, washed, resuspended and seeded at 1 x 10^5 cells in triplicate in a 96 well plate with 200uL of media. Alamar blue (Invitrogen) was then added at a 1:10 dilution and incubated at 37°C for 6 hours. Absorbance was read at 570nm and 600nm on a Synergy HTX Multi-mode reader. Percentage reduction in viability was calculated via the equation below and presented as percentage normalised to control. Alamar blue assay confirms redox potential of the cell, used as a substitute for cellular viability and proliferative activity.

$$\text{Percentage difference between treated and control cells} = \frac{(O2 \times A1) - (O1 \times A2)}{(O2 \times P1) - O1 \times P2)} \times 100$$

O1 = Molar extinction coefficient E of oxidised Alamar Blue at 570 nm
O2 = E of oxidised Alamar Blue at 600 nm
A1 = Absorbance of test wells at 570 nm
A2 = Absorbance of test wells at 600 nm
P1 = Absorbance of positive control wells at 570 nm
P2 = Absorbance of positive control wells at 600 nm

2.8.2. Cellular cytotoxicity

A CytoTox-Fluor cytotoxicity assay was purchased from Promega, UK. Cells were cultured in 6-well plates for 7, 14 and 21 days after calcification induction, harvested, counted and plated at 4 x 10^4 seeding density, in triplicate in 96 wells with 100 μL of media. An equal volume of complete CytoTox-Fluor cytotoxicity assay reagent was added, mixed via orbital shaking and incubated at 37°C for 30 minutes. Fluorescence was measured at 485nmEx/530Em on a Synergy HTX Multi-mode reader.

2.8.3. β-galactosidase senescence associated assay

To determine senescence associated β-galactosidase presence (87), cells were firstly cultured in 24 wells plates for four days in relevant culture medium. Cells were washed in PBS and fixed in 4% PFA for 15 minutes, before washing in 0.1 M phosphate buffer (pH 7.3) supplemented with 2 mM $MgCl_2$ twice for 5 minutes. Subsequently cells were stained with 1 mg/mL x-gal (Invitrogen) for 2 hours, before aspirating the stain and rewashing in the same buffer as before, and finally imaged on a Zeiss Primovert microscope with positive blue cells quantified using imageJ.

2.9. Calcification assays

2.9.1. Alkaline phosphatase assay

To determine the alkaline phosphatase activity during calcification of vSMCs, a colorimetric assay was performed. vSMCs were seeded at 0.5 x 10^6 in 6-well plates, cultured in relevant media and harvested at day 4 and day 7. Prior to harvesting, cells were washed once in PBS and then solubilised with 0.2 mL of pre-chilled 0.05% Trixon X-100 in PBS per well, freeze-thawed twice, scraped and sonicated for 30 seconds. Lysates were then centrifuged at 500*g* for 10 minutes at room temperature to discard cellular debris.

Protein concentrations were determined with a BCA assay. 20 μg of total protein was made up to 20 μL using 0.05% Triton X-100 in PBS and 180 μL of para-nitrophenyl phosphate (pNPP) (Thermo, UK) was added to each sample. A standard curve of p-nitrophenol (Thermo, UK) was prepared ranging between 1 mM and 1 M in Triton X-100 up to 20 μL, in 0.2 M increments, with 180 μL of pNPP added to each well, a blank was also prepared with 20 μL of Triton X-100. Both samples and standards were run in triplicate in a 96 well plate and incubated at 37°C for half an hour, until a colour change from clear to yellow was evident within the standard range.

The enzymatic reaction was subsequently stopped in all wells by the addition of 50 μL of 3 M NaOH. Samples were then read at 405nm using Synergy HTX Multi-mode plate reader. If ALP was present/active within the lysate the colourless pNPP substrate was converted into yellow p-nitrophenol, with the colour change being directly proportional to the amount of active ALP present in the lysate. ALP activity was calculated via the standard curve as nM p-nitrophenol converted/μg protein for each cell lysate sample (106).

2.9.2. Quantification of calcium deposition

A colorimetric calcium detection kit was purchased from AbCam (ab102505). Cells were harvested from confluent wells on 6-well plates at day 14 and day 21 (2 x 10^6 cells) and washed with PBS before being resuspended in 500 μL (or 4x the sample volume) of PBS with 0.1% NP-40 and incubated on ice. Cells were homogenised via a sonicator and centrifuged for 5 minutes at 4°C at top speed to remove insoluble

material. The supernatant was then transferred to fresh tubes and 50 μL of each sample was plated in triplicate with 90 μL of chromogenic reagent and 60 μL of calcium assay buffer in each well. Both samples and standards were mixed well and incubated for 10 minutes in the dark before being read at 575nm on a Synergy HTX Multi-mode reader.

2.9.3. Alizarin red staining and elution

Mineralisation was detected in culture via Alizarin red staining. Briefly, cells were washed three times in PBS before fixing with 4% PFA for 10 minutes. Fixed cells were then washed with PBS a further three times before incubating with 4% Alizarin red in distilled water on a rocker for 10 minutes. Excess stain was removed via washing with distilled water until the water ran clear. Stained cells were left to dry before imaging via the Zeiss Primovert microscope.

Alizarin red staining was eluted in order to quantify the level of mineralisation. Alizarin red stained cells were incubated with 600 μL 10% (v/v) Formic acid in distilled water for 15 minutes on a shaker. 200 μL of the resulting liquid was transferred into each well of a 96 well plate and absorbance was read at 405 nm on the Synergy HTX Multi-mode reader, with formic acid alone used as a negative control. Results were normalised to the control sample and presented as fold difference between the test sample and control.

2.10. Griess assay

The Griess assay was used to reflect the bioavailability of nitric oxide (NO_2) within the tissue culture medium. Briefly, the Griess assay measures nitrite concentration after conversion of nitrate to nitrite with nitrate reductase. It is based on a two-step diazotization reaction in which acidified NO_2- produces a nitrosating agent, which reacts with sulphanilamide to produce a diazonium ion. This ion is then coupled to N-1-napthylethylenediamine dihydrochloride to form the chromophore azo-derivative which absorbs light at 540nm (269).

Firstly, a preparation of the nitrate standard reference curve was produced between 100 μM and 0 μM, and 50 μL placed into a 96 well plate in duplicate, alongside all experimental samples. Once equilibrated to room temperature, 50 μL of the sulphanilamide solution was added to each well, followed by a 10 minute incubation in the dark. 50 μL of NED solute ion was then added to all wells, followed by another 10 minute incubation in the dark, absorbance was then read immediately at 540 nm on the Synergy HTX Multi-mode reader and presented as nitrite concentration (μM).

2.11. Chromatin Immunoprecipitation

A SimpleChIP kit #9003 (Cell Signalling) was used to perform chromatin immunoprecipitation (270). Cells were cultured until confluent in relevant media and harvested at day 4. Each immunoprecipitation required two T75 flasks per treatment. Cells were crosslinked in 20 mL culture medium with a final formaldehyde concentration of 1% for 10 minutes at room temperature. 2 mL of 10X glycine was added to each flask and mixed briefly then incubated for 5 minutes at room temperature. Cells were then washed twice with ice-cold PBS before adding 2 mL of ice cold PBS supplemented with 0.5% v/v 200X PIC. Cells were scraped and transferred to 15 mL tubes and centrifuged at 2000*g* for 5 minutes at 4°C. Supernatant was discarded and the pellet was resuspended in 1 mL of 1X Buffer A with DTT and PIC and incubated for 10 minutes on ice and mixed by inverting every 3 minutes. The nuclei suspension was then centrifuged for 2000*g* for 5 minutes at 4°C and the supernatant discarded. The pellet was resuspended in 1X Buffer B with DTT with repeated centrifugation, and the pellet subsequently resuspended in 100 μL of 1X Buffer B with DTT per prep. The sample was transferred to a 1.5 mL Eppendorf tube, with 0.5 μL Micrococcal nuclease added, mixed and incubated for 20 minutes at 37°C to digest DNA to 150-900bp fragments. The digest was stopped by adding 10 μL of 0.5 M EDTA and the tube placed on ice for 2 minutes. Nuclei were then pelleted by centrifuging at 16,000*g* for 1 minute at 4°C. The supernatant was removed, and pellet resuspended in 100 μL of 1X Chip Buffer + PIC and incubated on ice for 10 minutes. Lysates were then pulse-sonicated 5 times and incubated on ice and centrifuged at 9400*g* for 10 minutes at 4°C.

50 μL of chromatin was taken to validate chromatin digestion and concentration. 40 μL was mixed with 100 μL nuclease free water, 6 μL 5 M NaCl and 2 μL RNAase and incubated for 30 minutes at 37°C. Subsequently 2 μL of Proteinase K was added and mixed before incubation for 2 hours at 65°C. DNA was isolated via spin column extraction, washed in DNA wash buffer and purified in DNA elution buffer. 10 μL of purified DNA was taken and electrophoresed on a 1% agarose gel as previously described, alongside a 100bp Hyperladder (BioLine). DNA was identified as being between 150-900 bp long. DNA concentration was determined using a nanodrop spectrophotometer.

10 μg of digested cross-linked chromatin was used per immunoprecipitation. 400 μL of 1X ChIP Buffer and 2 μL of 200X PIC was added to chromatin and placed on ice. A ChIP grade antibody was then added to each sample at the appropriate concentration, before incubation overnight at 4°C whilst rotating. 30 μL of Protein G Magnetic Beads were then added to each IP and incubated for 2 hours at 4°C with rotation. Each sample was then placed on a magnetic separation rack until the solution was clear. The pelleted protein G magnetic beads were then washed with 1 mL of wash buffer three times before repeating the magnetic separation rack stage again. 150 μL of ChIP elution was then added to each IP and eluted for 30 minutes at 65°C on a thermomixer. Samples were then placed on a magnetic separation rack again and the supernatant transferred to a new tube. 7 μL 5 M NaCl and 2 μL proteinase K was added and incubated for 2 hours at 65°C. 750 μL of DNA Binding Buffer was then added to each sample and mixed before being transferred to a DNA spin column and centrifuged at 18500*g* for 30 seconds, where the collected liquid was discarded. The procedure was repeated twice more. 50 μL of DNA Elution buffer was added, and the centrifugation step repeated. The eluent contained purified DNA.

DNA was then to quantified for further use in qPCR. Primers were designed around conserved regions of known H3K27Ac marks near to each genes regulatory elements. 2 μL of DNA sample was added to each well containing 2 μL of 5 μM primers and 6 μL of Nuclease-free water. The samples within the PCR plate were then subjected to the following treatment: Initial denaturation 95°C for 3 minutes, followed by 40 cycles of denaturation at 95°C for 15 seconds and annealing and extension at 60°C for 60 seconds. Results were then analysed using the $2^{-\Delta\Delta Ct}$ method.

2.12. Cell cycle analysis

Flow cytometry was used to determine cell cycle, as well as nucleus size and area (271). Cells were grown in 6-well plates and harvested at day four of treatment. Media was removed from cells, washed twice, trypsinised and pelleted at 4°C. The pellet was resuspended in 500 μL of PBS and the cell count adjusted to 1 x 10^6 cells/mL. Subsequently 3 mL of ice cold 75% ethanol was added drop-wise to 500 μL of cell suspension whilst mixing. Cell suspension was then mixed again via a 20-gauge syringe and incubated overnight at -20°C. The following day, cells were centrifuged at 500*g* for 10 minutes at 4°C, to aspirate ethanol, and washed with PBS, mixed and then centrifuged as before. The pellet was resuspended in 250 μL of PBS and 12.5 μL of propidium Iodide (1 mg/mL) was added alongside 10 μL of RNase A (20 mg/mL) and mixed, before incubation in the dark for 30 minutes at 37°C. Samples were then centrifuged as before, removing staining solution, and resuspended in PBS within flow cytometry tubes. Flow cytometry was performed on a BD FACS Calibur (BD Biosystems) and analysed via FlowJo (FlowJo Inc).

2.13. Statistics

The statistical significance of all experimental data was determined via GraphPad Prism 6 Software (GraphPad, USA). The normality of all data was firstly determined via a Quantile-Quantile (Q-Q) plot, to confirm normal distribution of data, with a histogram plot produced to check for bimodality and a skewed distribution. Furthermore, a Shapiro-Wilk test was conducted on GraphPad to further confirm normality and homoscedasticity. Statistical significance was then determined via an unpaired T-test for normally distributed data sets with two independent groups. One-way analysis of variance (ANOVA) was used to compare the variance of group means within a normally distributed data set containing three or more groups with only one independent variable. Finally, a Two-way ANOVA was used to determine the variance of normally distributed data sets containing three or more groups with two independently defined categorical groups. Post-hoc analysis was conducted on all ANOVA tests using either Bonferroni or Tukey analysis. For data sets without normal distribution an unpaired, non-parametric Mann-Whitney test was used to confirm significance.(*$P<0.05$, **$P<0.005$, ***$P<0.001$).

3. SIRT1 activation reduces the osteogenic differentiation of vascular smooth muscle cells *in vitro* through a senescence and Runx2 dependent pathway

3.1. Introduction

3.1.1. Clinical problem of vascular calcification

Vascular calcification is highly correlated with an increased cardiovascular risk, especially within the diabetic patient (65, 272, 273), and as such there has been great emphasis on studies to determine the molecular process in which ectopic calcification develops. Whilst many imaging studies have been completed (73), the molecular basis remains unclear. With the development of calcification now accepted to be a cell mediated process resembling osteogenesis rather than a passive process as previously believed (274, 275), the key players within the mineralisation process are shown to maintain a fine balancing act between the reduction of inhibitory molecules and the induction of osteogenic differentiation factors, to keep vSMCs in line with the rest of the vessel (276, 277). Previous studies have shown that hydroxyapatite crystals form the final stage of the calcification process (278, 279), however the composition of these crystals and the factors triggering their development differ widely (280), depending on the disease conditions and the processes which drive the development of calcification.

3.1.2. Vascular calcification induced senescence

Cellular senescence is defined as the irreversible loss of proliferation potential, either due to replicative senescence; where the cells cease to divide as a result of telomere uncapping (266), or as part of the senescence associated secretory phenotype and has been linked to the deposition of a mineralised matrix within soft tissues (281, 282). vSMCs undergo senescence, in part, due to the differentiation to a senescence associated secretory phenotype, which can be triggered by activation of the tumour suppressor gene p53 and the cyclin-dependent kinase inhibitors that operate in conjunction with this pathway (89). Whilst senescence accumulates over the lifespan of all healthy humans, senescent cells are found

primarily in renewable or inflamed tissues, such as cells within the vascular system (283). In addition to permanent senescence, cells often acquire a range of morphological and functional changes, including a flatter and hypertrophic morphology (284), increasing expression of β-galactosidase and proinflammatory cytokines, as such as IL-6 and IL-8 (88), which can cause increased inflammation, perpetuating the cycle of senescence and inflammation. Whilst vSMCs within the vessel wall may exhibit increased migratory and proliferative capacity when first damaged (268), cells within the plaque which are constantly exposed to inflammation and damage gain this senescent phenotype (285), in which p21, p16 and β-galactosidase increase in expression and co-localise in the same vicinity inducing irreversible G1 cell cycle arrest (167). The links between senescence and vascular calcification have been developed from the osteogenic gene expression profile of SMCs undergoing a senescent change in phenotype.

3.1.3. Runx2 pathway in the process of cellular calcification

One of the proteins often linked with senescence is Runx2 (286, 287), which is also an osteogenic transcription factor that acts as a marker of vascular calcification (288, 289). In addition, within calcified vessels, proteomic analysis has confirmed an upregulation of a range of bone related transcription factors, which in addition to Runx2, include Msx2, Sox9, and Ostrix (290), all of which upregulate expression of both bone and chondrocytic proteins (291), and which are normally supressed within the contractile smooth muscle cell. With pro-osteogenic factors, such as BMPs (292) and inflammatory mediators such as TNFα (293) increased within the vessel wall prior to calcification (294), they bind to receptors on the cell surface, inducing a cascade of pro-osteogenic protein activation.

One such cell surface receptor; Pit-1 has been reported to increase activation following hyperglycaemia, leading to an influx of calcium and sodium into the cell (295), which forms the basis of the established *in vitro* model of calcification which is used today. Inhibition of sodium through the Pit-1 cotransporter has shown to inhibit osteogenic transcription factor Runx2 (296) and downstream production of osteocalcin and osteopontin, suggesting that phosphate is a key player within the activation of both Runx2 and matrix mineralisation. Concurrently, the increase in cellular calcium activates multiple signalling pathways, such as the *Wnt* (297),

MAPK (148) and ALP (298) leading to secretion of vesicles containing calcium and phosphate, which once secreted from the cell, bind to the matrix causing widespread tissue mineralisation. Previous studies have demonstrated that Runx2 knockout mice develop defective bone formation and decreased arterial calcification (299, 300) when compared to hyperphosphatemic conditions, suggesting Runx2 is required for vSMCs osteogenic differentiation. One of the pathways which modulate the Runx2 transcription factor in bone is the histone deacetylase, SIRT1 (301). Although SIRT1 has been linked to the development of vascular calcification (302), whether this is executed via Runx2 activation remains to be elucidated and will be part of the focus of this study.

3.1.4. SIRT1 as a regulator of vascular calcification

Sirtuin proteins, which have previously been shown to exert control over a range of metabolic functions, including insulin resistance and glucose sensing (303), have further been found to play a role in inhibiting hyperglycaemic induced calcification in both rat and mouse models (249, 304), via the inhibition of osteoblastic differentiation of the vSMCs, although the mechanism still remains unclear. SIRT1 activation is induced by the increase in NAD+ present within vSMCs, and the shift within the NADH/NAD+ ratio towards NADH observed in hyperglycaemic conditions may decrease SIRT1 expression (211, 305). This reduction in SIRT1 expression may potentially lead to negative effects within the cell and induce vSMC osteogenic differentiation (87).

3.2. Aim and Objectives

The aim of this chapter was ultimately to determine whether a lack of SIRT1 expression within a diabetic environment contributes to hyperglycaemic induced calcification in human smooth muscle cells *in vitro* and establish a mechanism of action. This was achieved via the following objectives:

i) Firstly, to determine if the *in*-vitro osteogenic model could mimic the vSMC phenotypic transition observed in the diabetic patients and by which pathway this model increased the development of calcification within the vSMCs.

ii) Secondly, this study sought to determine the expression level of SIRT1 in osteogenic and hyperglycaemic conditions.

iii) Thirdly, this study aimed to elucidate the role of senescence in vSMC during the development of calcification,

iv) And finally, this study sought to establish if SIRT1 modulation could affect both this development of cellular senescence and the overall development of calcification within the vSMCs.

3.3. Results

3.3.1. Hyperglycaemic conditions reduce SIRT1 expression

First, it was important to establish whether SIRT1 expression was modulated in the *in vitro* diabetic model. Cells were grown in 1) control, 2) osteogenic and 3) hyperglycaemic with osteogenic conditions as described in Chapter 2. Expression of SIRT1 was assessed using western blot analysis and localisation of SIRT1 was assessed by immunocytochemistry. Following 4 days pre-treatment, SIRT1 protein expression significantly decreased by 60% in hyperglycaemic conditions when compared to both control ($p<0.0001$) and osteogenic conditions ($p<0.0255$), with all blots normalised to α-tubulin (Fig. 3.1a). Fluorescent staining showed localisation of SIRT1 within the cytoplasm and the nucleus in the control conditions. There appeared to be a decrease in SIRT1 positive staining following 4 days of osteogenic treatment, with SIRT1 appearing to move from the nucleus to the cytoplasm as well as decreasing in fluorescence within hyperglycaemic conditions (Fig. 3.1b).

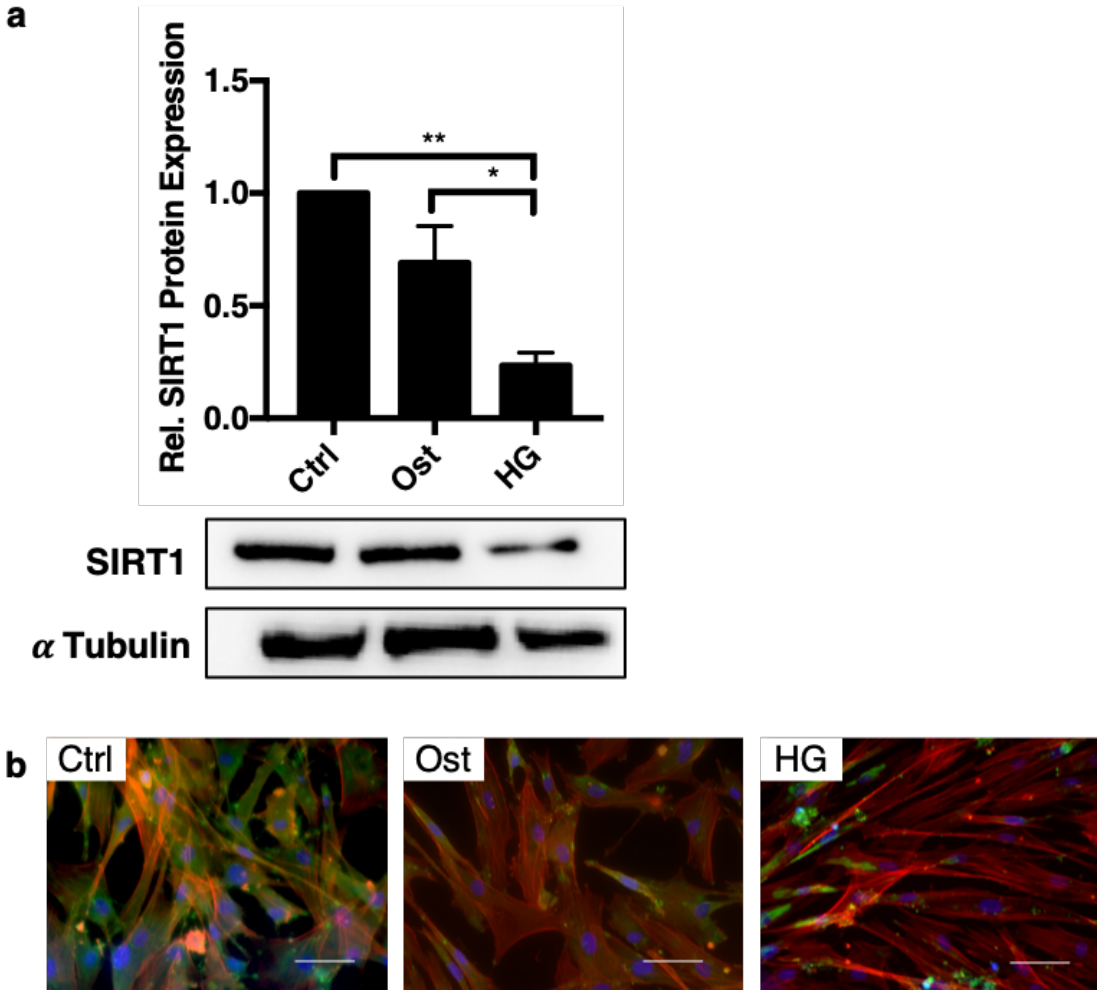

Fig. 3.1. SIRT1 expression decreased under hyperglycaemic conditions. The effect of control (Ctrl), $CaCl_2$ and BGP osteogenic (Ost) and osteogenic with high glucose (HG) conditions on SIRT1 expression following 4 days of treatment was assessed. **a)** 20 μg of protein lysate isolated from vSMCs treated for 4 days with control, osteogenic or hyperglycaemic conditions were examined. SIRT1 protein expression was decreased in hyperglycaemic conditions compared to both control and osteogenic treatments. Blots were re-probed with α-Tubulin shown as loading control (n=6) (One-way ANOVA, Tukey Post-Hoc test). **b**) vSMCs cultured for four days were stained for SIRT1. Phalloidin red, DAPI blue, SIRT1 green. (n=6). *P<0.05, **P<0.005. Scale Bars = 10µm. Mean ±SEM.

3.3.2. Hyperglycaemic conditions induce smooth muscle cell calcification

The next objective was to show whether hyperglycaemic conditions effected the calcification of vSMCs. Cells were treated with control, osteogenic or hyperglycaemic conditions for 21 days, fixed and stained with Alizarin red (Fig. 3.2a) which stains for matrix mineralisation. Alizarin red staining showed some mineralised nodules within the osteogenic conditions, which were lacking in control conditions. There was a clear increase in positive Alizarin red staining which when quantified showed a significant increase in the hyperglycaemic conditions compared to control cells ($p<0.0037$) (Fig. 3.2b). ALP activity was used as an early marker of osteogenic differentiation and as an important component of hard tissue formation and was measured at day 4 and day 7 timepoints. A significant increase in activity was observed at day 4 ($p<0.0107$) and day 7 ($p<0.0238$) in hyperglycaemic conditions compared to control, and a significant increase was also observed in hyperglycaemic conditions compared to osteogenic ($p<0.0238$) (Fig. 3.2c). A final validation of calcification was assessed using total calcium concentration in the three conditions at day 21. Calcium concentration tripled in the hyperglycaemic treatment compared to the control ($p<0.0023$), further supporting the Alizarin red staining (Fig. 3.2d).

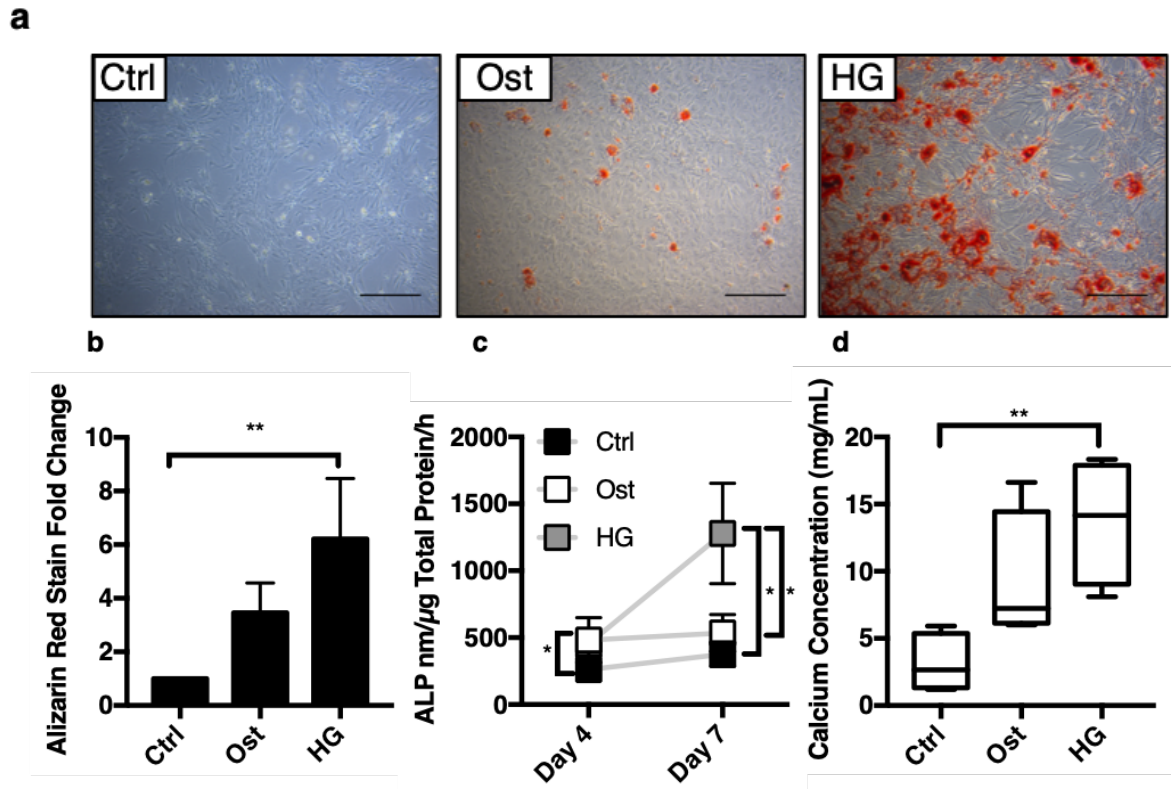

Fig. 3.2. Hyperglycaemic conditions induce smooth muscle cell mineralisation. The effect of control (Ctrl), $CaCl_2$ and BGP osteogenic (Ost) and osteogenic with high glucose (HG) conditions was examined. **a)** Representative micrographs show positive Alizarin red staining in osteogenic conditions at day 21, which is increased in high glucose osteogenic media (n=4 and 5FoV). **b)** Alizarin red staining quantified via elution was significantly increased in hyperglycaemic conditions compared to control (n=4) (One-way ANOVA, Tukey Post-Hoc test). **c)** ALP activity was assessed via the para-nitrophenyl phosphate colorimetric assay. ALP activity doubled by day 4 in hyperglycaemic conditions compared to control and increased by over a two-fold in hyperglycaemic conditions compared to osteogenic conditions by day 7 (n=5) (Two-way ANOVA, Tukey Post-Hoc test). **d)** Calcium concentration assessed via AbCam Kit (ab102505) at day 21 was increased four-fold in hyperglycaemic conditions compared to control treatment (n=5) (One-way ANOVA, Tukey Post-Hoc test). *P<0.05, **P<0.005, ***P<0.001. Scale Bars = 100µm. Mean ±SEM.

3.3.3. Hyperglycaemic conditions induce Runx2 activation

The calcification process was also confirmed on a molecular level, with Runx2, the master osteogenic transcription factor being examined. First, day 4 Runx2 mRNA abundance was measured using qPCR analysis and a significant increase was found in both hyperglycaemic conditions compared to osteogenic ($p<0.0050$) and control ($p<0.0.0002$) conditions (Fig. 3.3a) which also correlated with the change in protein levels. Runx2 protein expression significantly increased in osteogenic conditions compared to control ($p<0.045$) and doubled in hyperglycaemic conditions ($p<0.0232$) (Fig. 3.3b) which was expressed relative to the α-tubulin loading control. It was next of interest to determine if the increase in Runx2 protein levels correlated with its transcriptional activity status. The acetylation profile of the promotor region of the Runx2 gene was examined via ChIP. Since Runx2 acetylation is known to regulate the activation and production of Runx2 protein, the effect of hyperglycaemia on this process was investigated. Primers designed around a known H3K27Ac mark demonstrated an increase in the acetylation of the Runx2 promotor, with hyperglycaemic conditions demonstrating a doubling compared to osteogenic conditions ($p<0.0064$) and a five-fold increase compared to control ($p<0.0002$), when normalised to a 2% input and IgG pull-down control (Fig. 3.3c).

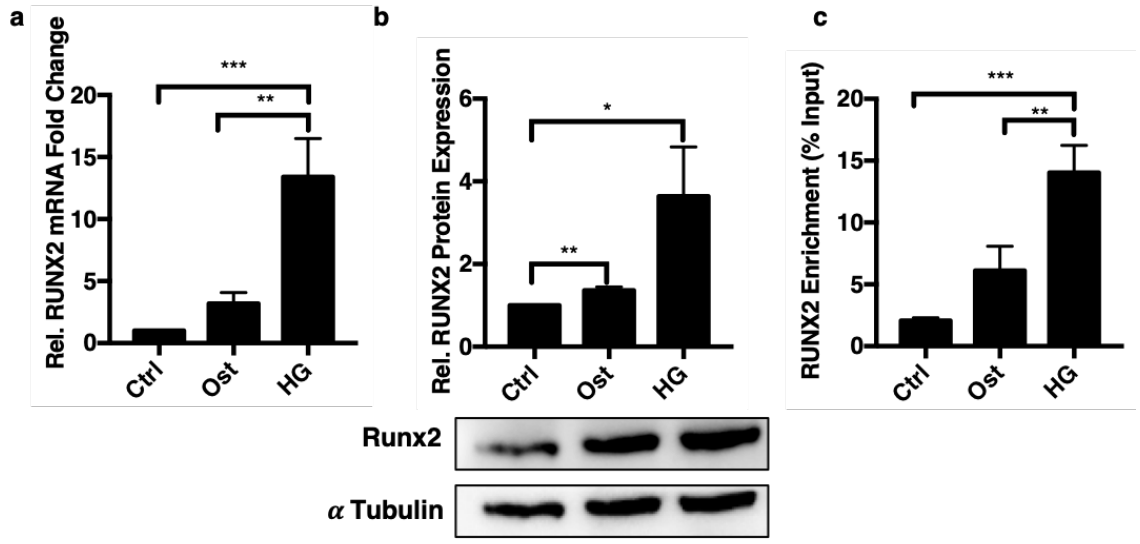

Fig. 3.3. **Hyperglycaemic conditions increase Runx2 promotor acetylation and protein expression.** The effect of control (Ctrl), $CaCl_2$ and BGP osteogenic (Ost) and osteogenic with high glucose (HG) conditions was examined. mRNA, Protein and DNA isolated from vSMCs at a day 4 timepoint was examined for Runx2 expression. **a)** Runx2 mRNA abundance was increased by over 10-fold in hyperglycaemic conditions compared to osteogenic and untreated controls (n=9) (One-way ANOVA, Tukey Post-Hoc test). **b)** Runx2 protein levels increased in hyperglycaemic conditions compared to untreated controls, western blots were quantified using densitometry and expressed relative to α-Tubulin shown as loading control (n=3) (One-way ANOVA, Tukey Post-Hoc test). **c)** Chromatin immunoprecipitation (ChIP) was conducted to determine the acetylation profile of the Runx2 promotor region. ChIP demonstrated a significant increase in acetylation of lysine within the Runx2 promotor in hyperglycaemic conditions compared to both osteogenic and control (n=3) (One-way ANOVA, Tukey Post-Hoc test). *P<0.05, **P<0.005, ***P<0.001. Mean ±SEM.

As the gene encoding the non-collagenous bone matrix protein OCN is a downstream target of Runx2 and known to be involved in vascular calcification (306), its expression was assessed at day 7 during the hyperglycaemia-induced vSMC calcification process. OCN positive staining was apparent in both osteogenic and hyperglycaemic treatments, with an apparent increase in OCN both in the cytoplasm and the nucleus in hyperglycaemic conditions when compared to control (Fig. 3.4a). The mean fluorescence of OCN assessed via ImageJ was significantly increased in both osteogenic and hyperglycaemic conditions compared to control ($p<0.0001$) (Fig. 3.4b) which mimicked the increased OCN mRNA at an earlier day 4 time point (Fig. 3.4c). OCN mRNA abundance doubled ($p<0.0209$) within osteogenic conditions at day 4 and increased 8-fold under hyperglycaemic conditions ($p<0.0004$) at the same timepoint.

Additional bone-related markers and downstream targets of Runx2 (307) were also analysed at the mRNA level at the day 4 time point (Fig. 3.4d). Both OPG and OPN expression showed no significant change between treatments at this time point. However, it is interesting to note that MSX2; a transcription factor critical for the development of chondrocyte/osteogenic differentiation (308) was significantly increased in hyperglycaemic conditions ($p<0.049$) (Fig. 3.4d).

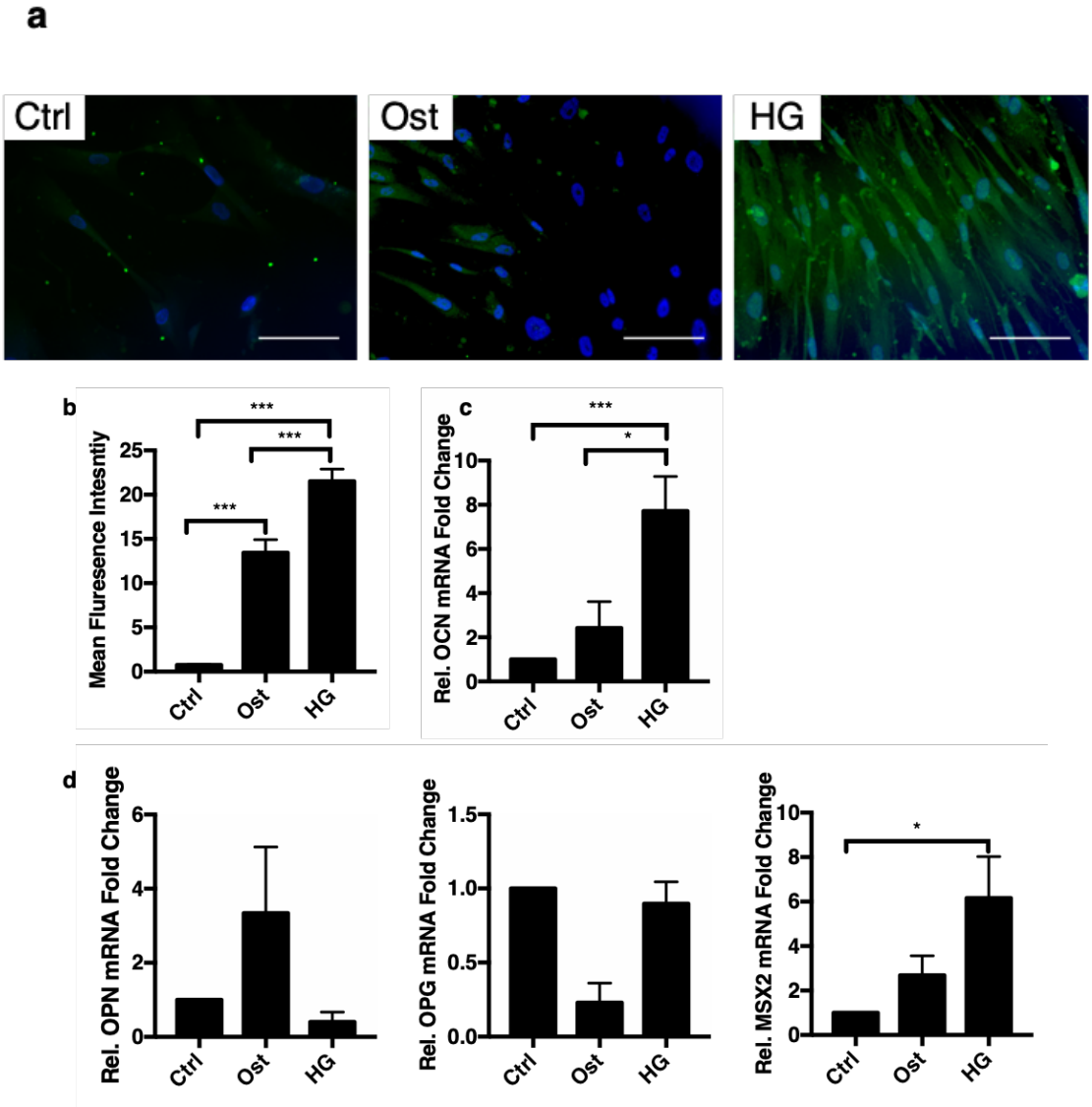

Fig. 3.4. Hyperglycaemic conditions increase protein expression of downstream markers of the Runx2 pathway *in vitro*. The effect of hyperglycaemia on calcification markers was examined. Three conditions were assessed; control (Ctrl), $CaCl_2$ and BGP osteogenic (Ost) and osteogenic with high glucose (HG). **a)** Following 4 days of treatment OCN protein localisation was assessed by fluorescent staining (n=4 and 5FoV). **b)** staining was quantified via ImageJ. OCN increased via a third in hyperglycaemic conditions compared to osteogenic conditions (n=4) (One-way ANOVA, Tukey Post-Hoc test). **c)** OCN mRNA abundance increased via four-fold in hyperglycaemic conditions compared to osteogenic at day 4 (n=9) (One-way ANOVA, Tukey Post-Hoc test). **d)** OPN, OPG and MSX2 mRNA expression was examined following 4 days of treatment. MSX2 expression significantly increased in hyperglycaemic conditions compared to control (n=4) (One-way ANOVA, Tukey Post-Hoc test). OCN green, DAPI blue. *P<0.05, **P<0.005, ***P<0.001. Scale Bars = 10µm. Mean ±SEM.

3.3.4. Diabetic patient vessels exhibit calcification markers

Having established the links between hyperglycaemic conditions and calcification in conjunction with a down-regulation of SIRT1 expression, it was next of interest to investigate SIRT1 expression and calcification marker expression in diabetic patient tissue compared to non-calcified tissue.

Diabetic patient popliteal arterial vessels were acquired from patients during lower limb amputation and were found to exhibit increased expression of calcification markers compared to non-calcified internal mammary artery controls. Positive Alizarin red staining shown in dark red stain was positive within the smooth muscle layer of the DM sections and is absent in the IMA control (Fig. 3.5a). Both Runx2 (Fig. 3.5b) and OCN (Fig. 3.5c) staining shown in black was increased in the diabetic patient vessels, localised to the medial layer and conversely absent in the IMA controls. Both the diabetic patient and the IMA vessels demonstrate positive αSMA staining suggesting the presence of vSMCs within the vessel, correlating with the location of calcification marker expression (Fig. 3.5d). Haematoxylin and Eosin staining was used to demonstrate the integrity of the section obtained from the vessel, where the cytoplasm of the cells stained pink, the nucleus in purple, and calcified areas were identified by the positively stained areas in dark purple (Fig. 5e). Osteopontin, a known marker of calcification was stained for and developed with brown DAB, whilst the samples were counterstained with Haematoxylin (Fig. 5f). Positive staining observed in the DM samples are shown in brown, compared to the lack of brown staining in the IMA control. A negative IgG control demonstrates the DAB staining is specific for the antibodies used (Fig. 3.5g).

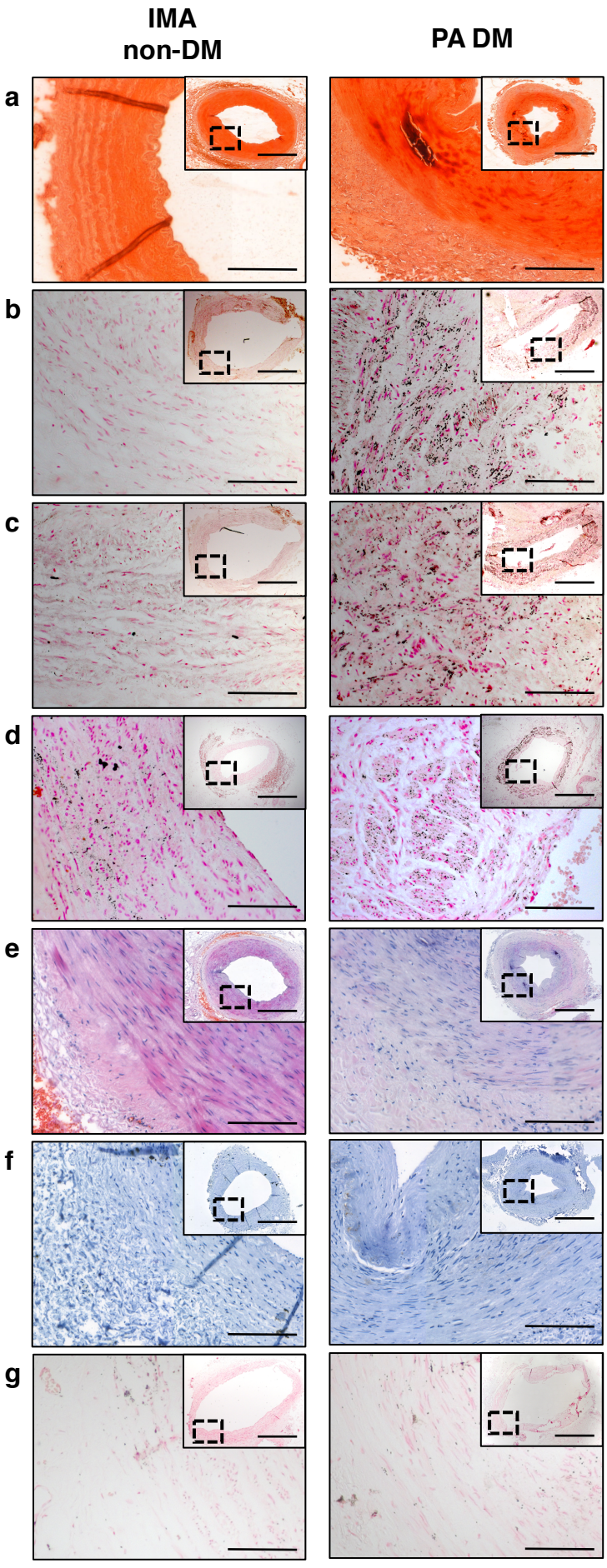

Fig. 3.5. Osteogenic marker expression is increased in diabetic patients. Internal mammary arteries (IMA) were harvested from non-diabetic patient undergoing CABG surgery and used as controls. Popliteal arteries (PA) were harvested from diabetic patients (DM) undergoing lower limb amputation. **a)** Alizarin red staining, positive staining shown by arrow (n=3). **b)** Runx2 staining, positive staining observed in the DM compared to the IMA. **c)** OCN staining, positive staining observed in the DM compared to the IMA **d)** αSMA staining **e)** H&E staining differentiating the cytoplasm in pink from the nucleus in blue. **f)** OPN staining showing the positive OPN staining in brown observed in the DM compared to the IMA **g)** IgG staining as a negative control. (n=6 for all). Scale bars = 200µm/20µm

3.3.5. Hyperglycaemic conditions induce cellular senescence and increase smooth muscle cell plasticity

Diabetic patients often exhibit decreased wound healing and a loss of a smooth muscle contractile phenotype within the vessels. A β-galactosidase assay was used to determine the development of senescence within vSMCs under *in vitro* hyperglycaemic conditions.

Positive blue staining at day 4 is shown in both osteogenic and hyperglycaemic conditions (Fig. 3.6a) with a significant increase in both osteogenic ($p<0.0417$) and hyperglycaemic ($p<0.006$) conditions compared to controls. Furthermore, a significant increase is apparent between osteogenic and hyperglycaemic conditions ($p<0.0115$) (Fig. 3.6b). Given that cells develop a senescent phenotype due to irreversible cell cycle arrest, the expression of cyclin-dependent kinase inhibitors was examined. p16 mRNA abundance significantly increased in hyperglycaemic conditions compared to both control ($p<0.0053$) and osteogenic ($p<0.0129$) conditions at day 4. Both p21 and master transcription factor p53 significantly increased mRNA abundance in hyperglycaemic conditions compared to controls ($p<0.0028$) ($p<0.0021$) respectively, however no significant difference was detected in the osteogenic condition at day 4 (Fig. 3.6c). Cell cytotoxicity showed no change in day 7 treatments under hyperglycaemic conditions, however by day 21 cytotoxicity was significantly greater in hyperglycaemic cells ($p<0.0001$) (Fig. 3.6d).

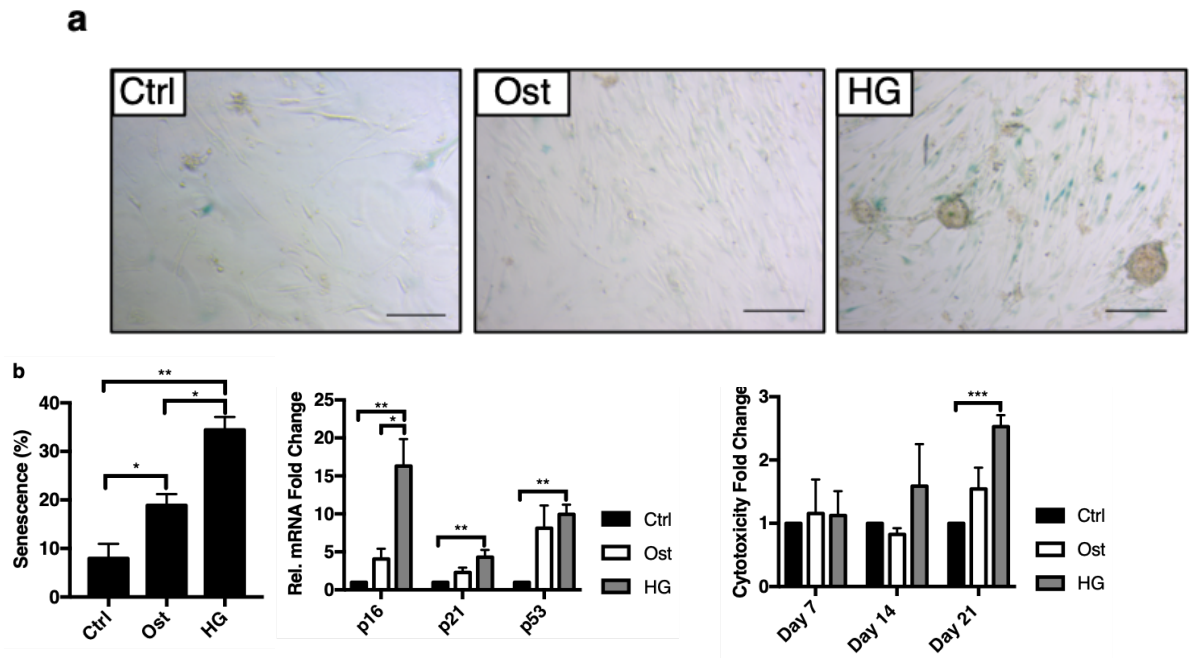

Fig. 3.6. **Hyperglycaemic conditions increased cellular senescence and associated markers.** Three treatment conditions were assessed; control (Ctrl), $CaCl_2$ and BGP osteogenic (Ost) and osteogenic with high glucose (HG). Positive cellular senescence represented via blue β-galactosidase activity observed in micrographs**. a)** Cells were cultured for 4 days in respective conditions and stained using x-gal substrate. Hyperglycaemia significantly increased β-gal staining (n=4 and 5FoV), **b)** staining quantification normalised to control treatment showed a significant increase in osteogenic and hyperglycaemic conditions compared to each other (n=4) (One-way ANOVA, Tukey Post-Hoc test). **c**) RNA harvested from treated cells at 4 day demonstrated cyclin-dependant kinase inhibitors p16 and p21 were significantly increased in hyperglycaemic conditions compared to control. p53 expression was increased in both osteogenic and hyperglycaemic conditions compared to control but showed no difference when compared to one another (n=4) (One-way ANOVA, Tukey Post-Hoc test). **d)** Cell cytotoxicity assessed by Promega assay (G9290) showed no significant increase at day 7, however hyperglycaemic treatment significantly increased cytotoxicity within the cells by day 21. (n=4) (Two-way ANOVA, Tukey Post-Hoc test). *P<0.05, **P<0.005. Scale Bars = 100µm. Mean ±SEM.

Since healthy vSMCs exhibit high levels of αSMA in order to maintain a contractile phenotype, the expression level was assessed via immunofluorescence within the model at day 4. Under hyperglycaemic conditions it was found that αSMA staining was diminished (Fig. 3.7a) with a significant decrease in both the hyperglycaemic ($p<0.0077$) and osteogenic ($p<0.0107$) conditions compared to the controls when quantified via imageJ (Fig. 3.7b).

Secondly, cellular proliferation was also examined to determine the activation of these cells under hyperglycaemic conditions. Whilst proliferation initially increased in a hyperglycaemic environment ($p<0.0034$) at day 14, by day 21 proliferation had decreased by 30% compared to controls ($p<0.0127$), correlating with the increase in senescence markers previously noted (Fig. 3.7c). 10,000 cells were examined from each sample under flow cytometry to determine cell cycle and size. Both nuclei area (Fig. 7d) and number (Fig. 3.7e) were examined. Nucleus number significantly decreased in hyperglycaemic conditions compared to controls ($p<0.0386$), corresponding with an enrichment in S phase (Fig. 3.7f) and a decrease in G1 phase.

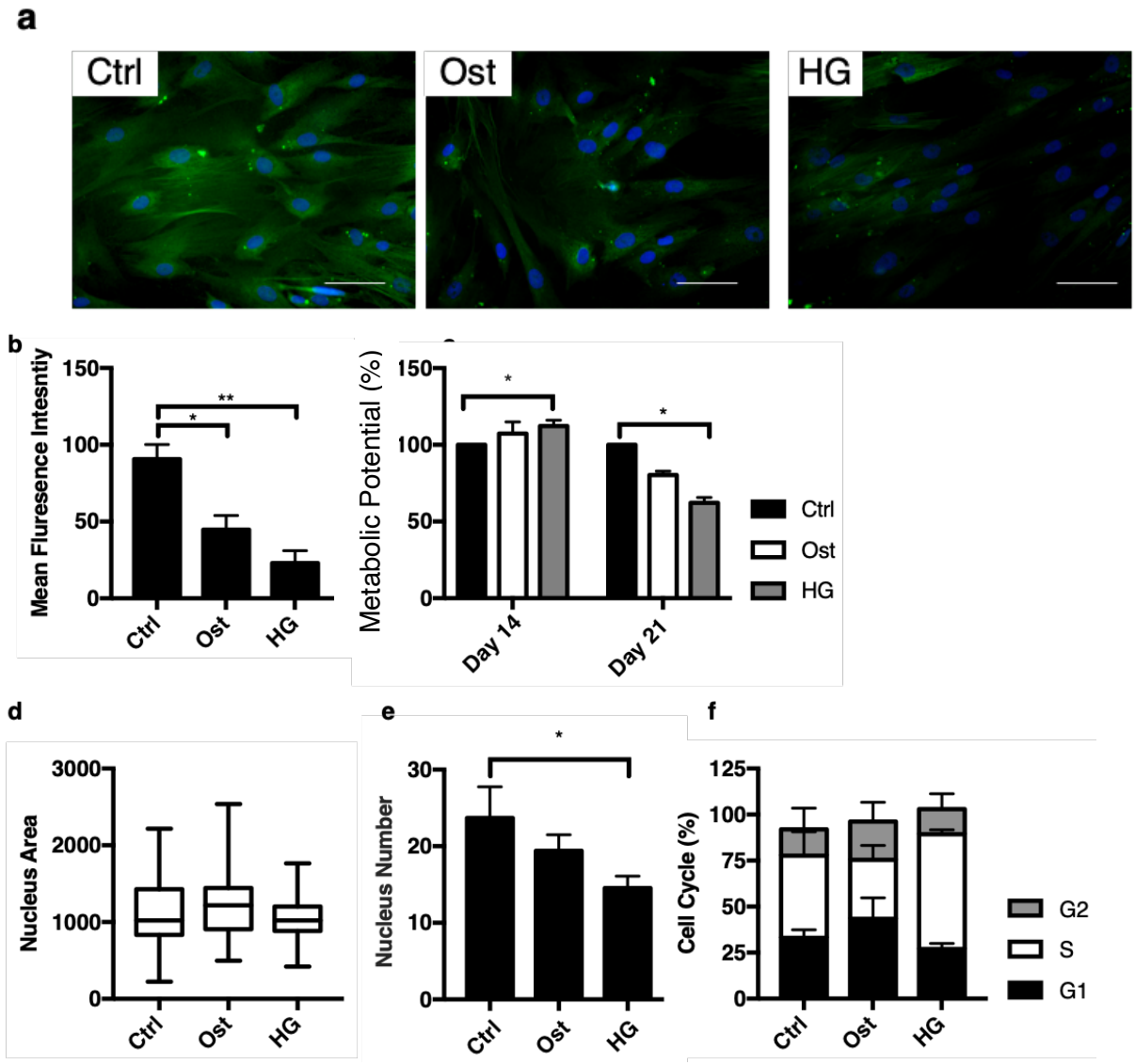

Fig. 3.7. Hyperglycaemic conditions modify cellular phenotype. The role of three treatment conditions; control (Ctrl), $CaCl_2$ and BGP osteogenic (Ost) and osteogenic with high glucose (HG). Were assessed on cellular proliferation and phenotype was examined. **a)** αSMA, a marker of smooth muscle contractility decreased staining intensity during 4 days of hyperglycaemic treatment (n=4 and 5FoV) **b)** staining quantified via ImageJ, significantly decreased in both osteogenic and hyperglycaemic conditions compared to controls (n=4) (One-way ANOVA, Tukey Post-Hoc test). **c)** Cellular proliferation confirmed via the blue assay increased at day 14 in hyperglycaemic conditions however it significantly decreased by day 21 (n=3) (Two-way ANOVA, Tukey Post-Hoc test). **d)** Nucleus area size confirmed via propodeum iodine staining under flow cytometry showed no significant change in hyperglycaemic conditions compared to control (n=4) (One-way ANOVA, Tukey Post-Hoc test) whereas **e)** nucleus number significantly decreased in hyperglycaemic conditions compared to control (n=4) (One-way

ANOVA, Tukey Post-Hoc test). **f)** Cell cycle phases were examined with flow cytometry. S phase increased in hyperglycaemic conditions compared to controls, whereas G1 phase decreased (n=4). αSMA green, DAPI blue. *P<0.05, **P<0.005, Scale Bars = 10μm. Mean ±SEM.

3.3.6. SIRT1 expression can be modulated via chemical and genetic approaches

The SIRT1 activator SRT1720 (Selleckchem) was used at a dose dependent concentration which was shown to have no negative effect on cell viability between the doses of 0-0.5 μM (Fig. 3.8a) as was SIRT1 inhibitor; Sirtinol (Selleckchem) between the doses of 0-10 μM (Fig. 3.8b), while at higher doses viability decreased. Therefore, SRT1720 and Sirtinol was used at 0.5 μM and 10 μM respectively henceforth. Control conditions were supplemented with DMSO at an equal concentration to that which is within the drug treated conditions, thus henceforth all control conditions; when compared to a drug treated condition, contain DMSO at a proven (309) sublethal concentration of 0.1% (1:1000).

SIRT1 activation increased SIRT1 mRNA expression by almost 15-fold ($p<0.0006$), whereas SIRT1 inhibition via Sirtinol reduced expression to under a third of untreated expression levels ($p<0.0001$) (Fig. 3.8c). Pharmacological modification of SIRT1 was mirrored in protein expression, with a three-fold increase observed with SRT1720 activation ($p<0.0010$) and a significant reduction observed in Sirtinol treatment ($p<0.0001$) compared to control (Fig. 3.8d). SIRT1 siRNA was used to confirm the effect of Sirtinol inhibition. SIRT1 siRNA reduced SIRT1 mRNA expression to a tenth compared to scrambled siRNA controls ($p<0.0001$) (Fig. 3.9a), which was also evident in protein expression ($p<0.0061$) (Fig. 3.9b).

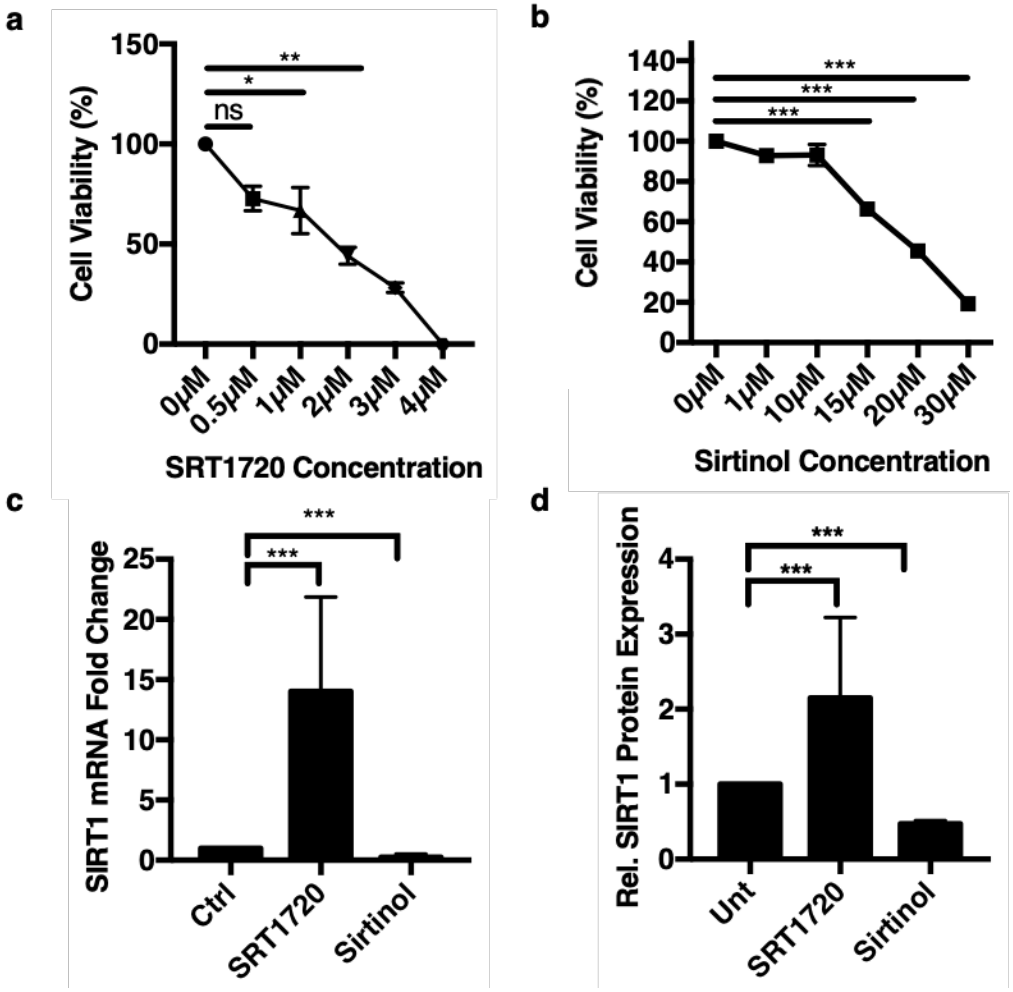

Fig. 3.8. SIRT1 modulation via chemical approaches. The effect of SIRT1 activators and inhibitors on SIRT1 expression was examined. Cells were treated with either the activator; SRT1720 or inhibitor; Sirtinol for 4 days prior to harvesting for RNA and protein or assessed for viability via the Alamar blue assay. Control samples were treated with the equivalent amount of DMSO (0.1%). **a)** SIRT1 activation via SRT1720 significantly reduced cell viability when used at doses over 0.5 μM (n=3) (Two-way ANOVA, Tukey Post-Hoc test). **b)** Sirtinol inhibition significantly reduced cell viability at over 10 μM (n=3) (Two-way ANOVA, post doc test). **c)** SIRT1 mRNA expression was significantly increased via 0.5μM SRT1720 activation, and significantly reduced via 10 μM Sirtinol inhibition. (n=4) (One-way ANOVA, Tukey Post-Hoc test), **d)** which was sustained to SIRT1 protein expression (n=3) (One-way ANOVA, Tukey Post-Hoc test). *P<0.05, **P<0.005, ***P<0.001. Mean ±SEM.

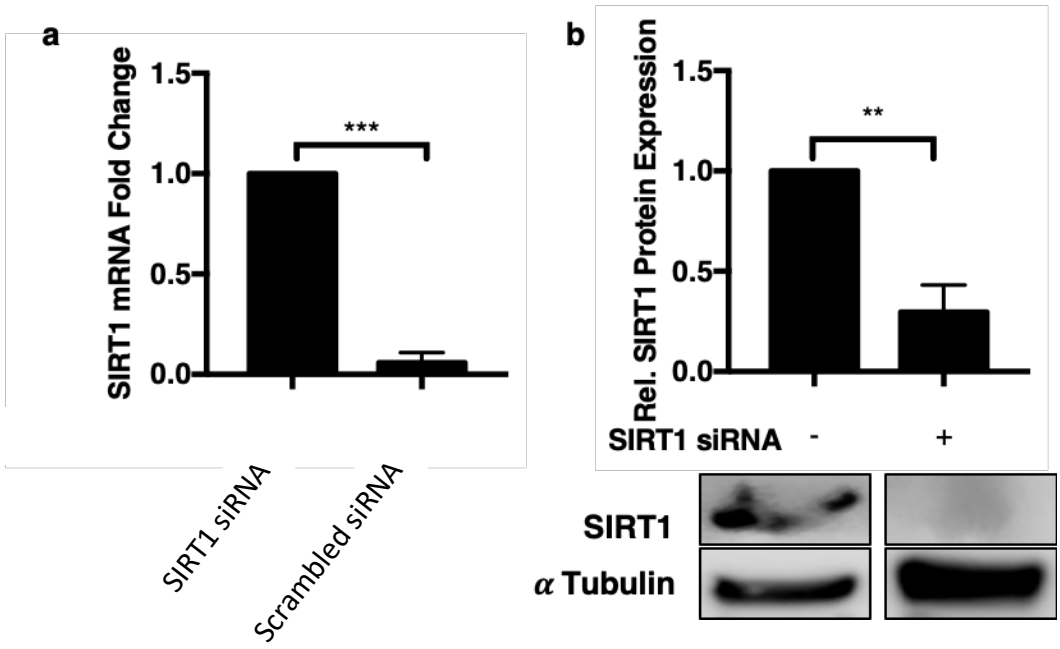

Fig. 3.9. SIRT1 knockdown via a genetic approach. The effect of SIRT1 siRNA and Scrambled siRNA on SIRT1 expression was examined. cells were cultured until confluence then placed in antibiotic free media for 2 hours before siRNA dissolved in TE buffer was added. PolyFect was used as a transfection reagent and left to incubate for 6 hours before media was replaced with calcifying media for 7 days. SIRT1 knockdown via siRNA significantly reduced SIRT1 **a)** mRNA (n=4) (Paired T-test) and **b)** in protein expression (n=4) (Paired T-test). *P<0.05, **P<0.005, ***P<0.001. Mean ±SEM.

3.3.7. Modulation of SIRT1 modifies smooth muscle cell mineralisation

Since previous literature has demonstrated that SIRT1 activation inhibits hyperphosphatemia-induced calcification through a premature senescence pathway (249), the impact of SIRT1 expression within the current hyperglycaemic model was assessed. Cell matrix calcification was examined in the three treatment groups via Alizarin red staining, ALP activity and total calcium content, to determine the effects of SIRT1 modulation. Where a small molecule activator or inhibitor was used to modulate SIRT1 expression, 0.1% DMSO was used in non-drug treated controls.

SIRT1 activation via SRT1720 was protective against calcified matrix deposition in both osteogenic ($p<0.0019$) and hyperglycaemic conditions ($p<0.0365$), evidenced by a reduction of Alizarin red staining at day 21 compared to untreated (Fig. 3.10a, top panel). Conversely, SIRT1 inhibition via Sirtinol significantly induced a more pronounced mineral deposition in hyperglycaemic conditions ($p<0.0332$) (Fig 9a lower panel), which was significant when quantified (Fig. 3.10b). However, control cells treated with either SRT1720 or Sirtinol did not show any positive calcification staining (Fig. 3.10b).

To further confirm the development of calcification, cells and their matrix were harvested at day 21 and their total calcium content assessed. A significant decrease was observed in hyperglycaemic conditions with the addition of SRT1720 compared to untreated ($p<0.0173$) (Fig. 3.10c), in which the opposite was found in both osteogenic ($p<0.0011$) and hyperglycaemic ($p<0.0002$) conditions with the addition of Sirtinol when compared to untreated.

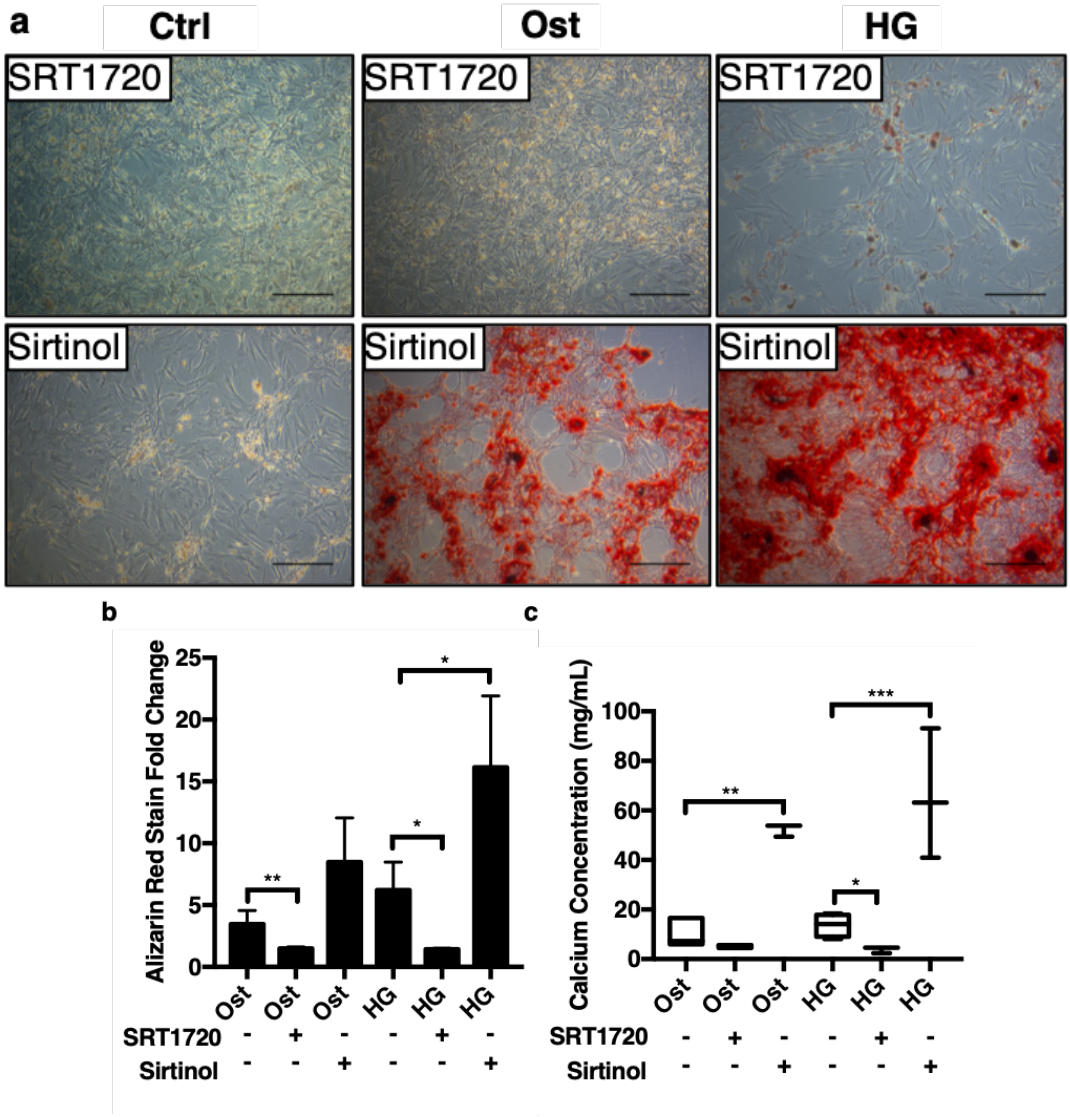

Fig. 3.10. Modulation of SIRT1 modifies smooth muscle cell mineralisation. The effect of SIRT1 activator SRT1720 (0.5 µM) and SIRT1 inhibitor Sirtinol (10 µM) on smooth muscle calcification was investigated, with 0.1% DMSO used within untreated controls. Three treatments were investigated; control (Ctrl), $CaCl_2$ and BGP osteogenic (Ost) and osteogenic with high glucose (HG). **a)** Representative micrographs demonstrate decreased staining with the addition 0.5 µM SRT1720 and increased staining with the addition of 10 µM Sirtinol following 21 days of treatment (n=4 and 5FoV**), b)** quantification confirms a significant increase in both osteogenic and hyperglycaemic conditions under 10 µM Sirtinol treated conditions compared to 0.5 µM SRT1720 and untreated (n=4) (Two-way ANOVA, Tukey Post-Hoc test). **c)** Total cellular calcium assessed at the same timepoint was significantly increased in 10 µM Sirtinol treated cells in both osteogenic and hyperglycaemic conditions and decreased under hyperglycaemic 0.5 µM SRT1720 conditions compared to control (n=4) (Two-way ANOVA, Tukey Post-Hoc test). *P<0.05, **P<0.005, ***P<0.001. Scale Bars = 100µm. Mean ±SEM.

To assess the early stage development of calcification, ALP activity was examined. ALP activity significantly increased in osteogenic conditions by day 4 ($p<0.0073$) and was sustained until day 7 with the addition of Sirtinol ($p<0.0007$) when compared to untreated osteogenic conditions. ALP activity reduced with the addition of SRT1720 compared to the untreated control cells, however this was not significant (Fig. 3.11a). In hyperglycaemic treatment little difference in ALP activity was found between Sirtinol and untreated conditions at day 7, however there was a decrease in SRT1720 treated cells, when compared to Sirtinol ($p<0.0280$) and untreated ($p<0.0322$) conditions (Fig. 3.11a). SIRT1 siRNA was not used to assess matrix calcification or calcium content of cells due to its short half-life and the apoptotic effect repeat transfection would have on the cells, however ALP activity could be assessed within the first seven days of siRNA treatment. ALP activity was increased in hyperglycaemic conditions following SIRT1 siRNA knockdown by day 7 when compared to scrambled siRNA controls ($p<0.0327$) (Fig. 3.11b).

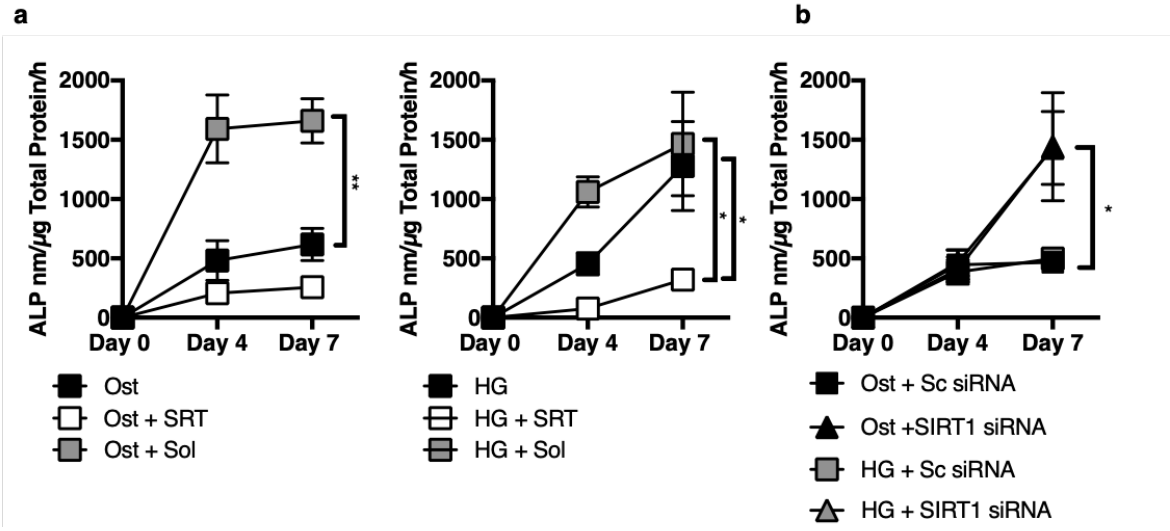

Fig. 3.11. **Modulation of SIRT1 modifies smooth muscle cell alkaline phosphatase activity**. The effect of SIRT1 activator SRT1720 (0.5 µM) and SIRT1 inhibitor Sirtinol (10 µM) on vSMC ALP activity was investigated, on two conditions; $CaCl_2$ and BGP osteogenic (Ost) and osteogenic with high glucose (HG). with 0.1% DMSO used within untreated control. **a)** SIRT1 activation decreased ALP activity in both osteogenic and hyperglycaemic conditions compared to SIRT1 inhibition (n=5) (Two-way ANOVA, Tukey Post-Hoc test). **b)** SIRT1 siRNA and scrambled control were used to confirm Sirtinol findings. SIRT1 siRNA significantly increased ALP activity in both osteogenic and high glucose conditions compared to scrambled siRNA. (n=4) (Two-way ANOVA, Tukey Post-Hoc test). *P<0.05, **P<0.005. Mean ±SEM.

Since SIRT1 activation and inhibition has now been demonstrated to inhibit and increase the development of vSMC calcification respectively, the transcriptional pathway targeted by SIRT1 was examined. The acetylation profile of Runx2 was again assessed following the addition of SIRT1 activator SRT1720. SRT1720 significantly decreased Runx2 acetylation in all conditions by day 4, with hyperglycaemic treatment causing a decrease by over 7-fold ($p<0.0001$) (Fig. 3.12a). With histone modifications around the H3K27Ac mark of Runx2 promotor region shown to be significantly downregulated with SIRT1 activation, the total mRNA and protein level was assessed. Runx2 mRNA was significantly increased in both osteogenic ($p<0.0001$) and hyperglycaemic ($p<0.0146$) conditions with the addition of Sirtinol (Fig. 3.12b), whereas there was a ten-fold decrease in Runx2 mRNA abundance when cells were treated with SRT1720 ($p<0.0206$).

Following mRNA analysis, protein expression of Runx2 at day 4 was also assessed. SRT1720 activation decreased protein expression by a third compared to untreated in hyperglycaemic conditions ($p<0.0057$) (Fig. 3.12c) whereas Sirtinol had the opposite effect, increasing Runx2 activity by over 3-fold ($p<0.001$) (Fig. 3.12d). siRNA inhibition of SIRT1 was confirmed to be effective up to 7 days after transfection (Fig. 3.9b). SIRT1 siRNA knockdown exhibited similar effects to Sirtinol treatment, significantly increasing Runx2 mRNA and protein expression at day 4 when compared to scrambled siRNA controls. mRNA abundance was significantly increased compared to hyperglycaemic conditions treated with scrambled siRNA ($p<0.0019$) (Fig. 3.13a). Greater variability was detected in Runx2 protein expression, with a significant increase in Runx2 expression found in hyperglycaemic conditions only ($p<0.0473$) (Fig. 3.13b).

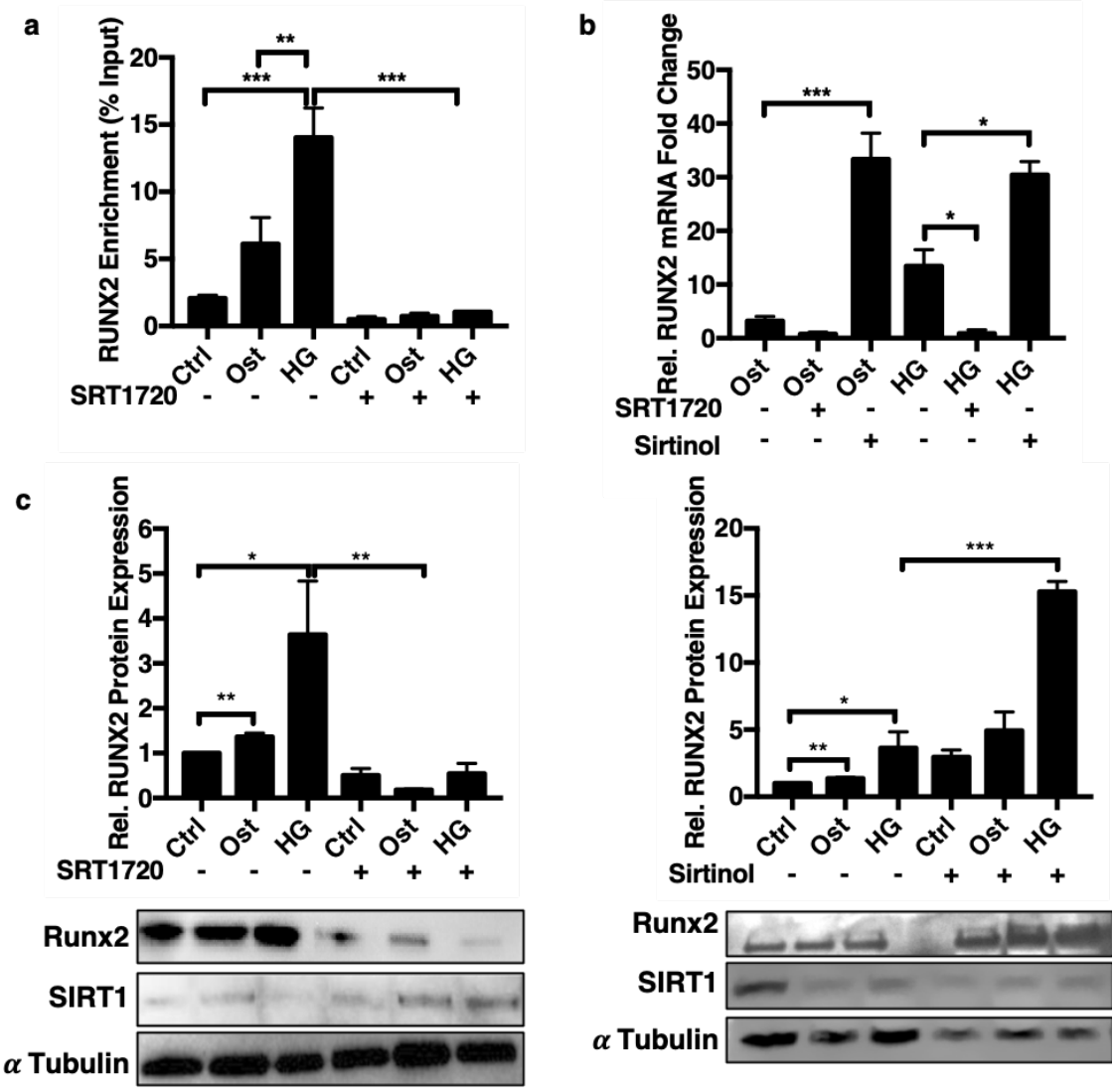

Fig. 3.12. Activation of SIRT1 modulates the Runx2 pathway. The effect of SIRT1 activator SRT1720 (0.5 μM) and SIRT1 inhibitor Sirtinol (10 μM) on the Runx2 pathway was investigated on control (Ctrl), $CaCl_2$ and BGP osteogenic (Ost) and osteogenic with high glucose (HG) with 0.1% DMSO used within untreated control. **a)** Acetylation of the Runx2 promotor region was significantly increased following 4 days of treatment in hyperglycaemic conditions compared to both the control and hyperglycaemic conditions treated with 0.5 μM SRT1720 (n=3) (Two-way ANOVA, Tukey Post-Hoc test). **b)** Runx2 mRNA expression significantly increased at the same timepoint in 10 μM Sirtinol treated conditions in both osteogenic and hyperglycaemic treatments whereas 0.5 μM SRT1720 decreased Runx2 expression (n=4) (Two-way ANOVA, Tukey Post-Hoc test). **c)** Runx2 protein expression also at day 4 significantly decreased with 0.5 μM SRT1720 activation in all treatments and increased in 10 μM Sirtinol treated conditions (n=3) (Two-way ANOVA, Tukey Post-Hoc test). *P<0.05, **P<0.005, ***P<0.001. Mean ±SEM.

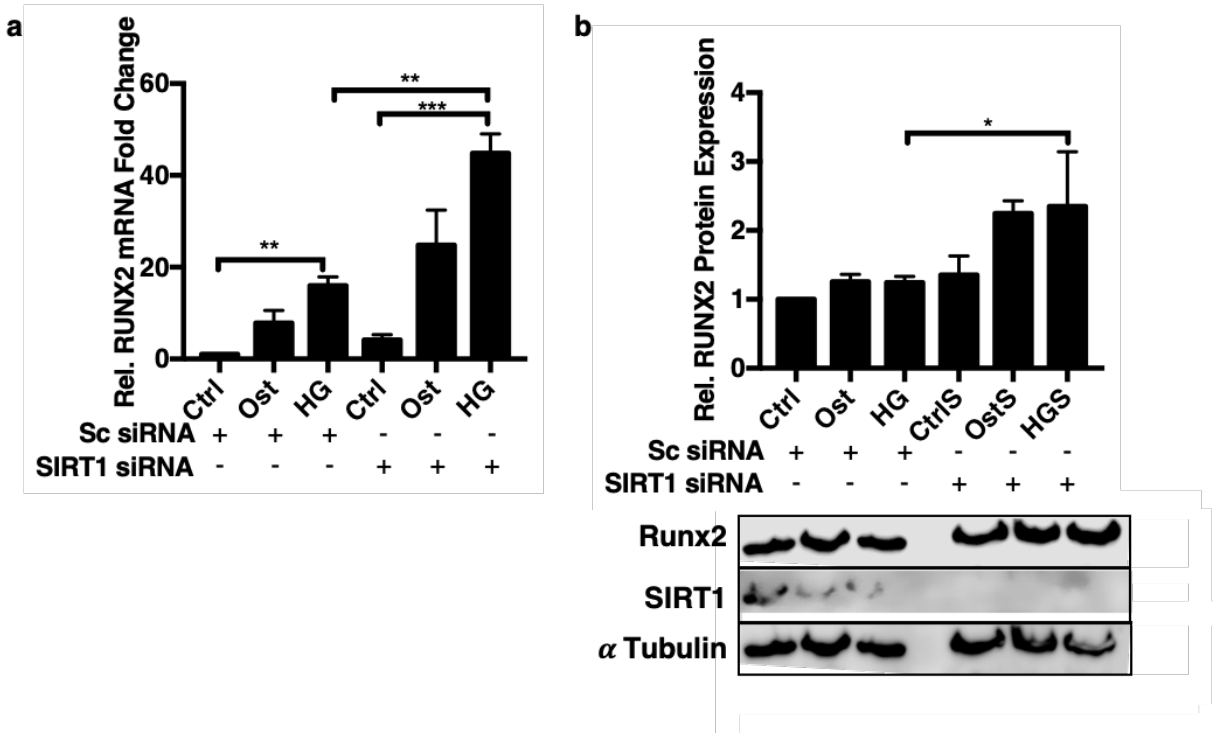

Fig. 3.13. Genetic knockdown of SIRT1 modulates the Runx2 pathway. The effect of SIRT1 siRNA and scrambled control on control (Ctrl), $CaCl_2$ and BGP osteogenic (Ost) and osteogenic with high glucose (HG). on the Runx2 pathway was investigated following 4 days of treatment. **a)** SIRT1 siRNA significantly increased Runx2 mRNA expression compared to scrambled siRNA (n=4) (Two-way ANOVA, Tukey Post-Hoc test). **b)** SIRT1 siRNA significantly decreased SIRT1 protein expression and increased Runx2 protein expression (n=3) (Two-way ANOVA, Tukey Post-Hoc test). *P<0.05, **P<0.005, ***P<0.001. Mean ±SEM.

3.3.8. SIRT1 activation negatively regulates proteins downstream in the Runx2 pathway

Whilst SIRT1 inhibition has been demonstrated to upregulate Runx2 expression, the effect of SIRT1 activation on downstream effector proteins within the Runx2 pathway is still unclear. OCN, concomitantly the most abundant non-collagenous peptide found in matrix mineralisation, has a known Runx2 binding element; osteoblast-specific cis-acting element 2 (OSE2; ACCACA) (310) and is therefore a good target to examine the downstream effects of SIRT1 on the Runx2 pathway. Expression of OCN was again examined at day 4 via fluorescent staining (Fig. 3.14a) and quantified via the mean fluorescent intensity (Fig. 3.14b). SIRT1 activation inhibited OCN expression in a similar trend to Runx2 expression, with no significant increase in OCN between osteogenic and hyperglycaemic conditions ($p<0.8140$) and a significant decrease compared to untreated cells in both osteogenic ($p<0.0176$) and hyperglycaemic treatments ($p<0.0001$). SIRT1 inhibition had the opposite effect, significantly increasing OCN expression at both osteogenic ($p<0.0001$) and hyperglycaemic treatments ($p<0.0030$) compared to untreated, however control cells treated with Sirtinol showed no significant increase in OCN staining (Fig. 3.14b). mRNA expression of OCN was significantly increased in Sirtinol treatment compared to osteogenic untreated conditions ($p<0.0001$). In hyperglycaemic conditions SRT1720 significantly decreased OCN mRNA expression compared to untreated ($p<0.0012$) and Sirtinol treatment ($p<0.0048$) the latter which was increased by 10-fold (Fig. 3.15a).

Msx2 activity followed a similar trend, with a significant increase in day 4 mRNA expression observed in osteogenic Sirtinol treated cells compared to untreated ($p<0.0001$) (Fig. 3.15b). OPN mRNA expression showed no change in osteogenic conditions irrespective of SIRT1 treatment. However, within hyperglycaemic conditions SIRT1 activation increased OPN expression 5-fold, with no significant change observed in Sirtinol treatment compared to control (Fig. 3.15c) ($p<0.0036$). Likewise, OPG followed a similar course, however osteogenic conditions showed a significant variation between SIRT1 activation; which increased OPG expression by over 20-fold ($p<0.0312$), as did hyperglycaemic conditions ($p<0.0243$). However, unlike OPN, no change in expression was observed between osteogenic and

hyperglycaemic SRT1720 treatment ($p<0.9999$) (Fig. 3.15d), suggesting that maybe the two proteins have different activators within the diabetic milieu.

Finally, SIRT1 siRNA knockdown was used to confirm the effect of SIRT1 inhibition on the downstream Runx2 pathway. OCN mRNA expression was significantly raised in SIRT1 knockdown treated cells compared to scrambled siRNA ($p<0.0206$) (Fig. 3.16a). Additionally, Msx2 mRNA expression was also examined and a significant increase was observed in both osteogenic ($p<0.0041$) and hyperglycaemic ($p<0.0003$) SIRT1 siRNA treated cells, however no change was observed in control, similar to Sirtinol treatment (Fig. 3.16b).

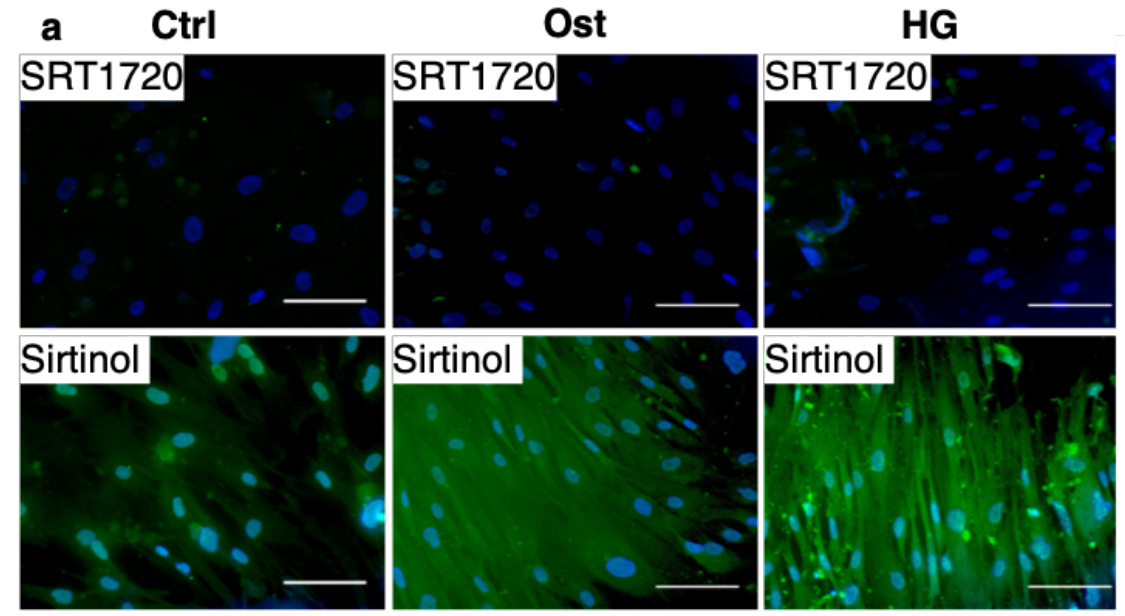

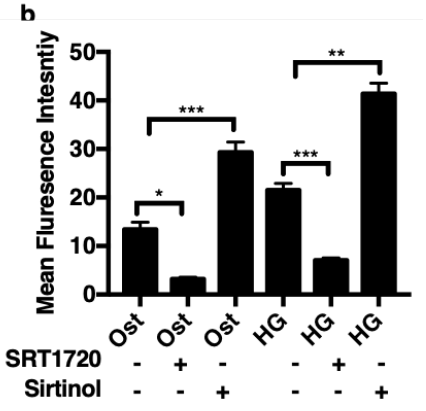

Fig. 3.14. SIRT1 modulates OCN expression downstream of the Runx2 pathway. The effect of SIRT1 activator SRT1720 (0.5 μM)and SIRT1 inhibitor Sirtinol (10 μM) on control (Ctrl), $CaCl_2$ and BGP osteogenic (Ost) and osteogenic with high glucose (HG) conditions in OCN production was investigated following 4 days of treatment, with 0.1% DMSO used within untreated control. **a)** OCN fluorescent staining was significantly decreased in all treatments with the addition of 0.5 μM SRT1720 and increased with the addition of 10 μM Sirtinol (n=3), **b)** this was confirmed by ImageJ quantification (n=3) (Two-way ANOVA, Tukey Post-Hoc test). OCN green, DAPI blue. $P<0.05$, $^{**}P<0.005$, $^{***}P<0.001$ Scale Bars = 10μm. Mean ±SEM.

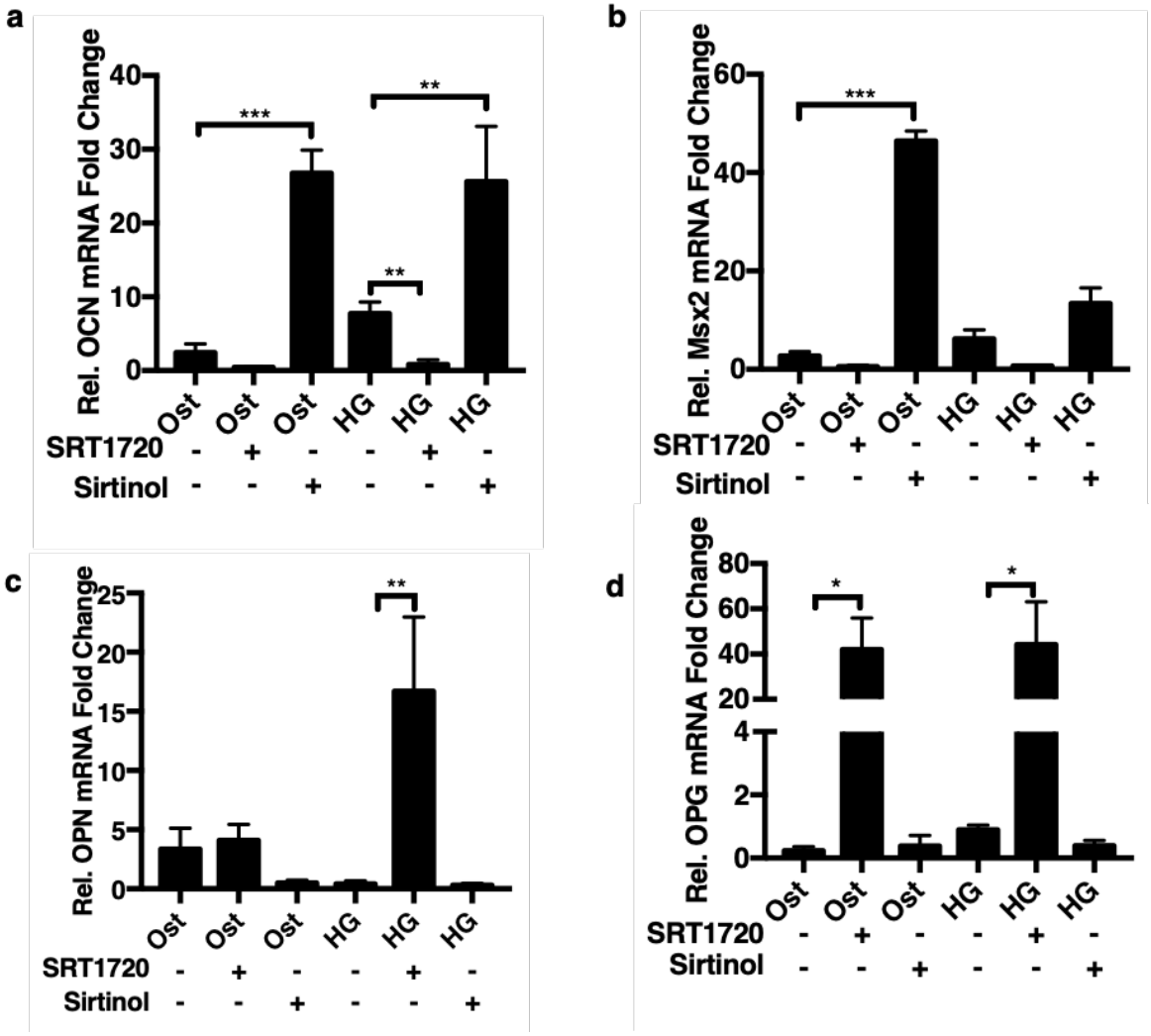

Fig. 3.15. SIRT1 modulates Runx2 downstream gene expression. The effect of SIRT1 activator SRT1720 (0.5 μM) and SIRT1 inhibitor Sirtinol (10 μM) on control (Ctrl), $CaCl_2$ and BGP osteogenic (Ost) and osteogenic with high glucose (HG) on downstream effector proteins within the Runx2 pathway was investigated, with 0.1% DMSO used within untreated controls. RNA harvested from day 4 treated cells was assessed. **a)** OCN (n=4) (Two-way ANOVA, Tukey Post-Hoc test) and **b)** MSX2 mRNA was significantly upregulated in both osteogenic and hyperglycaemic treatments with the addition of 10 μM Sirtinol (n=4) (Two-way ANOVA, Tukey Post-Hoc test). mRNA expression of osteogenic differentiation markers **c)** OPN (n=4) (Two-way ANOVA, Tukey Post-Hoc test) and **d)** OPG were examined at the same timepoint. OPN significantly increased in hyperglycaemic conditions when treated with 0.5 μM SRT1720 compared to both untreated and 10 μM Sirtinol treated conditions. OPG expression was significantly upregulated in both osteogenic and hyperglycaemic conditions with 0.5 μM SRT1720 compared to both untreated and 10 μM Sirtinol treatment (n=4) (Two-way ANOVA, Tukey Post-Hoc test). $P<0.05$, $^{**}P<0.005$, $^{***}P<0.001$. Mean ±SEM.

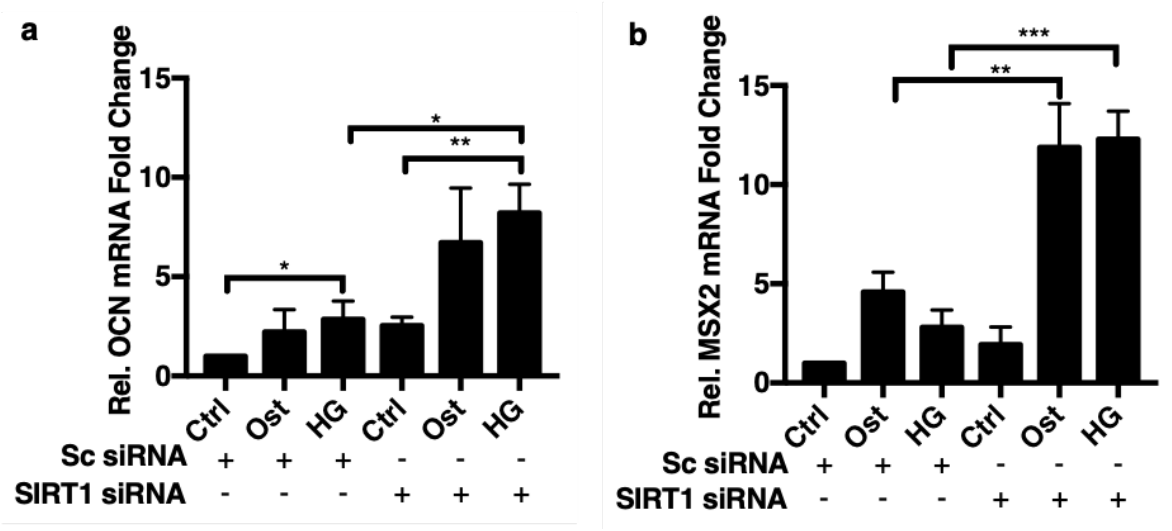

Fig. 3.16. SIRT1 siRNA increases downstream Runx2 marker expression. The effect of SIRT1 siRNA and scrambled siRNA on control (Ctrl), $CaCl_2$ and BGP osteogenic (Ost) and osteogenic with high glucose (HG) on downstream effector proteins in Runx2 pathway was investigated following 4 days of treatment after transfection. SIRT1 siRNA significantly increased expression of both **a)** OCN (n=4) (Two-way ANOVA, Tukey Post-Hoc test) and **b)** MSX2 mRNA compared to scrambled controls (n=4) (Two-way ANOVA, Tukey Post-Hoc test). $P<0.05$, $^{**}P<0.005$, $^{***}P<0.001$. Mean ±SEM.

3.3.9. SIRT1 inhibition increases cellular senescence under hyperglycaemic conditions

As demonstrated, SIRT1 activation reduces the induction of smooth muscle mineralisation. Recent studies have demonstrated the development of a senescence associated secretory phenotype concurrently alongside the development of calcification (311, 312) and therefore the effect of SIRT1 on cellular senescence was investigated.

β-galactosidase activity was again used to determine the presence of senescent cells, in association with cell cycle inhibitor expression analysis. SIRT1 activation via SRT1720 had little impact on cellular senescence in osteogenic conditions compared to untreated cells, however a significant decrease was observed in hyperglycaemic conditions compared to untreated ($p<0.0042$). Sirtinol inhibition of SIRT1 increased positive staining in osteogenic conditions by 50% ($p<0.0001$) and in hyperglycaemic conditions by over a third ($p<0.0030$) (Fig. 3.17a). SIRT1 siRNA knockdown was again used to confirm the pharmacological findings of Sirtinol. SIRT1 siRNA significantly increased β-galactosidase staining in both osteogenic ($p<0.0001$) and hyperglycaemic treatments ($p<0.0001$) by almost 6-fold with the scrambled siRNA demonstrating similar positive staining to untreated cells (Fig. 3.17b).

Following the finding that SIRT1 modulation could impact the development of hyperglycaemic induced senescence, the effect of SIRT1 on cell cycle kinase inhibitors was examined in order to tease out the mechanism underpinning the development of senescence within the diabetic mileu. p16 mRNA expression was significantly reduced when SIRT1 was activated in hyperglycaemic conditions ($p<0.0006$). Conversely SIRT1 inhibition increased hyperglycaemic induced p16 expression by almost a third ($p<0.0084$), with the control Sirtinol treatment significantly increasing p16 activation compared to untreated control ($p<0.0050$) (Fig. 3.18a).

p21 expression followed a similar trend to p16 expression, with a significant reduction in p21 in SRT1720 treatment under hyperglycaemic conditions compared to untreated ($p<0.0048$), with no significant difference between SRT1720 treated

control, osteogenic and hyperglycaemic treatments. Sirtinol treatment showed over a 50-fold increase of p21 expression in hyperglycaemic conditions compared to untreated hyperglycaemic conditions ($p<0.0001$), with a large increase in p21 mRNA expression compared when compared to Sirtinol control conditions ($p<0.0001$) (Fig. 3.18b).

Lastly, p53 expression was examined, with a significant decrease in expression observed in hyperglycaemic SRT1720 treated cells compared to hyperglycaemic untreated ($p<0.0079$), and a significant increase in hyperglycaemic Sirtinol treated cells when compared to hyperglycaemic untreated cells ($p<0.0004$) (Fig. 3.18c). Following this, acetylation of p53 promotor region was examined, as p53 promotor acetylation has been demonstrated to increase p21 expression, stabilise p53 expression and perpetuate a senescent phenotype (313). Enrichment of the lysine within the p53 promotor region was examined. SIRT1 activation significantly reduced enrichment in hyperglycaemic conditions ($p<0.0027$) (Fig. 3.18d), in concordance with the overall reduction of p53 mRNA when observed when treated with SIRT1 activator, SRT1720 (Fig. 3.18c).

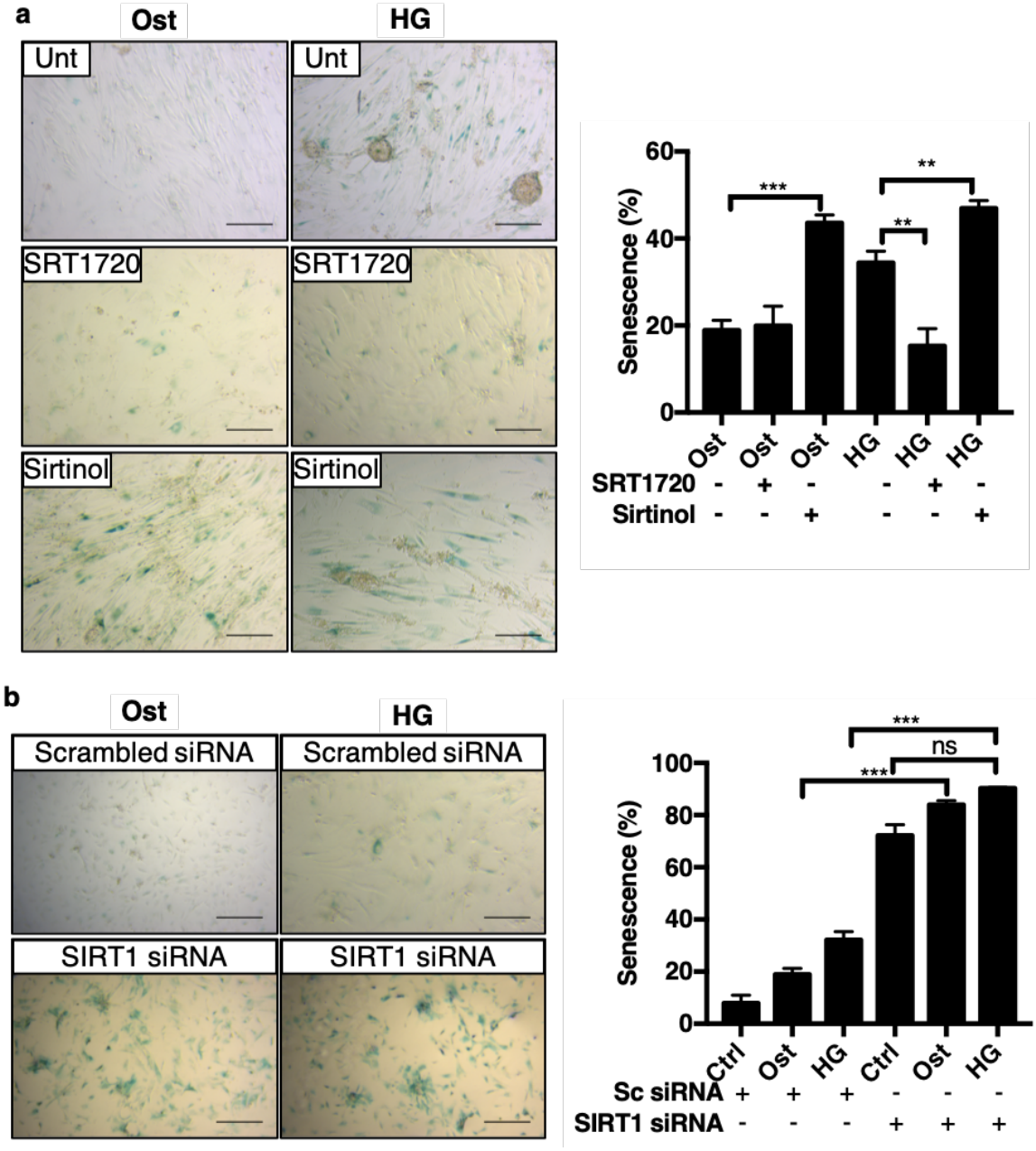

Fig. 3.17. SIRT1 modulation effects cellular senescence. The effect of SIRT1 activation via SRT1720 (0.5 μM) and SIRT1 inhibition via Sirtinol (10 μM) on cellular senescence was investigated following 4 days of treatment, with control (Ctrl), $CaCl_2$ and BGP osteogenic (Ost) and osteogenic with high glucose (HG) conditions and 0.1% DMSO used in untreated controls. SIRT1 siRNA was used to confirm Sirtinol results, with scrambled siRNA used as control. **a)** SIRT1 activation inhibits cellular senescence development under hyperglycaemic and osteogenic conditions, whereas SIRT1 inhibition via 10 μM Sirtinol significantly increased staining (n=4) (Two-way ANOVA, Tukey Post-Hoc test). **b)** SIRT1 siRNA increased cellular senescence regardless of glucose treatment, whereas scrambled siRNA showed no

significant increase in senescence (n=4) (Two-way ANOVA, Tukey Post-Hoc test). *P<0.05, **P<0.005, ***P<0.001 Scale Bars = 100µm. Mean ±SEM.

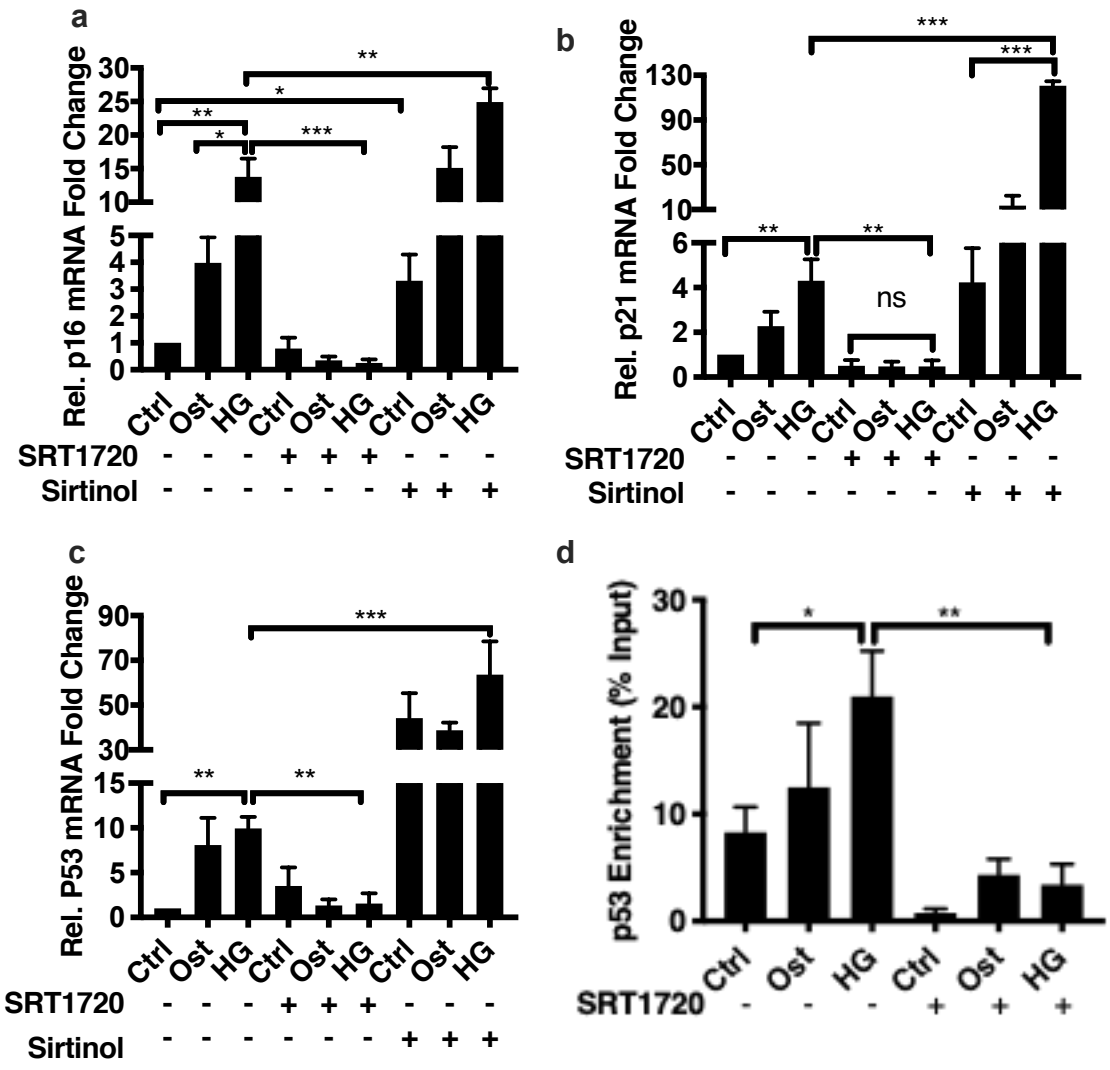

Fig. 3.18. SIRT1 modulation effects cellular senescence marker expression. The effect of SIRT1 activation via SRT1720 (0.5 µM) and SIRT1 inhibition via Sirtinol (10 µM) on cellular senescence was investigated following 4 days of treatment, with control (Ctrl), $CaCl_2$ and BGP osteogenic (Ost) and osteogenic with high glucose (HG) conditions and 0.1% DMSO used in untreated controls. **a)** p16 mRNA expression significantly reduced following SIRT1 activation and increased with SIRT1 inhibition as did (n=4) (Two-way ANOVA, Tukey Post-Hoc test) **b)** p21 (n=4) (Two-way ANOVA, Tukey Post-Hoc test) and **c)** p53 (n=4) (Two-way ANOVA, Tukey Post-Hoc test). **d)** p53 chromatin enrichment was significantly increased in hyperglycaemic conditions and reduced with SIRT1 activation (n=3) (Two-way ANOVA, Tukey Post-Hoc test). *P<0.05, **P<0.005, ***P<0.001. Mean ±SEM.

3.3.10. SIRT1 inhibition reduces smooth muscle cell proliferation and cell cycle progression

As previously reported, healthy, contractile vSMCs exhibit high levels of αSMA, allowing the cell to function as a contractile and motile unit. Previous data (Fig. 3.7a) suggest that this is lost during osteogenic differentiation under hyperglycaemic conditions, thus the effects of SIRT1 activation and inhibition on αSMA expression as a marker of contractility was compared between osteogenic and hyperglycaemic conditions (Fig. 3.19a).

SIRT1 activation with SRT1720, significantly increased αSMA expression in hyperglycaemic conditions at day 4 ($p<0.01512$), however no significant difference was observed between osteogenic and hyperglycaemic SIRT1 activated conditions. Sirtinol inhibition had the opposite effect, with a reduction in αSMA expression compared to untreated, in both osteogenic ($p<0.0199$) and hyperglycaemic treatments ($p<0.0108$) (Fig. 3.19b).

Since the phenotypic profile of a cell often affects its ability to proliferate and differentiate, the Alamar blue assay was conducted to assess its proliferative capacity. SIRT1 activation increased proliferation in hyperglycaemic conditions ($p<0.0247$), whereas SIRT1 inhibition significantly reduced proliferation in hyperglycaemic conditions compared to untreated ($p<0.0021$) (Fig. 3.20a).

To confirm the changes in cellular proliferation, cells were counted and seeded at equal density followed by four days of treatment, after which the number of nuclei within each sample was assessed by flow cytometry using propidium iodide. A significant increase in the number of nuclei between SRT1720 treated cells and untreated was in both control ($p<0.0144$) and hyperglycaemic conditions ($p<0.0015$) (Fig. 3.20b), correlating with the increase in proliferation previously noted (Fig. 3.20a). Conversely, a significant decrease in nucleus number was observed in Sirtinol treatment compared to SRT1720 treatment in hyperglycaemic conditions ($p<0.0028$).

Whilst nuclei number was assessed as a secondary marker of proliferation, nucleus area was also calculated to determine if cellular senescence was occurring between

G_0-G_1, as this would result in a doubling of the nuclear material but arresting of the cycle before the cell divided. However, no significant change was found with any treatments or media conditions (Fig. 3.20c).

Finally, cell cycle stage was assed via flow cytometry. The G1 phase within the cell cycle is often inhibited via p21 and p53 activation, and thus was reviewed to determine if this was the cause of cell cycle arrest within the model. Although none of the results were significant, the increasing trend towards greater G1 phase accumulation in Sirtinol treatment between osteogenic and hyperglycaemic conditions could suggest a possible increase in cell cycle arrest, compared to SRT1720 treated cells, in which the G1 phase percentage was lower than the control (Fig. 3.20d).

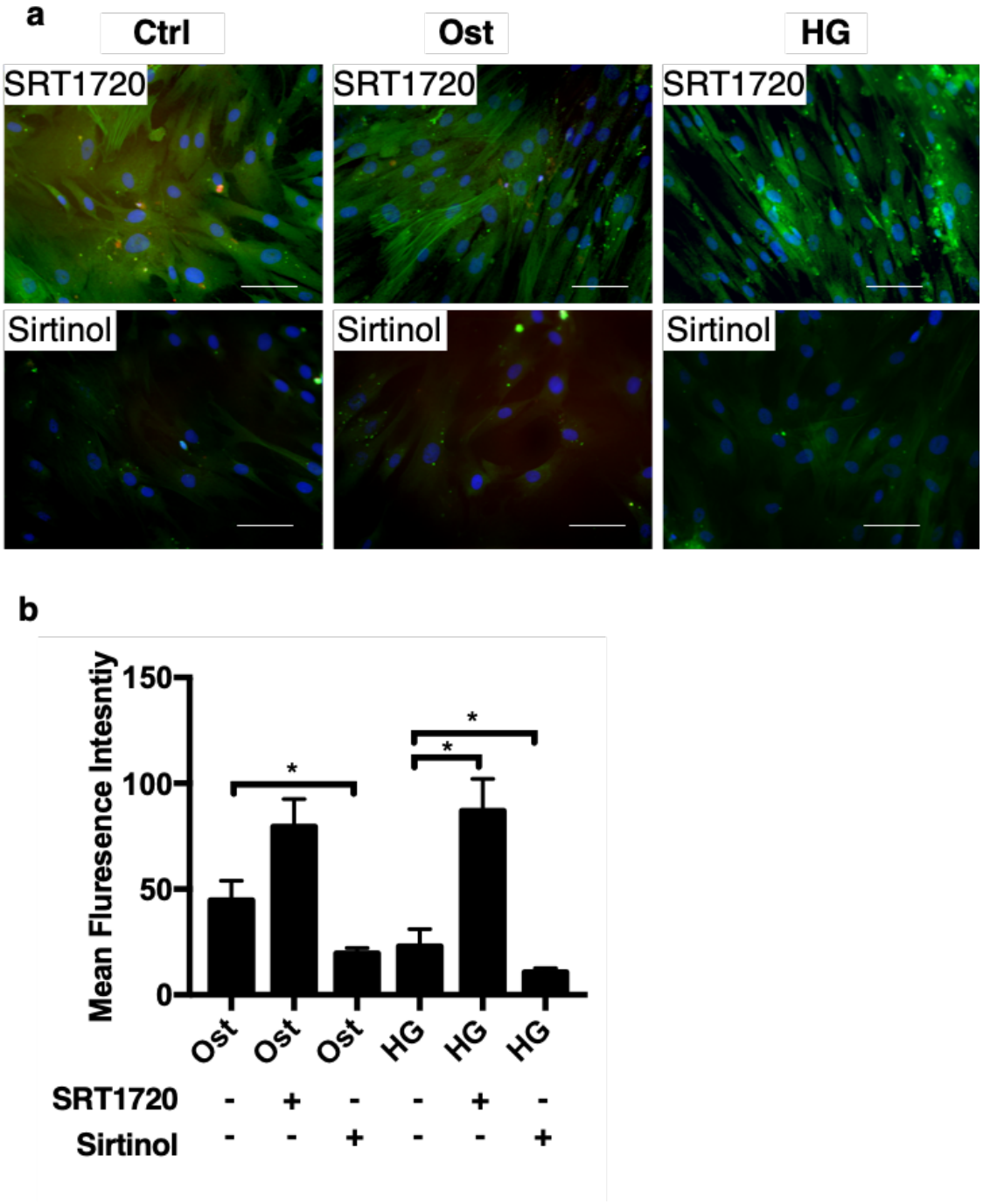

Fig. 3.19. SIRT1 modulation effects smooth muscle cell marker expression. The effect of SIRT1 activator SRT1720 and SIRT1 inhibitor Sirtinol on αSMA expression was investigated, with control (Ctrl), $CaCl_2$ and BGP osteogenic (Ost) and osteogenic with high glucose (HG) and 0.1% DMSO used in untreated controls. **a)** αSMA staining was conducted following 4 days of treatment and was significantly increased in all treatments with the addition of 0.5 µM SRT1720 and decreased with the addition of 10 µM Sirtinol **b**) this was confirmed by quantification (n=3) (Two-way ANOVA, Tukey Post-Hoc test). αSMA green, DAPI blue. *P<0.05. Scale Bars = 10µm. Mean ±SEM.

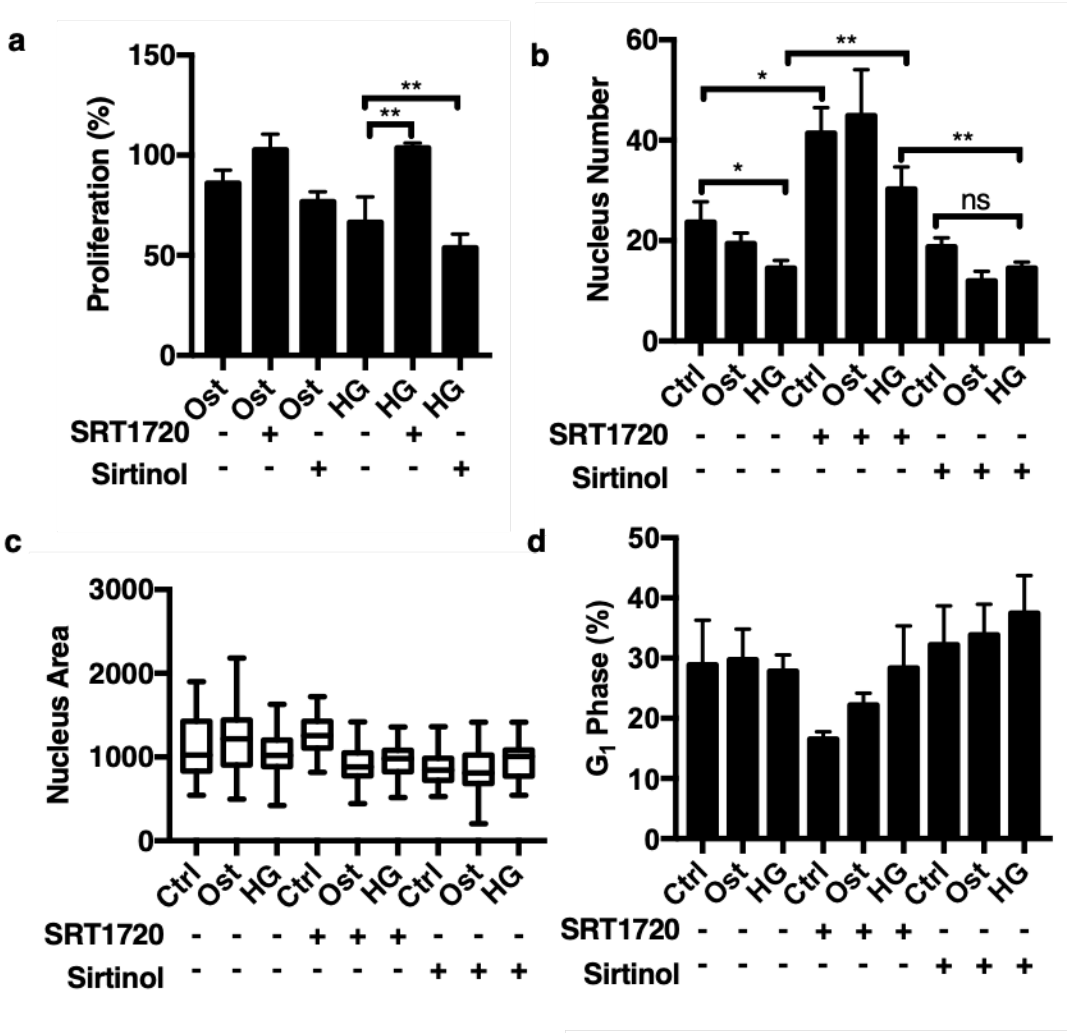

Fig. 3.20. SIRT1 modulation effects cellular proliferation and cell cycle progression. The effect of SIRT1 activator SRT1720 and SIRT1 inhibitor Sirtinol on proliferation and cell cycle was investigated, with control (Ctrl), $CaCl_2$ and BGP osteogenic (Ost) and osteogenic with high glucose (HG)and 0.1% DMSO used in untreated controls. **a)** Cellular proliferation was increased in all 0.5 μM SRT1720 treated conditions and decreased with the addition of Sirtinol (n=3) (Two-way ANOVA, Tukey Post-Hoc test). **b)** Nucleus number significantly instead with 0.5 μM SRT1720 treatment in hyperglycaemic conditions, and decreased in 10 μM Sirtinol treated conditions, however no difference was observed between the control and hyperglycaemic (n=4) (Two-way ANOVA, Tukey Post-Hoc test). **c)** Nucleus area showed no significant difference between treatments (n=4) (Two-way ANOVA, Tukey Post-Hoc test). **d)** Flow cytometry cell cycle analysis showed no change in G1 between untreated conditions, an increase was found in 10 μM Sirtinol treatment however this was not significant (n=4) (Two-way ANOVA, Tukey Post-Hoc test). *P<0.05, **P<0.005. Mean ±SEM.

3.4. Discussion

This is the first study to link the reduction of SIRT1 signalling with senescence and osteogenic differentiation within human vSMCs, correlating with diabetic tissue calcification, supporting the hypothesis that suppression of SIRT1 orchestrates the osteogenic trans-differentiation of vSMCs through a senescence pathway. These data show the convergence of both osteogenic and senescence pathways to support the process of mineralisation with the addition of glucose, inorganic phosphate and calcium *in-vitro,* which may be reflective of the diabetic environment *in-vivo*. Whilst this study focuses on the modulation of SIRT1 using pharmacological and genetic approaches, it is worth noting that a variety of SIRT1 polymorphisms have been linked to coronary artery calcification, cognitive impairment (314) and abnormal cholesterol metabolism and that specific SNPs have been demonstrated to increase long term survival in the total population, whereas interestingly, other SNPs have only shown a protective effect in overweight and obese subjects (303).

3.4.1 Marker expression correlates with reduction in SIRT1 expression

Firstly, this study demonstrates severe calcification occurring within the intima layer of the diabetic vessel wall, which is notably absent in the non-calcified IMA control. Histological staining shows the localisation of the calcification within the smooth muscle layer, with the dark Alizarin red staining correlating with the darkest parts of the αSMA stain, confirming the suggested calcification localisation. This development of calcification within the smooth muscle layer is further confirmed via the co-localisation of both Runx2 and OCN, which is absent within the IMA. Taken together these data suggest the correlation between the prevalence of calcification and the upregulation of proteins in association with the Runx2 pathway. With increased magnification to 40x, the localisation of OPN, OCN and Runx2 can be observed to be within the nucleus, as opposed to the IMA, where faint and diffuse Runx2 and OCN staining is located both with the cytoplasm and nucleus, suggesting an increase in osteogenic marker expression with the DM vessels. Previous studies have shown the nuclear localisation signal of Runx2 located on the c-terminus is activated through its acetylation via p300 (154), which neutralises the positive charge throughout the protein, making it more accessible to chromatin binding and subsequent transcription factor activation (315). With a lack of SIRT1 in these

diabetic samples, increased acetylation of Runx2 may occur in its reduction, leading to increased nuclear translocation and subsequently the development of calcification.

3.4.2. SIRT1 activation promotes negative regulation of the Runx2 pathway

To further investigate the mechanistical pathways involved, commercially available human coronary artery vSMCs from donors were purchased and grown under diabetic conditions; containing phosphate and calcium in the presence of high glucose to determine how SIRT1, or its absence, mediates the development of calcification. Whilst calcification was confirmed using previously reported markers of osteogenic differentiation including OPN, OPG, Msx2 and Alizarin red, the transcription factor Runx2 and associated pathway was examined under greater detail. Runx2 has fast emerged as a potent gene regulator associated with both tissue development and osteogenesis (316), determining the fate of cells, by regulating cell growth and differentiation down a variety of lineages (317, 318). Whilst null mutations of Runx2 can cause major defects during development, both loss and gain mutation have been pathologically associated with cancer (319), cardiovascular disease and skeletal malformations (320) depending on the biological timepoint. With Runx2 activation attributed to directly increasing OCN expression (142) the upregulation of both these proteins were reviewed in the presence of hyperglycaemic and osteogenic conditions. Both Runx2 and OCN expression increased in the presence of osteogenic conditions, and then further increased with the presence of hyperglycaemia, suggesting that hyperglycaemic conditions, which are manifested within diabetes, are likely to contribute to the development of calcification. With recent studies demonstrating the direct activation of ALP requiring Runx2 binding (298), the effect of osteogenic conditions on its expression was examined. ALP; an enzyme shown to catalyse reactions that induce calcification via the depletion of the potent calcification inhibitor, pyrophosphate, is suggested to be an early response to pathological stimuli such as calcium and phosphate. ALP activity was increased in osteogenic conditions compared to control and further increased in the hyperglycaemic environment. Since ALP activation is the first stage in the development of a calcified matrix, later timepoints were examined to determine if full calcification did develop under these conditions. Total cellular calcium content of the cells and associated matrix was assessed at day 21

alongside Alizarin red staining, both of which were upregulated in osteogenic conditions and again further upregulated in hyperglycaemic conditions, suggesting the link between the preliminary upregulation of ALP, Runx2 and Msx2 and the following matrix deposition. Whilst OPN and OPG expression was also examined, no significant change was observed at this earlier timepoint, with either the addition of osteogenic or hyperglycaemic media, suggesting there may be more to the control of the OPN-OPG axis than hyperglycaemia alone. Furthermore, both OPN and OPG are considered late stage markers of osteogenic differentiation, gained after treatment with high phosphate following the dramatic reduction of smooth muscle cell lineage markers (321-323) and thus a day 14 or day 21 timepoint might be more appropriate to observe a significant change in either proteins expression.

Since SIRT1 expression has been previously implicated in a range of both histone and non-histone target deacetylations, including senescence (324) and atherogenic pathways (325), its effect on the development on the Runx2 osteogenic pathway was examined. Activation of SIRT1 was achieved pharmacologically via SRT1720, whereas SIRT1 inhibition was achieved via both siRNA and the pharmacological inhibitor Sirtinol. SIRT1 activation promoted an abrupt inhibition of both Msx2 and Runx2 expression, leading to a downregulation of OCN expression and ALP activity, reducing the total matrix mineralisation and calcium content within the cells, correlating with previous animal studies which suggest SIRT1 could inhibit hyperphosphatemia induced calcification (249). The role of SIRT1 was further validated with the inhibition and genetic knockdown of SIRT1, the latter of which was sustained for 7 days. Runx2 activation was increased following the reduction of SIRT1, as were downstream markers OCN and ALP. Following 21-day treatment with Sirtinol, Alizarin red staining confirmed a significant increase in calcium matrix deposition, with cellular calcium five-times higher than cells treated only in hyperglycaemic conditions, suggesting the role of SIRT1 is increasingly important in the development of vascular calcification. This study extends and supports the previous rat findings that Runx2 activation can be negatively regulated via SIRT1 within vSMCs (249), however it is worth noting that studies in osteoblasts have been shown to be positively regulated by SIRT1, highlighting the differential regulatory properties of SIRT1 in different cell types (301).

3.4.3. Hyperglycaemia reduces expression of SIRT1

Another pathway in which this study and others (326, 327) hypothesise that SIRT1 could modify longevity is through glucose homeostasis. Since this study has demonstrated an inverse correlation between diabetic status and SIRT1 expression, a hyperglycaemic model was used to compare the direct effect of high glucose and increased calcium and phosphate on SIRT1 production. SIRT1 expression was reduced in osteogenic conditions but significantly reduced in hyperglycaemic conditions, with the expression of the remaining SIRT1 possibly being contained in the cytoplasm rather than in the nucleus thus inhibiting its activation, as previously observed in stressed endothelial cells (196) and further examined in Chapter 5. Increased glucose concentrations in the blood has been shown to produce pseudohypoxia (328) with glucose being quickly metabolised along the sorbitol pathway (329). Specifically, glucose is firstly reduced to the sugar alcohol sorbitol by aldose reductase, whilst NADPH is simultaneously oxidised to NADP+. Secondly, sorbitol is oxidised by sorbitol dehydrogenase to the ketonic monosaccharide fructose, reducing NAD+ to NADH, producing an increased concentration of NADH in the blood. This lack of NAD+ can be directly attributed to hyperglycaemia, causing a rate limiting step for SIRT1 activation, as without this co-factor SIRT1 is unable to deacetylate its targets. This hypothesis matches the diabetic blood assayed, as SIRT1 expression is significantly decreased when compared to healthy controls. (Fig. 4.1)

Relating this to the osteogenic pathway in diabetes, the Runx2 promotor region contains ten conserved lysine residues, all of which are possibly sites for acetylation. Furthermore, it is likely that osteogenic growth factors such as FGFs and BMPs (154) increase stability, acetylation and transcriptional activity of Runx2 via increased histone acetyltransferase activity via CBP and p300 protein levels, leading to an overall increase in acetylation. Under healthy conditions this balance would be restored via the activation of SIRT1 and subsequent deacetylation, however once the SIRT1 co-factor NAD+ is diminished via hyperglycaemia it is unable to competitively inhibit this acetylation, leading to an overactivation of the osteogenic differentiation pathway within the vSMCs (330). Since the diabetic patients within the study demonstrated a significant reduction in SIRT1 serum levels, the acetylation profile of the Runx2 promotor was examined. Gene

expression profiling combined with protein and ChIP analysis demonstrates not only a decrease in Runx2 expression as a direct result of SIRT1 activation, but also a decrease in promotor acetylation at H3K27Ac marks. Within hyperglycaemic conditions, the increase in Runx2 promotor acetylation correlated with a downregulation of SIRT1 expression in cells, suggesting that Runx2 activation may have a direct effect, or be directly influenced by the reduction of SIRT1 in vSMCs and contribute to their osteogenic differentiation.

Previous studies have suggested that minor allele carriers of specific SIRT1 SNPs have better glucose tolerance within overweight and obese patients (303), with little significant effect on healthy patients. This is correlated with mouse data, in which overexpression of SIRT1 in transgenic mice (331, 332) exhibits beneficial phenotypes such as improved glucose tolerance, indicating that specific SNPs, particularly those within the transcription factor binding site, may lead to a global overexpression of SIRT1, which would account for the increased tolerance to glucose in presence of both phosphate and calcium. These data are the first to suggest that the acetylation profile of Runx2 may be modulated within a diabetic model, suggesting a pathway by which SIRT1 may directly influence the activation of osteogenic trans differentiation within the vascular smooth muscle layer.

3.4.4. SIRT1 activation inhibits hyperglycaemia promoted loss of smooth muscle markers

Whilst changes to the overall vessel have been well documented in the diabetic vasculature, little research has been conducted on the morphological changes of vSMCs as a direct result of hyperglycaemic conditions. αSMA, a marker of contractile and healthy vSMCs was used to determine the phenotypic change of cells undergoing osteogenic treatment. Under control conditions the expression of αSMA maintained the straited spindle-like form, however once treated with osteogenic and hyperglycaemic conditions αSMA expression reduced, with cells becoming increasingly flattened and rhomboid shaped. SIRT1 activation allowed cells to maintain this spindle shape, with no significant decrease in αSMA expression observed between all SRT1720 treated cells. However, SIRT1 inhibition induced a greater morphological change within cells, with a significant reduction of αSMA and a greater number of cells losing their classic spindle-like shape (333).

Previous studies have demonstrated a quick increase in collagen fibre synthesis during hyperglycaemic treatment (334, 335), leading to the disorganisation of the fibres as they received mixed signals from both proliferative and osteogenic pathways, which this study confirms. Since the data presented in Chapter 4 confirmed the change in cellular morphology during hyperglycaemic treatment and in diabetic cells, the cell cycle and proliferation was assessed. Hyperglycaemic conditions induced no notable change in cells accumulating in G phase, however the nuclei number decreased after 4 days treatment, suggesting a reduction in the proliferative capacity in hyperglycaemic treatment, in-line with the hypothesis of glucose induced senescence, presented here and by others (336, 337). However, SIRT1 activation induced a significant increase in both nuclei number and overall proliferative capacity, suggesting that the cell cycle inhibition was reduced under hyperglycaemic conditions via SIRT1 activation. The opposite was confirmed with Sirtinol inhibition, with an increase in the number of cells arrested in G1 phase, suggesting an inhibition of the cell cycle, which may occur via the p16-Rb or p53 pathways (338).

3.4.5. SIRT1 activation inhibits development of a senescence associated secretory phenotype

Having demonstrated the morphological and phenotypic changes which occur during the osteogenic process, where vSMCs switch from a contractile, quiescent phenotype to a synthetic phenotype, thus acquiring an increased senescent capacity, the changes then manifest as a decrease in arterial compliance and an increase in arterial stiffness. Thus, whilst this study aimed to investigate the correlation between calcification and the modulation of SIRT1, it was important to establish, not only whether the morphological changes were a result of this relationship, but also if this was dependent on a senescence associated pathway. On a macro-level, SIRT1 has a wide array of targets which are linked to the modulation of the ‘senescence-associated secretory phenotype’ (324), which when acetylated can translocate to the nucleus, resulting in the development of premature cellular senescence. With this study and others confirming that the upregulation of hyperglycaemia (336) and hyperphosphatemia (339) leads to senescence via the p21 pathway, the effect of SIRT1 activation and inhibition was assessed. Pharmacological and genetic depletion of SIRT1 was shown to significantly increase

cellular senescence regardless of glucose or phosphate concentration within the media, suggesting a vital role for SIRT1 within the development of senescence. However, distinguishing whether the senescence or the calcification developed first was still unclear, as senescence has also been associated with vSMCs phenotypic changes alone. β-galactosidase staining, confirming lysosomal β-galactosidase accumulation was shown to appear at an earlier day 4 timepoint within untreated hyperglycaemic conditions and with the inhibition of SIRT1, compared to Alizarin red which was still negative at day 4 (data not shown). Therefore, it could be suggested that senescence is developing before the calcification. It may be that the downregulation of SIRT1, which was apparent from day 4 onwards, even in hyperglycaemic only treated cells, triggers the development of senescence, which in turn activates the vSMCs to differentiate into an osteogenic phenotype. This hypothesis is supported by the greater expression of Runx2 observed under day 4 in hyperglycaemic cells compared to normal glucose conditions, suggesting that Runx2 activation occurs more readily in the senescent environment. This is further confirmed by previous studies in mouse fibroblasts, in which overexpression of Runx2 induces greater positive β-galactosidase staining and a significant decrease in BrDu incorporation (340), which taken together, strengthens the findings that the senescent vSMC is a transient phenotype, increasing the sensitivity of these cells to begin the induction of calcification (167, 341).

Since SIRT1 expression has been long associated with a variety of proliferative and cell cycle pathways, the expression of both p16 and p21 was next examined in regard to the modulation of SIRT1. p53, commonly referred to as a tumour protein, is a tetrameric transcription factor, tightly regulated by posttranscriptional modifications (342). Regarded as a powerful tumour suppressor gene, it has the ability to inhibit cellular proliferation and induce immediate apoptosis via cell cycle arrest. Both p53 and its inducible cyclin-dependent kinase inhibitor p21 were significantly upregulated in hyperglycaemic conditions in which SIRT1 was diminished, and then further upregulated when SIRT1 was inhibited via Sirtinol. It has been shown previously that p53 acetylation is needed to induce the transactivation of p21 alongside other senescence markers, and that the deacetylation of p53 via SIRT1 reduces its stabilisation and half-life, therefore decreasing its overall cellular activity (343, 344). Recent research has demonstrated that within both neurons (345) and HUVECs (45) a hyperglycaemic environment

increases the acetylation of the p53 promotor, however the effect within the vSMCs is unknown. This is the first study to demonstrate that hyperglycaemic conditions can significantly increase the acetylation of the p53 promotor region around H3K27Ac marks, which correlates with the elevated p53 and p21 mRNA expression found in the *in-vitro* calcification experiments. To confirm that the modulation of p53 promotor acetylation was directly linked to SIRT1, SRT1720 activated cells were examined via ChIP and exhibited a significant decrease in enrichment, regardless of glucose or phosphate presence. Possibly suggesting that the p53 promoted senescence is more directly linked to the activation of SIRT1, rather than indirectly from the diabetic environment of the cells.

As SIRT1 is reduced within the diabetic patient, p53 is sustained at a constant state of acetylation and production, thus enhancing the production of the p53 target protein p21, within the cell (346). Since the promotor of SIRT1 contains two response elements to p53, it has been suggested that p53 may work to reduce SIRT1 expression in a negative feedback loop, thus propagating not only its stability but its production of p21, inducing cellular senescence. Genome-wide association studies have consistently found an association of p16 with increased diabetic risk (347). p16 is a tumour suppressor gene that inhibits cyclin D-dependent protein kinases, prohibiting G1-S transition within the cell cycle via the Rb pathway. Thus, it was next of interest to establish whether p16 expression was altered in the model. The data demonstrates that p16 expression was increased in both hyperglycaemic conditions and under pharmacological and genetic SIRT1 inhibition. An increase in p16 production has been reported when p300 acts to acetylate the appropriate sites on its promotor (348), findings which are supported by this study, which shows that a reduction of the deacetylase SIRT1 leads to an increase of p16 expression; however the mechanism by which this occurs remains to be elucidated. Based on the current findings, hyperglycaemic inhibition of SIRT1 leads to the increased production of p16 and p21, as well increased acetylation of p53, leading to a promotion of the senescent phenotype in vSMCs, acting as a basis for the development of smooth muscle calcification (Fig. 3.21).

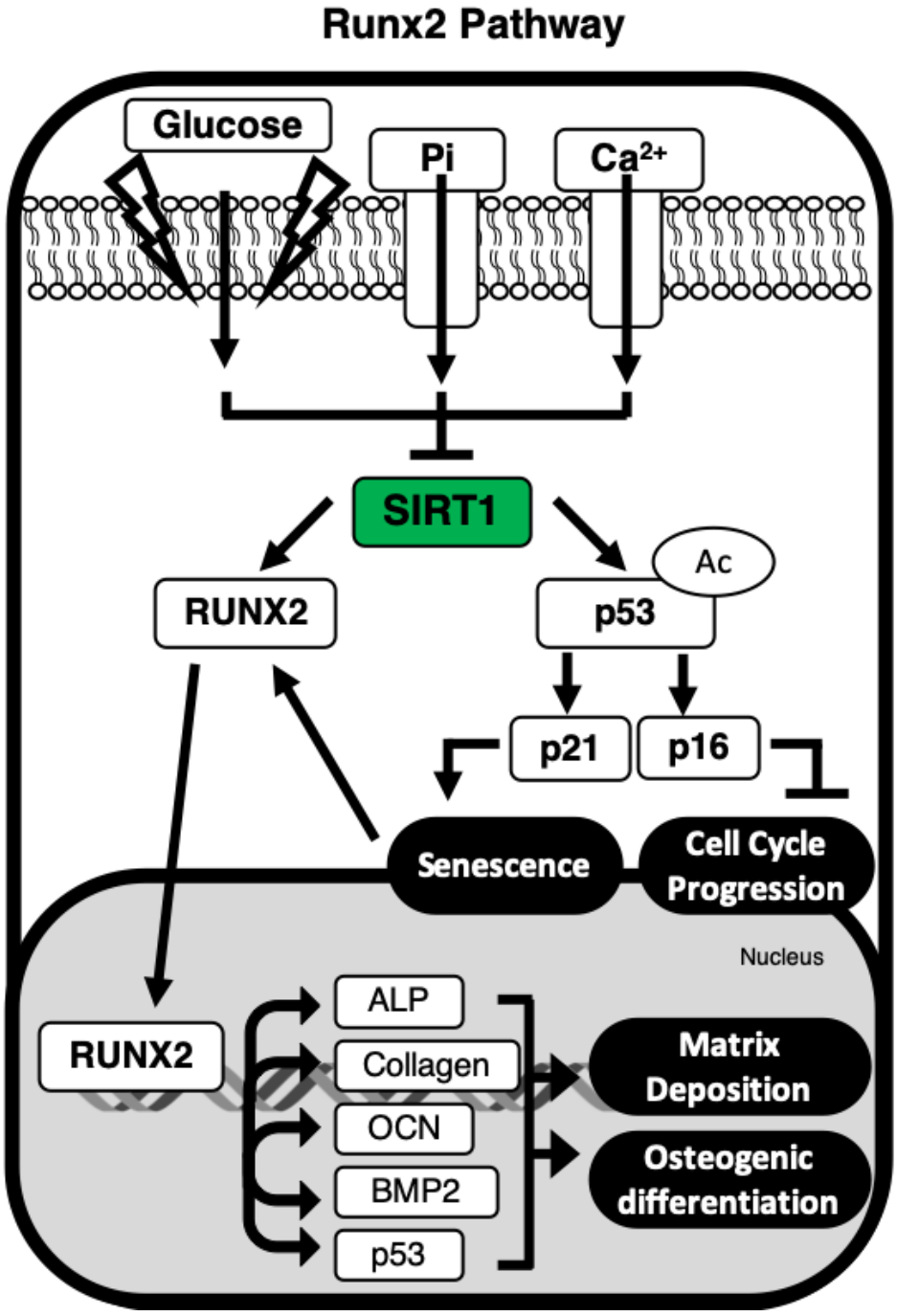

Fig. 3.21. Suggested model for the role of SIRT1 in the Runx2 calcification pathway. Hyperglycaemia coupled with hyperphosphatemia and increased cellular calcium leads to a decrease in SIRT1 expression. A lack of SIRT1 allows for increase p53 activation, resulting in p16 and p21 expression both of which upregulate cellular senescence and inhibit cell cycle progression. Cellular senescence increases Runx2 activity, leading to its nuclear translocation and binding to multiple promotor regions of osteogenic genes, which results in an increase in a calcified matrix deposition and osteogenic differentiation.

3.5 Limitations

Whilst this study clearly demonstrates the protective effect SIRT1 has on smooth muscle mineralisation, it is not without its limitations. Firstly, the use of a single timepoint to assess the expression of mRNA transcripts for OPN, OPG and OCN may have missed their expression as later stage osteogenic markers, which are upregulated once hydroxyapatite crystals have formed in response to the cell trying to inhibit the osteogenic process. Multiple timepoints for mRNA and protein analysis should be taken, however with the use of siRNA, SIRT1 suppression is not sustained beyond 7 days and therefore late timepoint expression changes could only be confirmed with small molecule modulation alone. Secondly ,the lack of long term genetic modification to overexpress and inhibit SIRT1 can be seen as a limitation. SIRT1 overexpression plasmids should be constructed in order to corroborate the SIRT1 activator data at day 21, through alizarin red staining and osteogenic differentiation markers of the cell, to confirm the change in SIRT1 expression is solely responsible for this effect, rather than a mechanism within the activator alone.

3.6. Conclusion

In conclusion, these data presented in Chapter 3 has demonstrated the protective effect of SIRT1 in a hyperglycaemic environment regarding the reduction of calcification development and suggests a relationship between calcification and cellular senescence. It could be suggested that the reduction of SIRT1 within a diabetic environment results in the induction of calcification, which acts in synergy with the induction of cellular senescence exacerbated by the presence of hyperglycaemia, forming a transient state in which vSMCs can undergo osteogenic differentiation. It will next be of interest to identify specific SNPs that are present within osteogenic and non-differentiating cells, and to probe further into the exact pathway by which damage sustained during hyperglycaemia within the vessel is modulated via SIRT1, which will be presented in the following chapters of this thesis.

4. Diabetic vascular smooth muscle cells exhibit increased migration and proliferation through activation of focal adhesion kinase and associated proteins via the ERK pathway, which can be attenuated via the activation of SIRT1

4.1. Introduction

4.1.1. The pathological impact of diabetes on the vasculature

Cardiovascular disease, of which atherosclerosis is a key pathology, is a leading cause of morbidity and mortality within diabetic patients, accounting for 1 in 7 of all deaths worldwide in the last two decades (273). Within the vasculature, smooth muscle and endothelial cells throughout the vessel wall constantly respond to repetitive injury, such as hypertension or DNA damage, leading to their dysfunction and dedifferentiation (349, 350). Healthy vSMCs exist in a quiescent contractile state in which stretch and contractile factors such as RhoA and calponin are upregulated. However, when the cell undergoes chronic stress and damage (351), it responds by downregulating its contractile phenotype and increasing its proliferative and migratory properties through pathways such as MAPK and PI3K (352, 353), in an attempt to repair and protect against future damage. Whilst both the contractile and synthetic phenotype exist as two extreme ends of the scale, the differentiation scale is a spectrum, with a mix between both phenotypes often present within a vessel (112). Once the vSMCs are dedifferentiated and proliferating at an increased rate, intimal hyperplasia can occur, leading to stenosis of the vessel, often resulting in decreased blood supply and the need for surgery and or amputation (354, 355).

Whilst the development of atherosclerosis and stenosis of the vessel can be attributed to three main modifiable risk factors; obesity, diabetes and smoking, the underlying molecular pathology remains unclear, with the current understanding being an interaction of multiple pathways regulating the increase of inflammatory cytokines and growth factors, leading to an extremely complex molecular network (356-359). However, recent studies have shown that there is a significant genetic

risk; independent of the three main risk factors described above, with smooth muscle differentiation and atherosclerotic development occurring under specific molecular signatures (360). Suggesting that there may be a more intrinsic reason why some patients are predisposed to such a poor outcome, something which will be addressed in the following chapter.

4.1.2. Role of cellular cytoskeletal reorganisation and focal adhesion formation in diabetic vessels

Smooth muscle cell migration plays an essential role in the tube formation of blood vessels during development (361, 362) and has been recently implicated in a variety of vascular pathologies, including pulmonary arterial hypertension (363, 364) and coronary artery disease (365), in which the intimal layer within the vessel thickens, reducing the lumen size and increasing pressure. Smooth muscle thickening may stem from the migration of proliferating progenitor cells such as CVCs to the site of damage (134), or the recruitment of circulating precursor cells into the smooth muscle layer via adhesion proteins.

In response to adhesive proteins within the ECM, cells form focal adhesions at the leading edge to strengthen their attachment to the ECM and induce retraction at the opposite rear edge (366, 367), dragging the cells towards to the focal adhesion via a mesh of F-actin, attached to the nucleus via intermediate filaments and microtubules (368). Once migrated forwards, the older focal adhesions are dismantled and new ones formed, following this cycle until the cell finishes migrating (369, 370). With increased damage of the vessel observed in diabetic patients, the normal, healthy basement membrane; composed of laminin and collagen IV is disrupted and the damaged areas filled with fibronectin. It is believed that this fibronectin mediates integrin cell surface receptors, activating focal adhesion formation proteins such as FAK and vinculin (371), leading to increased vSMC migration and proliferation, eventually resulting in the development of atherosclerosis and vessel stenosis. Whilst the increased migration of cells can be directly attributed to the formation of focal adhesions and the remodelling of the actin cytoskeleton, the activation and upregulation of the key motility and proliferation pathways such as MAPK and AKT (372-375) also play a key role in the vascular remodelling and widespread development of atherosclerosis. More recently these

pathways have been examined as possible druggable targets, with Metformin recently shown to reduce both ERK 1/2, PKC and ROS production in both mouse and clinical human models (376-379).

4.1.3. SIRT1 as a possible treatment for reduction of smooth muscle cell proliferation and migration in diabetes

One such possible target for the reduction in aberrant vSMC migration and proliferation may be the histone deacetylase SIRT1. With recent experimental data demonstrating the role of SIRT1 in upregulating adiponectin (380, 381), which plays a crucial role in protecting against insulin resistance and atherosclerosis within the adipose tissue and the loss of SIRT1 impairing pancreatic beta cell insulin secretion and glucose sensing (382), SIRT1 has become a promising candidate as a multi-organ diabetes treatment (383). As proliferation of vSMCs is known to increase under hyperglycaemic conditions (384) which also increases their migratory response towards insulin growth factor (385); both of which are increased in diabetes. SIRT1 may be able to blunt this effect through hyperglycaemic control, therefore reducing the remodelling of the vessel and ultimately reducing diabetic associated vascular dysfunction.

4.2. Aim and Objectives

The overall aim of this chapter was to determine the differences between diabetic and healthy smooth muscle cells, both on a morphological and molecular level.

i) Firstly, to elucidate if diabetic cells exhibited different morphological and physiological traits when compared to healthy vSMCs and if this affects their proliferative and migratory ability.

ii) Secondly this study sought to establish if diabetic cells produced greater focal adhesions compared to healthy vSMCs.

iii) And finally, this study aimed to determine if SIRT1 modulation could affect this development of focal adhesions and proliferative and migratory properties of diabetic vSMCs.

4.3. Results

4.3.1. Diabetic patients exhibit decreased SIRT1 levels

Vessels harvested from type II diabetic patients undergoing lower limb amputation were compared to IMA tissue leftover from CABG surgery. Von Kossa staining; shown in black, positively stained for phosphate deposits within the diabetic vessels which was localised to the smooth muscle layer and was negative in the IMA controls, demonstrating the vessel was calcified (Fig. 4.1a). Positive SIRT1 staining was detected in the IMA vessel in black, localised to both the smooth muscle layer and the endothelial layer, whilst being reduced in the diabetic vessel (Fig. 4.1b).

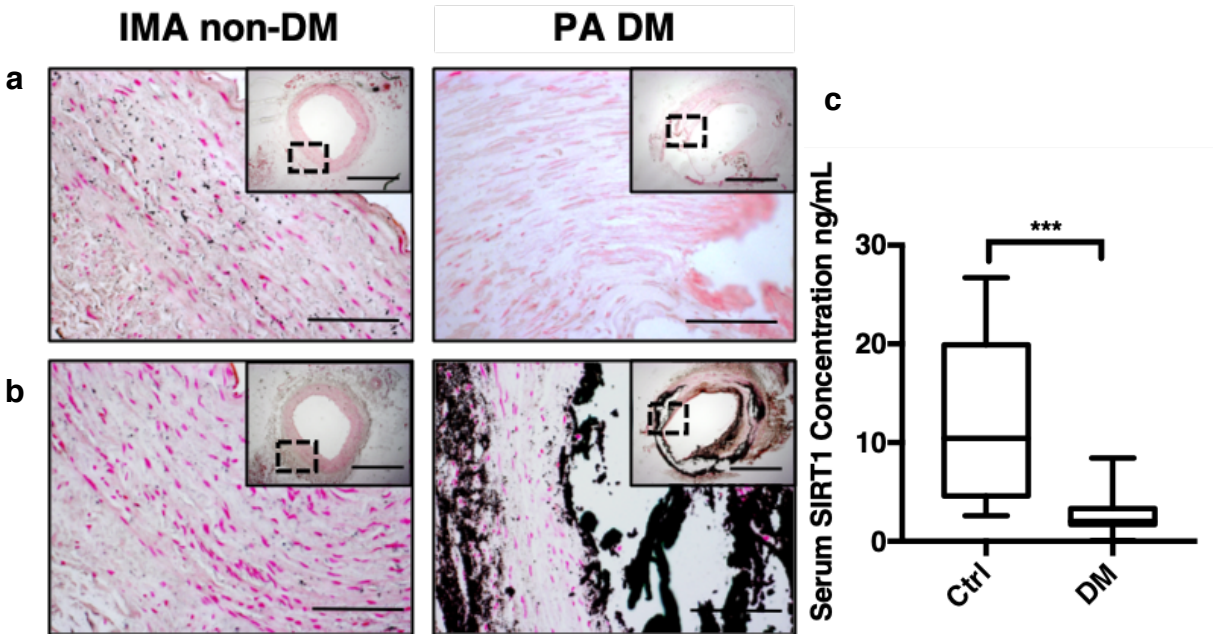

Fig. 4.1. Diabetic patients exhibit a decreased level of SIRT1. Vessels harvested from DM patients undergoing limb amputation and healthy controls from IMA leftover after CABG surgery. **a)** Diabetic vessels exhibit increased phosphate deposition in black, typical of vessel calcification, whereas IMA showed no positive staining (n=6). **b)** Vessels were stained for SIRT1 in black (n=6). **c)** Serum taken from diabetic patients exhibited significantly less SIRT1 than healthy controls when assessed via ELISA (n=20) (Mann-Whitney Unpaired Test). *P<0.05, **P<0.005 ***P<0.001. Scale bars = 200µm/20µm Mean ±SEM.

Since SIRT1 expression was confirmed to be reduced within the vessel, SIRT1 expression within the serum was also measured to confirm a system-wide reduction in SIRT1. Serum from diabetic patients was significantly reduced when compared to healthy controls ($p<0.0001$), correlating with vSMCs SIRT1 expression (Fig. 4.1c).

Following conformation of calcification within the patient's vessel via immunohistochemistry, 6 independent patient vSMCs were extracted from vessels, and cultured. vSMCs were stained with αSMA to confirm smooth muscle cell phenotype, with vSMCs from healthy controls also stained as a control (Fig. 4.2a). vSMCs were then stained with SIRT1 to determine expression. SIRT1 expression was reduced in diabetic vSMCs compared to non-diabetic vSMCs (Fig. 4.2b). mRNA (Fig. 4.2c) and protein expression (Fig. 4.2d) confirmed a significant reduction in SIRT1 expression when compared to non-diabetic vSMCs ($p<0.0022$) ($p<0.0022$) respectively.

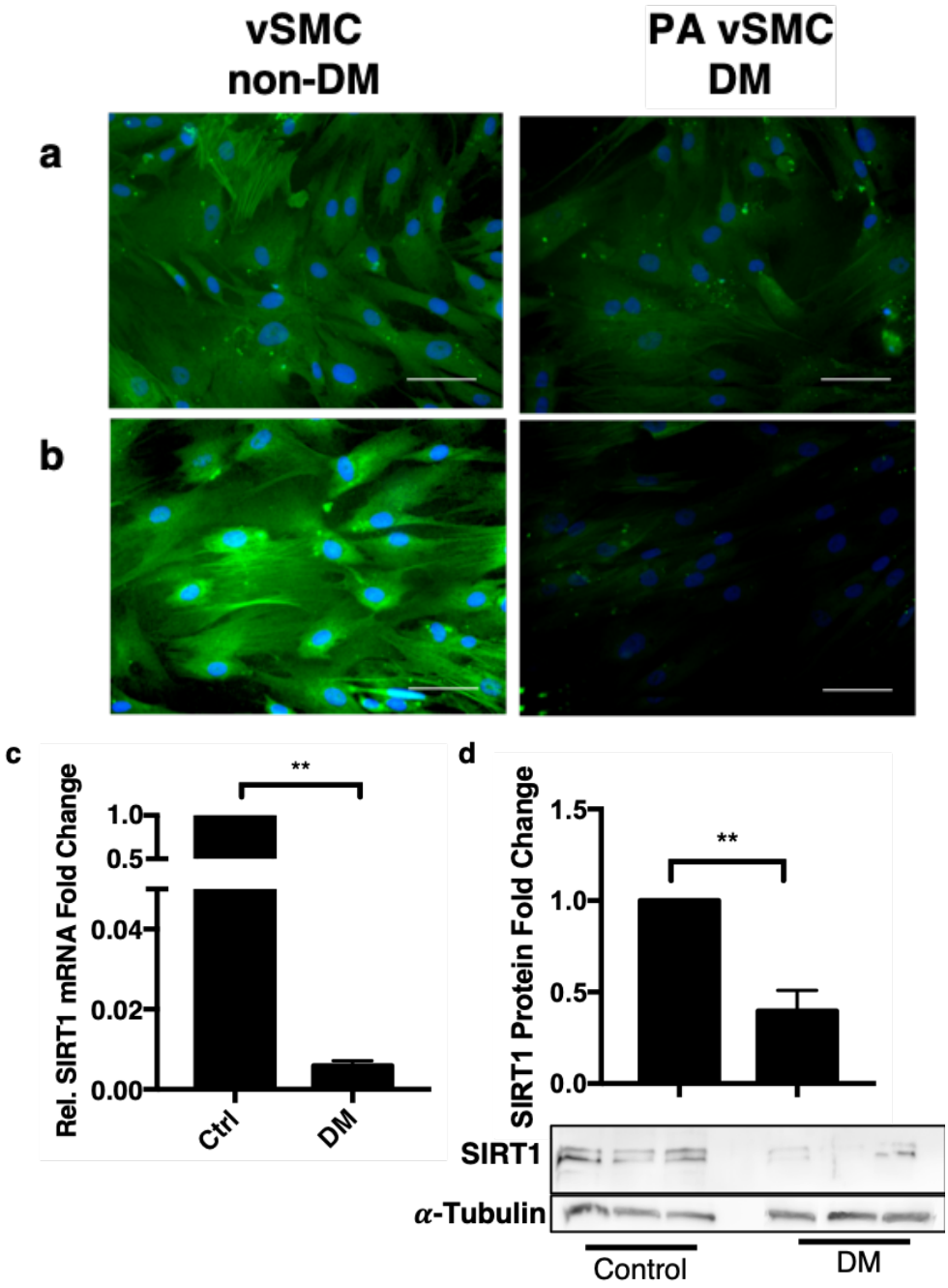

Fig. 4.2. Diabetic patient vSMCs exhibit a decreased level of SIRT1. Healthy vSMCs were purchased and DM vSMCs were harvested from diabetic vessels following DM patients undergoing limb amputation. Both cell groups were cultured in 5.5mM glucose until 80% confluence and fixed or harvested for further analysis. **a)** vSMCs stained for αSMA to confirm presence of vSMCs only (n=6) (Unpaired T-test), **b)** cells were stained for SIRT1 in green, which is decreased in the DM vSMCs compared to healthy vSMCs (n=6). **c)** SIRT1 mRNA and **d)** protein was significantly reduced in DM vSMCs compared to healthy vSMCs (n=6) (Unpaired T-test). SIRT1 green, DAPI blue. *P<0.05, **P<0.005 ***P<0.001. Scale Bars = 10µm. Mean ±SEM.

4.3.2. Morphological differences between diabetic and non-diabetic vascular smooth muscle cells

Cells were harvested from donor vessels as described within Chapter 2 and cultured either in control conditions; 5 mM DMEM supplemented with 10% FBS, or high glucose conditions; 25 mM DMEM supplemented with 10% FBS. Important to note; unlike conditions described in Chapter 3 and Chapter 5, cells were not supplemented with $CaCl_2$ or BGP in culture.

vSMCs derived from non-diabetic origin clearly exhibit the 'hill and valley' morphology, however vSMCs derived from diabetic patients displayed morphological differences, with a more dense and disorganised spread (Fig. 4.3a). The actin-based cytoskeleton morphology was compared with and without four days pre-treatment with SIRT1 activator; SRT1720. The cytoskeleton of DM vSMCs appears more rhomboid-like, with the non-diabetic vSMCs appearing more classically spindle shaped. When comparing cytoskeleton organisation, non-diabetic cells appeared more aligned and organised, with longer straighter F-Actin fibres, whereas diabetic vSMCs exhibited a more disorganised network of shorter fibres facing many directions and often layered on top of each other. With the addition of the SIRT1 activator SRT720, the F-Actin seemed to align more under both control and high glucose conditions, with fibres seeming to be longer and more uniform, comparable to the observation of non-diabetic cells (Fig. 4.3b).

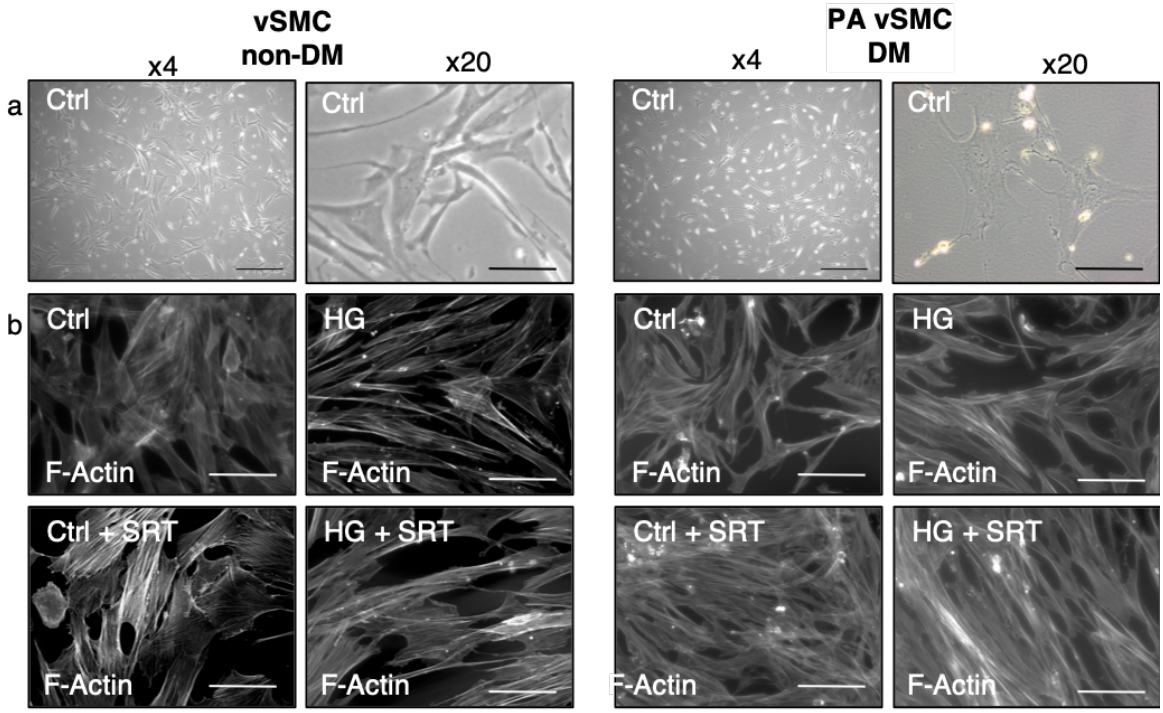

Fig. 4.3. Photomicrographs of diabetic and non-diabetic vSMCs. Diabetic vSMCs exhibit changes in morphology compared to healthy vSMCs. Diabetic cells were explanted from patients undergoing lower limb amputation and grown out from vessels in culture before culturing to 80% confluence and imaging. Cells were cultured in 5.5mM glucose (Ctrl), 25mM glucose (HG) with either 0.1% DMSO or 0.5 µM SRT1720 treatment for 4 days prior to imaging. Control cells purchased from Caltag were also grown until 80% confluence and imaged. **a)** Diabetic vSMCs exhibit a decrease in 'hill and valley' morphology when compared to healthy vSMCs, and at high however DM vSMCs do not appear spindle-like, rather rhombus shaped (n=6). **b)** F-Actin stained with phalloidin demonstrates decreased organisation of the actin-based cytoskeleton which appears to be better organized in the healthy controls. (n=6). Scale bar=10µm.

4.3.3. Diabetic vascular smooth muscle cells exhibit increased proliferative capacity

Cells from diabetic and non-diabetic vessels were seeded at equal densities and cultured in normal glucose (5 mM) or high glucose (25 mM) for 7 days. Proliferation was determined by measurement of the non-toxic reducing agent Alamar blue. Diabetic vSMCs cultured in both control ($p<0.0209$) and high glucose ($p<0.0002$) proliferated at a significantly greater rate than the non-diabetic vSMCs over 7 days. The addition of SIRT1 activator SRT1720 to diabetic vSMCs reduced proliferation by 5% under control conditions after 7 days, and by almost 10% in high glucose conditions, however neither of these were significant (Fig. 4.4a).

Since low levels of NO seem to favour proliferation (386) and SIRT1 is known to increase overall production of NO, the Griess assay was used to determine NO generation from cells cultured for 4 days in control conditions. NO was reduced by almost half in the diabetic vSMC media compared to non-diabetic vSMCs ($p<0.0001$), however with the inclusion of SIRT1 activator SRT1720, there was a significant increase NO production within diabetic vSMCs ($p<0.0001$), which was not significantly different to non-diabetic patients ($p<0.3944$) (Fig. 4.4b).

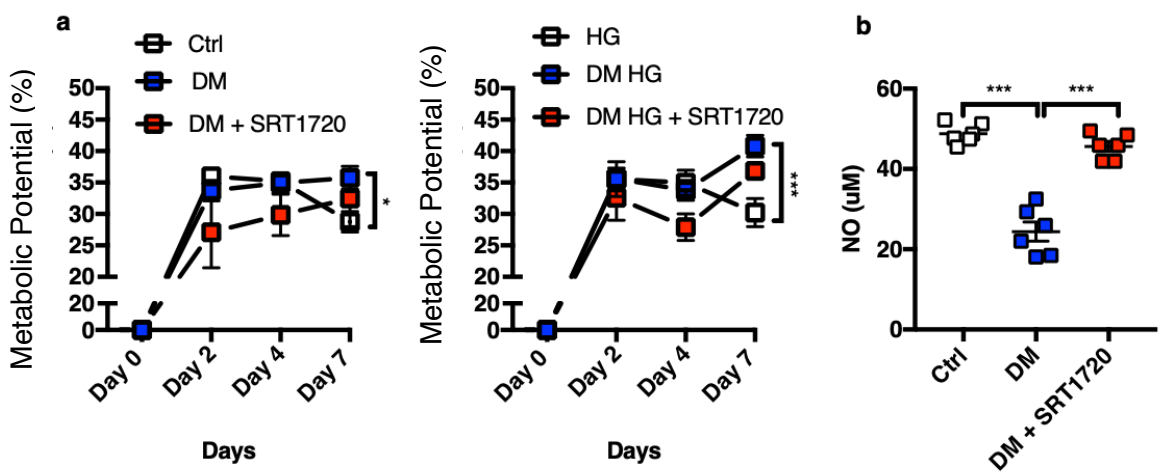

Fig. 4.4. Diabetic vSMCs exhibit increased proliferation and decreased nitric oxide availability. Cells harvested from DM vSMCs were compared to healthy controls. Cells were cultured in 5.5mM glucose (Ctrl), 25mM glucose (HG) with either 0.1% DMSO or 0.5 µM SRT1720 treatment. **a)** Cells were seeded at equal densities and proliferation was measured over a week via the Alamar blue assay. DM vSMCs proliferation was significantly increased compared to healthy vSMCs, addition of SIRT1 activator 0.5 µM SRT1720 reduced this after 7 days. DM vSMCs grown in high glucose media exhibited significantly more proliferation when compared to normal glycaemic conditions and proliferated significantly more than healthy vSMCs after 7 days. SIRT1 activation reduced DM vSMC proliferation via 5% (n=6) (Two-way ANOVA, Tukey Post-Hoc test). **b)** NO released into the media after 4 days of culture was analysed via the Griess assay. NO was significantly reduced in DM patients compared to control; both of which were supplemented with 0.1% DMSO to equivalate toxicity, and 0.5 µM SRT1720 increased NO by 50% (n=6) (One-way ANOVA, Tukey Post-Hoc test). *P<0.05, **P<0.005 ***P<0.001. Mean ±SEM.

4.3.4. Diabetic induced migration and adhesion within smooth muscle cells is reduced under SIRT1 activation following hyperglycaemic treatment

As cells from diabetic origins have been reported to exhibit increased adhesive and migratory properties in order to form dense atherosclerotic plaques within a shorter time frame (387, 388), the vSMCs harvested from diabetic patients were examined for these traits.

Equal densities of cells were seeded for 45 minutes and 3 hours, before washing, fixing and counting, to determine their adhesive properties. After 45 minutes, diabetic vSMCs demonstrated significantly greater adhesion compared to cells of a non-diabetic origin in control glucose conditions ($p<0.0001$). High glucose treated diabetic vSMC exhibited significantly greater adhesion than both diabetic cells grown in control glucose media ($p<0.0001$) and non-diabetic vSMCs ($p<0.0071$), with the addition of SIRT1 activator significantly reducing the diabetic vSMCs adhesion by 10% ($p<0.0001$). Following incubation for 3 hours, this trend was reversed in the control treatment, with non-diabetic vSMCs demonstrating increased adhesion, which was significantly greater than both diabetic vSMCs ($p<0.0150$) and diabetic vSMCs treated with SRT1720 ($p<0.0095$) (Fig. 4.5a).

Since diabetic patient vSMCs exhibit increased invasive properties within the vessels which leads to faster development of atherosclerosis, with a greater chance of vessel stenosis, the migratory capacity of diabetic vSMCs determined using a modified Boyden chamber technique in which cells migrate through a semi-permeable membrane, with PDGF-BB used as a chemoattractant. In non-diabetic vSMCs, increased glucose concentration within the media induced no change in their migratory properties after six hours. However, when compared to vSMCs from a diabetic origin, the migration of diabetic vSMCs was found to be 50% higher in the control media ($p<0.0001$), and even greater within the high glucose treatments ($p<0.0001$). Following SIRT1 activation, no change in migratory property was observed in diabetic vSMCs treated with control media compared to those left untreated. Furthermore, SIRT1 activated diabetic vSMCs demonstrate significantly greater migration than the vSMCs from non-diabetic origin ($p<0.0001$). Conversely, once treated with high glucose and SRT1720, diabetic vSMCs significantly reduced their capacity by almost a fifth after 6 hours ($p<0.0003$) (Fig. 4.5b).

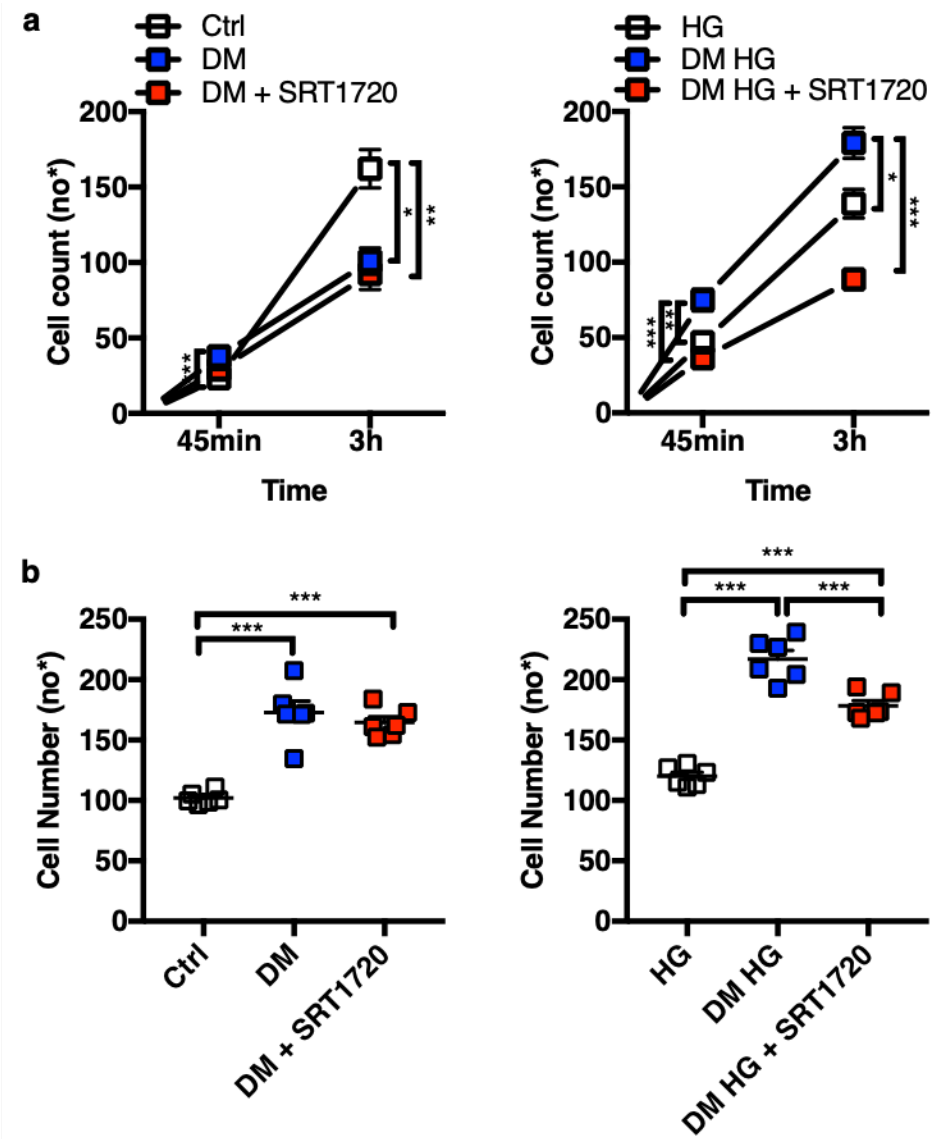

Fig. 4.5. Adhesion and migration of diabetic vSMCs was reduced with SIRT1 activation. Cells harvested from DM vSMCs were compared to healthy controls. Cells were cultured in 5.5mM glucose (Ctrl), 25mM glucose (HG) with either 0.5 µM SRT1720 or 0.1% DMSO to equivalate toxicity. **a)** Cells were counted and seeded in equal densities in 24 well plates and left to adhere. Adhesion was confirmed over 3 hours. Under normal glucose conditions DM vSMCs adhered significantly less than healthy vSMCs, with SIRT1 activation having no significant impact on adhesion. High glucose treatment increased DM vSMC adhesion via 50% after 3 hours, with a significant reduction in adhesion with SIRT1 activation (n=6) (Two-Way ANOVA, Tukey Post-Hoc test). **b)** A modified Boyden chamber was used to measure cell migration. Cells were counted and seeded at equal densities within the top chamber of the plate. DM cell migration was significantly higher in both control and hyperglycaemic treatments compared to healthy vSMCs. SIRT1 activation reduced migration in hyperglycaemic conditions only (n=6) (One-way ANOVA, Tukey Post-Hoc test). *P<0.05, **P<0.005 ***P<0.001. Mean ±SEM.

4.3.5. Focal adhesion formation is reduced following SIRT1 activation

Previous studies have demonstrated the link between glucose concentration and focal adhesions within a diabetic setting (389, 390), and since a reduction in focal adhesions has been shown to reduce the migratory properties of vSMCs, the role of SIRT1 on focal adhesion production was examined. Immunofluorescence was used to establish the expression of F-Actin and vinculin; the latter, a cytoskeleton associated protein which directly controls focal adhesion formation with actin (391).

Staining of vSMCs from a diabetic origin showed an increase in positive vinculin staining when cultured in high glucose media for 4 days, with a remodelling of the spread of vinculin adhesions appearing to move from the tips of the cells to the centre of the cells, where they became less spindle-like and more rhomboid shaped. Comparatively, when localising vinculin in cells from a non-diabetic origin, although overall vinculin staining was much lower, the focal adhesion formations did not move from the tips of the cells, even under high glucose conditions. The role of SIRT1 in both control and high glucose conditions was also examined by pre-treating the cells for 4 days with SIRT1 activator; SRT1720, followed by fixing and staining.

Within the cells from a diabetic origin, a large decrease in vinculin staining was observed in both control and high glucose conditions, with vinculin adhesions appearing on the tips of the cells, again rather than the middle of the cells, and the spindle-like shape of the cells was retained in high glucose treatment, rather than the diabetic rhomboid shape. Within cells from a non-diabetic origin, SIRT1 activation reduced positive vinculin staining to a very low level, with the cells retaining their spindle shape in both control and high glucose conditions (Fig. 4.6a).

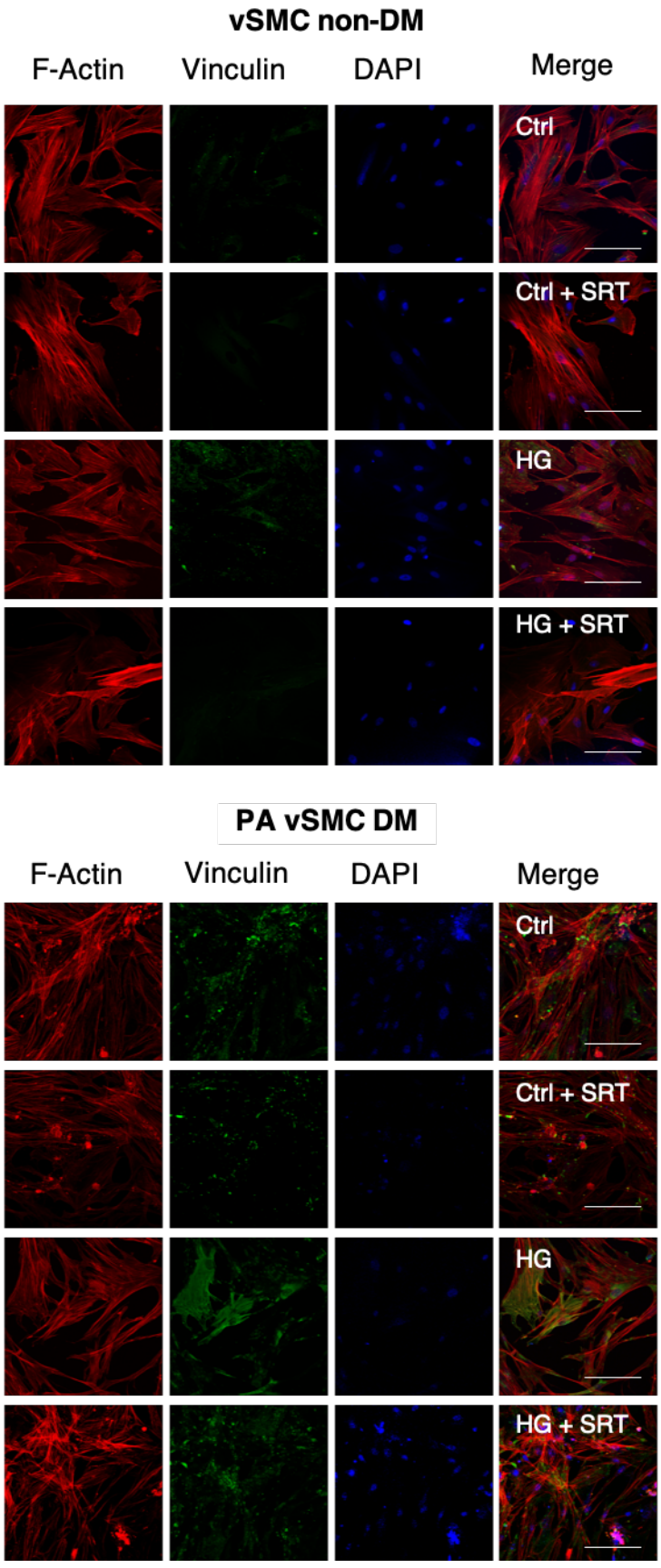

Fig. 4.6. SIRT1 activation reduced diabetic vSMC vinculin expression. Cells harvested from DM vSMCs were compared to healthy controls. Cells were cultured in 5.5mM glucose (Ctrl), 25mM glucose (HG) with either 0.5 µM SRT1720 or 0.1% DMSO to equivalate toxicity.. Cells were treated for 4 days in culture before fixing and staining. Vinculin staining was increased in hyperglycaemic conditions compared to control in both DM and healthy vSMCs, with DM vSMCs exhibiting greater vinculin staining in all four treatments. SIRT1 activation via 0.5 µM SRT1720 reduced vinculin staining under high and normal glucose conditions (n=6). F-Actin red, vinculin green, DAPI blue. Scale Bars = 5µm.

To validate the theory that focal adhesions were playing a role in the diabetic environment, localisation of a second focal adhesion protein; paxillin, was also examined. Previous studies demonstrated the role of paxillin and vinculin to be intertwined (392, 393), with both having control over the migratory ability of the cell, as well as the reorganisation of the cytoskeleton following an influx of Ca^{2+} signalling, all of which are upregulated following high glucose conditions, which is a hallmark of diabetic patients.

Within DM vSMCs, paxillin was overall more pronounced under immunofluorescent staining than cells from a non-diabetic origin, regardless of the glucose concentration or drug treatment. Within diabetic cells, 4-day treatment with high glucose media induced a greater level of staining compared to control conditions, however the pattern of distribution was much the same, with the cells all assuming a more rhomboid cytoskeleton shape compared to the healthy spindle shape. Activation of SIRT1 via SRT1720 reduced paxillin staining in the control conditions, with the overall cytoskeleton shape of the cell remaining unchanged. SIRT1 activation under high glucose conditions had little effect on paxillin expression, with the localisation of the paxillin adhesions appearing to be in a similar cellular location, as when cultured in the absence of SIRT1 activator; SRT1720, which was evident as lining the edges of the actin cytoskeleton as before.

However, within cells from a non-diabetic origin, the differentiation between SIRT1 activated and untreated was much more pronounced. Since paxillin expression was almost non-determinable in control glucose conditions, SIRT1 activation had little effect on the overall paxillin expression of non-diabetic cells, maintaining a similar cytoskeleton structure as without SIRT1 activation. Within the high glucose conditions, a large reduction in paxillin was observed with SIRT1 activation, with paxillin only lining a few of the actin cytoskeleton edges, rather than over most of the cells as per the high glucose only treatment. As with the vinculin staining, SIRT1 activation notably reorganised the actin cytoskeleton, with the rhomboid shape cells present in high glucose conditions being absent and the cells acquiring the spindle-like shape of healthy vSMCs (Fig. 4.7a).

Total cellular protein was also extracted from cells at the same day 4 timepoint, with paxillin expression examined by western blotting and normalised to α-tubulin, to strengthen the data obtained from the immunocytochemical staining. A significant 3-fold increase in paxillin expression was detected in diabetic cells compared to those from a non-diabetic origin ($p<0.0032$), and over 50% reduction found with the addition of SRT1720 to the diabetic cells ($p<0.0094$) (Fig. 4.7b).

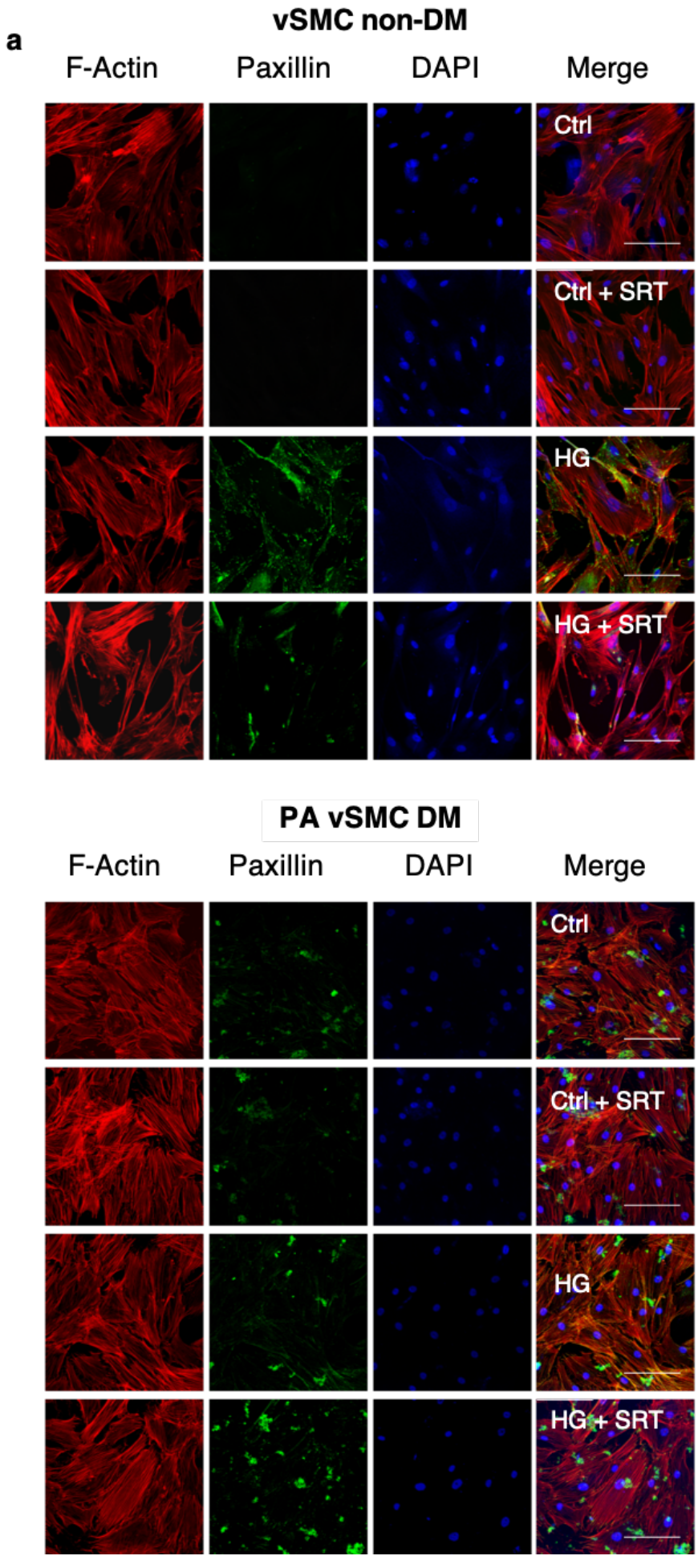
a
vSMC non-DM
F-Actin
Paxillin
DAPI
Merge
Ctrl
Ctrl + SRT
HG
HG + SRT
PA vSMC DM
F-Actin
Paxillin
DAPI
Merge
Ctrl
Ctrl + SRT
HG
HG + SRT

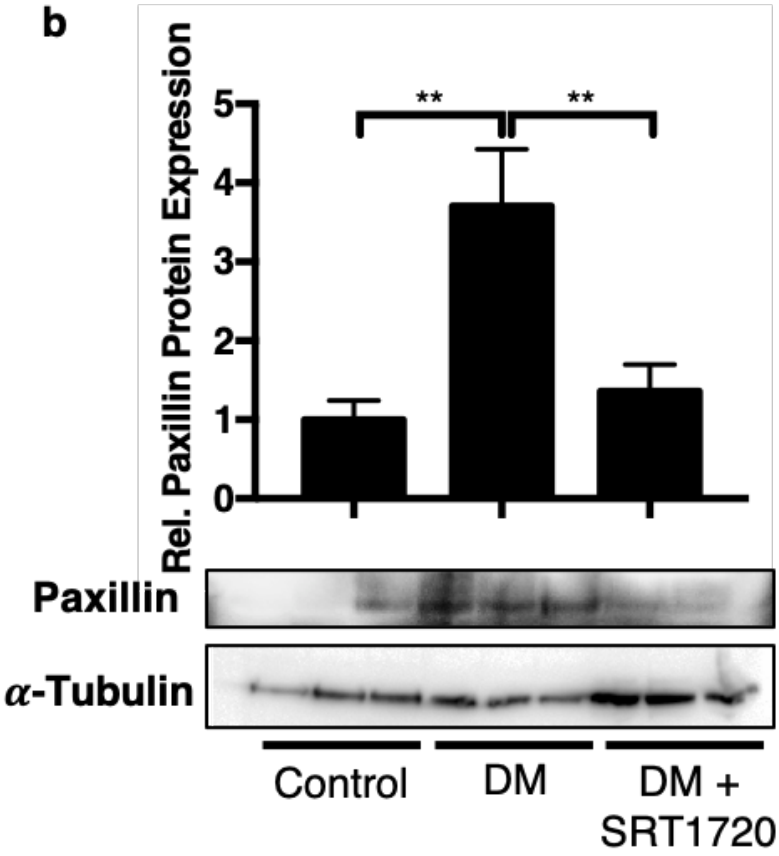

Fig. 4.7. SIRT1 activation reduced diabetic vSMC paxillin expression. Cells harvested from DM vSMCs were compared to healthy controls following 4 days of culture. Cells were cultured in 5.5mM glucose (Ctrl), 25mM glucose (HG) with either 0.5 μM SRT1720 or 0.1% DMSO to equivalate toxicity. **a)** Paxillin staining was increased in hyperglycaemic conditions compared to control in both DM and healthy vSMCs. DM vSMCs exhibited greater paxillin staining in control media compared to healthy vSMCs. SIRT1 activation via 0.5 μM SRT1720 reduced paxillin staining under high and normal glucose conditions in both DM and healthy vSMCs (n=6). **b)** Protein was harvested from cells following 4 days of treatment and paxillin expression assessed. Paxillin expression was significantly increased in DM vSMCs compared to healthy vSMCs. SIRT1 activation significantly reduced paxillin protein expression in DM vSMCs (n=6) (One-way ANOVA, Tukey Post-Hoc test). F-Actin red, paxillin green, DAPI blue. *P<0.05, **P<0.005. Scale Bars = 5μm. Mean ±SEM.

As paxillin is a key substrate for FAK (394), the expression of FAK relative to glucose concentration and SIRT1 activation was also examined. Since diabetic-insulin resistant adipose tissue has been shown to express increased levels of FAK (395), leading to remodelling of the ECM, increased vSMC invasion and FAK interaction with migratory and survival proteins p53 (396) and ERK (397), FAK expression in diabetic vSMCs was also examined via immunofluorescence.

FAK expression was relatively low within control conditions in both cells from a non-diabetic and diabetic origin, with slight staining observed on the tips of the spindles of the cells. Hyperglycaemic conditions increased FAK expression in both diabetic and non-diabetic cells, with both sets of cells again losing their spindle-like shape in favour or a more rhomboid cytoskeleton. FAK expression appeared disorganised in diabetic cells, with no distinct staining on the end of the actin filaments, compared to the cells from a non-diabetic origin, in which FAK expression appeared to line the outside of the actin cytoskeleton. SIRT1 activation via SRT1720 in diabetic cells reduced FAK expression in high glucose conditions, however no distinct change in staining was observed in the control conditions with and without SIRT1 activation. In cells from a non-diabetic origin, SIRT1 activation made little difference to FAK expression, with no significant staining apparent in control glucose conditions, and little change found in high glucose conditions with SIRT1 activation (Fig. 4.8a).

As before, total protein was extracted for western blot analysis at the same day 4 timepoint as staining, and expression of total and phosphorylated FAK was normalised to α-tubulin and analysed. Total FAK expression was significantly increased in diabetic cells compared to cells from a non-diabetic origin ($p<0.0175$), with SIRT1 activation reducing the expression of FAK in diabetic cells, however this was not significant ($p<0.1071$) (Fig. 4.8b). Phosphorylated FAK was found to be significantly increased 5-fold in diabetic cells ($p<0.0155$) when compared to controls, with a significant reduction observed following the addition of SIRT1 activator SRT1720 ($p<0.0242$), which reduced phosphorylated FAK to the levels observed in non-diabetic cells (Fig. 4.8c).

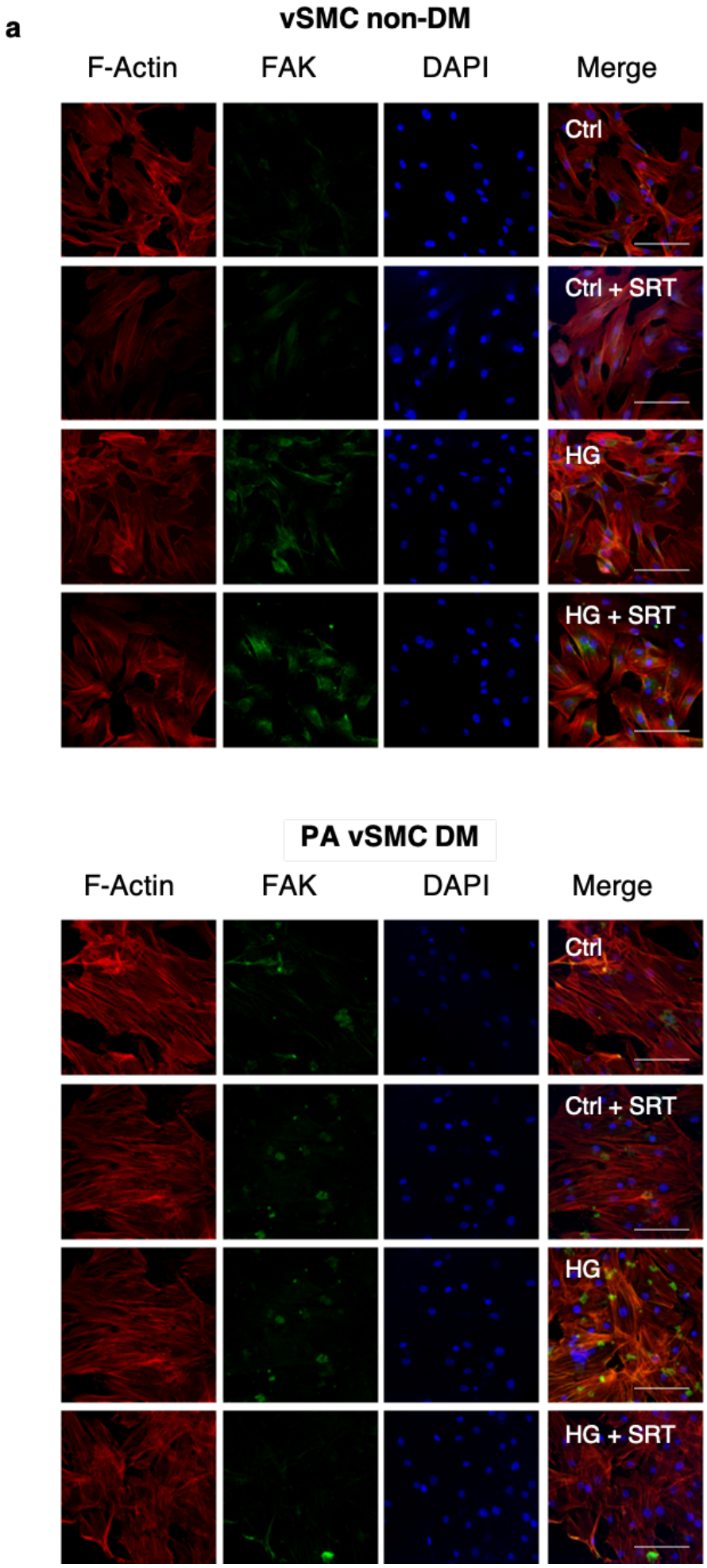
a
vSMC non-DM
F-Actin
FAK
DAPI
Merge
Ctrl
Ctrl + SRT
HG
HG + SRT
PA vSMC DM
F-Actin
FAK
DAPI
Merge
Ctrl
Ctrl + SRT
HG
HG + SRT

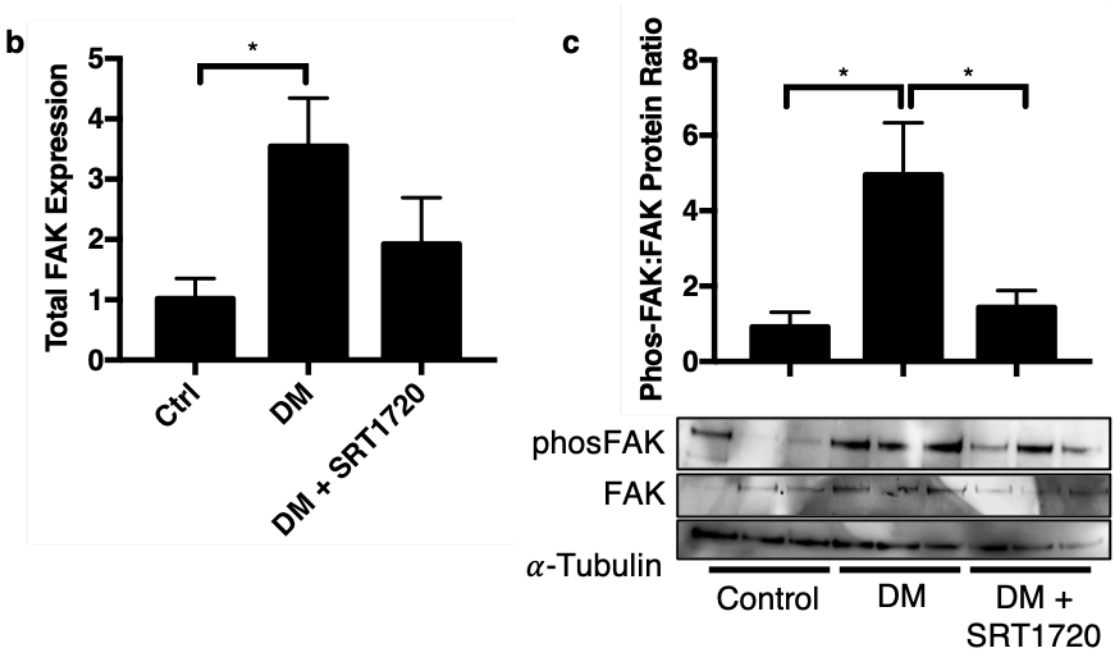

Fig. 4.8. SIRT1 activation reduced diabetic vSMC focal adhesion kinase activation. Cells harvested from DM vSMCs were compared to healthy controls after 4 days of treatment. Cells were cultured in 5.5mM glucose (Ctrl), 25mM glucose (HG) with either 0.5 μM SRT1720 or 0.1% DMSO to equivalate toxicity. **a)** FAK staining was increased in hyperglycaemic conditions compared to control in both DM and healthy vSMCs. DM vSMCs exhibited greater FAK staining in hyperglycaemic media compared to control conditions. SIRT1 activation via 0.5 μM SRT1720 reduced FAK staining under high and normal glucose conditions in both DM and healthy vSMCs (n=6). **b)** Total FAK expression was significantly increased in DM vSMCs compared to healthy controls (n=6) (One-way ANOVA, Tukey Post-Hoc test). **c)** phosphorylated FAK expression was significantly increased in DM vSMCs compared to healthy vSMCs, which was reduced with the activation of SIRT1 (n=6) (One-way ANOVA, Tukey Post-Hoc test). F-Actin red, focal adhesion kinase green, DAPI blue. *P<0.05. Scale Bars = 5μm. Mean ±SEM.

4.3.6. Activation of the ERK and AKT pathways is upregulated in diabetic vascular smooth muscle cells

Since proliferation (Fig. 4.4a), adhesion (Fig. 4.5a) and migration (Fig. 4.5b) production were all upregulated in cells from diabetic patients, the mechanistic pathways underpinning this process were interrogated. Given that MAPK pathway has been previously linked to impairing the function of diabetic cells (398, 399), the activation of this both MEK and ERK were investigated via western blot within the vSMC model.

MEK phosphorylation was significantly increased in diabetic cells compared to control ($p<0.0260$) (Fig. 4.9a), however no significant difference was found in the total expression of MEK when normalised to α-tubulin (Fig. 4.9b). Downstream of MEK, ERK expression was also examined. ERK phosphorylation was increased 3-fold in diabetic cells compared to those from a non-diabetic origin ($p<0.0043$) (Fig. 4.9c), with total ERK expression also increased in diabetic compared to non-diabetic cells when normalised to α-tubulin ($p<0.0384$) (Fig. 4.9d). In order to examine the pathway further, AKT; known to play a role in NO production and endothelial dysfunction within diabetic vessels, was also investigated. AKT phosphorylation was significantly increased in cells from diabetic patients compared to control ($p<0.0245$) (Fig. 4.9e), with total AKT expression also increased in diabetic cells compared to control and normalised to α-tubulin ($p<0.0010$) (Fig. 4.9f).

Furthermore, having demonstrated that activation of SIRT1 attenuates cellular proliferation and focal adhesion formation in vSMCs, the effect of SIRT1 activation on these pathways was again examined via western blot. SIRT1 activation within diabetic cells significantly reduced ERK phosphorylation to lower than control levels ($p<0.0028$) (Fig. 4.10a), however no reduction in total ERK expression was found when normalised to α-tubulin (Fig. 4.10b). Finally, AKT phosphorylation in diabetic cell was reduced to near control levels with the addition of the SIRT1 activator ($p<0.0245$) (Fig. 4.10c), whilst total AKT expression was significantly reduced to less than control when normalised to α-tubulin ($p<0.0001$) (Fig. 4.10d).

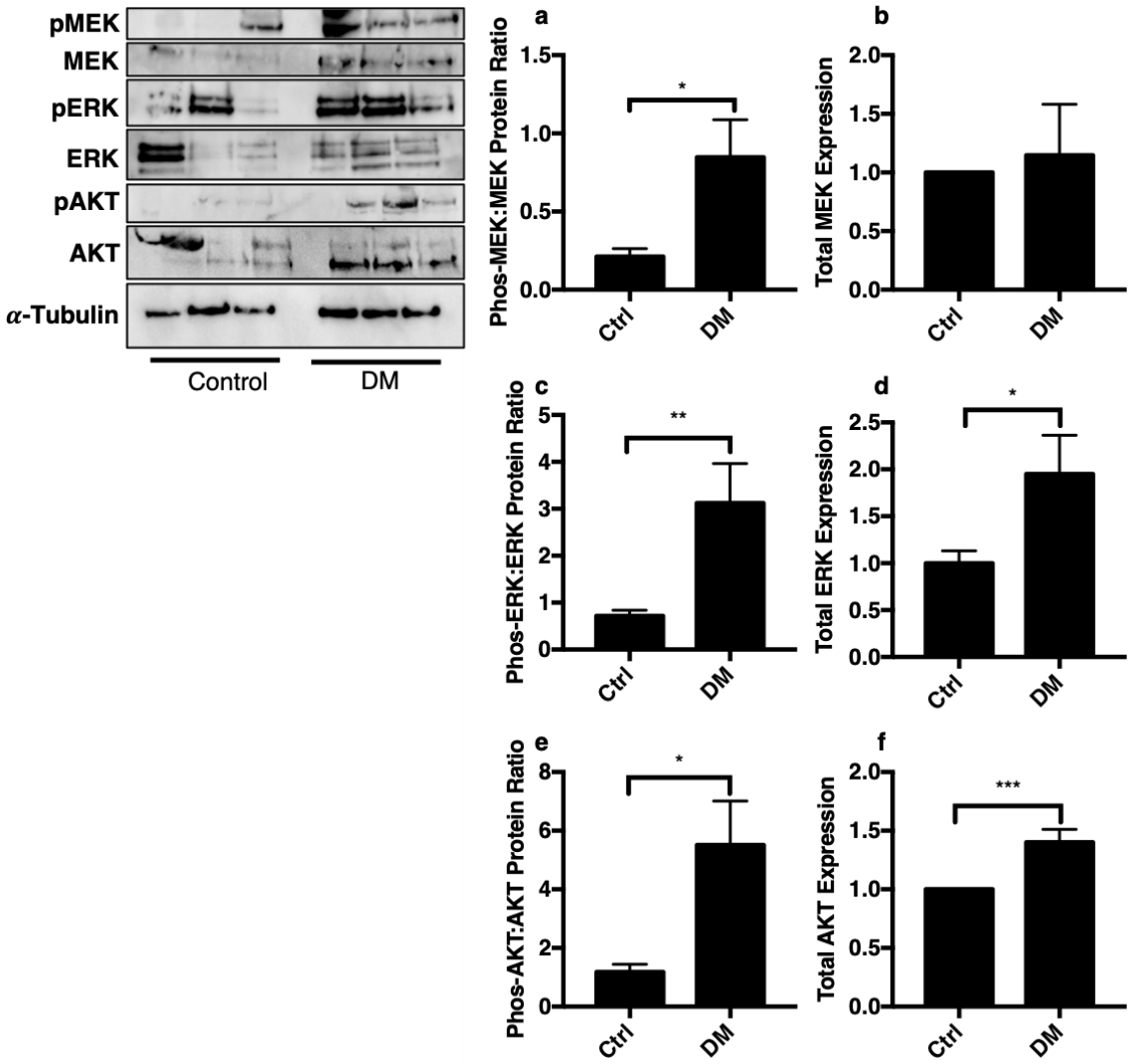

Fig. 4.9. MAPK and AKT activation are increased in diabetic vSMCs. Cells harvested from DM vSMCs were compared to healthy controls. Cells were cultured in control media until confluence when protein was isolated. Cells were cultured in 5.5mM glucose. **a**) DM vSMCs exhibited increased MEK phosphorylation compared to healthy controls (n=6), **b)** however no change in total MEK was found (n=6). **c)** Diabetic vSMCs exhibit significantly increased phosphorylated ERK when compared to healthy vSMCs (n=6), and **d)** significantly more total ERK was also observed (n=6). **e)** Diabetic vSMCs exhibit significantly increased phosphorylated AKT (n=6) and **f)** total AKT when compared to healthy vSMCs (n=6). (Unpaired T-test conducted **a-f**). *P<0.05, **P<0.005. Mean ±SEM.

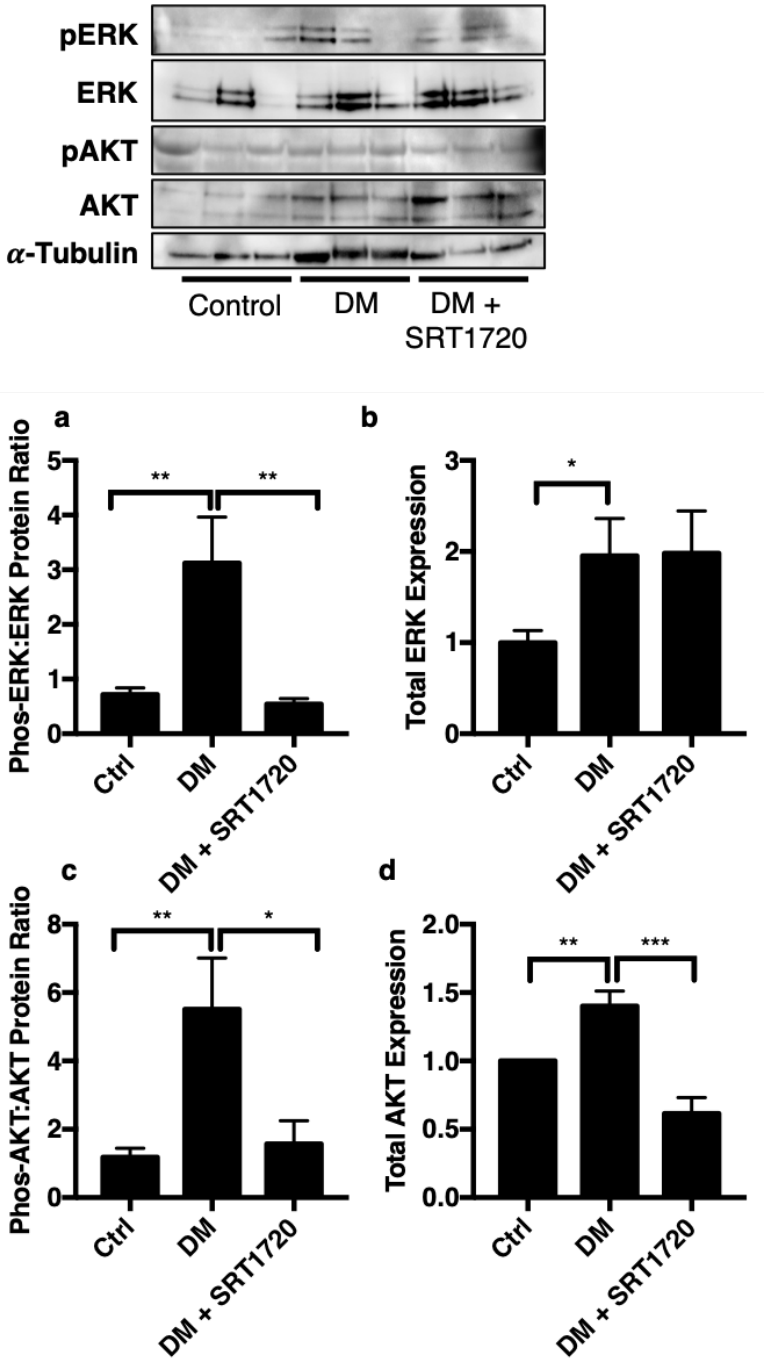

Fig. 4.10. ERK and AKT activation is reduced in diabetic vSMCs with the addition of SIRT1 activator SRT1720. Cells harvested from DM vSMCs were compared to healthy controls. All cells were cultured for 4 days in treatment media. Cells were cultured in 5.5mM glucose (Ctrl), 25mM glucose (HG) with either 0.5 µM SRT1720 or 0.1% DMSO to equivalate toxicity. **a)** SIRT1 activator 0.5 µM SRT1720 reduced ERK phosphorylation via a factor of three (n=6), **b)** but had little effect on total ERK expression (n=6). **c)** SIRT1 activation significantly reduced AKT phosphorylation in diabetic vSMCs compared to healthy controls and (n=6), **d)** reduced total AKT expression below healthy control levels (n=6) (One-way ANOVA, Tukey Post-Hoc test conducted **a-d**). *P<0.05, **P<0.005 ***P<0.001. Mean ±SEM.

4.4. Discussion

Whilst the phenotypic heterogeneity of vSMCs has been well established (117), little is known about the changes occurring in long-term diabetic patients, something which this study sought to address using an *in vitro* model. Atherosclerosis, a leading killer within cardiovascular disease is a chronic inflammatory disease leading to narrowing of the lumen and plaque development (400), resulting in intimal hyperplasia caused predominantly by vSMCs. This study utilised a model of vascular injury produced by chronic high glucose to stimulate hyperproliferation and migration within vSMC, to determine the role of SIRT1 on this invasive process.

4.4.1. Distinct changes in morphology are present between diabetic and non-diabetic vascular smooth muscle cells

With emerging bodies of evidence suggesting that vascular remodelling may be due to inherent morphological differences between diabetic and non-diabetic vSMCs (268), the morphology of cells from both origins was examined. Typically, vSMC morphology can be divided into two distinct phenotypes; a spindle-shaped phenotype commonly derived from healthy origins cultured in normoglycemic media, with the classic hill and valley appearance. Secondly a rhomboid shaped phenotype, often derived from a damaged vessel, which appears flatter with a greater surface area compared to its *healthier* counterparts. The latter morphology is often reported to be found within intimal legions caused via stent implantations (401), either from invasion or an *in situ* morphological change (402). In this study, under light microscope observation, cells from diabetic patients appeared to lose their spindle-like morphology, instead they appeared to be spread along the dish, as opposed to cells from a non-diabetic origin, which appeared to become aligned and maintain this spindle like morphology. Changes within the F-Actin cytoskeleton have been reported within the diabetic endothelial layer (403) causing restructuring, increasing microvascular leakage, with diffuse F-actin staining and areas of loss was evident. This study demonstrated a similar change in F-actin structure, with a reduction of organisation and directionality with the F-Actin, leading to an increase in cells overlapping compared to the non-diabetic vSMCs, which appeared more organised and striated. Whilst it is important to note that the two cell sub-types;

diabetic and non-diabetic used in this study arise from different vascular beds, previous comparative studies between the two vascular beds show no significant difference in the percentage of vSMCs within a plaque, nor is there a significant difference in the type of calcification presence between the two. Moreover, there was no significant difference observed between Runx2 and ALP mRNA expression, neither did Alizarin red staining demonstrate a significant difference in their mineralisation capacity, further suggesting that whilst these vascular bed locations remain distinct, the vSMCs which occupy the vessels are phenotypically comparable (404).

4.4.2. High glucose conditions reduce actin organisation and increase proliferation

With hyperglycaemia being a key independent risk factor for cardiovascular disease (405, 406), the effect of glucose on cells from diabetic and non-diabetic origins was examined. F-Actin staining demonstrated that diabetic cells under high glucose conditions have a further reduction in their organisation and structure, with little to no striated pattern observed. When compared to their diabetic counterparts, non-diabetic cells appear to line up under high glucose conditions, with an elongation in the cell morphology observed as they maintain the spindle-like shape typically associated with smooth muscle. Previous studies have suggested that vascular muscle cells from diabetic patients acquire a hypercontractile phenotype (407-409), similar to the remodelling of airways during asthma, suggesting a general mechanism for smooth muscle tissue reorganisation (410). This may give reason to the lack of organisation observed within diabetic vSMCs, with the hypercontractility resulting in the disorganisation and restructuring on the monolayer as observed within this study.

It has been widely reported that NO, a key metabolic and vascular regulator is dysregulated within a wide range of tissue in diabetic patients (411). This study confirms a decrease in NO availability produced by the diabetic smooth muscle, even after four days culture *ex-vivo* in normal glucose levels. With NO known to inhibit proliferation and induce cell death within vSMC, this downregulation fuels the hypothesis that the trans-differentiation of diabetic vSMCs reduces their synthetic quiescent phenotype, leading to a hyperproliferative state, which provides the

perfect environment for atherosclerotic development. Additionally, NO activity within the intimal layer has been reported to exert paracrine effects on bone-marrow derived endothelial progenitor cells (386, 412, 413); a subset of adult stem cells which are recruited to sites of vascular injury, promoting endothelial regeneration and neovascularisation. With this lack of NO generation in diabetic cells, their paracrine ability to induce vascularisation and endothelial repair may be partially inhibited, leading to a perpetuating positive feedback loop towards vascular dysregulation.

With hypermotility of cells being a defining feature of the diabetic smooth muscle layer (268, 414), and hypermotility and proliferation intrinsically linked, the effect of high glucose on proliferation, migration and adhesion was examined. Diabetic cells exhibited greater proliferation under control glucose conditions compared to cells from a non-diabetic origin, with this disparity observed to an even greater extent under high glucose conditions. With diabetic induced proliferation reportedly mediated via a variety of signalling mediators such as Notch (415, 416), MAPK (417) and AKT (418), these were investigated. AKT and ERK are often considered to control the process of smooth muscle development, and with diabetic vSMCs suggested to be dedifferentiated, it is proposed that over-activation of these pathways may be reverting these cells to a proliferative and migratory juvenile state (352, 419). Akt phosphorylation was significantly increased in cells from a diabetic origin compared to control cells, as was total AKT expression, to a lesser extent. AKT overexpression has been shown to decrease the contractile response within rats (420), and this correlates with the data presented here, suggesting that the reduction of key smooth muscle markers such as αSMA and the increase in AKT activation; both total and phosphorylated, could result in the diabetic vSMCs dedifferentiating and losing the contractile quiescent phenotype.

The MAPK pathway was also examined as pro-proliferation pathway. With MEK and ERK activation shown to degrade senescence inducer p21 (421, 422), and thus allowing cells to continue through the cell cycle even with DNA damage from vascular injury, it was hypothesised that these would be upregulated in diabetic vSMCs. Phosphorylation of MEK was found to be upregulated in cells from a diabetic origin, with no total change in MEK expression noted. Downstream of MEK,

ERK1/2 was also upregulated, with diabetic patient cells exhibiting significantly greater phosphorylated and total amounts of ERK compared to non-diabetic vSMCs. With the clinical development of MAPK inhibitors coming to the forefront of cancer treatment due to their ability to inhibit cell proliferation, the impact of this on diabetic vascular disease has started to be examined (423-425). As MEK/ERK signalling is activated via a range of mitogens and growth factors, and downstream ERK1/2 catalyses numerous cytoplasmic and nuclear targets, it could be considered a useful bottleneck to attenuate aberrant proliferation following vascular injury. Diabetic adipose tissue has been demonstrated to have a dysregulated adipocytokine expression profile (426) and increased lipid activity, with ERK activation sequestered via PD184352 restoring these levels back to normal conditions (423). Whilst this was beyond the scope of this study, as the patient cells have been exposed to hyperglycaemia and thus upregulated ERK signalling for 20+ years, this model may demonstrate that the basis of the animal model is applicable to human cells, and that MAPK inhibition may be a viable future option for future vascular diabetic treatment.

Since both AKT and MAPK pathways have been implicated in increased invasive properties of multiple cell types and these were both found to be upregulated in diabetic patients, the adhesive properties of diabetic cells were examined. Cellular adhesion was significantly lower in diabetic patient cells in control glucose compared to cells from a non-diabetic origin, however this was reversed in high glucose conditions, with diabetic cells found to adhere significantly more, suggesting a glucose induced adhesion related pathway may be activated to a greater extent in diabetic cells.

Whilst current research has again focused mainly on the role of MAPK and ERK in cancer cell adhesion to a matrix (427), parallels can be drawn with vascular disease. Following vascular injury, smooth muscle within the intimal layer lays down excessive matrix, which under high glucose and hyperphosphatemic conditions may start to calcify, contributing to increased vascular dysfunction and the trans-differentiation of vSMCs to a more osteogenic phenotype. Given that overactive ERK signalling in cancer cells promotes an increase in cell matrix adhesion (428, 429), and with cell detachment leading to further upregulation of these pathways

until the cells re-adhere (430), one could propose a similar mechanism under the inflammatory diabetic environment, possibly resulting in the increased adhesion and intimal hyperplasia observed within diabetic vessels. vSMC migration, a key contributor to the development of atherosclerotic plaques, was therefore assessed using PDGF-BB as a chemoattractant. As expected, migration was increased in both control and high glucose conditions after 6 hours in diabetic cells compared to non-diabetic. This correlates with diabetic induced migration observed *in vitro* (268, 431) with an upregulation required for the development of atherosclerosis and intimal hyperplasia (432), often corresponding with an increase in focal adhesion and F-actin remodelling, as found within this study.

4.4.3. Reduction of SIRT1 within the diabetic patient correlates with increased vessel calcification

Within the diabetic patient, calcification deposition within the vessel; shown via black Von Kossa staining; was significantly greater compared to the IMA control, with the staining localised to the intimal layer of the vessel wall and hyperplasia visible within the vessel. SIRT1 histological staining was inversely correlated with Von Kossa staining, with a reduction in staining observed in the smooth muscle layer within the vessel, which was greater within the IMA. With this study being among the first to show an inverse correlation between SIRT1 histological staining and calcification in human diabetic vessels (87), the SIRT1 levels within serum were also examined, to further demonstrate this relationship. Diabetic patients exhibited significantly decreased SIRT1 levels within their serum, possibly suggesting an overall decrease in expression, or perhaps that SIRT1 has shuttled into the nucleus via its NLS, which occurs during cellular stress (196). To further probe the expression of SIRT1 within diabetic patients, cells harvested from diabetic and non-diabetic origins were examined for SIRT1 expression. A significant decrease in both mRNA and protein expression in diabetic patients correlated with the fluorescent staining, which demonstrates a reduction of SIRT1, which was found within both the cytoplasm and the nucleus in cells from a non-diabetic origin. This study extends the results of previous findings (249), suggesting a correlation between the reduction of SIRT1 and the development of diabetic vascular dysregulation within the intimal layer, however the underlying mechanism of this remains unclear.

4.4.4. SIRT1 reduces diabetic induced migration and adhesion under hyperglycaemic conditions

SIRT1 activation has been found to exert a wide range of benefits, both to the vascular system and metabolism, with the activator SRT1720 shown to increase mouse lifespan by up to almost 10% over a three year period (433). In this study, SIRT1 activation within diabetic vSMCs was shown to reduce the disorganisation of the actin cytoskeleton, with the cells appearing more striated and more akin to the cells from non-diabetic origins. SIRT1 activation also appeared to reduce the rhomboid shape of the cells, even under high glucose conditions, with the spindle like 'hill and valley' morphology appearing to be somewhat restored.

With a reduction of SIRT1 demonstrated in diabetic patients, and diabetic vSMCs showing a significant increase in proliferation, the effect of SIRT1 activation on proliferation was examined. Whilst diabetic vSMC proliferation was greater than that observed in the non-diabetic cells, SIRT1 activation demonstrated a decrease under both control and high glucose conditions following a similar trend to the diabetic cells. SIRT1 promoting a reduction in cellular proliferation has recently been confirmed in a range of *in-vivo* and *in-vitro* models, however a wide variety of molecular pathways have been attributed to this (434-436). Further examination of the MAPK pathway suggested a reduction in ERK phosphorylation following SIRT1 activation. This is the first study to demonstrate a human vascular smooth muscle model in which activation of SIRT1 reduces phosphorylation of ERK, and thus decreases its downstream activation. Previous studies in rat chondrocytes suggest that a lack of SIRT1 leads to a hyperacetylation of ERK, allowing for increased self-phosphorylation and thus overactivation and increased proliferation, something which this data corroborates (437). Once phosphorylated, ERK is translocated to the nucleus during G1 phase, which is crucial for the activation of a range of tertiary complex factors and growth related proteins (438), leading to a reorganisation of the actin cytoskeleton (439) as observed within this study. Since these data suggest both a systemic and vSMC localised decrease of SIRT1 within diabetic patients, it could be suggested that this lack of SIRT1 may permit the over-acetylation of a range growth factor targets, leading to the intimal hyperplasia often observed in diabetic vessels.

Additionally, a key marker of vascular calcification and diabetes; high intracellular calcium as demonstrated via the Von Kossa staining, has been linked to increased proliferation. Increased calcium ions have been shown to activate cellular matrix deposition as a means to remove excessive calcium from the cytoplasm, which has a range of downstream negative effects; activation of ERK signalling being one of them (440), which in turn increases proliferation. Furthermore, excess intracellular calcium may play a role within the AKT proliferation pathway. It has been well established that cyclic stretch within cells; such as those undergoing osteogenic differentiation and cytoskeleton remodelling, results in an influx of calcium into the cytoplasm (441-443). Alongside increased cyclic stretch, calcium influx allows increased phosphorylation of multiple proteins involved in the activation of the AKT pathway, permitting increased cellular proliferation. These data demonstrate that AKT phosphorylation was significantly decreased in diabetic cells with the addition of SIRT1 activator SRT1720, as was total AKT expression. Elevated AKT activation has been linked with a range of anti-apoptotic effects in a multitude of cancers and p53 inhibition, with resveratrol shown to reduce aberrant proliferation and induce normal cell apoptosis and p53 activity (444). Under healthy basal conditions in which SIRT1 is at a 'normal' level, AKT activation is at a minimum, but within diabetic samples, hyperglycaemia (445) a change in insulin levels (446) and a lack of SIRT1 may attribute to the significant rise of phosphorylation of AKT, leading to hyperactivation of this pathway, again forcing this hyperproliferative phenotype found in diabetic smooth muscle.

With AKT phosphorylation directly regulating the production of focal adhesions and cellular adhesion to a matrix (447), the effect of SIRT1 on cellular adhesion was also examined. AKT phosphorylation correlated with an increase in cellular adhesion under high glucose, with SIRT1 activation reducing these adhesive properties after both 45 minutes and sustained to three hours. With cell migration linked to the remodelling and activation of the cellular cytoskeleton, SIRT1 substrates were reviewed to determine a link (448). Interestingly, Cortactin, an F-actin binding protein with established roles in protrusive actin dynamics (449) is found to be a substrate via co-immunoprecipitation experiments with SIRT1 (448). Within cancer cells, SIRT1 inhibition is suggested to decrease cellular adhesion and migration (450), the opposite is found within these data. However, with the role of SIRT1 still

under investigation, both within cancer and cell migration more generally, both findings may be correct under different physiological conditions (451). Caloric restriction; a known activating process of SIRT1, inhibits proliferation and reduces tumorigenesis (452), however SIRT1 has also been shown to increase Cortactin led migration (453), a key pathway in the development of cancer, suggesting that whilst high levels of SIRT1 may upset homeostasis, it is clear that a lack of SIRT1 is detrimental. Since diabetic patients exhibit significantly lower levels of SIRT1 than the general population and cancer patients exhibit significantly higher (454), the activation of SIRT1 within this study may increase SIRT1 expression to a *healthy* level, which is located somewhere between the two pathologies and far below the levels found in migratory cancer cells. Therefore, within this model SIRT1 activation is reducing the migration and adhesion properties of diabetic vSMCs, however this is not to say that overexpression of SIRT1 may have opposite effects, however this remains outside the scope of this study but an interesting area for future investigation.

4.4.5. Focal adhesion formation is increased within diabetic vascular smooth muscle cells

Focal adhesion complexes regulate a range of cellular functions, inducing adhesion, apoptosis and migration, and are considered crucial for linking the ECM to the actin cytoskeleton (455), allowing for the transmission of force within a vessel and overall vascular remodelling within a pathological setting. Among the hundreds of proteins which are contained within a single focal adhesion (456), vinculin, paxillin and FAK are especially important for connecting the matrix-integrin complex with downstream signalling molecules and actin stress fibres. This study sought for the first time to examine the change in focal adhesion formation within diabetic human vSMCs and the role of SIRT1 activation within this process.

Depletion of vinculin has been demonstrated to lead to dramatic changes in cell motility and focal adhesion size (457-459), and more recently was proposed as a key player in the regulation of cell adhesion (391). Whilst the structure of vinculin has been well characterised *in vitro,* its expression level within diabetic patients is less well understood (460). Expression of vinculin was low in cells from a non-diabetic origin compared to the diabetic samples, with an increase observed in both

when treated within a high glucose environment. Previous studies have shown that in diabetic patients, specifically those with either uncontrolled insulin or high glucose, there is an increased susceptibility to form focal adhesions (333, 389, 461), leading to aberrant migration and adhesion, found commonly in the narrowing of vessel lumen and their overall occlusion.

Following an increase in vinculin, paxillin, a multifunction and multidomain focal adhesion adapter protein is recruited and phosphorylated at specific Tyr and Ser residues (462). Expression of paxillin was shown to be upregulated in diabetic samples compared to those from a non-diabetic origin, with activation again increased in high glucose conditions compared to control conditions. As paxillin acts as a scaffolding protein, it has duel effect on the maintenance of focal adhesion structure, with its activation and phosphorylation observed at the front motile end of the cells focal adhesion, in which it binds the ECM and enhances lamellipodial protrusions, allowing the cell to migrate forward (463). Conversely, dephosphorylation of paxillin leads to the dismantling of the focal adhesion located at the back of the cell, allowing cellular release from the ECM as it migrates forwards.

With paxillin shown to localise with inactive ERK at the tips of actin filaments and phosphorylate (389), this pathway is self-enhanced. Activated ERK phosphorylates paxillin, following which both proteins are upregulated in the presence of high glucose, suggesting the activation of these pathways observed within the diabetic patient may be somewhat controllable by the reduction or inhibition of this cyclic pathway. Phosphorylation of paxillin has been demonstrated to associate not only with FAK, leading to further development of focal adhesions and increased migration, but also with the downstream effector; AKT (464). Phosphorylation of paxillin at tyrosine residues has been confirmed to increase AKT phosphorylation, which corresponds with the data in this study (464, 465). Activation of AKT via paxillin has been identified as an important mechanism for cancer growth (464). With this finding relatable to the increased proliferation observed within diabetic vSMCs, it could be suggested that overactivation of both focal adhesion proteins and associated AKT signalling may be responsible for the proliferative and migratory phenotype of diabetic vSMCs.

Finally, FAK; a cytoplasmic tyrosine kinase located within focal adhesions has been implicated as a key mediator for integrin signalling as well as cell surface receptors, leading to increased migration and proliferation in a variety of both cardiovascular and cancer related cell types (466, 467). Cells, both diabetic and non-diabetic, cultured under control glucose conditions exhibited little FAK staining, however FAK was greatly upregulated in the high glucose conditions, more notably within diabetic patient cells. FAK activation, which depends upon its phosphorylation, was significantly upregulated in diabetic patients, something which has been proven to be glucose induced (389) and thus could suggest reasoning for the upregulation within diabetic patients, who are often hyperglycaemic. Additionally, phosphorylated FAK directly phosphorylates paxillin (468), which acts as an adapter protein through FAK to increase the link between the actin cytoskeleton and integrin complex (467), remodelling the cytoskeleton for cell spreading and increased migration, resulting in vessel wall remodelling and the narrowing of the lumen.

Furthermore, FAK has been demonstrated to activate the ERK pathway in a similar manner to paxillin activation, with FAK able to phosphorylate ERK at focal adhesions alongside Src, increasing the scaffold formation surrounding the development of focal adhesions (469). Previous studies have demonstrated FAK inhibition, both as a reduction of total protein and inhibition of FAK phosphorylation, reduces cellular sensitivity and F-actin remodelling in response to glucose (470). This previous data, when considered alongside these current data, may suggest a pathway in which increased FAK activation in response to chronic high glucose induces MAPK downstream activation, leading to the vascular remodelling and increased intimal hyperplasia observed in diabetic patients.

4.4.6. SIRT1 activation reduces the occurrence of focal adhesion formation

Having previously demonstrated the effectiveness of SIRT1 activation on decreasing cellular proliferation and migration, possibly through an ERK/AKT mediated pathway, it was investigated whether SIRT1 may have a role in focal adhesion lead migration (Fig. 4.11). Activation of SIRT1 reduced the expression of vinculin, paxillin and FAK to varying degrees within diabetic vSMCs, with a significant reduction of FAK phosphorylation when treated for 4 days prior to lysis. Whilst not widely reviewed within vascular remodelling, resveratrol; a SIRT1

activator, has been used in cancer models to reduce FAK activation (471), in order to reduce the rate of proliferation and migration and to induce apoptosis. With growing similarities drawn between cancer and cardiovascular risk in diabetes (472-474), it seems a fair comparison to suggest this mechanism may act in a similar way, with a lack of SIRT1 allowing for increased acetylation of both FAK and paxillin, modulating microtubule and centrosome polarisation which leads to an increased trafficking of cells during migration (475). Given that a reduction of SIRT1 within the diabetic patient is a key finding within this study, activation of SIRT1 may reduce this acetylation of focal adhesion associated proteins, reducing their activation and thus cellular migration, however more co-localisation studies should be conducted to confirm the direct relationship between SIRT1 and focal adhesion proteins.

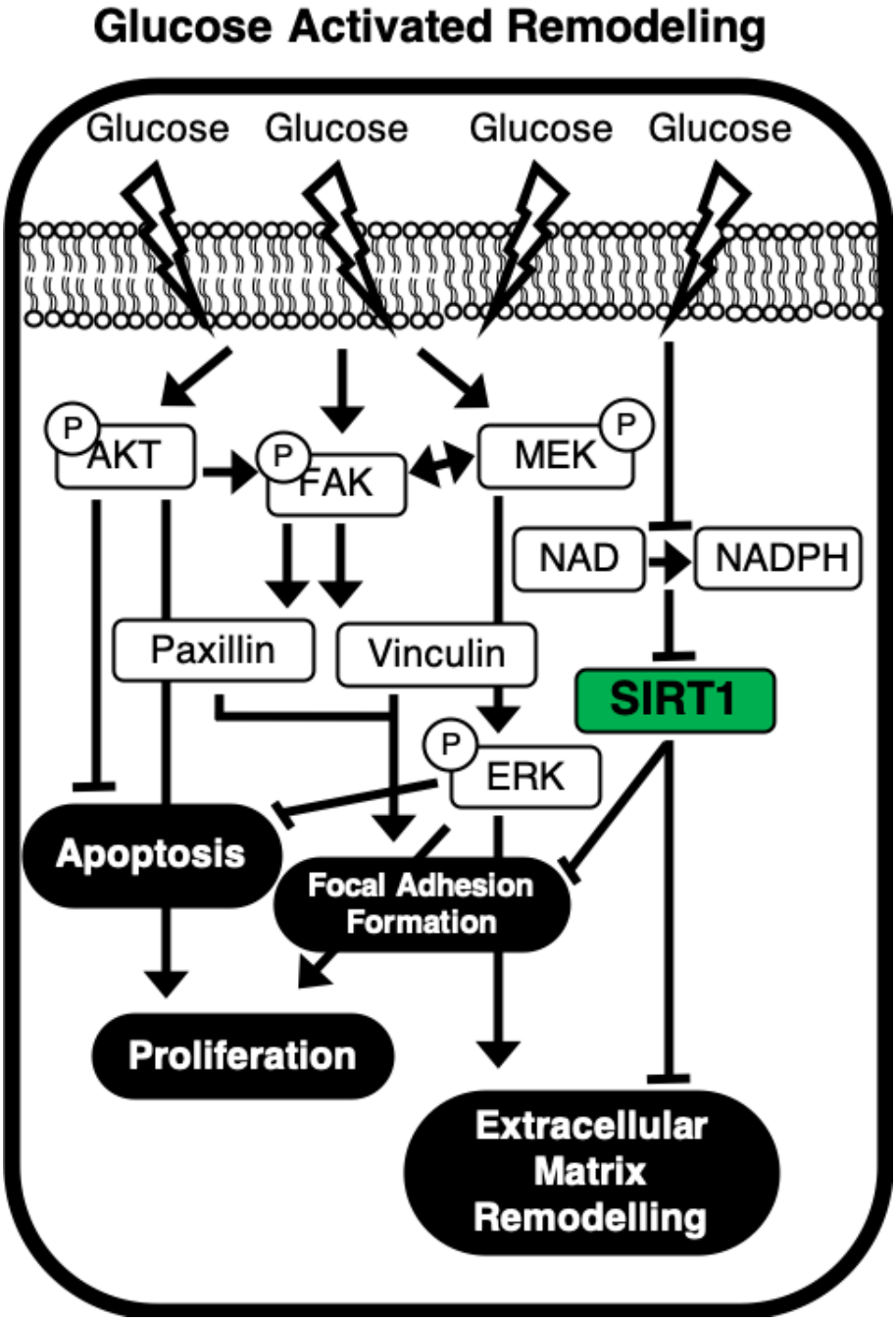

Fig. 4.11. Suggested mechanism for the role of SIRT1 in glucose activated focal adhesion formation. Firstly, hyperglycaemia reduces NAD to NADPH conversion, reducing SIRT1 substrate availability and therefore activation. Hyperglycaemia induces FAK activation which auto-phosphorylates and phosphorylates AKT and ERK, leading to an increase in vinculin and paxillin expression resulting in extracellular matrix remodelling and focal adhesion formation.

4.5. Limitations

Whilst this chapter clearly demonstrates the difference in focal adhesion formation, migration and proliferation between diabetic and non-diabetic vSMCs, it is not without its limitations. Firstly, the difference between the two vascular beds in which vSMCs were harvested from; coronary arteries used for the control, and popliteal artery used for the diabetic patients is not an ideal comparison, due to the difference in cyclic stretch and sheer stress each vessel will face, leading to a different time course and possible differentiation pathway activation. However previous studies have demonstrated (404) that this discrepancy in vascular beds does not affect vSMCs osteogenic potential, it is worth considering when comparing data between the two. Furthermore, since the CA vSMCs are purchased from a supplier, the process of extraction will undoubtedly be different, leading to different culture conditions, which may affect their phenotype prior to treatment. Secondly throughout this thesis and within this chapter, the comparison of IMA to PA vessels when undertaking IHC staining is also a limitation. For the most useful data set, healthy PA vessels should be compared to the calcified PA DM vessels, however healthy popliteal vessels are not easily obtainable, non-calcified IMA sections were used. However, with the vSMCs within IMA known not to calcify (86) whilst they do not make a good comparison for the vascular bed, histologically they demonstrate the phenotype of a non-osteogenic, non-calcified vessel well.

4.6. Conclusion

In conclusion, the experiments described within this chapter demonstrate the inherent differences between vSMCs from a diabetic and non-diabetic origin, highlighting the morphological and phenotypic differences between them. Moreover, these data suggest an upregulation of the MAPK pathway as a crucial link between the increased proliferation and migration commonly observed in diabetic cells, and the increase development of focal adhesions, which may be fuelling this aggressive phenotype. Furthermore, this study shows that activation of SIRT1 may be able to reduce diabetic high glucose induced proliferation and migration, through a downregulation of ERK1/2 phosphorylation and focal adhesion assisted migration. Further investigation into the mechanism in which SIRT1 may reduce focal adhesion activation should be examined, and the precise relationship between FAK and ERK should also be considered.

5. Loss of SIRT1 in diabetes accelerates DNA damaged induced smooth muscle mineralisation *in vitro* and reduces activation of the DNA repair MRN complex

5.1 Introduction

5.1.1. The prevalence of diabetic induced calcification

The occurrence of diabetes is fast becoming a global epidemic, with almost 9% of the population affected (273). Diabetes is associated with elevated oxidative stress, arising from hyperglycaemia through the activation of the polyol pathway (476), due to poor patient glycaemic control (477) and finally resulting in increased cardiovascular risk. One of the key co-morbidities associated with diabetes is vascular calcification (65, 478), a major cause of mortality within the western world, in which calcium and lipoprotein accumulate within the blood vessels, leading to the formation of fatty streak lesions and matrix deposition (479). At a molecular level, advanced vascular calcification is associated with cellular senescence (480, 481), telomere erosion and persistent DNA damage (121, 158) in response to various cellular stresses such as hyperglycaemia and reactive oxygen species production, further promoting the development of matrix deposition within the vessel. However, the mechanism by which hyperglycaemic conditions increase DNA damage and the pathways underpinning this, is still unclear.

5.1.2. DNA damage response pathways

The DNA Damage Response (DDR) is a collection of canonical pathways, which, following a stress factor, stimulate a variety of sensor proteins including MRE11 RAD50, NBS1 (MRN complex) (482) and the histone variant H2AX (483). The DDR represents a multitude of signal transduction pathways which sense DNA damage and replicative stress and regulate the physiological processes which determine whether a cell undergoes DNA repair, enters irreversible senescence, or, in cases of severe damage, undergoes apoptosis. Firstly The MRN complex has been implicated in several aspects of DSBs, from initial detection, to triggering DDR signalling pathways and facilitating repair (484). Considered to be a flexible scaffold, the MRN complex binds to the DNA break, bridging over the broken DNA, before

activating the checkpoint signalling pathway (161). These sensors are then phosphorylated via recruited transducer members of the protein family phosphatidylinositol 3-kinase-like protein kinases (PIKKs) such as Ataxia Telanglectasia Mutated (ATM) to the site of damage (162). Subsequently, this leads to the activation of effector molecules such as checkpoint kinases and p53, which ultimately contribute to an arrest in the cell cycle, followed by DNA repair or apoptosis. Furthermore, recruitment of ATM by the MRN complex contributes to the activation and phosphorylation of the H2AX protein, which when phosphorylated directly binds to binding partner MDC1, further enhancing the MRN-ATM binding and contributing to the positive feedback loop which allows spreading of γH2AX over mega-base domains around the DSBs (485), in order to provide a platform for further recruitment of other DDR proteins. Following activation of the repair complex, damage undergoes repair either through nonhomologous end joining (NHEJ), or homolog recombination, the latter which only occurs during S or G phase after replication has been completed (160). Following successful repair, γH2AX is dephosphorylated by protein phosphatase 2a and the cell returns to its pre-senescent phenotype (486).

5.1.3. The role of SIRT1 in DNA damage sensing

Sirtuin 1 (SIRT1) is a NAD+ dependent deacetylase, with roles in longevity, aging, glucose metabolism and calcification (211, 305). Having previously been reported that a reduction of SIRT1 leads to increased smooth muscle calcification (87, 487, 488), the effect of SIRT1 on DNA damage and repair has been examined. It is now understood that SIRT1 binds and regulates tumour suppressor p53, which following DNA damage, deacetylates p53 and attenuates its ability to act as a transcription factor (489). Consequently, SIRT1 activation has been suggested to increase cell survival under DNA damage conditions (490), however its role in diabetes-associated DNA damage is yet to be investigated. Furthermore, a functional link has been shown between SIRT1 and NBS1 in increasing the resistance to DNA damage (491). However SIRT1 activators, specifically SRT1720, which has been shown to operate as a possible therapeutic for type II diabetes models (254), has been found to increase phosphorylated ATM in DNA damage models and reduces lag time in the initiation of DNA repair (492). Thus, making SIRT1 an interesting target for examination within a DNA damage diabetic model.

5.2. Aim and Objectives

The aim of this part of the study was ultimately to determine whether a lack of SIRT1 expression within a diabetic environment contributes to hyperglycaemic induced DNA damage and subsequent repair in human smooth muscle cells *in vitro* and establish a mechanism of action. This was achieved via the following objectives:

i) Firstly, to establish if diabetic patient vessels and vSMCs isolated from diabetic patients exhibit DNA damage markers.

ii) Secondly, to determine if the *in*-vitro calcification model induced DNA damage within vSMCs, if this was significantly greater under hyperglycaemic conditions compared to control and comparable to the damage observed in DM vSMCs.

iii) Thirdly, to elucidate whether SIRT1 activation or inhibition impacted the level of damage sustained to the cells, when treated with a known inducer of DNA damage; H_2O_2.

iv) And finally, to identify which mechanistic pathway could be responsible for the disparity in DNA damage in different SIRT1 environments.

5.3. Results

5.3.1. Diabetic patients exhibit DNA damage and decreased SIRT1 expression

Firstly, it was important to establish the prevalence of DNA damage within the diabetic vessels compared to control. Diabetic popliteal arterial vessels taken from patients undergoing lower limb amputation were examined histologically for calcification, senescence and DNA damage markers, and compared to non-calcified IMA harvested from CABG surgery patients. Von Kossa staining positively identified calcification via a precipitation reaction with the phosphate ions present, with Von Kossa staining negative within the smooth muscle and endothelium of the IMA samples (Fig. 5.1a). To confirm the presence of SIRT1 within the smooth muscle layer, SIRT1 was stained for, within both diabetic and control samples. Positive staining was decreased in the diabetic patient compared to the IMA, in which SIRT1 was found ubiquitously expressed within both the endothelium and the smooth muscle layer (Fig. 5.1b). Since senescence is often associated within DNA damage and calcification, Sudan Black (Fig. 5.1c) and p21 (Fig. 5.1d) staining were used to confirm the presence of senescence located within the smooth muscle layer. Both Sudan Black and p21 were positively stained within the diabetic vessel, with little to no staining observed within the IMA control. Furthermore, the TUNEL assay was used to confirm the fragmentation of DNA within the vessels via the attachment of a tagged form of dUTP to 3' ends of double and single stranded DNA breaks. Positive TUNEL staining was observed in all diabetic vessel samples examined, compared to the IMA which was negative (Fig. 5.1e). γH2AX staining was used to confirm the presence of DSBs. Staining was negative within the IMA vessel. Conversely, positive staining was observed both within the smooth muscle layer and the adventitia within the diabetic vessels (Fig. 5.1f). Since DNA damage repair protein complexes are assembled within minutes of damage occurring (493) and sustained until the damage is repaired to prevent cellular apoptosis, vessels removed from diabetic patients were assessed for presence of ATM and the MRN complex and compared to non-calcified IMA tissue. Positive staining confirmed the presence of ATM, RAD50 MRE11 and NBS1 within the smooth muscle layer of the diabetic vessel. Within the IMA controls faint ATM staining was observed throughout the vessel, however no positive staining was observed for MRE11, RAD50 or NBS1 (Fig. 5.1g-j).

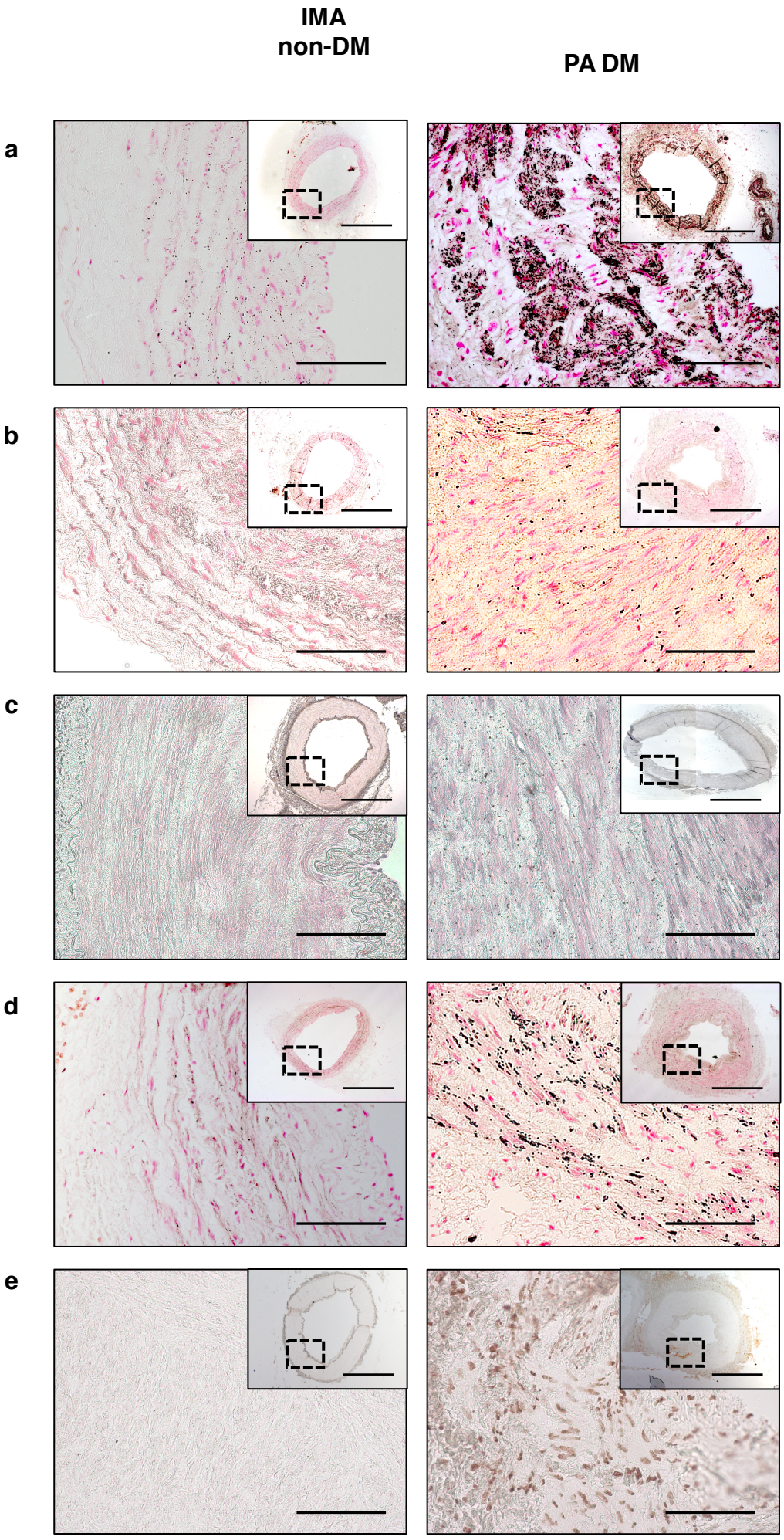
IMA
non-DM
PA DM
a
b
c
d
e

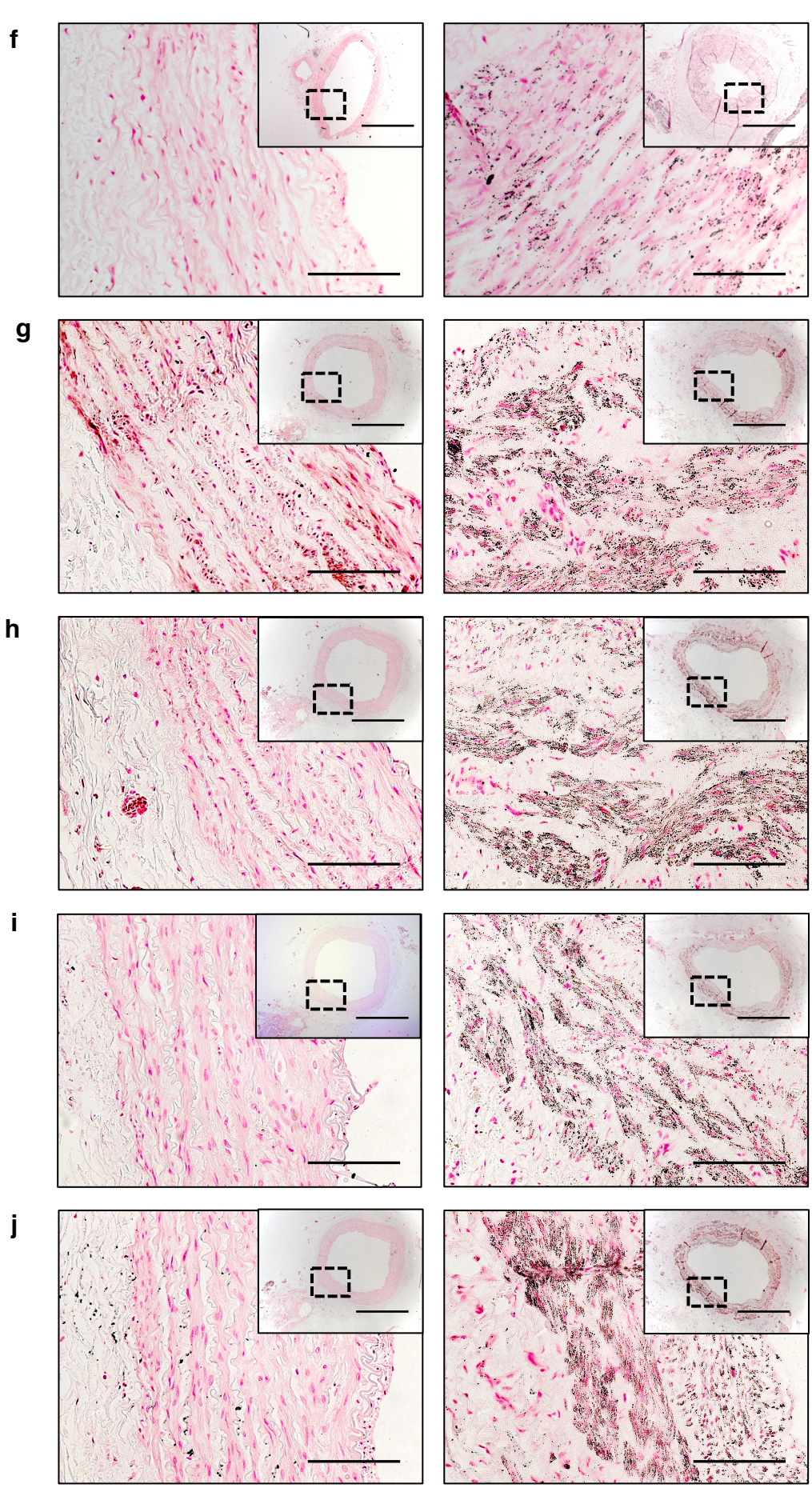
IMA
non-DM
PA DM
f
g
h
i
j

Fig. 5.1. Diabetic patient vessels exhibit increased DNA damage and senescence marker expression. Representative micrographs of popliteal arteries harvested from diabetic patients (DM) undergoing lower limb amputation and internal mammary artery (IMA) taken from non-diabetic patients. **a)** DM vessels showed positive Von Kossa staining compared to IMA controls, demonstrating an increase of phosphate within the vessel. **b)** SIRT1 expression was diminished in the DM patient vessel compared to the IMA control. DM vessels showed increased senescence markers **c)** lipofuscin (Sudan B) and **d)** p21 when compared to non-calcified IMA (n=3). **e)** A TUNEL assay was performed on both IMA and DM sections, demonstrating an increase in double stranded DNA nicks in the DM compared to IMA. **f)** γH2A.X staining was increased in DM patients and lacking in the IMA samples. **g)** DM patients showed an increase in ATM staining compared to IMA, **h)** MRE11 **i)** RAD50 **j)** NBS1 staining was increased in DM patients compared to IMA controls. (n=6). Scale bar=200µm/20µm. Mean ±SEM.

5.3.2. Cells harvested from diabetic patients exhibit low SIRT1 expression and increased DNA damage

To determine whether DNA damage was increased in vSMCs isolated from patients with diabetes and if this correlated with SIRT1 expression, known markers of DNA damage were analysed in an *in vitro* cell culture model. Following culture until 80% confluence in control 5 mM glucose conditions, cells were harvested and combined with agarose to determine DNA damage using electrophoresis via the comet assay.

vSMCs harvested from calcified popliteal vessels demonstrated a greater level of persistent DNA damage compared to healthy vSMC controls, indicated by a significantly larger tail moment ($p<0.0001$) and tail percentage ($p<0.0001$) (Fig. 5.2) compared to non-calcified controls. Telomere length confirmed via qPCR was also significantly decreased by over a quarter in diabetic vSMCs compared to healthy controls ($p<0.0095$) (Fig. 5.3a). Conversely, cellular senescence observed via p21 (Fig. 5.3b) and p53 (Fig. 5.3c) mRNA abundance was increased in diabetic patient cells compared to controls ($p<0.0022$), ($p<0.0476$) respectively. mRNA expression of ATM, a protein known to phosphorylate γH2AX, was upregulated three-fold in diabetic vSMCs compared to healthy controls ($p<0.0476$) (Fig. 5.3d).

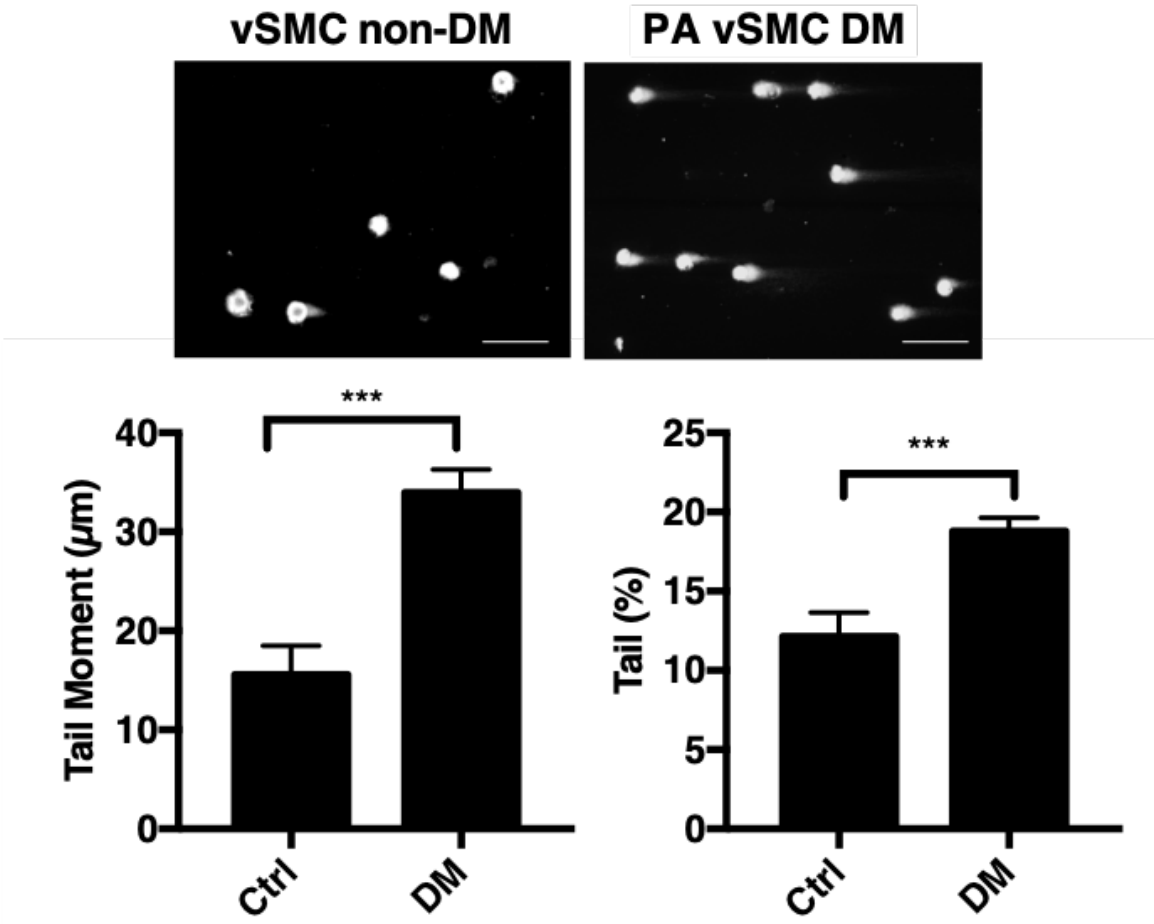

Fig. 5.2. Diabetic patient vSMCs exhibit DNA damage. vSMCs harvested from diabetic patients undergoing lower limb amputation demonstrated increased DNA damage compared to healthy controls. Cells were cultured in 5.5mM DMEM. Cells were cultured to 80% confluence within 6 well plates before harvesting. Double stranded DNA breaks were assessed via the comet assay. Tail DNA percentage increase by over a third in DM vSMCs compared to control, as did tail moment (n=6) (Unpaired T-test). *P<0.05, **P<0.005, ***P<0.001. Scale Bars = 100μm. Mean ±SEM.

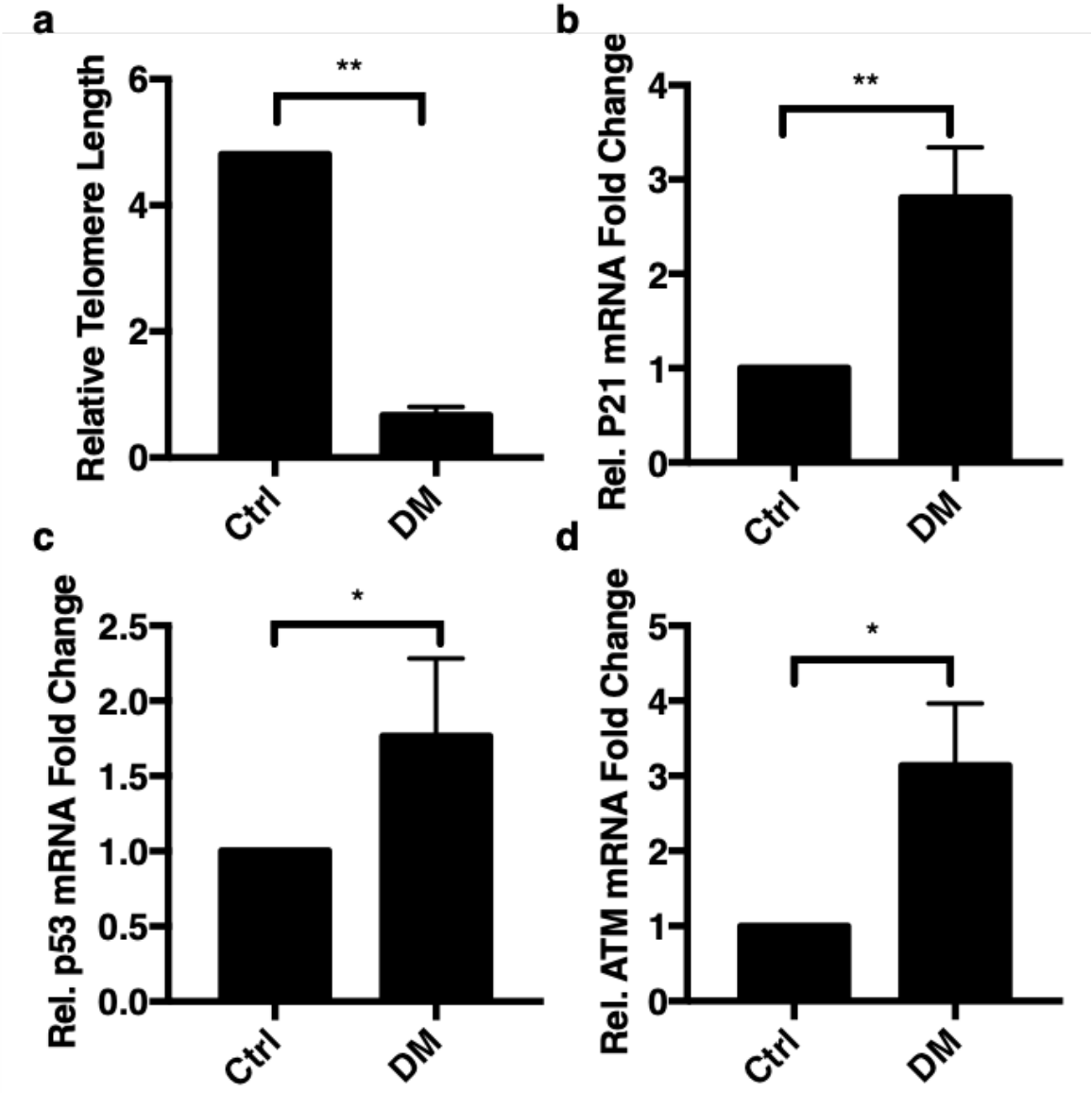

Fig. 5.3. Diabetic patient vSMCs exhibit decreased telomere length and increase senescence and DNA damage marker gene expression. vSMCs harvested from diabetic patients undergoing lower limb amputation demonstrated increased DNA damage marker expression compared to healthy controls. Cells were cultured in 5.5mM DMEM. **a)** DM samples showed a significant decrease in telomere length; assessed via qPCR, compared to healthy vSMCs (n=6). **b)** p21 mRNA expression was significantly increased in DM vSMCs compared to healthy controls (n=6), as was **c)** p53 (n=6) and **d)** ATM mRNA expression (n=6). (Unpaired T-test conducted **a-d**) *P<0.05, **P<0.005, ***P<0.001. Scale Bars = 100µm. Mean ±SEM.

5.3.3. Hyperglycaemic conditions induce DNA damage

Phosphorylation of histone H2AX at Ser139 is considered to be an early marker of DNA damage, which correlates with the development of DSBs (485). To determine how a diabetic environment modulates DNA damage in vSMCs, a well-established *in-vitro* calcification model was used. Briefly, three conditions were used within the model; untreated control conditions, containing 5 mM of glucose. Untreated osteogenic conditions, containing 5 mM glucose alongside 5 mM BGP and 2.6 mM $CaCl_2$, and finally untreated hyperglycaemic conditions, containing 25 mM glucose alongside 5 mM BGP and 2.6 mM $CaCl_2$.

Control cells had a baseline of 12 γH2AX foci per cell, with many cells exhibiting no foci at all (Fig. 5.4a). However, when cultured in hyperglycaemic conditions, cells exhibited significantly more foci when compared to both control ($p<0.0041$) and osteogenic ($p<0.0092$) conditions. To confirm the immunocytochemistry data, total protein harvested at day 4 was assessed for γH2AX expression via western blot, with a significant increase found in hyperglycaemic conditions compared to both control ($p<0.0072$) and osteogenic ($p<0.0079$) conditions (Fig. 5.4b). As the tumour suppressor p53 has previously been reported to mediate cell cycle arrest in hyperglycaemic conditions (87), p21 foci activation, the product of p53 activation during hyperglycaemic treatment, was examined. p21 foci were significantly upregulated by over a third in hyperglycaemic conditions compared to control ($p<0.0326$), however no difference was found in osteogenic conditions alone, when compared to control (Fig. 5.5a). A comet assay was used to determine naturally occurring DSBs in the *in-vitro* model. Tail moment was significantly increased in hyperglycaemic conditions compared to both osteogenic ($p<0.0001$) and control ($p<0.0001$) and furthermore a two-fold increase was observed in tail percentage between control and osteogenic ($p<0.0001$) and control and hyperglycaemic ($p<0.0001$) (Fig. 5.5b).

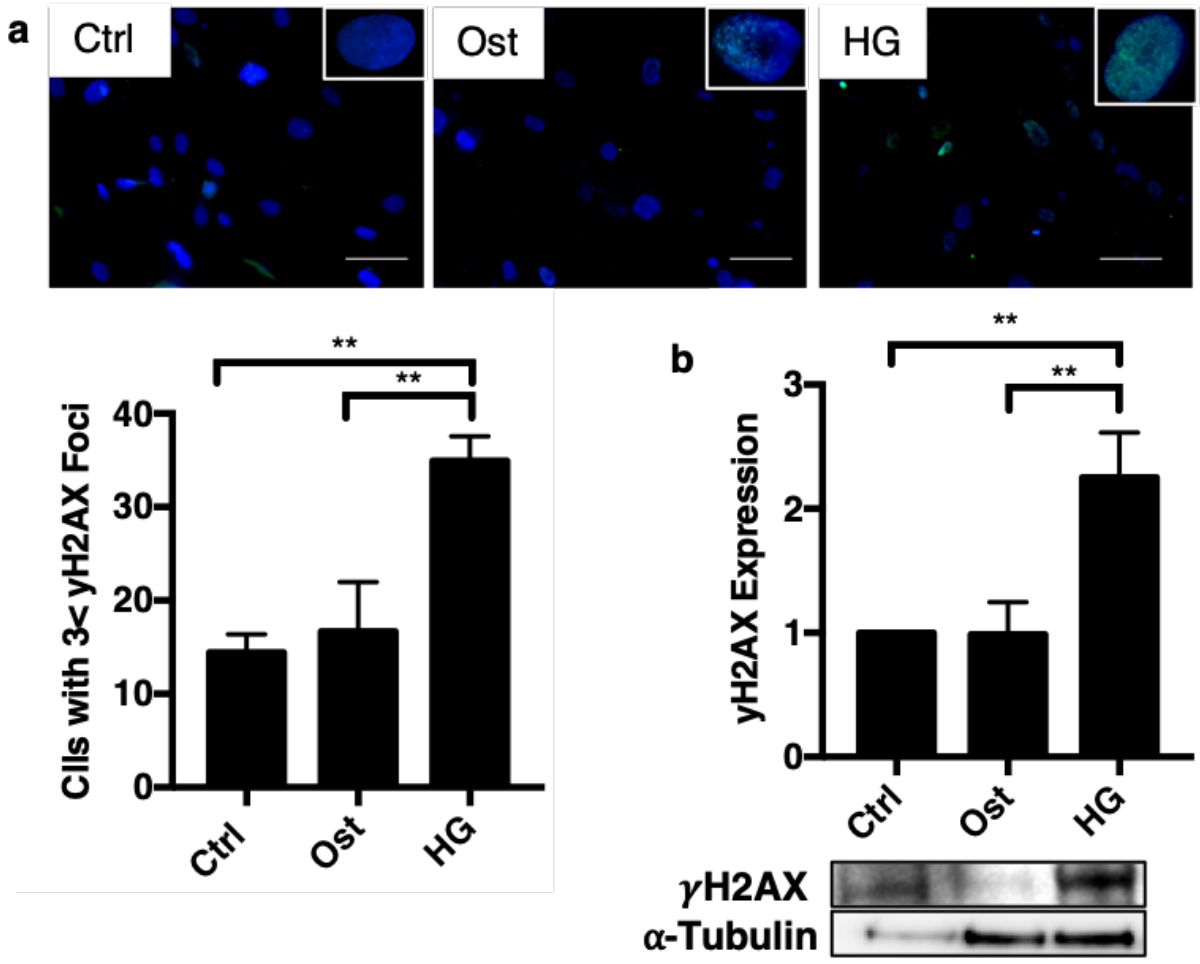

Fig. 5.4. Hyperglycaemic conditions increase DNA damage marker γH2AX expression. The effect of $CaCl_2$ and BGP in high glucose conditions was assessed**.** Three treatments were investigated; control (Ctrl), $CaCl_2$ and BGP osteogenic (Ost) and osteogenic with high glucose (HG). **a)** cells were cultured for 4 days in relevant media before fixing and staining for γH2AX foci. Foci count via ImageJ was significantly increased in hyperglycaemic conditions compared to both osteogenic and control (n=3) (One-way ANOVA, Tukey Post-Hoc test). **b)** protein harvested from all three treatments at the same timepoint showed significantly greater γH2AX expression in hyperglycaemic conditions compared to control and osteogenic condition (n=7) (One-way ANOVA, Tukey Post-Hoc test). DAPI blue, γH2AX green. *P<0.05, **P<0.005, ***P<0.001. Scale Bar = 10μm. Mean ±SEM.

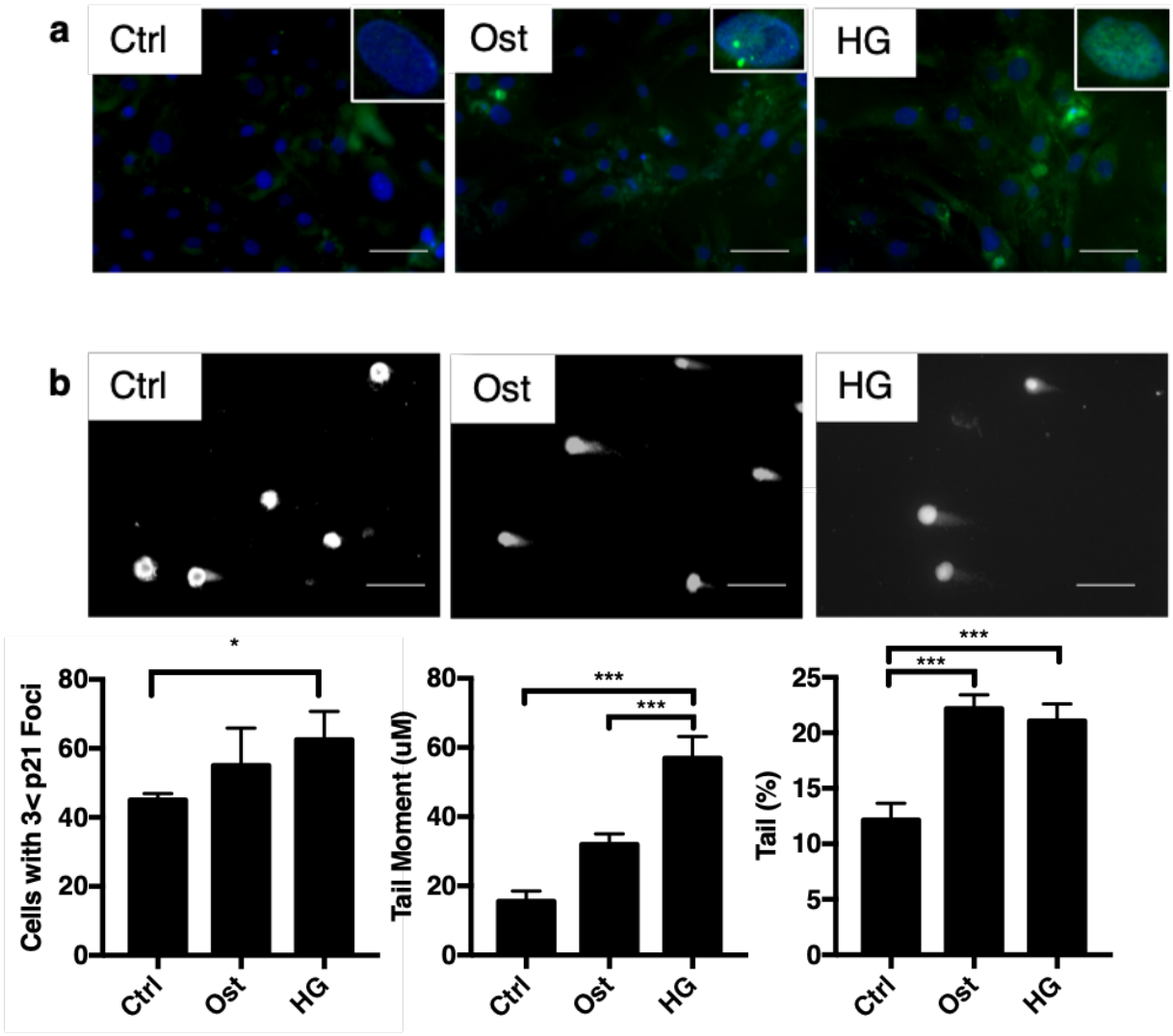

Fig. 5.5. Hyperglycaemic conditions increase DNA damage marker expression. The effect of three treatments were investigated; control (Ctrl), $CaCl_2$ and BGP osteogenic (Ost) and osteogenic with high glucose (HG). **a)** Following 4 days of treatment and subsequent fixing and staining, senescence marker p21 was significantly more pronounced in hyperglycaemic conditions compared to control (n=3) (One-way ANOVA, Tukey Post-Hoc test). **b)** DSBs assessed via the comet assay were significantly increased in hyperglycaemic conditions compared to control, demonstrated via tail moment and percentage of DNA within the tail (n=3) (One-way ANOVA, Tukey Post-Hoc test). DAPI blue, p21 green. *P<0.05, **P<0.005, ***P<0.001. Scale Bar = 10µm. Mean ±SEM.

5.3.4. SIRT1 attenuates DNA damage induced osteogenic differentiation

Firstly, to determine how DNA damage affects calcification in a diabetic environment, cells were cultured in the previously described, control, osteogenic and hyperglycaemic conditions in the presence or absence of 200μM H_2O_2 and SIRT1 activator; SRT1720 (0.5 μM), resulting in the following 9 conditions; untreated control, untreated osteogenic, untreated hyperglycaemic, H_2O_2 control, H_2O_2 osteogenic, H_2O_2 hyperglycaemic, and H_2O_2 SRT1720 control, H_2O_2 SRT1720 osteogenic and finally H_2O_2 SRT1720 hyperglycaemic conditions.

Cells treated with H_2O_2 alone exhibited increased calcification after 7 days when compared to those left untreated in both osteogenic ($p<0.0431$) and hyperglycaemic ($p<0.0468$) conditions. SIRT1 activation alongside H_2O_2 reduced Alizarin red staining significantly in both osteogenic ($p<0.0420$) and hyperglycaemic ($p<0.0471$) conditions (Fig. 5.6a). ALP activity was increased by day 4 in hyperglycaemic conditions compared to control, under both untreated ($p<0.0002$) and H_2O_2 conditions ($p<0.0004$). A significant increase was also noted between osteogenic and hyperglycaemic untreated conditions ($p<0.0029$). Moreover, a significant increase was found between osteogenic and hyperglycaemic treatments under H_2O_2 conditions ($p<0.0110$), with a significant increase in ALP activity under H_2O_2 hyperglycaemic conditions when compared to untreated hyperglycaemic conditions ($p<0.0001$). Finally, a reduction in ALP activity was observed when treated with SRT1720 and H_2O_2 when compared to H_2O_2 conditions alone under hyperglycaemic conditions ($p<0.0011$) (Fig. 5.6b).

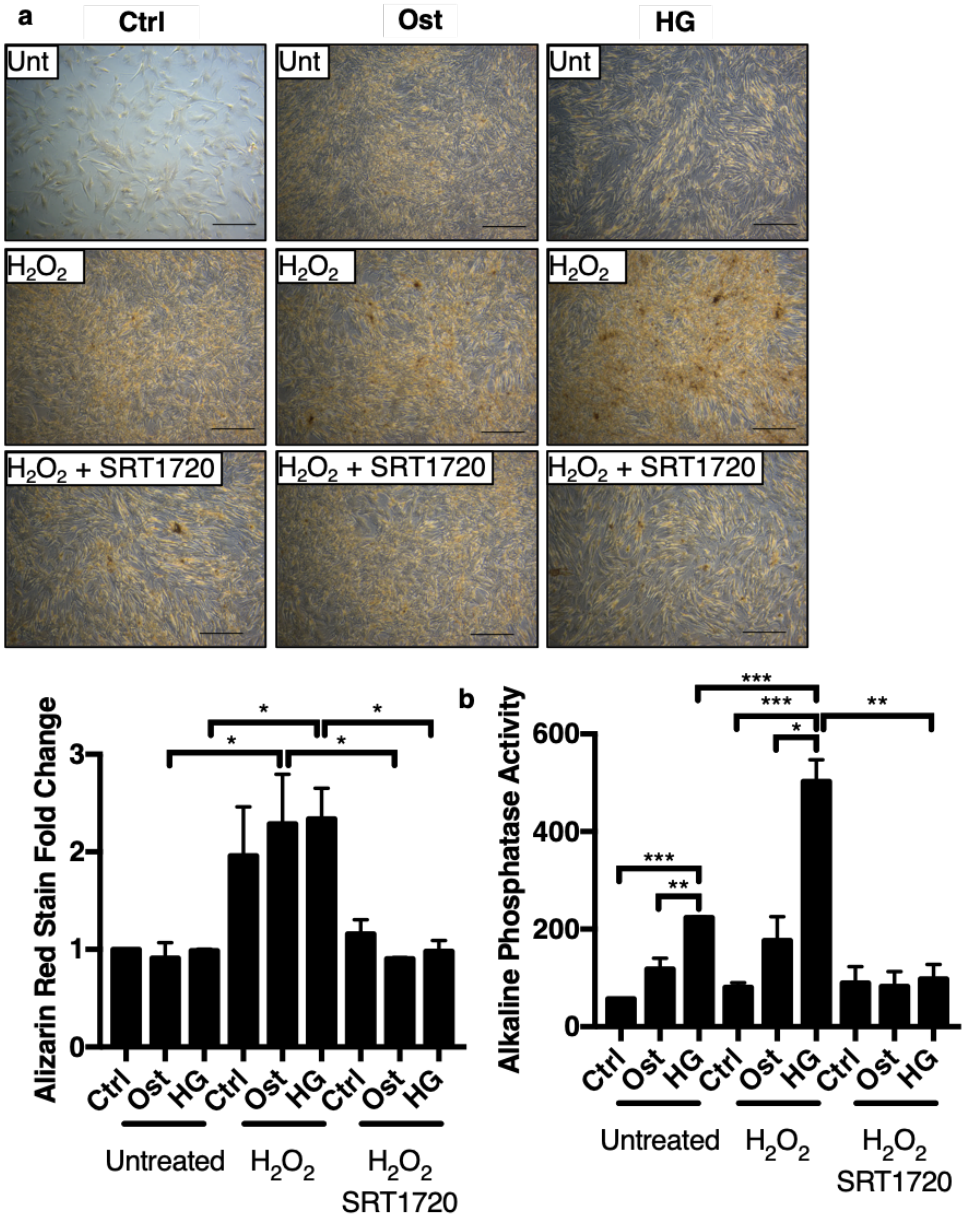

Fig. 5.6. SIRT1 activation inhibits DNA damage induced smooth muscle calcification. H_2O_2 treatment induces osteogenic smooth muscle cell differentiation through the Runx2 pathway. The effect of SIRT1 activator SRT1720 on smooth muscle calcification was investigated, with 0.1% DMSO used within untreated controls. Three treatments were investigated; control (Ctrl), $CaCl_2$ and BGP osteogenic (Ost) and osteogenic with high glucose (HG). 200 μM H_2O_2 was used to induce DNA damage. **a)** Alizarin red staining at day 7 showed no increase in untreated hyperglycaemic conditions, however an increase was seen in H_2O_2 treatment, which was reduced with 0.5 μM SRT1720 pre-incubation (n=3) (Two-way ANOVA, Tukey Post-Hoc test). **b)** Day 4 ALP activity was increased in H_2O_2 treatment and reduced in all 0.5 μM SRT1720 conditions (n=3) (Two-way ANOVA, Tukey Post-Hoc test). *P<0.05, **P<0.005, ***P<0.001. Scale Bar = 100μm. Mean ±SEM.

To confirm the development of osteogenic differentiation, Runx2 and OCN mRNA expression was examined following 4 days of treatment. Both Runx2 (Fig. 5.7a) and OCN (Fig. 5.7b) were upregulated in H_2O_2 treated hyperglycaemic conditions compared to untreated hyperglycaemic conditions ($p<0.0035$) ($p<0.0425$) respectively. Runx2 activation increased between untreated control and untreated hyperglycaemic conditions ($p<0.0188$). Additionally, Runx2 mRNA expression increased in control conditions between H_2O_2 treated and untreated cells ($p<0.0288$), with a significant reduction in Runx2 mRNA abundance when cells were treated with SRT1720 in hyperglycaemic conditions under the presence of H_2O_2 ($p<0.0001$). OCN mRNA abundance increased significantly between control H_2O_2 treated cells and both osteogenic H_2O_2 ($p<0.0081$) and hyperglycaemic H_2O_2 ($p<0.0425$) treated cells. Finally, following treatment with SRT1720 under hyperglycaemic H_2O_2 conditions, OCN mRNA expression decreased over 30-fold ($p<0.0009$) when compared to hyperglycaemic H_2O_2 conditions alone.

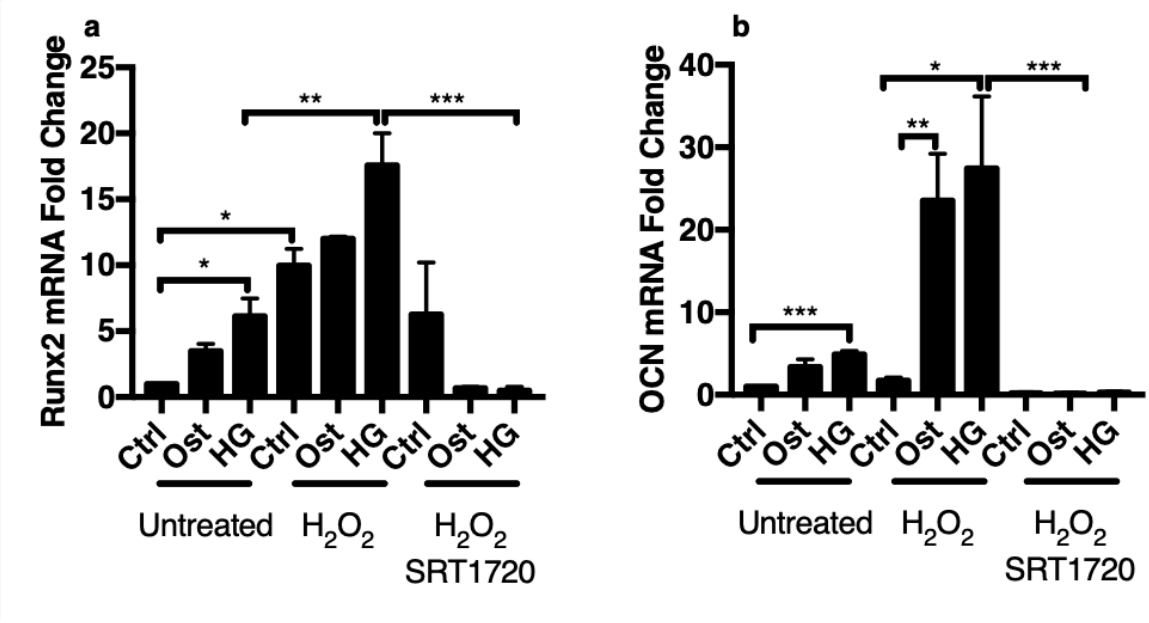

Fig. 5.7. SIRT1 activation inhibits DNA damage induced osteogenic markers. 30 minutes of 200 μM H_2O_2 treatment induces osteogenic marker expression within vSMCs. Cells were pre-treated for 4 days; with SIRT1 activator; SRT1720 with 0.1% DMSO used within untreated controls to equivalate toxicity. Three treatments were investigated; control (Ctrl), $CaCl_2$ and BGP osteogenic (Ost) and osteogenic with high glucose (HG), before 30 minutes of exposure to H_2O_2 and subsequent harvesting for RNA. **a)** Runx2 mRNA expression was significantly increased during hyperglycaemic treatment, and further increased when treated with H_2O_2, but reduced with 0.5 μM SRT1720 pre-incubation (n=4) (Two-way ANOVA, Tukey Post-Hoc test). **b)** OCN mRNA expression was significantly increased in both osteogenic and hyperglycaemic conditions with H_2O_2 treatment and was significantly reduced in 0.5 μM SRT1720 treated cells (n=4) (Two-way ANOVA, Tukey Post-Hoc test). *P<0.05, **P<0.005, ***P<0.001. Mean ±SEM.

5.3.5. SIRT1 translocation increased following DNA damage

Given the observed increase in osteogenic markers following treatment with H_2O_2, the effect of H_2O_2 on SIRT1 expression was assessed. Following 4 days of treatment, cells were fixed and stained for with SIRT1 and F-Actin marker phalloidin. SIRT1 staining appeared to reduce following osteogenic treatment, with a greater reduction observed under hyperglycaemic conditions. An increase in SIRT1 staining was shown across all three H_2O_2 treated conditions compared to untreated (Fig. 5.8a).

To confirm the fluorescent staining, protein was harvested at the same timepoint and assessed via western blot. Following osteogenic ($p<0.0493$) and hyperglycaemic ($p<0.0008$) treatments, SIRT1 expression significantly decreased as expected (previously demonstrated in Fig. 3.1a), however following H_2O_2 treatment, SIRT1 expression was increased in all three conditions, with a significant upregulation detected between the hyperglycaemic conditions ($p<0.0041$) (Fig. 5.8b). Interestingly, a small reduction in SIRT1 expression was observed when comparing H_2O_2 treated osteogenic and hyperglycaemic conditions ($p<0.0138$), however this was still higher than the comparative condition left untreated.

Following this, the translocation of SIRT1 following H_2O_2 treatment was assessed at the same timepoint, using a nuclear fractionation kit (Abcam). In untreated conditions, there was a relatively even distribution of SIRT1 between the cytoplasm and the nucleus. However, when treated with H_2O_2 under hyperglycaemic conditions, SIRT1 was retained almost entirely to the cytoplasm instead of being translocated to the nucleus ($p<0.0005$) (Fig. 5.8c). Moreover, an increase in cytoplasmic SIRT1 was found between control and both osteogenic ($p<0.0075$) and hyperglycaemic ($p<0.0031$) conditions following H_2O_2 treatment.

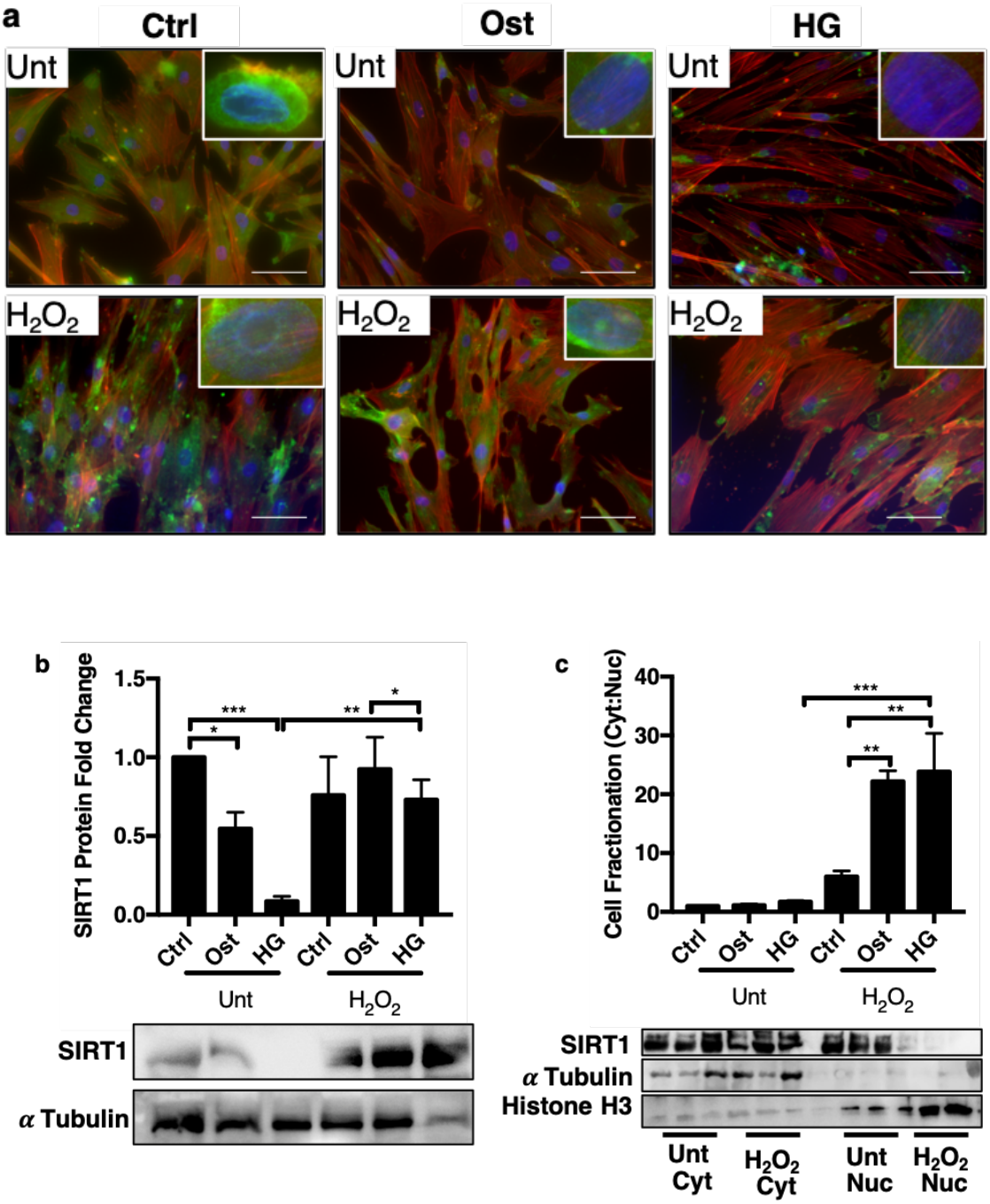

Fig. 5.8. SIRT1 expression is increased following DNA damage but reduced in the nucleus. 30 minutes of 200 µM H_2O_2 treatment induces SIRT1 expression reduces nuclear SIRT1 expression. **a)** Following 4 days treatment in three conditions; control (Ctrl), $CaCl_2$ and BGP osteogenic (Ost) and osteogenic with high glucose (HG), cells were treated with H_2O_2 and immediately fixed and stained. SIRT1 expression appears to be decreased in hyperglycaemic treatments compared to controls in both untreated and H_2O_2 treated vSMCs (n=3). **b**) Concurrent with staining, cells were harvested for protein following DNA damage.

SIRT1 expression significantly reduced following hyperglycaemic treatment and was significantly increased following H_2O_2 treatment in all three treatments (n=3) (Two-way ANOVA, Tukey Post-Hoc test). **c)** Cell fractionation was conducted to determine the subcellular location of SIRT1 following DNA damage. Fractionation demonstrated a significant shift in SIRT1 expression from the nucleus into the cytoplasm following H_2O_2 damage, with an increase in cytoplasmic SIRT1 in hyperglycaemic treatment compared to control (n=3) (Two-way ANOVA, Tukey Post-Hoc test). SIRT1 green, F-actin red, DAPI blue. *P<0.05, **P<0.005, ***P<0.001. Scale Bars = 100μm. Mean ±SEM.

5.3.6. SIRT1 activation protects against DNA damage

Having demonstrated the reduction of SIRT1 correlating with an increase in DNA damage, the effect of SIRT1 modulation was examined in vSMCs following recovery from the DSBs induced by H_2O_2. vSMCs were treated for 4 days with SIRT1 activator SRT1720 (0.5 μM) or SIRT1 inhibitor Sirtinol (10 μM), before staining and counting of γH2AX foci within the nucleus or undergoing single cell electrophoresis via the comet assay.

Cells were either left untreated and stained or treated with 200 μM of H_2O_2 for 30 minutes and left to recover in fresh complete media before staining at 1 hour and 3-hour time points. γH2AX staining showed no significant change before H_2O_2 treatment following 4 days of pre-treatment with either SRT1720 or Sirtinol (Fig. 5.9a). Following 30 minutes of H_2O_2 treatment, a significant increase was observed in foci number between SRT1720 treated hyperglycaemic cells and Sirtinol hyperglycaemic cells ($p<0.0147$) (Fig. 5.9b). Finally, following 3 hours of recovery, a significant decrease was observed in control conditions, between untreated and SRT1720 ($p<0.0001$) and a significant increase between untreated and Sirtinol treated cells ($p<0.0282$). In osteogenic conditions following 3 hours recovery, a significant increase was observed between Sirtinol and SRT1720 treated cells ($p<0.0088$). Lastly, under hyperglycaemic conditions after 3 hours recovery, SRT1720 reduced foci count by over half compared to Sirtinol treatment ($p<0.0001$) with SRT1720 treated cells expressing 40% less foci than untreated conditions ($p<0.0039$). Sirtinol activation increased foci accumulation by over 20% compared to untreated ($p<0.0037$) (Fig. 5.9c). All data was analysed via ImageJ (Fig. 5.9d).

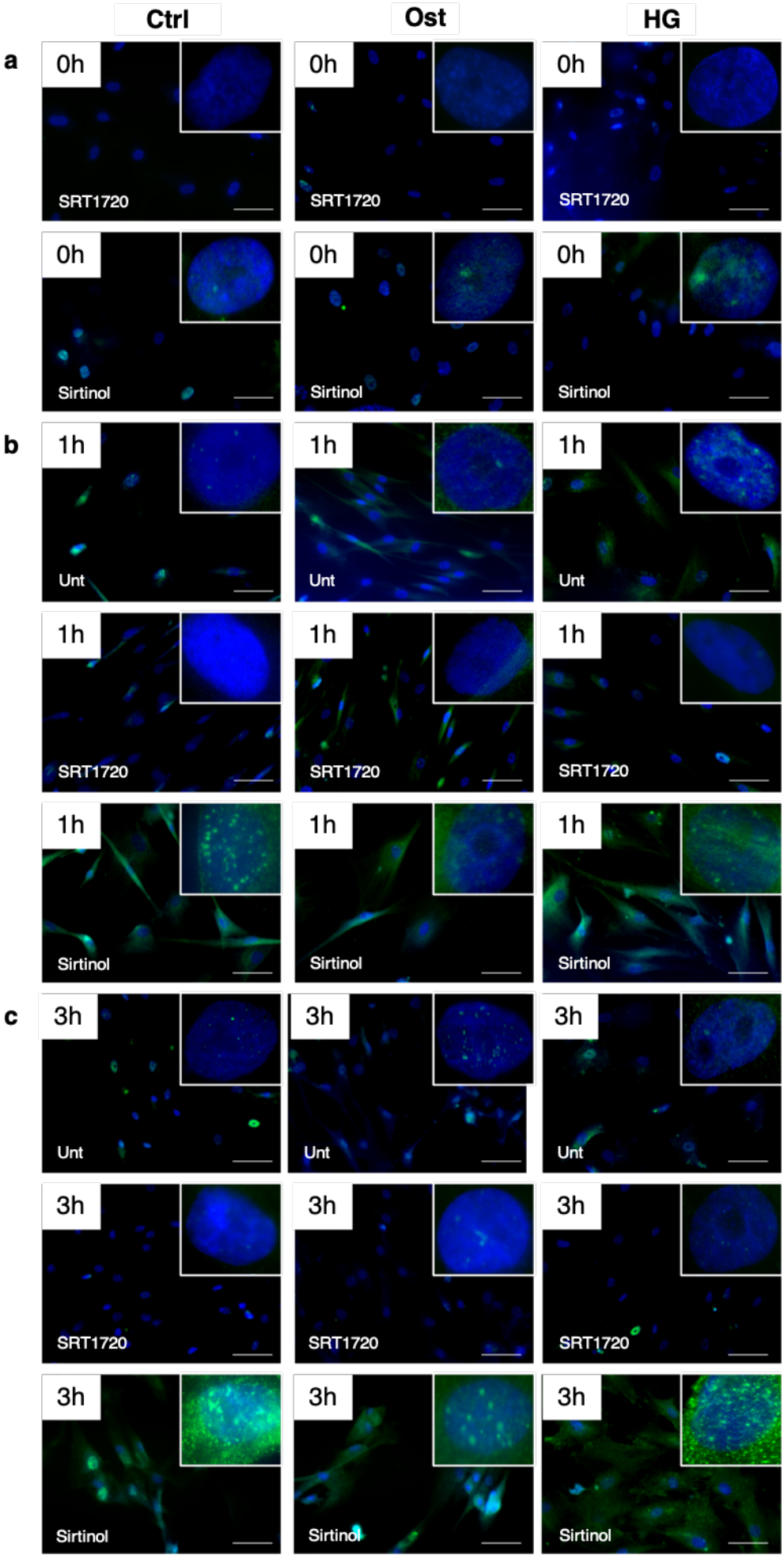
Ctrl
Ost
HG
a
0h
SRT1720
Sirtinol
b
1h
Unt
c
3h

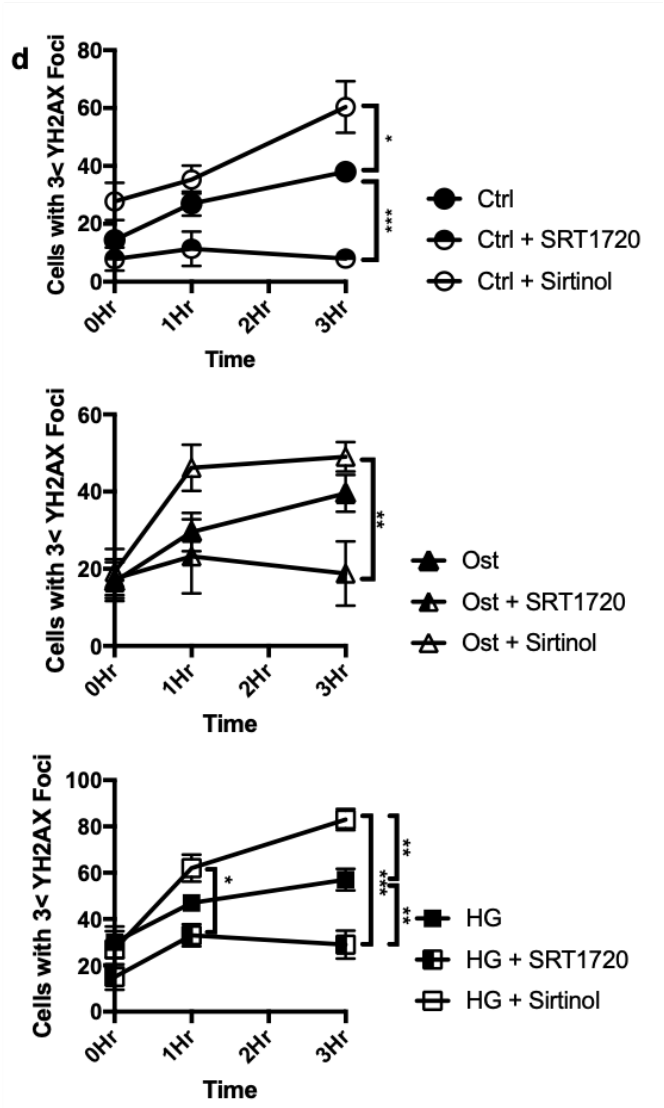

Fig. 5.9. SIRT1 activation decreases DNA damage marker γH2AX expression. Presence of γH2AX was confirmed via fluorescent staining. The effect of SIRT1 activator SRT1720 and SIRT1 inhibitor Sirtinol was investigated, with 0.1% DMSO used within untreated controls. Three treatments were investigated; control (Ctrl), $CaCl_2$ and BGP osteogenic (Ost) and osteogenic with high glucose (HG). 200 μM H_2O_2 was used to induce DNA damage. Pre-treatment of cells with 0.5 μM SRT1720 for 4 days before damage decreased γH2AX foci accumulation both **a)** before and **b)** after DNA damage via H_2O_2, and **c)** reduced the perpetuation of DNA damage after 3h. Conversely, 10 μM Sirtinol treatment increased **b)** cellular response to DNA damage demonstrated via γH2AX staining, which **c)** prolonged the damage response 3h after initial damage (n=3) **d)** quantification of all foci via ImageJ (Two-way ANOVA, Tukey Post-Hoc test). Cells were either supplemented with 0.5 μM SRT1720, 10 μM Sirtinol or 0.1% DMSO to equivalate toxicity. DAPI blue, γH2AX green, images shown on previous page. *P<0.05, **P<0.005, ***P<0.001. Scale Bar = 10μm. Mean ±SEM.

DSBs were again assessed by the comet assay. Following pre-treatment for 4 days with SIRT1 activator SRT1720 (0.5 μM) or SIRT1 inhibitor Sirtinol (10 μM), cells were either left untreated or treated with 200 μM of H_2O_2 for 30 minutes and left to recover in fresh media before DNA was isolated and underwent electrophoresis to assess DNA damage.

Head percentage was maintained at 90% with SRT1720 treated cells in the control environment, which was significantly greater than both the untreated ($p<0.0001$) and Sirtinol ($p<0.0001$) treatment after 3h recovery period, with Sirtinol inhibition of SIRT1 significantly reducing head percentage compared to control ($p<0.0001$) (Fig 5.10b). Osteogenic conditions showed no significant difference before damage and 1h following H_2O_2 damage, however a 20% repair in head percentage was observed in SRT1720 treated cells after 3h recovery compared to untreated ($p<0.0490$). Interestingly, a 10% recovery was detected in Sirtinol treated cells following a 3h incubation, however this trend was not significant. Hyperglycaemic conditions demonstrated the greatest decrease in head percentage when comparing Sirtinol to untreated and SRT1720 treated cells, with a significant drop observed in Sirtinol treatment after 3h when compared to SRT1720 ($p<0.0001$) and untreated ($p<0.0001$). Furthermore, SRT1720 maintained 20% greater DNA within the head of the comet compared to untreated after 3 hours recovery ($p<0.0001$). Moreover, SRT1720 treated cells showed no significant difference between all three conditions when comparing head percentage, whereas untreated and Sirtinol treatment significantly reduced head percentage between control and hyperglycaemic conditions ($p<0.0001$) ($p<0.0001$) respectively.

Tail moment, an index of induced DNA damage taking into consideration both migration and relative amount of DNA in the tail, was also used to assess the DNA damage and subsequent repair. Within control treatment, tail moment did not vary significantly between 0h and 3h after damage, however a significant increase in moment was identified between Sirtinol ($p<0.0001$) and untreated ($p<0.0001$), compared to SRT1720 treatment. There was no significant difference between osteogenic and hyperglycaemic treatment regarding tail moment, however the addition of SRT1720 significantly reduced tail moment when compared to Sirtinol and untreated in both osteogenic ($p<0.0001$), ($p<0.0001$) and hyperglycaemic

($p<0.0001$), ($p<0.0001$) conditions. Finally, a significant increase in tail moment was observed between Sirtinol and untreated in both osteogenic ($p<0.0001$) and hyperglycaemic ($p<0.0001$) conditions (Fig. 5.10a-d).

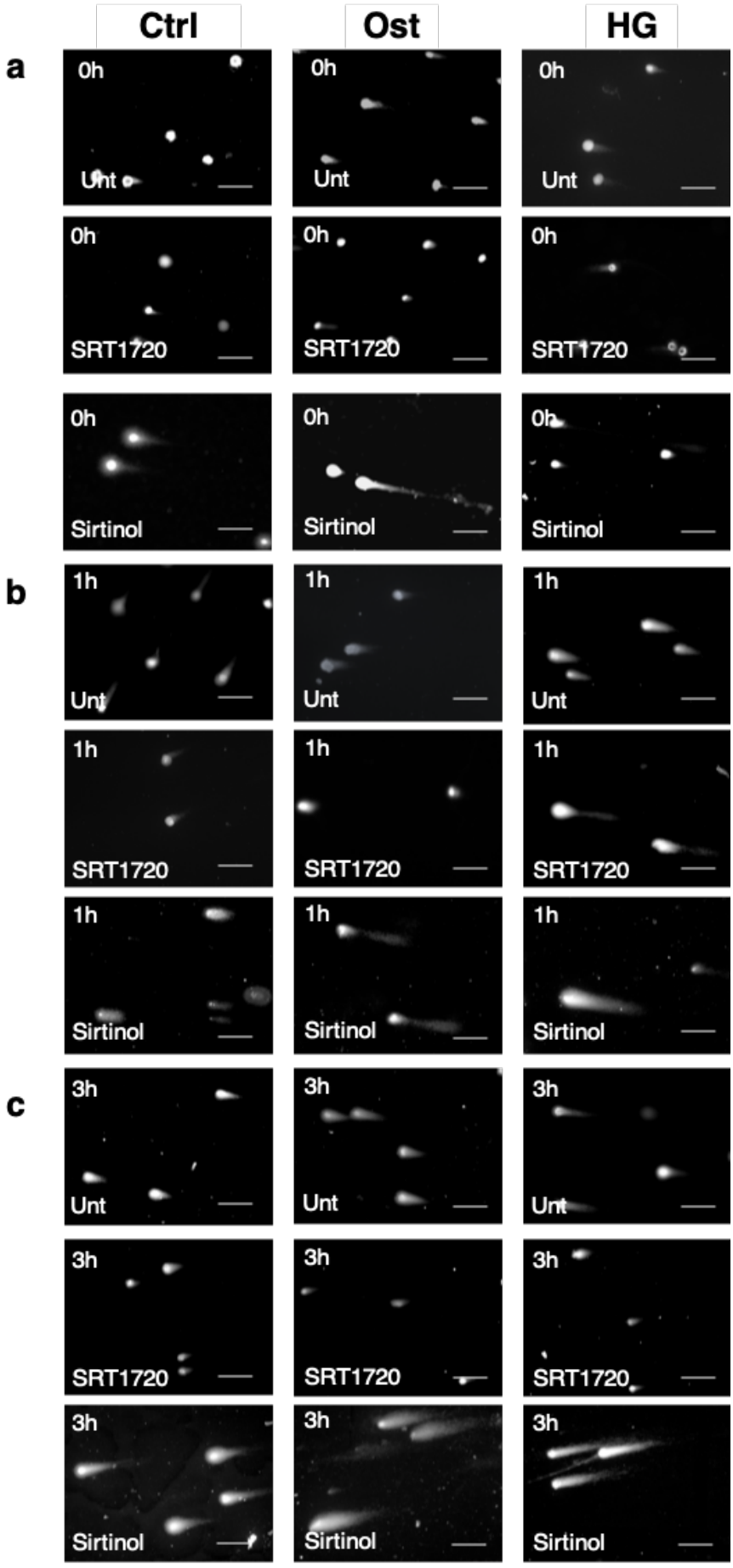
Ctrl
Ost
HG
a
0h
Unt
0h
SRT1720
0h
Sirtinol
b
1h
Unt
1h
SRT1720
1h
Sirtinol
c
3h
Unt
3h
SRT1720
3h
Sirtinol

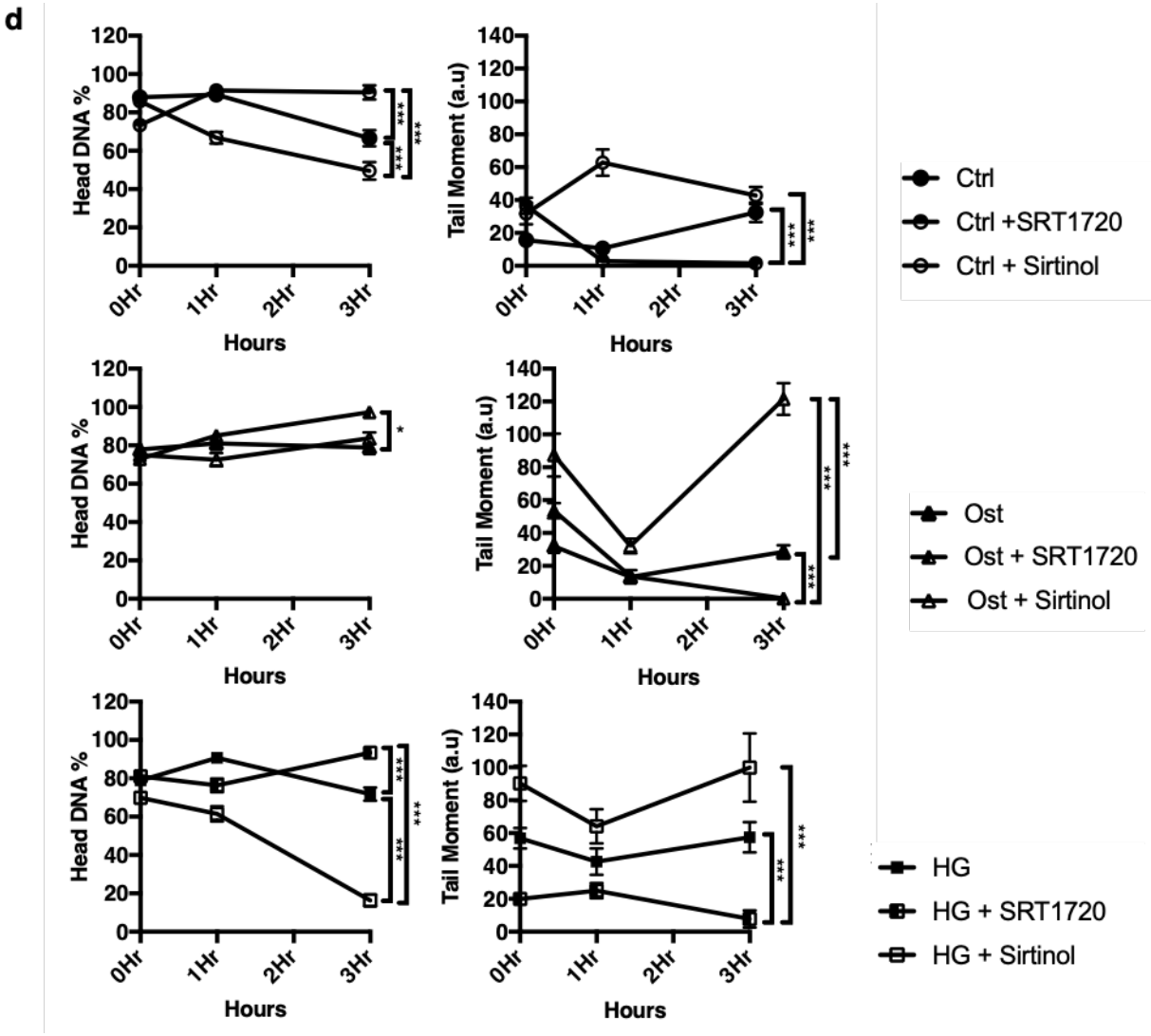

Fig. 5.10. SIRT1 activation protects against DSB formation. DSBs were determined via the comet assay. The effect of SIRT1 activator SRT1720 and SIRT1 inhibitor Sirtinol was investigated, with 0.1% DMSO used within untreated controls. Three treatments were investigated; control (Ctrl), $CaCl_2$ and BGP osteogenic (Ost) and osteogenic with high glucose (HG). 200 μM H_2O_2 was used to induce DNA damage. **a)** Following 4 days of pre-treatment in respective conditions, DNA damage was assessed before induction of damage via H_2O_2. No significant change was seen in either tail moment or head percentage in 0.5 μM SRT1720, 10 μM Sirtinol or untreated conditions. **b)** Following 30 minutes treatment with H_2O_2 cells were harvested immediately and assessed for damage. No significant change was seen between 0.5 μM SRT1720, 10 μM Sirtinol and untreated conditions. **c)** Following damage, cells were left to recover for 3 hours in complete media and the DNA was again assessed. In control conditions head DNA percentage significantly

decreased and tail moment significantly increased following 10 μM Sirtinol treatment, a pattern which was also seen in both osteogenic and hyperglycaemic conditions. 0.5 μM SRT1720 treatment had the inverse effect, with a decrease in time taken to repair seen compared to untreated conditions (n=3). **d)** Quantification of all slides conducted on ImageJ to demonstrate significance. (n=3) (Two-way ANOVA, Tukey Post-Hoc test). Corresponding images shown on previous page. *P<0.05, **P<0.005, ***P<0.001. Scale Bar = 10μm. Mean ±SEM.

5.3.7. SIRT1 activation reduces chromatin acetylation and increases MRN activation

Once DNA damage has been detected within the cell, sensor proteins are recruited to the damage sites and orchestrate the formation of multiprotein complexes for DDR activation (494). Initially H2AX is bound to DSBs, where it binds and is phosphorylated via an active acetylated ATM. This phosphorylation binds NBS1 first, forming a trimeric complex with MRE11 and RAD50, tethering the MRN complex to the DNA damage site before translocating to the nucleus and forming distinct foci with γH2AX at DSBs (484).

Since DDR activation is primarily activated by ATM phosphorylation (493), its activation profile was considered. Firstly, ChIP was performed to determine the acetylation profile of the promotor region within the ATM gene. Acetylation was significantly increased in a hyperglycaemic environment compared to osteogenic conditions ($p<0.0054$), with SIRT1 activation significantly reducing acetylation around the H3K27Ac mark in hyperglycaemic conditions ($p<0.0074$) (Fig. 5.11a). Acetylation of the MRN complex was then examined. Acetylation of the MRE11 promotor region did not significantly change under hyperglycaemic conditions, nor with the activation of SIRT1 in either three treatments. Conversely, RAD50 promotor acetylation was significantly increased following hyperglycaemic treatment compared to control ($p<0.0019$) and osteogenic conditions ($p<0.0010$), with SIRT1 activation significantly reducing acetylation in hyperglycaemic conditions ($p<0.0012$). Finally, NBS1 promotor acetylation was significantly increased following hyperglycaemic treatment in untreated conditions compared to control ($p<0.0002$) and reduced following SIRT1 activation within the same condition ($p<0.0002$).

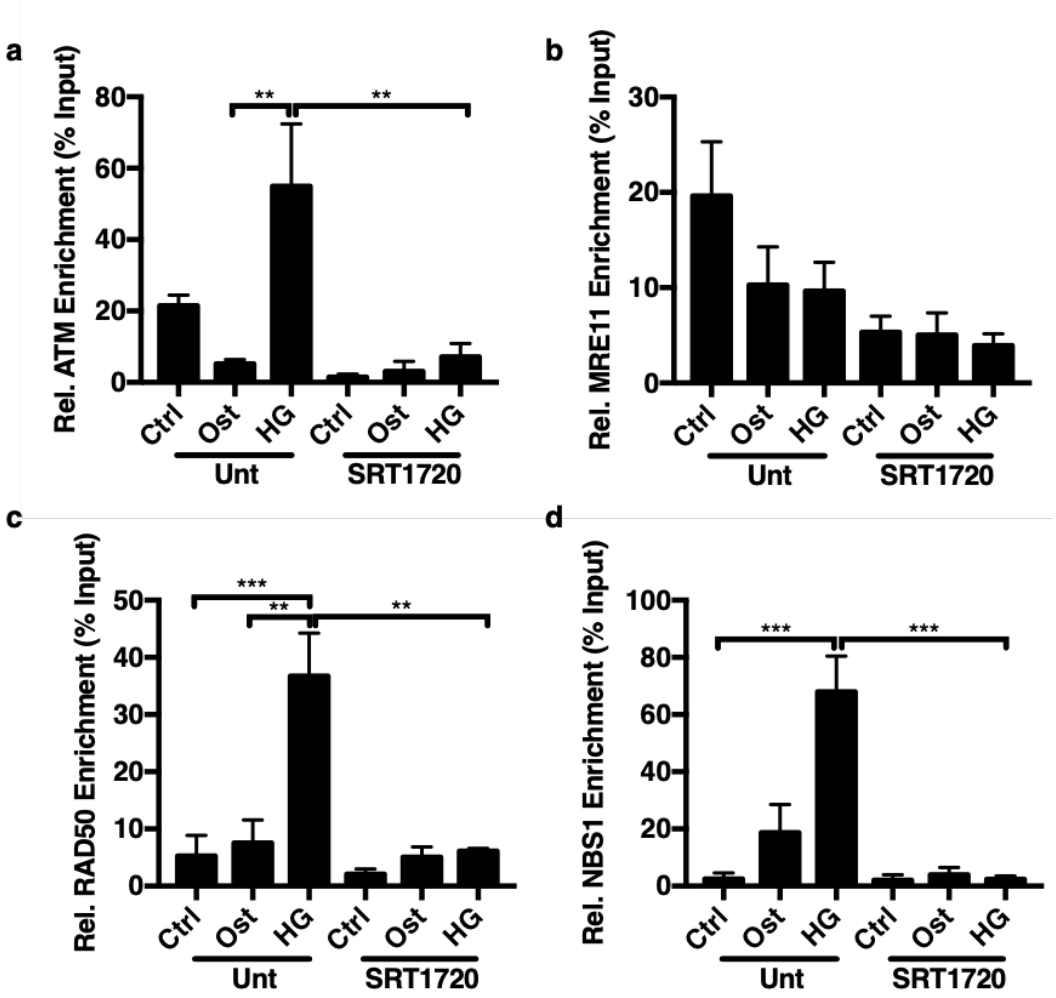

Fig. 5.11. SIRT1 activation reduces promotor acetylation of MRN complex. Following 4 days of treatment in three conditions; control (Ctrl), $CaCl_2$ and BGP osteogenic (Ost) and osteogenic with high glucose (HG), in the effect of SIRT1 activator SRT1720 was investigated, with 0.1% DMSO used within untreated controls. Chromatin immunoprecipitation was performed with an anti-acetyl-lysine antibody to assess the acetylation profile of the ATM and MRN complex. **a)** ATM promotor acetylation was increased during hyperglycaemic treatment and was significantly reduced following treatment with 0.5 µM SRT1720 (n=3). **b)** MRE11 promotor acetylation was decreased in hyperglycaemic conditions and further reduced with the activation of SIRT1, however this was not significant (n=3). **c)** RAD50 promotor acetylation was significantly decreased when cells were cultured in a hyperglycaemic environment with 0.5 µM SRT1720 when compared to untreated hyperglycaemic conditions (n=3). **d)** Acetylation of the NBS1 promotor was significantly increased in hyperglycaemic conditions compared to control and decreased when cells were cultured in a hyperglycaemic environment with 0.5 µM SRT1720 (n=3). (Two-way ANOVA, Tukey Post-Hoc test conducted **a-d**). *P<0.05, **P<0.005, ***P<0.001. Mean ±SEM.

Following assessment of the promotor acetylation, the impact of SIRT1 activation under DNA damage inducing conditions on protein expression was examined. Total ATM expression was increased in untreated hyperglycaemic compared to control ($p<0.0038$) concurrently upregulated with γH2AX protein expression, which was also increased in a hyperglycaemic environment (Fig. 5.4b). Of note, H_2O_2 increased the baseline expression of ATM, with a significant reduction identified within the hyperglycaemic treatment compared to untreated hyperglycaemic conditions following H_2O_2 damage ($p<0.0021$). Furthermore, ATM expression was found to be significantly upregulated with SIRT1 activation after H_2O_2 damage, with a significant increase observed in both osteogenic ($p<0.0001$) and hyperglycaemic ($p<0.0001$) conditions compared to H_2O_2 damage alone, with a 50% increase found when comparing control and osteogenic H_2O_2 SRT1720 treated cells ($p<0.0030$) (Fig. 5.12a).

Activation of the MRN complex was next examined. No significant change in phosphorylation of MRE11 was found between all three untreated and H_2O_2 damaged cells. However, when SIRT1 was activated within a H_2O_2 DNA damage inducing environment, MRE11 phosphorylation significantly increased in hyperglycaemic conditions between untreated ($p<0.0001$) and H_2O_2 damage alone ($p<0.0001$). Additionally, a significant increase was found under hyperglycaemic conditions compared to osteogenic under SRT1720 H_2O_2 conditions ($p<0.0303$) (Fig. 5.12b). Next, RAD50 protein expression was examined. RAD50 expression under hyperglycaemic conditions was significantly increased compared to untreated cells ($p<0.0146$), however a 4-fold increase was observed when pre-treated with SRT1720, which was a significant increase when compared to hyperglycaemic untreated ($p<0.0001$) and H_2O_2 hyperglycaemic conditions ($p<0.0001$). Moreover, under control conditions, RAD50 expression increased 3-fold with SIRT1 activation when compared to H_2O_2 alone ($p<0.0001$). Finally, no change was found in NBS1 phosphorylation following H_2O_2 treatment, irrespective of condition. However, a significant increase was observed in both osteogenic ($p<0.0001$) and hyperglycaemic ($p<0.0015$) conditions following SIRT1 activation under H_2O_2 conditions, compared to H_2O_2 alone. Likewise, a 5-fold increase was observed in hyperglycaemic H_2O_2 SRT1720 treated cells compared to untreated ($p<0.0002$) (Fig. 5.12d).

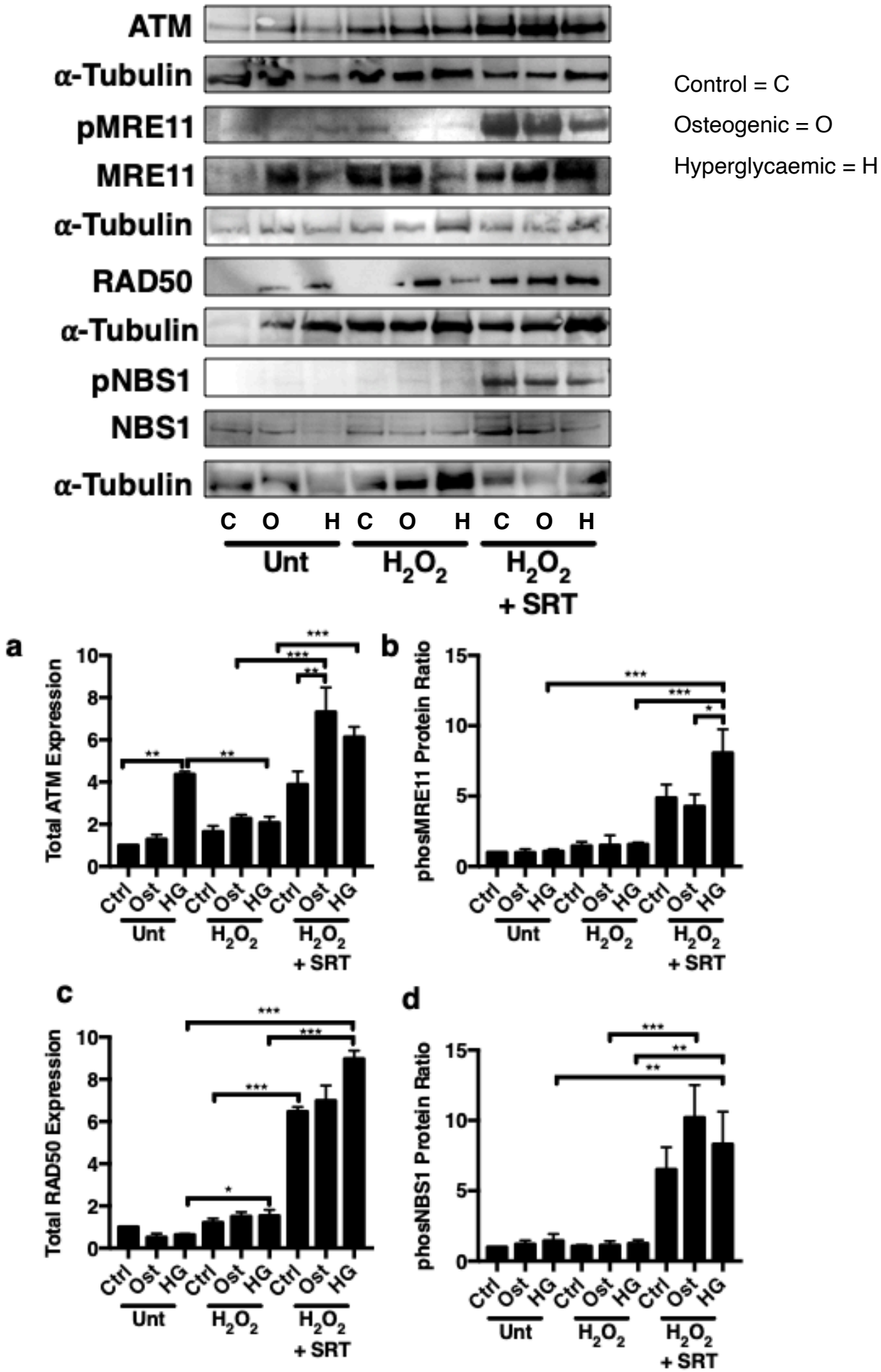
ATM
α-Tubulin
pMRE11
MRE11
α-Tubulin
RAD50
α-Tubulin
pNBS1
NBS1
α-Tubulin
C O H C O H C O H
Unt
H2O2
H2O2 + SRT
Control = C
Osteogenic = O
Hyperglycaemic = H
a
Total ATM Expression
b
phosMRE11 Protein Ratio
c
Total RAD50 Expression
d
phosNBS1 Protein Ratio
Ctrl Ost HG
Unt
H2O2
H2O2 + SRT

Fig. 5.12. SIRT1 activation reduces MRN complex activation. Following 4 days of treatment in previously noted conditions, protein expression of ATM and the MRN complex was assessed. Cells were either supplemented with 0.5 μM SRT1720 or 0.1% DMSO to equivalate toxicity and cultured in three conditions; control (Ctrl), $CaCl_2$ and BGP osteogenic (Ost) and osteogenic with high glucose (HG). **a)** ATM protein expression was increased under hyperglycaemic conditions compared to controls and decreased following DNA damage. ATM expression was further increased with the treatment of 0.5 μM SRT1720 under DNA damage conditions (n=3). **b**) MRE11 protein phosphorylation was increased following treatment with 0.5 μM SRT1720 (n=3). **c)** RAD50 protein expression was significantly increased following H_2O_2 treatment, and further upregulated in all three conditions with SIRT1 activation (n=3). **d)** Phosphorylation of NBS1 was significantly increased following SIRT1 activation (n=3). (Two-way ANOVA conducted, Tukey Post-Hoc test **a-d**) *P<0.05, **P<0.005, ***P<0.001. Mean ±SEM.

5.4. Discussion

SIRT1 has been previously identified as a longevity gene and was found to be downregulated within diabetic patients (Chapter 4) (87, 495). Upregulation of SIRT1 has been shown to slow a range of degenerative diseases via regulation of energy balance and protection against cellular senescence and apoptosis (496, 497). Vascular calcification, a highly prevalent pathology, is associated with major cardiovascular events, in which vSMCs play an integral role in mediating the development of calcification via osteogenic differentiation and the development of vesicles that deposit calcium-phosphate hydroxyapatite crystals along the matrix. Whilst previous studies have focused on the development of DNA damage within atherosclerotic plaques (159, 497, 498), this is the first *in-vitro* study to demonstrate that DNA damage-activated osteogenic differentiation in vSMCs may be perpetuated via a loss of SIRT1. Furthermore, suggesting that restoring SIRT1 levels may further activate the MRN DNA repair complex and return cells to their normal quiescent state, instead of undergoing senescence and apoptosis.

5.4.1. DNA damage is prevalent within the diabetic patient

This study clearly demonstrates an increased presence of DNA damage markers such as γH2AX and the MRN complex within calcified popliteal vessels from diabetic patients when compared to a non-calcified IMA, alongside a lack of SIRT1 staining, which correlates with previously published data demonstrating a reduction of SIRT1 within diabetic serum (87). Additionally, senescence markers Sudan Black, p21 and the TUNEL assay suggest the development of calcification correlates with increased DNA damage in areas which lack SIRT1; however, the precise mechanism underlying the relationship between reduced SIRT1 activity in calcification is not known. Furthermore, vSMCs harvested from calcified vessels were assessed for DNA damage and SIRT1 expression. SIRT1 expression was reduced in diabetic vSMCs compared to healthy controls, with a significant upregulation of p53, p21 and a decrease in telomere length, suggesting that an integral part of the diabetic vSMCs phenotype is the development of a senescent state and an increase in DNA damage, in agreement with previous findings (129, 341). Interestingly, ATM expression was upregulated in diabetic vSMCs compared to non-diabetic vSMCs, suggesting that whilst the DNA repair response is activated within these diabetic

cells, the response mechanism may be inhibited further down the pathway than ATM and that whilst this part of the repair mechanism is upregulated, it is unable to prevent a senescent phenotype from developing.

To further investigate the mechanistic pathways involved, a human coronary artery smooth muscle cell model was used; where vSMCs were grown in osteogenic conditions in the presence or absence of hyperglycaemic, also in the presence of absence of H_2O_2 to induce DNA damage and the SIRT1 activator; SRT1720 and inhibitor; Sirtinol. Hyperglycaemic conditions were found to increase the rate of DNA damage in vSMCs within culture, with both γH2AX and p21 foci numbers significantly increasing in hyperglycaemic conditions compared to control, alongside the increase in both tail percentage and tail length of comets following 4 days of hyperglycaemic treatment. Whilst vSMCs within normal vessels are characterised as having low levels of osteogenic marker expression, this study demonstrated that an increase in osteogenic markers Runx2 and OCN occurred following DNA damage; with hyperglycaemic conditions exacerbating their expression. Additionally, ALP activity and Alizarin red staining was also increased within H_2O_2 damaged cells. Although SIRT1 has multiple functions, this is the first study to directly link the increase in SIRT1 activity to a reduction in DNA damage induced calcification and osteogenic differentiation of vSMCs.

5.4.2. An increase in cellular SIRT1 levels following DNA damage increases DNA repair

Following DNA damage, SIRT1 expression was increased within H_2O_2 damaged cells, and upon further investigation via cell fractionation, SIRT1 levels were found to be significantly reduced within the nucleus following DNA damage, with SIRT1 translocating to the cytoplasm. Whilst previous work has been conducted on SIRT1 as a nuclear shuttling partner for a variety of transcription factors (499, 500), there is little knowledge surrounding whether SIRT1 originates within the cytoplasm or the nucleus. These data demonstrate the possible translocation of SIRT1 from the nucleus to the cytoplasm following treatment with hyperglycaemic, DNA damaging conditions. However, further investigation through techniques such as time lapse photography could confirm that shuttling occurs, rather than a degradation of SIRT1 in one subcellular location and an increase within the other. Previous studies have

suggested that phosphorylation of SIRT1 at Ser-164 (501) may inhibit the nuclear translocation of SIRT1, allowing its retention in the cytoplasm and overall reduction in activity, and this may offer an explanation as to the lack of improvement observed in the DNA damage response, even though SIRT1 activity is increased during H_2O_2 induced damage.

To further evaluate the role of SIRT1 in H_2O_2 induced DNA damage, SIRT1 was inhibited via Sirtinol and activated via SRT1720. The presence of γH2AX was confirmed via quantification of foci accumulation in the nucleus. Inhibition of SIRT1 demonstrated an increase in foci, which exponentially increased during a 3h recovery time. Conversely, γH2AX staining for cells treated with SRT1720 peaked at 1h following H_2O_2 treatment, with a reduction in γH2AX staining detected at three hours. Previous studies have suggested a mechanism in which SIRT1 physically interacts with acetyl-transferase Tip60, inhibiting the acetylation of γH2AX and thus reducing the cellular response, something these data corroborates (502-504). Furthermore, SIRT1 knockout cells have demonstrated increased sensitivity to radiation induced DNA damage and are more likely to undergo cell death than wild-type cells (505), again suggesting that there is a role for deacetylation within this pathway, and it may be required in order for cells not to develop a senescent or apoptotic phenotype.

5.4.3. DNA repair through the MRN complex is not fully activated in a reduced SIRT1 environment

DNA damage was also assessed via the comet assay, with SIRT1 activation significantly reducing comet length after 3 hours, suggesting activation of a repair pathway, with SIRT1 inhibition having converse effects. Further examination of the DNA repair pathways demonstrated phosphorylation of both NBS1 and MRE11 within SIRT1 activated cells, which may account for the repair observed in DNA damaged cells following SIRT1 activation. Previous studies have suggested that following DNA damage, NBS1 and SIRT1 are both recruited to the chromatin, and associated with one another, causing deacetylation of NBS1, a prerequisite to its activation (491). These findings are corroborated by this study, with SIRT1 activation found to reduce acetylation around the H3K27ac mark within the transcription start site, suggesting that an increase in deacetylation promotes

production of the NBS1 protein, allowing for an active MRN repair complex to be produced. In addition, within hyperglycaemic conditions, acetylation of the NBS1 promotor is significantly increased, with no change in production or phosphorylation of the NBS1 protein, suggesting that whilst hyperglycaemic conditions are sufficient to induce DNA damage, they do not activate the DNA repair complex; MRN, possibly due to the reduction of SIRT1 within the cells. These data further suggest that SIRT1 activation is required for the phosphorylation of MRE11 following DNA damage via the ATM kinase, which is simultaneously upregulated alongside SIRT1 activation. Previous studies have demonstrated that phosphorylation of MRE11 via ATM at s676 and s678 is important in the response to DNA DSBs and is dependent on the activation and presence of NBS1 (506). This is consistent with the data presented here, suggesting that both MRE11 and NBS1 must be phosphorylated in order for repair to occur. Interestingly, RAD50 expression significantly increased following DNA damage within hyperglycaemic conditions, however no increase in DNA repair was observed via the comet assay. This is in line with previous studies that found that the phosphorylation of both MRE11 and NBS1 may be more critical to MRN activation than RAD50 production (507).

5.5 Limitations

Whilst this study clearly demonstrates the role of SIRT1 in the protection of diabetic conditions induced DNA damage, it is not without its limitations. Firstly, the use of an immediate and severe damaging agent; H_2O_2, instead of a longer term, slower and more persistent DNA damage intervention (such as sustained hyperglycaemia for weeks, or months), means this model is not a true representation of the DNA damage caused by diabetes. DNA damage and the subsequent vascular calcification develops over a course of 20-40 years in most cases, and whilst this model allows the researcher the ability to look at expression and mechanisms throughout the entire process, it does not mimic diabetic damage exactly.

5.6. Conclusion

In summary these data suggest a model in which DNA repair through the MRN complex is not fully activated by a diabetic environment, possibly due to reduction of SIRT1 within the patient. Reduction of SIRT1 may lead to increased acetylation of NBS1, blocking its phosphorylation sites, thereby inhibiting further activation of ATM and the formation of the MRN complex, and ultimately DNA repair (508) (Fig. 5.13). This work builds on previous studies suggesting that a reduction of SIRT1 may be responsible for inducing a pro-apoptotic, pro-calcification environment in which DNA repair though p53 is inhibited (343, 509, 510). Furthering the hypothesis by demonstrating that an increase in SIRT1 expression promotes MRN activation resulting in increased DNA repair and cell survival. Most importantly this work highlights the growing interest and importance in the role of DNA damage in vascular calcification, a pathology for which there is no current treatment, thus demonstrating the need for the development of treatments for targeted DNA damage.

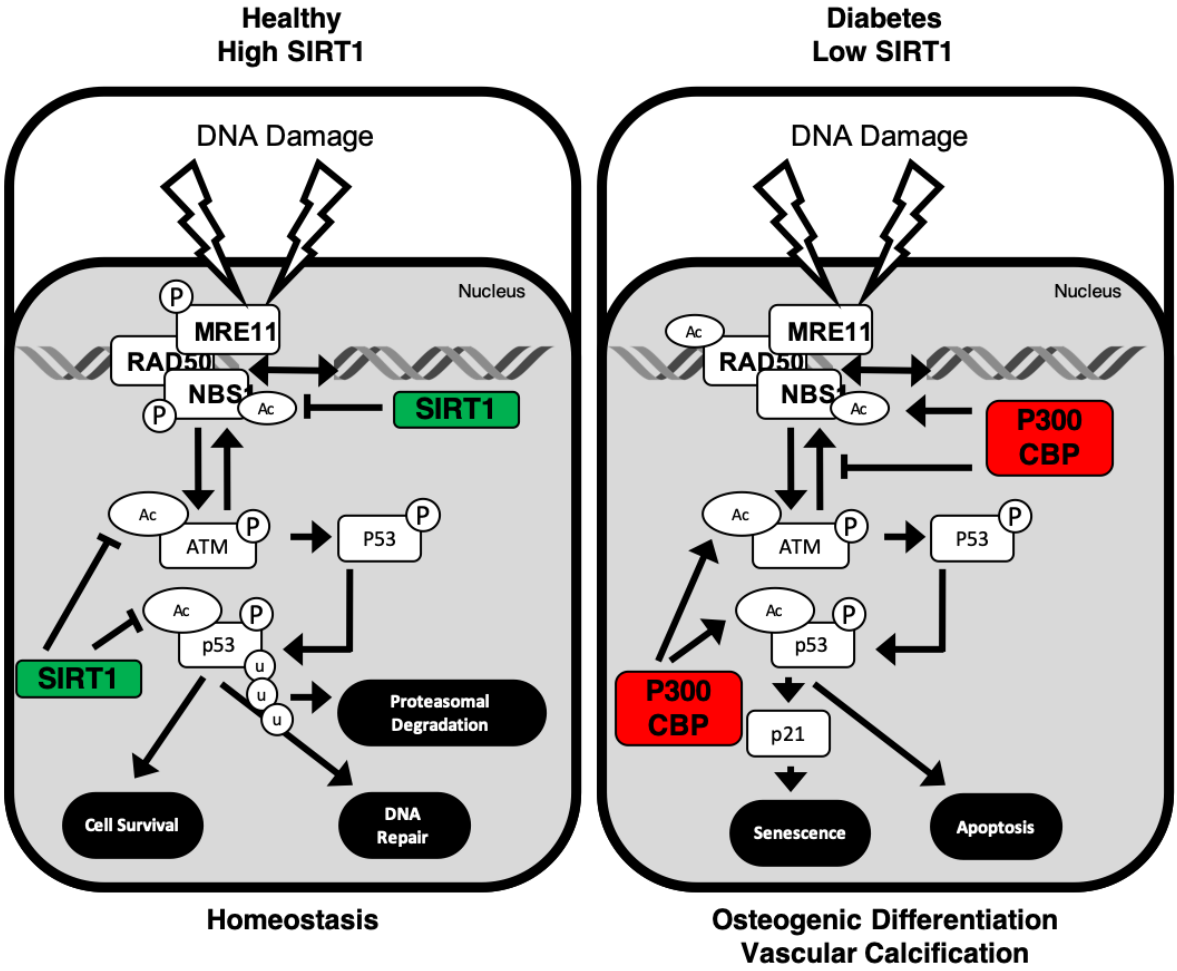

Fig. 5.13. Suggested mechanism for the role of SIRT1 in DNA damage induced calcification. SIRT1 activation during DNA damage increases phosphorylation of the MRN complex, leading to p53 acetylation and its subsequent ubiquitination, resulting in DNA repair and increased cell survival. Within a low SIRT1 diabetic environment DNA damage induces acetylation of the MRN complex and reduces phosphorylation. Acetylation induces p53 activation resulting in increased senescence and apoptosis, ultimately resulting in calcification.

6. Conclusions and Future Works

6.1. General Discussion

Vascular calcification is a leading pathology in aged and diabetic vessels, with the severity of the disease correlating with enlarging deposits of calcium and phosphate hydroxyapatite crystals in major arteries, resulting in increased morbidity and mortality (478, 511, 512). Clinically, vascular calcification is now accepted as a reliable predictor of coronary heart disease and achieving any level of control over this process requires a greater understanding of the mechanisms involved, bridging multiple feedback loops and crosstalk between different organ systems. Whilst previously considered a passive and degenerative pathology, calcification is now recognised as a pathobiological process sharing many features with bone formation, and it is these mechanistic pathways that this thesis sought to investigate. Throughout this body of work an *in-vitro* model of vascular calcification has been utilised to investigate the mechanisms in which high glucose and osteogenic medium may promote vascular calcification and has demonstrated the role of SIRT1 within these signalling pathways and the clinical relevance of SIRT1 to this pathology (Fig. 6.1)

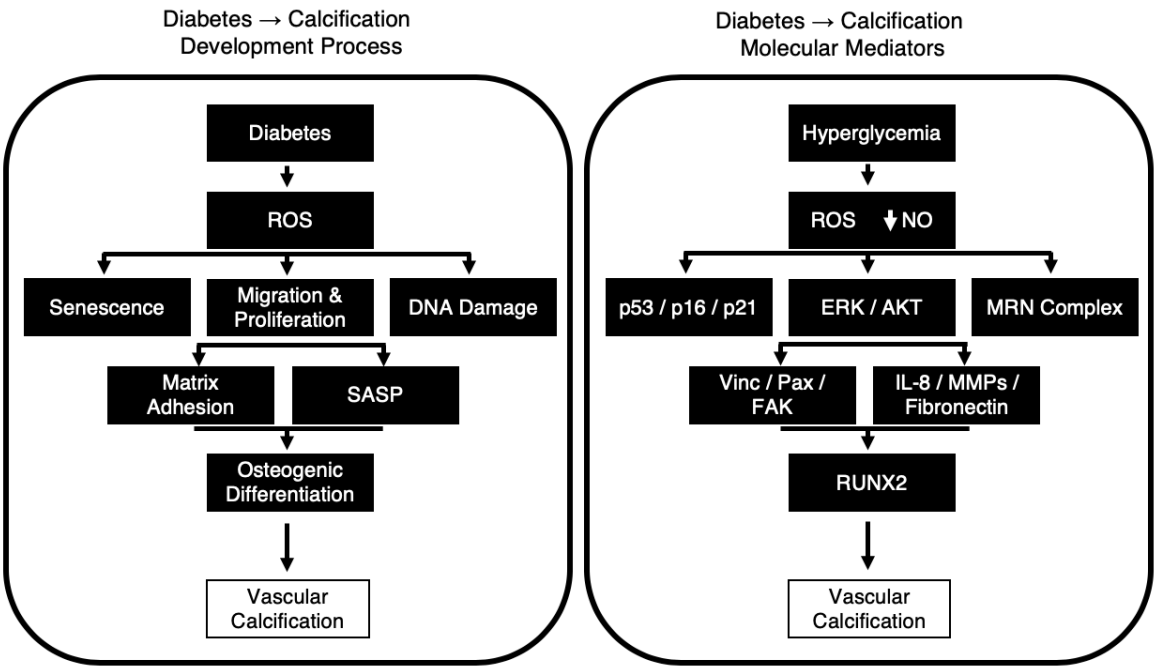

Figure 6.1. **Suggested mechanism of diabetic induced vascular calcification.** Diabetic hyperglycemia increases ROS production, decreasing nitric oxide production. This loss of nitric oxide activates quiescent cells to increase cellular migration and proliferation, whilst becoming susceptible to increased DNA damage and the development of a senescence associated phenotype (SASP). This induces an inflammatory environment with an increase in focal adhesion production, further increasing intima thickening and leading to the development of the osteogenic phenotype within vSMCs, ultimately resulting in the development of vascular calcification. LH section; Processes involved in calcification development. RH section; molecular mediators – boxes without arrows suggests an increase. ROS; reactive oxygen species, SASP; senescence associated secretory phenotype, NO_2; nitric oxide, MRN complex; MRE11 RAD50 NBS1, Vinc; Vinculin, Pax; Paxillin, FAK; Focal Adhesion Kinase, MMPs; Matrix Metalloproteinases.

This study has sought to determine the role of SIRT1 within the vascular calcification process and has achieved that through key findings. Firstly, this is the first study linking the reduction of SIRT1 signalling in a human diabetic vascular environment, in concordance with previous studies suggesting a loss of SIRT1 plays a crucial role in high glucose induced senescence in endothelial cells (495) and atherosclerotic calcification models in both mice and rats (249, 341). SIRT1 expression localised to the vascular smooth muscle layer of the vessels in calcified tissue is diminished in areas with positive Alizarin red and Von Kossa staining, suggesting an inverse correlation between the two. Additionally, activation of the DNA damage repair complex; MRN, was increased within the smooth muscle layer of the vessel, however DNA damage was still observed. Thus, suggesting that whilst the DNA damage repair mechanism may be activated in response to the damage observed, the repair mechanism is not fully switched on and may be an ill-fated attempt to repair damage.

DNA damage has been widely reported as a possible trigger for the increase of calcification in atherosclerotic models (158, 159, 513), and is something these data agree with, demonstrating a significant increase in Runx2 and ALP activity following H_2O_2 induced damage when compared to the untreated model of hyperglycaemia. Furthermore, this study confirms reports suggesting that DNA damage reduces ATM activation (479), therefore blunting phosphorylation of the DNA repair mechanism, the MRN complex. Moreover, this body of work and others demonstrate increased SIRT1 activation increases ATM expression (492, 514) therefore activating downstream DNA damage repair pathways. This suggests a possible mechanism in which a hyperglycaemic, hyperphosphatemic environment induces DNA damage and where the repair process is inhibited due to a decrease in ATM activation, leading to cellular senescence and finally the development of vascular calcification. This study confirms that DNA damage significantly increases the rate and severity of hyperglycaemic calcification, with an increase in γH2AX foci correlating with the increase in Runx2 expression. In addition, this induction of DNA damage may induce a senescence associated secretory phenotype, demonstrated via an increase of p53, p21 and p16 expression as well as β-galactosidase staining, which has been shown here and elsewhere (129, 515) to increase the development of calcification.

Inhibition of both DNA damage and senescence through SIRT1 activation demonstrates a reduction in calcification suggesting a crucial role for SIRT1 in these pathways, through epigenetic gene regulation, observed within this study at histone 3 lysine 27. The dynamics of H3K27 acetylation within DNA regulatorily regions play a fundamental role in the precise timing and level of gene transcription (516), marking both active promotors and distal enhancers. Aberrant H3K27ac marks have a suggested involvement in a range of disease pathologies (517, 518), including vascular disease (519). Here, the increase in H3K27ac marks around the promotor regions of p53, RAD50, NBS1 and Runx2 were found to correlate with an increase in senescence, calcification and the inability to repair DNA breaks effectively. SIRT1 activation however, significantly reduced acetylation of all the aforementioned promotor regions, thus suggesting that SIRT1 may be a key regulator within this process, however much greater in depth analysis of the acetylation patterns of these promotor regions must be undertaken in order to further confirm this.

Furthermore, this study demonstrates the inherent phenotypic differences between diabetic and healthy vSMCs and suggests a possible mechanism behind the invasive process observed in intimal hyperplasia prior to calcification (520). Hypermotility and hyperproliferation within diabetic vSMCs (521, 522) and their progenitors (523, 524) are responsible for the development of restenosis following angioplasty and are critical in the pathological processes of vascular diseases such as atherosclerosis and coronary heart disease. Therefore, a reduction in their proliferation and migration towards inflammatory markers and growth factors may produce a feedback loop to regulate vSMC proliferation and vascular neointimal hyperplasia (525).

Moreover, this work suggests that the inherent loss of organisation within the vSMC structure may occur as a result of a lack of SIRT1 within the diabetic patient; which leads to the disorganisation and overlapping of cells within the vessel. This in turn may lead to microvascular leakage (526, 527) and the possibility of leukocyte infiltration into the intimal layer of the vessel (528), further inducing an inflammatory environment in which a calcified plaque could form. Moreover, with the activation of SIRT1 eliciting an increase in organisation of the cytoskeleton and a reduction of ERK activation; the latter of which has been noted to increase an invasive

phenotype in other cell types (122, 333, 429, 438), this study suggests that reactivation of both ERK and AKT within a diabetic vSMC may be responsible for the development of this migratory phenotype. This may suggest a dedifferentiation of the cells to an immature phenotype coupled with a reduction of contractility which collaborates with the reduction of αSMA observed when compared to healthy vSMCs cultured in the same environment. Interestingly, phosphorylated ERK has been shown to degrade p21 and increase cell cycle progression even after DNA damage (421, 529), allowing proliferation and migration to continue, perpetuating the pathology. With an increase in DNA damage found in the diabetic vSMCs as well as an increase in cellular proliferation and adhesion, a DNA damage mechanism in which vSMCs increase their focal adhesion production to further migrate and proliferate within the vessel before senescing and calcifying is supported by this body of work as a whole.

6.2. Future Work

Whilst both the *in-vitro* and *ex-vivo* data within this study has convincingly shown that SIRT1 plays a critical role in inhibiting osteogenic differentiation within vSMCs, it remains clear that there are many key questions still to be answered.

Firstly, whilst these data demonstrate the concurrent decrease in SIRT1 within both patient vSMCs and serum, it remains to be elucidated how SIRT1 is shuttled between the two, or by which precise signalling mechanism SIRT1 is downregulated within a diabetic patient. One such possible way in which to determine this is to observe the expression levels of SIRT1 within the extracellular vesicles either within the blood, or that are released from the vSMCs. Recent studies employing new high-resolution microscopy technologies have shown extracellular vesicles from cardiac tissues closely resemble matrix vesicles released from bone, however they are phenotypically distinct (530). It would therefore be of use to determine the contents of these vesicles to investigate not only whether SIRT1 transcripts are present and up or downregulated in a diabetic patient, but also to see if osteogenic-inducing transcripts were also being transferred in this manner, and thus contributing to the increase in calcification. Interestingly, an emerging role for extracellular vesicles and the micro RNAs within them, as an inducer of the senescence associated secretory phenotype has been reported in lung disease (531) and since this is the suggested mechanism for the development of vSMC calcification through the Runx2 pathway (87), it would be interesting to examine whether this was the case within this model. To this end, isolated extracellular vesicles would ideally undergo RNA sequencing to unbiasedly determine the expression of RNA transcripts, before confirming the expression change with qPCR.

With increasing amounts of research highlighting the distinct subpopulations and overall heterogeneity within vSMCs (117), it is clear that what was once considered a population of ‘vascular smooth muscle cells’ is now a heterogenous population composed of cells with distinct proteomic and transcriptional signatures from each other and that investigations into their disease pathology should be conducted as such (117). Therefore, further experiments on vSMCs harvested from the diabetic patient cohort should have their RNA sequenced individually; scRNA-seq, in order

to isolate unique markers of the vSMCs that calcify and those that do not. These markers should be then assessed via qPCR to confirm the results of the scRNA-seq. With this approach, future patient samples within the laboratory could then undergo fluorescence-activated cell sorting and cells from all distinct subpopulations should be separated out and cultured separately, with the theory that one or more of the subpopulations might contain a pro-calcifying phenotype whilst others may be anti-osteogenic. This pro-calcification marker could then be treated as a biomarker and used downstream to stratify a patients likelihood of developing calcification. Additionally, the use of exciting new technologies such as SCoPE-MS (532); single cell proteomics by mass spectrometry, could be used to confirm the upregulated transcript identified by scRNA-seq was increased at protein level. With western blotting tremendously variable at best, techniques such as SCoPE-MS would not only increase the ability to identify and quantify thousands of proteins in a single experiment but would use significantly less of the patient sample to do so, leaving more sample to run further conformational analysis at a later date.

With the process of smooth muscle mineralisation resulting in the calcification of the ECM deposited by vSMCs, future studies looking at the matrix deposited by the vSMCs might offer valuable insights into the process of calcification. With this study and others (333) demonstrating the inherent differences in migratory and adhesive properties of cells from a diabetic origin compared to healthy controls, their ability to degrade or produce a matrix should be assessed to determine if this contributes to osteogenic differentiation of vSMCs. With the reduction of basement membrane proteins known to promote phenotypic modulation of vSMCs (115, 533, 534), levels of matrix degrading proteases such as MMPs should be assessed, in order to determine whether they contribute to the development of calcification. Since SIRT1 is known to be a negative regulator of MMP9 in diabetic retinal cells (535) and MMP13 in osteoblasts (536) it could be hypothesised that the activation of SIRT1 observed within these data to inhibit vSMC osteogenic differentiation could also play an inhibitory role in matrix remodelling and hydroxyapatite crystal deposition. Furthermore, the mitochondrial capacity of diabetic vSMCs should be examined via seahorse stress tests, in order to determine if increased DNA damage and the development of smooth muscle calcification correlates with mitochondrial dysfunction (373). With previous studies demonstrating the loss of mitochondrial

respiration in atherosclerosis promoting a necrotic core (195, 328), it would be of interest to link the speed of osteogenic differentiation with mitochondrial function to determine its role in the development of vascular calcification.

Furthermore, from a more clinical perspective it may be useful to determine the NAD+ levels within the blood of the diabetic and healthy patients, in order to confirm if SIRT1 activity is further decreased due to a lack of available NAD+ in a hyperglycaemic environment to catalyse deacetylase reactions. With NAD+ utilised in a variety of inflammatory and metabolic pathways, many simple assays have been developed to determine its level. Liquid chromatography with tandem mass spectrometry has been well described to measure NAD+ within both blood and cells to a good chromatographic resolution of at least 17 metabolites using an amino phase column with polar selectivity (537). In addition, within the *in vitro* tissue culture model used, a simple NADPH assay could be utilised and the levels of NADPH measured via a spectrophotometer (538, 539), thus giving the opportunity to compare both NADPH/NAD+ levels within the patients' blood and cells. As the balance between NADH and NAD+ is severely perturbed within a diabetic patient, the correlation between NAD+, SIRT1 levels and severity of calcification may provide useful insight into whether restoration of this imbalance may increase the effectiveness of SIRT1, or whether it is independently decreased compared to SIRT1.

6.3. Conclusion

In conclusion, this thesis has examined the role of SIRT1 throughout different phases of the vascular calcification process pertaining to vascular smooth muscle cells. Significantly, these data demonstrate the inherent differences between diabetic and healthy smooth muscle cells, with a reduction of SIRT1 identified in diabetic patients. Furthermore, these data suggest that the lack of SIRT1 inhibits complete DNA repair, leading to the dysregulation and dedifferentiation of smooth muscle cells into an osteogenic phenotype, in which they gain migratory properties before developing a senescence associated secretory phenotype and mineralising, causing pathological calcification and leading to the need for clinical intervention.

7. Appendix

Name	Company	Catalogue number	Raised in	Working concentration	Target size
SIRT1	AbCam	Ab12193	Rabbit	1:5000	80 kDa
α-Tubulin	AbCam	Ab7291	Mouse	1:1000	50 kDa
Runx2	R&D	AF2006	Goat	1:500	57 kDa
Osteocalcin	R&D	MAB1419	Mouse	1:500	
α-SMA	AbCam	Ab5694	Rabbit	1:1000	
Osteopontin	R&D	Ab214050	Rabbit	1:2000	
Vinculin	CST	13901	Rabbit	1:5000	
Phalloidin	Fluka	77418		1:5000	
Paxillin	BD	610051	Mouse	1:5000	68 kDa
Phospho-Focal Adhesion Kinase (Tyr925)	CST	3284	Rabbit	1:1000	125 kDa
Focal Adhesion Kinase	CST	3285	Rabbit	1:1000	125 kDa
Phospho-Mitogen-Activated Protein Kinase Kinase (S218/S222) (S222/226)	R&D	MAB8407	Rabbit	1:250	50 kDa
Mitogen-Activated Protein Kinase Kinase	R&D	AF2079	Goat	1:250	50 kDa
Phospho-Extracellular-Signal Regulated Kinase ½ (T202/Y204) (T185/Y187)	R&D	MAB1018	Rabbit	1:250	130 kDa
Extracellular-Signal Regulated Kinase 1/2	R&D	MAB1578	Mouse	1:250	130 kDa
Phospho-Protein Kinase B (S473)	R&D	AF887	Rabbit	1:250	60 kDa
Protein Kinase B	R&D	MAB2055	Mouse	1:250	60 kDa
p21	AbCam	Ab109119	Rabbit	1:1000	
γ-H.2AX (S139)	AbCam	Ab11174	Rabbit	1:1000	14 kDa
ATM	AbCam	Ab78	Mouse	1:1000	350kDa
Phospho-Mre11 (S676)	CST	4859	Rabbit	1:1000	81 kDa
Mre11	CST	4847	Rabbit	1:1000	81 kDa
Phospho-Nbs1 (S343)	CST	3001	Rabbit	1:1000	95 kDa
Nbs1	CST	14956	Rabbit	1:1000	95 kDa
Rad50	CST	3427	Rabbit	1:1000	153 kDa
Histone H3	CST	4620	Rabbit	1:1000	17 kDa
Acetylated Lysine	AbCam	Ab21623	Rabbit	1:500	
IgG	AbCam	Ab238531	Rabbit	1:2000	150 kDa
Goat anti-Mouse HRP	Dako	P0447	Goat	1:1000	
Goat anti-Rabbit HRP	Dako	P0448	Goat	1:1000	
Rabbit anti-Goat HRP	Dako	P0449	Rabbit	1:1000	

Table. 7.1. Antibodies used throughout thesis. Antibodies were diluted to appropriate concentrations in blocking solution before used.

Primer name	Company	Accession number	Sequence	Product size
SIRT1	Invitrogen	NM_001142498.1	CTGGACAATTCCAGCCATCT GGGTGGCAACTCTGACAAAT	63 bp
Runx2	Invitrogen	NM_001024630.3	CCCCACGACAACCCACCAT CACTCCGGCCCACAAATCTC	289 bp
GAPDH	Invitrogen	NM_001256799.2	CCACCCATGGCAAATTCCATG TCTAGACGGCAGGTCAGGTCC ACC	26 bp
B-Actin	Invitrogen	NM_001101.4	AGAGCTACGAGCTGCCTGAC AGCACTGTGTTGGCGTACAG	184 bp
Osteocalcin	Invitrogen	NM_199173.5	CATGAGAGCCCTCACAAGAGC GACACCCTAGAC	315 bp
Osteopontin	Invitrogen	NM_000582.2	CAGCTTTACAACAAATACCCAG AT TTACTTGGAAGGGTCTGTGGG	98 bp
Osteoprotegerin	Invitrogen	NM_002546.3	GTTAACCCTGGAGCTTTCTGC ATCGCCTGCCTTTGATCAGT	114 bp
Msx2	Invitrogen	NM_002449.4	TTACCACATCCCAGCTCCTC CCTGGGTCTCTGTGAGGTTC	111 bp
p16	Invitrogen	NM_214646.1	CGTGGACCTGGCTGAGGAGC ACGAAAGCGGGGTGGGTTGT	234
p21	Invitrogen	NM_000389.4	CTCAGGGTCGAAAACGGCGG GTGGGCGGATTAGGGCTTCCT	95 bp
p53	Invitrogen	NM_000546.5	TAGCGATGGTCTGGCCCCTCC GATGGGCCTCCGGTTCATGC	202 bp
Col3a1	Invitrogen	NM_000090.3	ATGCACGTCTACATTAAGGAAC TC TGCCCTCAGTGTCCAGTATG	204 bp
Col6a1	Invitrogen	NM_001848.2	TCACTCCTCTCCCTGTGGTTAT GGTTGACCTCGGTGGATGTG	321 bp
TelO	Invitrogen		CGGTTTGTTTGGGTTTGGGTTT GGGTTTGGGTTTGGGTT GGCTTGCCTTACCCTTACCCTT ACCCTTACCCTTACCCT	60 bp

Table. 7.2. DNA oligonucleotide primers used for quantitative real-time PCR.

Primers were obtained from Invitrogen in lyophilized form and reconstituted to 100 μM with sterile distilled water and frozen at -20°C until further use. Working solutions were made fresh by diluting primer stocks 1:10 in fresh sterile distilled water.

Chip primer name	Company	Sequence	Product size
RAD50	Invitrogen	CTTAGGAGCAGAAGCGTCCC TCCTAAGGTCGCTGTAGCCT	49 bp
p53	Invitrogen	CCTGCGTCTGGAACTGGAAT AGAGTGCAATGATGGGTCGTT	96 bp
NBS1	Invitrogen	TGGCGCTCTCCATACTCTCT GTGAAGGGTCTTGTCCTCGG	98 bp
MRE11	Invitrogen	GTCTGCGGAGGAACACCTTT GATGTGGTGGGGGTTGTCTC	97 bp
ATM	Invitrogen	TCTCAGCAACAGTGGTTAGGT CAGACAGAGTGCTTTCTTTGGTG	93 bp
Runx2	Invitrogen	AGGAGTAAGCGATACGGACG GGAAGTAGCTCGCTCGGG	98 bp

Table. 7.3. DNA oligonucleotide primers used for chromatin immunoprecipitation quantitative PCR. Primers were obtained from Invitrogen in lyophilized form and reconstituted to 100 μM with sterile distilled water and frozen at -20°C until further use. Working solutions were made fresh by diluting primer stocks 1:10 in fresh sterile distilled water and used immediately.

8. Bibliography

1. Pagidipati NJ, Gaziano TA. Estimating Deaths From Cardiovascular Disease: A Review of Global Methodologies of Mortality Measurement. Circulation. 2013;127(6):749-56.
2. Roth GA, Huffman MD, Moran AE, Feigin V, Mensah GA, Naghavi M, et al. Global and regional patterns in cardiovascular mortality from 1990 to 2013. Circulation. 2015;132(17):1667-78.
3. Roth G, Johnson, C., Abajobir, A., Abd-Allah, Foad., Abera, S., Abyu, G., Ahmed, M, Aksut, B., Alam, T., Alam, K., Alla, F., Alvis-Guzman, N.,Amrock, S., Ansari, H., Arnlov, H., Asayesh, H., Atey, T., Avila-Burgos, L., Murray, C.,. Global, Regional, and National Burden of Cardiovascular Diseases for 10 Causes, 1990 to 2015. Journal of the American College of Cardiology. 2017;70(1):1-25.
4. Dutta P, Courties G, Wei Y, Leuschner F, Gorbatov R, Robbins CS, et al. Myocardial infarction accelerates atherosclerosis. Nature. 2012;487(7407):325-9.
5. Shah MS, Brownlee M. Molecular and Cellular Mechanisms of Cardiovascular Disorders in Diabetes. Circ Res. 2016;118(11):1808-29.
6. Wang H, Eitzman DT. Acute myocardial infarction leads to acceleration of atherosclerosis. Atherosclerosis. 2013;229(1):18-22.
7. Gimbrone MA, Jr., Garcia-Cardena G. Vascular endothelium, hemodynamics, and the pathobiology of atherosclerosis. Cardiovasc Pathol. 2013;22(1):9-15.
8. Thubrikar MJ. Correlate blood pressure, not blood flow, with atherosclerosis. Eur J Cardiothorac Surg. 2013;43(4):838-9.
9. Paneni F, Diaz Canestro C, Libby P, Luscher TF, Camici GG. The Aging Cardiovascular System: Understanding It at the Cellular and Clinical Levels. J Am Coll Cardiol. 2017;69(15):1952-67.
10. North BJ, Sinclair DA. The intersection between aging and cardiovascular disease. Circ Res. 2012;110(8):1097-108.
11. Dworatzek E, Mahmoodzadeh S. Targeted basic research to highlight the role of estrogen and estrogen receptors in the cardiovascular system. Pharmacol Res. 2017;119:27-35.
12. Blenck CL, Harvey PA, Reckelhoff JF, Leinwand LA. The Importance of Biological Sex and Estrogen in Rodent Models of Cardiovascular Health and Disease. Circ Res. 2016;118(8):1294-312.
13. Pool LR, Ning H, Lloyd-Jones DM, Allen NB. Trends in Racial/Ethnic Disparities in Cardiovascular Health Among US Adults From 1999-2012. J Am Heart Assoc. 2017;6(9).
14. Karmali KN, Lloyd-Jones DM. Implementing Cardiovascular Risk Prediction in Clinical Practice: The Future Is Now. J Am Heart Assoc. 2017;6(4).
15. Guthold R, Gretchen, Stevens, Riley, Leanne, Bull, Fiona. Worldwide trends in insufficient physical activity from 2001 to 2016: a pooled analysis of 358 population-based surveys with 1·9 million participants - The Lancet Global Health. The Lancet Global Health. 2018;6(10).
16. Sheri R. Colberg RJS, Jane E. Yardley, Michael C. Riddell, David W. Dunstan, Paddy C. Dempsey, Edward S. Horton, Kristin Castorino and Deborah F. Tate. Physical Activity/Exercise and Diabetes: A Position Statement of the American Diabetes Association. Diabetes Care. 2016;39(11).
17. Ezzati M, Henley SJ, Thun MJ, Lopez AD. Role of smoking in global and regional cardiovascular mortality. Circulation. 2005;112(4):489-97.

18. Can A, Castro VM, Ozdemir YH, Dagen S, Yu S, Dligach D, et al. Association of intracranial aneurysm rupture with smoking duration, intensity, and cessation. Neurology. 2017;89(13):1408-15.
19. Sasco AJ, Secretan MB, Straif K. Tobacco smoking and cancer: a brief review of recent epidemiological evidence. Lung Cancer. 2004;45 Suppl 2:S3-9.
20. Virdis A, Giannarelli C, Neves MF, Taddei S, Ghiadoni L. Cigarette smoking and hypertension. Curr Pharm Des. 2010;16(23):2518-25.
21. Santanam N, Sanchez R, Hendler S, Parthasarathy S. Aqueous extracts of cigarette smoke promote the oxidation of low density lipoprotein by peroxidases. FEBS Lett. 1997;414(3):549-51.
22. Martinet W, Knaapen MW, De Meyer GR, Herman AG, Kockx MM. Elevated levels of oxidative DNA damage and DNA repair enzymes in human atherosclerotic plaques. Circulation. 2002;106(8):927-32.
23. Bekkering S, Quintin J, Joosten LA, van der Meer JW, Netea MG, Riksen NP. Oxidized low-density lipoprotein induces long-term proinflammatory cytokine production and foam cell formation via epigenetic reprogramming of monocytes. Arterioscler Thromb Vasc Biol. 2014;34(8):1731-8.
24. Ross R. The pathogenesis of atherosclerosis: a perspective for the 1990s. Nature. 1993;362(6423):801-9.
25. Ghosh A, Pechota LV, Upchurch GR, Jr., Eliason JL. Cross-talk between macrophages, smooth muscle cells, and endothelial cells in response to cigarette smoke: the effects on MMP2 and 9. Mol Cell Biochem. 2015;410(1-2):75-84.
26. Collaboration NRF. Worldwide trends in diabtes sience 1980: a pooled analysis of 751 population-based studies with 4.4 million participants. The Lancet. 2016;387(10027):1513-30.
27. Seuring T, Archangelidi O, Suhrcke M. The Economic Costs of Type 2 Diabetes: A Global Systematic Review. Pharmacoeconomics. 2015;33(8):811-31.
28. Röder PV, Wu B, Liu Y, Han W. Pancreatic regulation of glucose homeostasis. Exp Mol Med. 2016;48(3):e219-.
29. Du XL, Edelstein D, Dimmeler S, Ju Q, Sui C, Brownlee M. Hyperglycemia inhibits endothelial nitric oxide synthase activity by posttranslational modification at the Akt site. J Clin Invest. 2001;108(9):1341-8.
30. Salt A, Morrow, V., Brandie, F., Connell, J., Petrie, J. High Glucose Inhibits Insulin-stimulated Nitric Oxide Production without Reducing Endothelial Nitric-oxide Synthase Ser1177 Phosphorylation in Human Aortic Endothelial Cells. Journal of Biological Chemistry. 2003;278:18791-7.
31. Tousoulis D, Kampoli AM, Tentolouris C, Papageorgiou N, Stefanadis C. The role of nitric oxide on endothelial function. Curr Vasc Pharmacol. 2012;10(1):4-18.
32. Assar ME, Angulo J, Rodriguez-Manas L. Diabetes and ageing-induced vascular inflammation. J Physiol. 2016;594(8):2125-46.
33. Förstermann U, Xia N, Li H. Roles of Vascular Oxidative Stress and Nitric Oxide in the Pathogenesis of Atherosclerosis. Circulation Research. 2017;120:713-35.
34. Prevention CfDCa. National Diabetes Statistics Report. Centers for Disease Control and Prevention, US Department of Health and HUman Services. 2017.
35. Schram MT, Sep SJ, van der Kallen CJ, Dagnelie PC, Koster A, Schaper N, et al. The Maastricht Study: an extensive phenotyping study on determinants of type 2 diabetes, its complications and its comorbidities. Eur J Epidemiol. 2014;29(6):439-51.
36. Sorensen BM, Houben AJ, Berendschot TT, Schouten JS, Kroon AA, van der Kallen CJ, et al. Prediabetes and Type 2 Diabetes Are Associated With Generalized

Microvascular Dysfunction: The Maastricht Study. Circulation. 2016;134(18):1339-52.
37. Moulik PK, Mtonga R, Gill GV. Amputation and mortality in new-onset diabetic foot ulcers stratified by etiology. Diabetes Care. 2003;26(2):491-4.
38. Vinik AI, Nevoret ML, Casellini C, Parson H. Diabetic neuropathy. Endocrinol Metab Clin North Am. 2013;42(4):747-87.
39. Shu J, Santulli G. Update on peripheral artery disease: Epidemiology and evidence-based facts. Atherosclerosis. 2018;275:379-81.
40. Association AD. Peripheral Arterial Disease in People With Diabetes. 2003.
41. Krishnan B, Babu S, Walker J, Walker AB, Pappachan JM. Gastrointestinal complications of diabetes mellitus. World J Diabetes. 2013;4(3):51-63.
42. Aroda VR, Knowler WC, Crandall JP, Perreault L, Edelstein SL, Jeffries SL, et al. Metformin for diabetes prevention: insights gained from the Diabetes Prevention Program/Diabetes Prevention Program Outcomes Study. Diabetologia. 2017;60(9):1601-11.
43. Goldberg RB, Aroda VR, Bluemke DA, Barrett-Connor E, Budoff M, Crandall JP, et al. Effect of Long-Term Metformin and Lifestyle in the Diabetes Prevention Program and Its Outcome Study on Coronary Artery Calcium. Circulation. 2017;136(1):52-64.
44. Mary A, Hartemann A, Liabeuf S, Aubert CE, Kemel S, Salem JE, et al. Association between metformin use and below-the-knee arterial calcification score in type 2 diabetic patients. Cardiovasc Diabetol. 2017;16(1):24.
45. Zhang E, Guo Q, Gao H, Xu R, Teng S, Wu Y. Metformin and Resveratrol Inhibited High Glucose-Induced Metabolic Memory of Endothelial Senescence through SIRT1/p300/p53/p21 Pathway. PLoS One. 2015;10(12).
46. Arunachalam G, Samuel SM, Marei I, Ding H, Triggle CR. Metformin modulates hyperglycaemia-induced endothelial senescence and apoptosis through SIRT1. Br J Pharmacol. 2014;171(2):523-35.
47. Matheus AM, Tannus LRM, Cobas RA, Palma CCS, Negrato CA, Gomes Mde B. Impact of Diabetes on Cardiovascular Disease: An Update. Int J Hypertens. 2013;2013.
48. Koistinen MJ. Prevalence of asymptomatic myocardial ischaemia in diabetic subjects. Bmj. 1990;301(6743):92-5.
49. Leon BM, Maddox TM. Diabetes and cardiovascular disease: Epidemiology, biological mechanisms, treatment recommendations and future research. World J Diabetes. 2015;6(13):1246-58.
50. Sarapultsev P, Yushkov B, Sarapultsev A. Prevalence of arrhythmias in patients with type 2 diabetes and the role of structural changes in myocardium in their development. Diabetes Metab Syndr. 2017;11 Suppl 2:S567-s76.
51. Tribouilloy C, Rusinaru D, Mahjoub H, Tartiere JM, Kesri-Tartiere L, Godard S, et al. Prognostic impact of diabetes mellitus in patients with heart failure and preserved ejection fraction: a prospective five-year study. Heart. 2008;94(11):1450-5.
52. Thiruvoipati T, Kielhorn CE, Armstrong EJ. Peripheral artery disease in patients with diabetes: Epidemiology, mechanisms, and outcomes. World J Diabetes. 2015;6(7):961-9.
53. Einarson TR, Acs A, Ludwig C, Panton UH. Prevalence of cardiovascular disease in type 2 diabetes: a systematic literature review of scientific evidence from across the world in 2007–2017. Cardiovasc Diabetol. 2018;17.

54. Movahed MR, Hashemzadeh M, Jamal MM. The prevalence of pulmonary embolism and pulmonary hypertension in patients with type II diabetes mellitus. Chest. 2005;128(5):3568-71.
55. Yau JW, Rogers SL, Kawasaki R, Lamoureux EL, Kowalski JW, Bek T, et al. Global prevalence and major risk factors of diabetic retinopathy. Diabetes Care. 2012;35(3):556-64.
56. Singh R, Kishore L, Kaur N. Diabetic peripheral neuropathy: current perspective and future directions. Pharmacol Res. 2014;80:21-35.
57. Gheith O, Farouk N, Nampoory N, Halim MA, Al-Otaibi T. Diabetic kidney disease: world wide difference of prevalence and risk factors. J Nephropharmacol. 2016;5(1):49-56.
58. Luchsinger JA, Tang MX, Stern Y, Shea S, Mayeux R. Diabetes mellitus and risk of Alzheimer's disease and dementia with stroke in a multiethnic cohort. Am J Epidemiol. 2001;154(7):635-41.
59. Raman R, Pal SS, Adams JS, Rani PK, Vaitheeswaran K, Sharma T. Prevalence and risk factors for cataract in diabetes: Sankara Nethralaya Diabetic Retinopathy Epidemiology and Molecular Genetics Study, report no. 17. Invest Ophthalmol Vis Sci. 2010;51(12):6253-61.
60. Kozhevnikova SA, Budnevskiy AV, Ovsyannikov ES, Malysh EY, Belov VN. Chronic obstructive pulmonary disease and diabetes: a look at the epidemiology, pathogenetic mechanisms, treatment. Patol Fiziol Eksp Ter. 2016;60(4):122-7.
61. Tung YC, Lee SS, Tsai WC, Lin GT, Chang HW, Tu HP. Association Between Gout and Incident Type 2 Diabetes Mellitus: A Retrospective Cohort Study. Am J Med. 2016;129(11):1219.e17-.e25.
62. Bhatt HB, Smith RJ. Fatty liver disease in diabetes mellitus. Hepatobiliary Surg Nutr. 2015;4(2):101-8.
63. Stabley J, Towler, DA.,. Arterial Calcification in Diabetes Mellitus. Atherosclerosis, Thrombosis and Vascular Biology. 2017;37:205-17.
64. Demer LL, Tintut Y, Nguyen KL, Hsiai T, Lee JT. Rigor and Reproducibility in Analysis of Vascular Calcification. Circ Res. 2017;120(8):1240-2.
65. Durham AL, Speer MY, Scatena M, Giachelli CM, Shanahan CM. Role of smooth muscle cells in vascular calcification: implications in atherosclerosis and arterial stiffness. Cardiovasc Res. 2018;114(4):590-600.
66. Rumberger JA, Simons DB, Fitzpatrick LA, Sheedy PF, Schwartz RS. Coronary artery calcium area by electron-beam computed tomography and coronary atherosclerotic plaque area. A histopathologic correlative study. Circulation. 1995;92(8):2157-62.
67. Raggi P, Shaw LJ, Berman DS, Callister TQ. Prognostic value of coronary artery calcium screening in subjects with and without diabetes. J Am Coll Cardiol. 2004;43(9):1663-9.
68. Amann K. Media Calcification and Intima Calcification Are Distinct Entities in Chronic Kidney Disease. Clinical Journal of American Society of Nephrology. 2008;3(6):1599-605.
69. Kockelkoren R, Vos A, Van Hecke W, Vink A, Bleys RL, Verdoorn D, et al. Computed Tomographic Distinction of Intimal and Medial Calcification in the Intracranial Internal Carotid Artery. PLoS One. 2017;12(1):e0168360.
70. Lanzer P, Boehm M, Sorribas V, Thiriet M, Janzen J, Zeller T, et al. Medial vascular calcification revisited: review and perspectives. Eur Heart J. 2014;35(23):1515-25.
71. Chistiakov DA, Sobenin IA, Orekhov AN, Bobryshev YV. Mechanisms of medial arterial calcification in diabetes. Curr Pharm Des. 2014;20(37):5870-83.

72. Johnson RC, Leopold JA, Loscalzo J. Vascular calcification: pathobiological mechanisms and clinical implications. Circ Res. 2006;99(10):1044-59.
73. Wang Y, Osborne MT, Tung B, Li M, Li Y. Imaging Cardiovascular Calcification. J Am Heart Assoc. 2018;7(13).
74. Souza A, Bream, P., Elliott, L,. Chest Film Detection of Coronary Artery Calcification. The Value of the CAC Triangle. Radiology. 1978;129(1).
75. Reinsch N, Mahabadi AA, Lehmann N, Möhlenkamp S, Hoefs C, Sievers B, et al. Comparison of dual-source and electron-beam CT for the assessment of coronary artery calcium scoring. Br J Radiol. 2012;85(1015):e300-6.
76. Mohammedi K, Potier L, Belhatem N, Matallah N, Hadjadj S, Roussel R, et al. Lower-extremity amputation as a marker for renal and cardiovascular events and mortality in patients with long standing type 1 diabetes. Cardiovasc Diabetol. 2016;15.
77. Organisation WH. Global Health Estimates 2016: Deaths by Cause, Age, Sex, by Country and by Region, 2000-2016. 2018.
78. Rafael Carmena JB. Diabetogenic Action of Statins: Mechanisms | SpringerLink. Current Atherosclerosis Reports. 2019.
79. Tsuyoshi Tabuchi MS, Tomonori Itoh, Motoyuki Nakamura. MicroRNA-34a regulates the longevity-associated protein SIRT1 in coronary artery disease: effect of statins on SIRT1 and microRNA-34a expression. Clinical Science. 2012;123(3):161-71.
80. Hlatky MA, Boothroyd DB, Reitz BA, Shilane DA, Baker LC, Go AS. Adoption and Effectiveness of Internal Mammary Artery Grafting in Coronary Artery Bypass Surgery Among Medicare Beneficiaries. J Am Coll Cardiol. 2014;63(1):33-9.
81. Fumiyuki Otsuka KY, Kenichi Sakakura , Renu Virmani. Why is the mammary artery so special and what protects it from atherosclerosis? Annals of Cardiothoracic Surgery. 2018;2(4):519-26.
82. Doenst T, Haverich, A., Serruys, P., Bonow, R., Kappetien, P., Falk, V., Velazquez, E., Diegeler, A., Sigusch, H.,. PCI and CABG for Treating Stable Coronary Artery Disease. Journal the American College of Cardiology. 2018;73(8).
83. Shroff R, Long, D., Shanahan, C.,. Mechanistic Insights into Vascular Calcification in CKD. Journal of the American Society of Nephrology. 2013;24(2).
84. Back M, Aranyi T, Cancela ML, Carracedo M, Conceicao N, Leftheriotis G, et al. Endogenous Calcification Inhibitors in the Prevention of Vascular Calcification: A Consensus Statement From the COST Action EuroSoftCalcNet. Front Cardiovasc Med. 2018;5:196.
85. Schurgers LJ, Akbulut AC, Kaczor DM, Halder M, Koenen RR, Kramann R. Initiation and Propagation of Vascular Calcification Is Regulated by a Concert of Platelet- and Smooth Muscle Cell-Derived Extracellular Vesicles. Front Cardiovasc Med. 2018;5.
86. Bakhshian Nik A, Hutcheson JD, Aikawa E. Extracellular Vesicles As Mediators of Cardiovascular Calcification. Front Cardiovasc Med. 2017;4.
87. Bartoli-Leonard F, Wilkinson FL, Schiro A, Inglott FS, Alexander MY, Weston R. Suppression of SIRT1 in Diabetic Conditions Induces Osteogenic Differentiation of Human Vascular Smooth Muscle Cells via RUNX2 Signalling. Scientific Reports. 2019;9(1):878.
88. Gardner SE, Humphry M, Bennett MR, Clarke MC. Senescent Vascular Smooth Muscle Cells Drive Inflammation Through an Interleukin-1α–Dependent Senescence-Associated Secretory Phenotype. Arterioscler Thromb Vasc Biol. 2015;35(9):1963-74.

89. Coppé JP, Desprez PY, Krtolica A, Campisi J. The Senescence-Associated Secretory Phenotype: The Dark Side of Tumor Suppression. Annu Rev Pathol. 2010;5:99-118.
90. Ndip A, Williams A, Jude EB, Serracino-Inglott F, Richardson S, Smyth JV, et al. The RANKL/RANK/OPG signaling pathway mediates medial arterial calcification in diabetic Charcot neuroarthropathy. Diabetes. 2011;60(8):2187-96.
91. Shroff RC, Shah V, Disease I, Hiorns MP, Radiology Departments GOSHUIoCH, London , UK, Schoppet M, et al. The circulating calcification inhibitors, fetuin-A and osteoprotegerin, but not Matrix Gla protein, are associated with vascular stiffness and calcification in children on dialysis. Nephrology Dialysis Transplantation. 2008;23(10):3263-71.
92. Sardana. M. I, V., Swapna, V., Uzma, K., Ali, T., Maheshwara, K., Ahmed, SA., Beraun, M., Drummen, N., Vermer, C., Akers, S., Chirinos, J.,. Inactive Matrix Gla-Protein and Arterial Stiffness in Type 2 Diabetes Mellitus. American Journal of Hypertension. 2017;30(2):196-201.
93. Westenfeld R, Schäfer C, Krüger T, Haarmann C, Schurgers LJ, Reutelingsperger C, et al. Fetuin-A Protects against Atherosclerotic Calcification in CKD. J Am Soc Nephrol. 2009;20(6):1264-74.
94. Sage AP, Tintut Y, Demer LL. Regulatory mechanisms in vascular calcification. Nat Rev Cardiol. 2010;7(9):528-36.
95. New SE, Aikawa E. Role of extracellular vesicles in de novo mineralization: an additional novel mechanism of cardiovascular calcification. Arterioscler Thromb Vasc Biol. 2013;33(8):1753-8.
96. Malhotra R, Burke MF, Martyn T, Shakartzi HR, Thayer TE, O'Rourke C, et al. Inhibition of Bone Morphogenetic Protein Signal Transduction Prevents the Medial Vascular Calcification Associated with Matrix Gla Protein Deficiency. PLoS One. 2015;10(1).
97. Schurgers LJ, Spronk HM, Skepper JN, Hackeng TM, Shanahan CM, Vermeer C, et al. Post-translational modifications regulate matrix Gla protein function: importance for inhibition of vascular smooth muscle cell calcification. J Thromb Haemost. 2007;5(12):2503-11.
98. Theuwissen E, Smit E, Vermeer C. The Role of Vitamin K in Soft-Tissue Calcification. Adv Nutr. 2012;3(2):166-73.
99. Barrett H, O'Keeffe M, Kavanagh E, Walsh M, O'Connor EM. Is Matrix Gla Protein Associated with Vascular Calcification? A Systematic Review. Nutrients. 2018;10(4).
100. Furmanik M, Shanahan CM. Endoplasmic Reticulum Stress in Arterial Smooth Muscle Cells: A Novel Regulator of Vascular Disease. Curr Cardiol Rev. 2017;13(2):94-105.
101. Jansen F, Yang X, Franklin BS, Hoelscher M, Schmitz T, Bedorf J, et al. High glucose condition increases NADPH oxidase activity in endothelial microparticles that promote vascular inflammation. Cardiovasc Res. 2013;98(1):94-106.
102. Byon CH, Javed A, Dai Q, Kappes JC, Clemens TL, Darley-Usmar VM, et al. Oxidative Stress Induces Vascular Calcification through Modulation of the Osteogenic Transcription Factor Runx2 by AKT Signaling*. J Biol Chem. 2832008. p. 15319-27.
103. Ndip A, Wilkinson FL, Jude EB, Boulton AJ, Alexander MY. RANKL-OPG and RAGE modulation in vascular calcification and diabetes: novel targets for therapy. Diabetologia. 2014;57(11):2251-60.
104. Brodeur MR, Bouvet C, Bouchard S, Moreau S, Leblond J, Deblois D, et al. Reduction of advanced-glycation end products levels and inhibition of RAGE

signaling decreases rat vascular calcification induced by diabetes. PLoS One. 2014;9(1):e85922.
105. Deng L, Wang, Y., Peng, Y., Wu, Y., Ding, Y., Jiang, Y., Shen, Z., Fu, Q.,. Osteoblast-derived microvesicles: A novel mechanism for communication between osteoblasts and osteoclasts. Bone. 2015;79:37-42.
106. Kapustin AN, Davies JD, Reynolds JL, McNair R, Jones GT, Sidibe A, et al. Calcium Regulates Key Components of Vascular Smooth Muscle Cell–Derived Matrix Vesicles to Enhance Mineralization. Circulation Research. 2011.
107. Nielsen LB, Pedersen FS, Pedersen L. Expression of type III sodium-dependent phosphate transporters/retroviral receptors mRNAs during osteoblast differentiation. Bone. 2001;28(2):160-6.
108. Golub EE. Role of Matrix Vesicles in Biomineralization. Biochim Biophys Acta. 2009;1790(12):1592-8.
109. Kapustin AN, Shanahan CM. Calcium regulation of vascular smooth muscle cell-derived matrix vesicles. Trends Cardiovasc Med. 2012;22(5):133-7.
110. Ngai D, Lino M, Bendeck MP. Cell-Matrix Interactions and Matricrine Signaling in the Pathogenesis of Vascular Calcification. Front Cardiovasc Med. 2018;5:174.
111. Hsu JJ, Lim J, Tintut Y, Demer LL. Cell-matrix mechanics and pattern formation in inflammatory cardiovascular calcification. Heart. 2016;102(21):1710-5.
112. Rensen S, Doevendans P, van Eys G. Regulation and characteristics of vascular smooth muscle cell phenotypic diversity. Neth Heart J. 2007;15(3):100-8.
113. Brozovich F, Nicholson C, Degen C, Gao YZ, Aggarwal M, Morgan K. Mechanisms of Vascular Smooth Muscle Contraction and the Basis for Pharmacologic Treatment of Smooth Muscle Disorders. Pharmacol Rev. 2016;68(2):476-532.
114. Allahverdian S, Chaabane C, Boukais K, Francis GA, Bochaton-Piallat ML. Smooth muscle cell fate and plasticity in atherosclerosis. Cardiovasc Res. 2018;114(4):540-50.
115. Yamamoto M, Yamamoto K, Noumura T. Type I collagen promotes modulation of cultured rabbit arterial smooth muscle cells from a contractile to a synthetic phenotype. Exp Cell Res. 1993;204(1):121-9.
116. Frid MG, Aldashev AA, Dempsey EC, Stenmark KR. Smooth muscle cells isolated from discrete compartments of the mature vascular media exhibit unique phenotypes and distinct growth capabilities. Circ Res. 1997;81(6):940-52.
117. Dobnikar L, Taylor AL, Chappell J, Oldach P, Harman JL, Oerton E, et al. Disease-relevant transcriptional signatures identified in individual smooth muscle cells from healthy mouse vessels. Nature Communications. 2018;9(1):4567.
118. Gomez D, Owens GK. Smooth muscle cell phenotypic switching in atherosclerosis. Cardiovasc Res. 2012;95(2):156-64.
119. Nguyen AT, Gomez D, Bell RD, Campbell JH, Clowes AW, Gabbiani G, et al. Smooth Muscle Cell Plasticity: Fact or Fiction? Circ Res. 2013;112(1):17-22.
120. Sandison ME, Dempster J, McCarron JG. The transition of smooth muscle cells from a contractile to a migratory, phagocytic phenotype: direct demonstration of phenotypic modulation. J Physiol. 2016;594(21):6189-209.
121. Bennett MR, Sinha S, Owens GK. Vascular smooth muscle cells in atherosclerosis. Circ Res. 2016;118(4):692-702.
122. Al-Ayoubi A, Tarcsafalvi A, Zheng H, Sakati W, Eblen ST. ERK activation and nuclear signaling induced by the loss of cell/matrix adhesion stimulates anchorage-independent growth of ovarian cancer cells. J Cell Biochem. 2008;105(3):875-84.

123. Cheng Z, Sundberg-Smith LJ, Mangiante LE, Sayers RL, Hakim ZS, Musunuri S, et al. Focal adhesion kinase regulates smooth muscle cell recruitment to the developing vasculature. Arterioscler Thromb Vasc Biol. 2011;31(10):2193-202.
124. Fincham V, James M, Frame M, Winder S. Active ERK/MAP kinase is targeted to newly forming cell–matrix adhesions by integrin engagement and v-Src. EMBO J. 2000;19(12):2911-23.
125. Miyamoto S, Teramoto H, Coso OA, Gutkind JS, Burbelo PD, Akiyama SK, et al. Integrin function: molecular hierarchies of cytoskeletal and signaling molecules. J Cell Biol. 1995;131(3):791-805.
126. D'Souza DR, Salib MM, Bennett J, Mochin-Peters M, Asrani K, Goldblum SE, et al. Hyperglycemia regulates RUNX2 activation and cellular wound healing through the aldose reductase polyol pathway. J Biol Chem. 2009;284(27):17947-55.
127. Fiorentino TV, Prioletta A, Zuo P, Folli F. Hyperglycemia-induced oxidative stress and its role in diabetes mellitus related cardiovascular diseases. Curr Pharm Des. 2013;19(32):5695-703.
128. Kong JG, Park JB, Lee D, Park EY. Effect of High Glucose on Stress-Induced Senescence of Nucleus Pulposus Cells of Adult Rats. Asian Spine J. 2015;9(2):155-61.
129. Liu Y, Drozdov I, Shroff R, Beltran LE, Shanahan CM. Prelamin A accelerates vascular calcification via activation of the DNA damage response and senescence-associated secretory phenotype in vascular smooth muscle cells. Circ Res. 2013;112(10):e99-109.
130. Komori T. Regulation of osteoblast differentiation by transcription factors. J Cell Biochem. 2006;99(5):1233-9.
131. Sinha S, Iyer D, Granata A. Embryonic origins of human vascular smooth muscle cells: implications for in vitro modeling and clinical application. Cell Mol Life Sci. 2014;71(12):2271-88.
132. Cheng JK, Wagenseil JE. Extracellular Matrix and the Mechanics of Large Artery Development. Biomech Model Mechanobiol. 2012;11(8):1169-86.
133. Leszczynska A, Murphy JM. Vascular Calcification: Is it rather a Stem/Progenitor Cells Driven Phenomenon? Front Bioeng Biotechnol. 2018;6:10.
134. Tintut Y, Alfonso Z, Saini T, Radcliff K, Watson K, Bostrom K, et al. Multilineage potential of cells from the artery wall. Circulation. 2003;108(20):2505-10.
135. Yamazaki T, Mukouyama Y. Tissue Specific Origin, Development, and Pathological Perspectives of Pericytes. Front Cardiovasc Med. 2018;5(78).
136. Li SL, Reddy MA, Cai Q, Meng L, Yuan H, Lanting L, et al. Enhanced proatherogenic responses in macrophages and vascular smooth muscle cells derived from diabetic db/db mice. Diabetes. 2006;55(9):2611-9.
137. Roy S, Sala R, Cagliero E, Lorenzi M. Overexpression of fibronectin induced by diabetes or high glucose: phenomenon with a memory. Proc Natl Acad Sci U S A. 1990;87(1):404-8.
138. El-Osta A, Brasacchio D, Yao D, Pocai A, Jones PL, Roeder RG, et al. Transient high glucose causes persistent epigenetic changes and altered gene expression during subsequent normoglycemia. J Exp Med. 2008;205(10):2409-17.
139. Yao D, Brownlee M. Hyperglycemia-induced reactive oxygen species increase expression of the receptor for advanced glycation end products (RAGE) and RAGE ligands. Diabetes. 2010;59(1):249-55.

140. Yuan T, Yang T, Chen H, Fu D, Hu Y, Wang J, et al. New insights into oxidative stress and inflammation during diabetes mellitus-accelerated atherosclerosis. Redox Biol. 2019;20:247-60.
141. Hink U, Tsilimingas N, Wendt M, Munzel T. Mechanisms underlying endothelial dysfunction in diabetes mellitus: therapeutic implications. Treat Endocrinol. 2003;2(5):293-304.
142. Franceschi RT, Xiao G, Jiang D, Gopalakrishnan R, Yang S, Reith E. Multiple Signaling Pathways Converge on the Cbfa1/Runx2 Transcription Factor to Regulate Osteoblast Differentiation. Connect Tissue Res. 2003;44(Suppl 1):109-16.
143. Bartoli-Leonard F, Wilkinson FL, Langford-Smith AWW, Alexander MY, Weston R. The Interplay of SIRT1 and Wnt Signaling in Vascular Calcification. Front Cardiovasc Med. 2018;5.
144. Boström KI, Jumabay M, Matveyenko A, Nicholas SB, Yao Y. Activation of Vascular Bone Morphogenetic Protein Signaling in Diabetes Mellitus. Circ Res. 2011;108(4):446-57.
145. Rutkovskiy A, Stensløkken KO, Vaage IJ. Osteoblast Differentiation at a Glance. Med Sci Monit Basic Res. 222016. p. 95-106.
146. Tyson KL, Reynolds JL, McNair R, Zhang Q, Weissberg PL, Shanahan CM. Osteo/chondrocytic transcription factors and their target genes exhibit distinct patterns of expression in human arterial calcification. Arterioscler Thromb Vasc Biol. 2003;23(3):489-94.
147. Zhang S, Xiao Z, Luo J, He N, Mahlios J, Quarles LD. Dose-Dependent Effects of Runx2 on Bone Development. J Bone Miner Res. 242009. p. 1889-904.
148. Gu X, Masters KS. Role of the MAPK/ERK pathway in valvular interstitial cell calcification. Am J Physiol Heart Circ Physiol. 2009;296(6):H1748-57.
149. Xiao G, Jiang D, Thomas P, Benson MD, Guan K, Karsenty G, et al. MAPK pathways activate and phosphorylate the osteoblast-specific transcription factor, Cbfa1. J Biol Chem. 2000;275(6):4453-9.
150. Hu Y, Chan E, Wang SX, Li B. Activation of p38 mitogen-activated protein kinase is required for osteoblast differentiation. Endocrinology. 2003;144(5):2068-74.
151. Huang J, Huang H, Wu M, Li J, Xie H, Zhou H, et al. Connective tissue growth factor induces osteogenic differentiation of vascular smooth muscle cells through ERK signaling. Int J Mol Med. 2013;32(2):423-9.
152. Li Y, Ge C, Franceschi RT. MAP Kinase-Dependent RUNX2 Phosphorylation Is Necessary for Epigenetic Modification of Chromatin During Osteoblast Differentiation. J Cell Physiol. 2017;232(9):2427-35.
153. Yang Y, Sun Y, Chen J, Bradley WE, Dell'Italia LJ, Wu H, et al. AKT-independent activation of p38 MAP kinase promotes vascular calcification. Redox Biol. 2018;16:97-103.
154. Jeon EJ, Lee KY, Choi NS, Lee MH, Kim HN, Jin YH, et al. Bone morphogenetic protein-2 stimulates Runx2 acetylation. J Biol Chem. 2006;281(24):16502-11.
155. Martinez-Moreno JM, Munoz-Castaneda JR, Herencia C, Oca AM, Estepa JC, Canalejo R, et al. In vascular smooth muscle cells paricalcitol prevents phosphate-induced Wnt/beta-catenin activation. Am J Physiol Renal Physiol. 2012;303(8):F1136-44.
156. Javed A, Bae J-S, Afzal F, Gutierrez S, Pratap J, Zaidi SK, et al. Structural Coupling of Smad and Runx2 for Execution of the BMP2 Osteogenic Signal. 2008.

157. Phimphilai M, Zhao Z, Boules H, Roca H, Franceschi RT. BMP Signaling Is Required for RUNX2-Dependent Induction of the Osteoblast Phenotype. J Bone Miner Res. 2006;21(4):637-46.
158. Muller KH, Hayward R, Rajan R, Whitehead M, Cobb AM, Ahmad S, et al. Poly(ADP-Ribose) Links the DNA Damage Response and Biomineralization. Cell Rep. 2019;27(11):3124-38.e13.
159. Shah A, Gray K, Figg N, Finigan A, Starks L, Bennett M. Defective Base Excision Repair of Oxidative DNA Damage in Vascular Smooth Muscle Cells Promotes Atherosclerosis. Circulation. 2018;138(14):1446-62.
160. Chatterjee N, Walker GC. Mechanisms of DNA damage, repair, and mutagenesis. Environ Mol Mutagen. 2017;58(5):235-63.
161. Lamarche BJ, Orazio NI, Weitzman MD. The MRN complex in Double-Strand Break Repair and Telomere Maintenance. FEBS Lett. 2010;584(17):3682-95.
162. Uziel T, Lerenthal Y, Moyal L, Andegeko Y, Mittelman L, Shiloh Y. Requirement of the MRN complex for ATM activation by DNA damage. EMBO J. 2003;22(20):5612-21.
163. Burma S, Chen BP, Murphy M, Kurimasa A, Chen DJ. ATM phosphorylates histone H2AX in response to DNA double-strand breaks. J Biol Chem. 2001;276(45):42462-7.
164. Chang HHY, Pannunzio NR, Adachi N, Lieber MR. Non-homologous DNA end joining and alternative pathways to double-strand break repair. Nat Rev Mol Cell Biol. 2017;18(8):495-506.
165. Yang K, Guo R, Xu D. Non-homologous end joining: advances and frontiers. Acta Biochim Biophys Sin (Shanghai). 2016;48(7):632-40.
166. Kang YJ, Yan CT. Regulation of DNA repair in the absence of classical non-homologous end joining. DNA Repair (Amst). 2018;68:34-40.
167. Nakano-Kurimoto R, Ikeda K, Uraoka M, Nakagawa Y, Yutaka K, Koide M, et al. Replicative senescence of vascular smooth muscle cells enhances the calcification through initiating the osteoblastic transition. Am J Physiol Heart Circ Physiol. 2009;297(5):H1673-84.
168. MacDonald BT, Tamai K, He X. Wnt/β-Catenin Signaling: Components, Mechanisms, and Diseases. Developmental Cell. 2009;17(1):9-26.
169. Wang S, Yang Z, Gao Y, Li Q, Su Y, Wang Y, et al. Pyruvate kinase, muscle isoform 2 promotes proliferation and insulin secretion of pancreatic beta-cells via activating Wnt/CTNNB1 signaling. Int J Clin Exp Pathol. 2015;8(11):14441-8.
170. Cai T, Sun D, Duan Y, Wen P, Dai C, Yang J, et al. WNT/beta-catenin signaling promotes VSMCs to osteogenic transdifferentiation and calcification through directly modulating Runx2 gene expression. Exp Cell Res. 2016;345(2):206-17.
171. R Nusse AB, J Papkoff, P Scambler, G Shackleford, A McMahon, R Moon, H Varmus. A new nomenclature for int-1 and related genes: The Wnt gene family. Cell. 1991;64(2):231.
172. Westendorf JJ, Kahler RA, Schroeder TM. Wnt signaling in osteoblasts and bone diseases. Gene. 2004;341:19-39.
173. Gao C, Xiao G, Hu J. Regulation of Wnt/β-catenin signaling by posttranslational modifications. Cell Biosci. 42014. p. 13.
174. Wang Y, Li YP, Paulson C, Shao JZ, Zhang X, Wu M, et al. Wnt and the Wnt signaling pathway in bone development and disease. Front Biosci (Landmark Ed).19:379-407.
175. González-Sancho JM, Greer YE, Abrahams CL, Takigawa Y, Baljinnyam B, Lee KH, et al. Functional Consequences of Wnt-induced Dishevelled 2

Phosphorylation in Canonical and Noncanonical Wnt Signaling*. J Biol Chem. 2882013. p. 9428-37.
176. Gaur T, Lengner CJ, Hovhannisyan H, Bhat RA, Bodine PV, Komm BS, et al. Canonical WNT signaling promotes osteogenesis by directly stimulating Runx2 gene expression. J Biol Chem. 2005;280(39):33132-40.
177. Sun J, Khalid S, Rozakis-Adcock M, Fantus IG, Jin T. P-21-activated protein kinase-1 functions as a linker between insulin and Wnt signaling pathways in the intestine. Oncogene. 2009;28(35):3132-44.
178. Astudillo P, Larrain J. Wnt signaling and cell-matrix adhesion. Curr Mol Med. 2014;14(2):209-20.
179. Günther T, Poli C, Müller JM, Catala-Lehnen P, Schinke T, Yin N, et al. Fhl2 deficiency results in osteopenia due to decreased activity of osteoblasts. EMBO J. 242005. p. 3049-56.
180. Hsu JJ, Tintut Y, Demer LL. Vitamin D and Osteogenic Differentiation in the Artery Wall. Clin J Am Soc Nephrol. 2008;3(5):1542-7.
181. Shobeiri N, Adams MA, Holden RM. Vascular calcification in animal models of CKD: A review. Am J Nephrol. 2010;31(6):471-81.
182. King AJ. The use of animal models in diabetes research. Br J Pharmacol. 2012;166(3):877-94.
183. Lee YT, Lin HY, Chan YWF, Li KHC, To OTL, Yan BP, et al. Mouse models of atherosclerosis: a historical perspective and recent advances. Lipids Health Dis. 2017;16.
184. Ognen Ivanovski IN. Animal models of vascular calcification. Atherosclerosis. 2012;222(2):576.
185. von Scheidt M, Zhao Y, Kurt Z, Pan C, Zeng L, Yang X, et al. Applications and Limitations of Mouse Models for Understanding Human Atherosclerosis. Cell Metab. 2017;25(2):248-61.
186. Getz GS, Reardon CA. Animal Models of Atherosclerosis. Arterioscler Thromb Vasc Biol. 2012;32(5):1104-15.
187. Mulligan-Kehoe MJ. The vasa vasorum in diseased and nondiseased arteries. Am J Physiol Heart Circ Physiol. 2010;298(2):H295-305.
188. Excellence NIfHaC. Type 2 Diabetes: Prevention in People at High Risk. NICE; 2018.
189. Klar AJ, Fogel S, Macleod K. MAR1-a Regulator of the HMa and HMalpha Loci in SACCHAROMYCES CEREVISIAE. Genetics. 1979;93(1):37-50.
190. Haigis MC, Sinclair DA. Mammalian sirtuins: biological insights and disease relevance. Annu Rev Pathol. 2010;5:253-95.
191. Mendes KL, Lelis DF, Santos SHS. Nuclear sirtuins and inflammatory signaling pathways. Cytokine Growth Factor Rev. 2017;38:98-105.
192. Lynch CJ, Shah ZH, Allison SJ, Ahmed SU, Ford J, Warnock LJ, et al. SIRT1 undergoes alternative splicing in a novel auto-regulatory loop with p53. PLoS One. 2010;5(10):e13502.
193. Davenport A, Huber, H., Hoelz, A.,. Structural and FUnctional ANalysis of Human SIRT1. Journal of Molecular Biology. 2014;426(3):526-41.
194. Tanno M, Sakamoto, J., Miura, T., Shimamoto, K., Horio, Y.,. Nucleocytoplasmic Shuttling of the NAD+-dependent Histone Deacetylase SIRT1. Journal of Biological Chemistry. 2007.
195. Hou J, Chong ZZ, Shang YC, Maiese K. Early apoptotic vascular signaling is determined by Sirt1 through nuclear shuttling, forkhead trafficking, bad, and mitochondrial caspase activation. Curr Neurovasc Res. 2010;7(2):95-112.

196. Yanagisawa S, Baker JR, Vuppusetty C, Koga T, Colley T, Fenwick P, et al. The dynamic shuttling of SIRT1 between cytoplasm and nuclei in bronchial epithelial cells by single and repeated cigarette smoke exposure. PLoS One. 2018;13(3).
197. Byles V, Chmilewski LK, Wang J, Zhu L, Forman LW, Faller DV, et al. Aberrant Cytoplasm Localization and Protein Stability of SIRT1 is Regulated by PI3K/IGF-1R Signaling in Human Cancer Cells. Int J Biol Sci. 2010;6(6):599-612.
198. Wu J, Jin Z, Zheng H, Yan LJ. Sources and implications of NADH/NAD+ redox imbalance in diabetes and its complications. Diabetes Metab Syndr Obes. 2016;9:145-53.
199. Tong L, Denu JM. Function and metabolism of sirtuin metabolite O-acetyl-ADP-ribose. Biochim Biophys Acta. 2010;1804(8):1617-25.
200. Liou GG, Tanny JC, Kruger RG, Walz T, Moazed D. Assembly of the SIR complex and its regulation by O-acetyl-ADP-ribose, a product of NAD-dependent histone deacetylation. Cell. 2005;121(4):515-27.
201. Chou CC, Li YC, Gartenberg MR. Bypassing Sir2 and O-acetyl-ADP-ribose in transcriptional silencing. Mol Cell. 2008;31(5):650-9.
202. Gomes A, Yong, J., Kiew, K., Aydin, E., Khongkow, M., Laohasinnarong, S., Lam, E. Sirtuin1 in Acetylation of Downstream Target Proteins. Histone Deacetylases: Methods and Protocols, Methods in Molecular Biology. 2016;1436.
203. Ma P, Schultz RM. Histone deacetylase 1 (HDAC1) regulates histone acetylation, development, and gene expression in preimplantation mouse embryos. Dev Biol. 2008;319(1):110-20.
204. Katan-Khaykovich Y, Struhl K. Dynamics of global histone acetylation and deacetylation in vivo: rapid restoration of normal histone acetylation status upon removal of activators and repressors. Genes Dev. 2002;16(6):743-52.
205. Boily G, Seifert EL, Bevilacqua L, He XH, Sabourin G, Estey C, et al. SirT1 regulates energy metabolism and response to caloric restriction in mice. PLoS One. 2008;3(3):e1759.
206. McBurney MW, Yang X, Jardine K, Hixon M, Boekelheide K, Webb JR, et al. The mammalian SIR2alpha protein has a role in embryogenesis and gametogenesis. Mol Cell Biol. 2003;23(1):38-54.
207. Wang Y. Molecular Links between Caloric Restriction and Sir2/SIRT1 Activation. Diabetes Metab J. 2014;38(5):321-9.
208. Ruggenenti P, Abbate M, Ruggiero B, Rota S, Trillini M, Aparicio C, et al. Renal and Systemic Effects of Calorie Restriction in Patients With Type 2 Diabetes With Abdominal Obesity: A Randomized Controlled Trial. Diabetes. 2017;66(1):75-86.
209. Walsh ME, Shi Y, Van Remmen H. The effects of dietary restriction on oxidative stress in rodents. Free Radic Biol Med. 2014;66:88-99.
210. Li C, Feng F, Xiong X, Li R, Chen N. Exercise coupled with dietary restriction reduces oxidative stress in male adolescents with obesity. J Sports Sci. 2017;35(7):663-8.
211. Cantó C, Auwerx J. Targeting SIRT1 to improve metabolism: all you need is NAD+? Pharmacol Rev. 2012;64(1):166-87.
212. Poljsak B. NAMPT-Mediated NAD Biosynthesis as the Internal Timing Mechanism: In NAD+ World, Time Is Running in Its Own Way. Rejuvenation Research. 2018;21(3).
213. Zhang T, Berrocal JG, Frizzell KM, Gamble MJ, DuMond ME, Krishnakumar R, et al. Enzymes in the NAD+ salvage pathway regulate SIRT1 activity at target gene promoters. J Biol Chem. 2009;284(30):20408-17.

214. Anderson RM, Bitterman KJ, Wood JG, Medvedik O, Sinclair DA. Nicotinamide and PNC1 govern lifespan extension by calorie restriction in Saccharomyces cerevisiae. Nature. 2003;423(6936):181-5.
215. Luna A, Aladjem MI, Kohn KW. SIRT1/PARP1 crosstalk: connecting DNA damage and metabolism. Genome Integr. 2013;4:6.
216. Ray Chaudhuri A, Nussenzweig A. The multifaceted roles of PARP1 in DNA repair and chromatin remodelling. Nat Rev Mol Cell Biol. 2017;18(10):610-21.
217. Hwang J, Yao H, Caito S, Sundar IK, Rahman I. Redox regulation of SIRT1 in inflammation and cellular senescence. Free Radic Biol Med. 2013;0:95-110.
218. Wang C, Chen L, Hou X, Li Z, Kabra N, Ma Y, et al. Interactions between E2F1 and SirT1 regulate apoptotic response to DNA damage. Nat Cell Biol. 2006;8(9):1025-31.
219. Yi J, Luo J. SIRT1 and p53, effect on cancer, senescence and beyond. Biochim Biophys Acta. 2010;1804(8):1684-9.
220. Sasaki T, Maier B, Koclega KD, Chruszcz M, Gluba W, Stukenberg PT, et al. Phosphorylation regulates SIRT1 function. PLoS One. 2008;3(12):e4020.
221. Nasrin N, Kaushik VK, Fortier E, Wall D, Pearson KJ, de Cabo R, et al. JNK1 Phosphorylates SIRT1 and Promotes Its Enzymatic Activity. PLoS One. 2009;4(12).
222. Zschoernig B, Mahlknecht U. Carboxy-terminal phosphorylation of SIRT1 by protein kinase CK2. Biochem Biophys Res Commun. 2009;381(3):372-7.
223. Michan S, Sinclair, D.,. Situins in mammals: Insights into their biological function. Biochemical Journal. 2007;404(1):1-13.
224. Pandithage R, Lilischkis R, Harting K, Wolf A, Jedamzik B, Luscher-Firzlaff J, et al. The regulation of SIRT2 function by cyclin-dependent kinases affects cell motility. J Cell Biol. 2008;180(5):915-29.
225. Liu X, Wang D, Zhao Y, Tu B, Zheng Z, Wang L, et al. Methyltransferase Set7/9 regulates p53 activity by interacting with Sirtuin 1 (SIRT1). Proc Natl Acad Sci U S A. 2011;108(5):1925-30.
226. Yang Y, Fu W, Chen J, Olashaw N, Zhang X, Nicosia SV, et al. SIRT1 sumoylation regulates its deacetylase activity and cellular response to genotoxic stress. Nat Cell Biol. 2007;9(11):1253-62.
227. Kornberg MD, Sen N, Hara MR, Juluri KR, Nguyen JV, Snowman AM, et al. GAPDH mediates nitrosylation of nuclear proteins. Nat Cell Biol. 2010;12(11):1094-100.
228. Vinciguerra M, Santini MP, Martinez C, Pazienza V, Claycomb WC, Giuliani A, et al. mIGF-1/JNK1/SirT1 signaling confers protection against oxidative stress in the heart. Aging Cell. 2012;11(1):139-49.
229. Gao Z, Zhang J, Kheterpal I, Kennedy N, Davis RJ, Ye J. Sirtuin 1 (SIRT1) protein degradation in response to persistent c-Jun N-terminal kinase 1 (JNK1) activation contributes to hepatic steatosis in obesity. J Biol Chem. 2011;286(25):22227-34.
230. Revollo JR, Li X. The ways and means 6 that fine tune Sirt1 activity. Trends Biochem Sci. 2013;38(3):160-7.
231. Guo Y, Xu A, Wang Y. SIRT1 in Endothelial Cells as a Novel Target for the Prevention of Early Vascular Aging. J Cardiovasc Pharmacol. 2016;67(6):465-73.
232. Zhang W, Huang Q, Zeng Z, Wu J, Zhang Y, Chen Z. Sirt1 Inhibits Oxidative Stress in Vascular Endothelial Cells. Oxid Med Cell Longev. 2017;2017.
233. Mattagajasingh I, Kim CS, Naqvi A, Yamamori T, Hoffman TA, Jung SB, et al. SIRT1 promotes endothelium-dependent vascular relaxation by activating endothelial nitric oxide synthase. Proc Natl Acad Sci U S A. 2007;104(37):14855-60.

234. Chen HZ, Wan YZ, Liu DP. Cross-talk between SIRT1 and p66Shc in vascular diseases. Trends Cardiovasc Med. 2013;23(7):237-41.
235. Heiss C, Rodriguez-Mateos A, Kelm M. Central Role of eNOS in the Maintenance of Endothelial Homeostasis. Antioxid Redox Signal. 2015;22(14):1230-42.
236. Sandoo A, van Zanten JJV, Metsios GS, Carroll D, Kitas GD. The Endothelium and Its Role in Regulating Vascular Tone. Open Cardiovasc Med J. 2010;4:302-12.
237. Ignarro LJ, Harbison RG, Wood KS, Kadowitz PJ. Activation of purified soluble guanylate cyclase by endothelium-derived relaxing factor from intrapulmonary artery and vein: stimulation by acetylcholine, bradykinin and arachidonic acid. J Pharmacol Exp Ther. 1986;237(3):893-900.
238. Miranda MX, van Tits LJ, Lohmann C, Arsiwala T, Winnik S, Tailleux A, et al. The Sirt1 activator SRT3025 provides atheroprotection in Apoe-/- mice by reducing hepatic Pcsk9 secretion and enhancing Ldlr expression. Eur Heart J. 2015;36(1):51-9.
239. Miao H, Zeng H, Gong H. microRNA-212 promotes lipid accumulation and attenuates cholesterol efflux in THP-1 human macrophages by targeting SIRT1. Gene. 2018;643:55-60.
240. Zeng HT, Fu YC, Yu W, Lin JM, Zhou L, Liu L, et al. SIRT1 prevents atherosclerosis via liverXreceptor and NFkappaB signaling in a U937 cell model. Mol Med Rep. 2013;8(1):23-8.
241. Fan W, Fang R, Wu X, Liu J, Feng M, Dai G, et al. Shear-sensitive microRNA-34a modulates flow-dependent regulation of endothelial inflammation. J Cell Sci. 2015;128(1):70-80.
242. Guo R, Liu B, Wang K, Zhou S, Li W, Xu Y. Resveratrol ameliorates diabetic vascular inflammation and macrophage infiltration in db/db mice by inhibiting the NF-kappaB pathway. Diab Vasc Dis Res. 2014;11(2):92-102.
243. Chong ZZ, Wang S, Shang YC, Maiese K. Targeting Cardiovascular Disease with Novel SIRT1 Pathways. Future Cardiol. 2012;8(1):89-100.
244. Zhang QJ, Wang Z, Chen HZ, Zhou S, Zheng W, Liu G, et al. Endothelium-specific overexpression of class III deacetylase SIRT1 decreases atherosclerosis in apolipoprotein E-deficient mice. Cardiovasc Res. 2008;80(2):191-9.
245. Hou J, Wang S, Shang YC, Chong ZZ, Maiese K. Erythropoietin employs cell longevity pathways of SIRT1 to foster endothelial vascular integrity during oxidant stress. Curr Neurovasc Res. 2011;8(3):220-35.
246. Guo R, Li W, Liu B, Li S, Zhang B, Xu Y. Resveratrol protects vascular smooth muscle cells against high glucose-induced oxidative stress and cell proliferation in vitro. Med Sci Monit Basic Res. 2014;20:82-92.
247. Tomayko EJ, Cachia AJ, Chung HR, Wilund KR. Resveratrol supplementation reduces aortic atherosclerosis and calcification and attenuates loss of aerobic capacity in a mouse model of uremia. J Med Food. 2014;17(2):278-83.
248. Mattison J, Wang, M., Bernier, M., Zhang, J., Park, SS., Maudsley, S., An, SS., Santhanam, L., Martin, B., Faulkner, S., Sosnowska, D., Csiszar, A.m Herbert, RL., Tilmont, EM., Ungvari, Z., Pearson, KJ., Lakatta, EG., de Cabo, R.,. Resveratrol prevents high fat/sucrose diet-induced central arterial wall inflammation and stiffening in nonhuman primates. Cell Metabolism. 2014;20(1):183-90.
249. Takemura A, Iijima K, Ota H, Son BK, Ito Y, Ogawa S, et al. Sirtuin 1 retards hyperphosphatemia-induced calcification of vascular smooth muscle cells. Arterioscler Thromb Vasc Biol. 2011;31(9):2054-62.

250. Villalba JM, Alcaín FJ. Sirtuin activators and inhibitors. Biofactors. 2012;38(5):349-59.
251. Howitz KT, Bitterman KJ, Cohen HY, Lamming DW, Lavu S, Wood JG, et al. Small molecule activators of sirtuins extend Saccharomyces cerevisiae lifespan. Nature. 2003;425(6954):191-6.
252. Borra MT, Smith BC, Denu JM. Mechanism of human SIRT1 activation by resveratrol. J Biol Chem. 2005;280(17):17187-95.
253. Hubbard BP, Sinclair DA. Small molecule SIRT1 activators for the treatment of aging and age-related diseases. Trends Pharmacol Sci. 2014;35(3):146-54.
254. Milne JC, Lambert PD, Schenk S, Carney DP, Smith JJ, Gagne DJ, et al. Small molecule activators of SIRT1 as therapeutics for the treatment of type 2 diabetes. Nature. 2007;450(7170):712.
255. Bonkowski MS, Sinclair DA. Slowing ageing by design: the rise of NAD(+) and sirtuin-activating compounds. Nat Rev Mol Cell Biol. 2016;17(11):679-90.
256. Dai H, Kustigian L, Carney D, Case A, Considine T, Hubbard BP, et al. SIRT1 Activation by Small Molecules: Kinetic and biophysical evidence for direct interaction of enzyme and activator. J Biol Chem. 2010;285(43):32695-703.
257. Baksi A, Kraydashenko O, Zalevkaya A, Stets R, Elliott P, Haddad J, et al. A phase II, randomized, placebo-controlled, double-blind, multi-dose study of SRT2104, a SIRT1 activator, in subjects with type 2 diabetes. Br J Clin Pharmacol. 2014;78(1):69-77.
258. Venkatasubramanian S, Noh RM, Daga S, Langrish JP, Mills NL, Waterhouse BR, et al. Effects of the small molecule SIRT1 activator, SRT2104 on arterial stiffness in otherwise healthy cigarette smokers and subjects with type 2 diabetes mellitus. Open Heart. 2016;3(1):e000402.
259. Noh RM, Venkatasubramanian S, Daga S, Langrish J, Mills NL, Lang NN, et al. Cardiometabolic effects of a novel SIRT1 activator, SRT2104, in people with type 2 diabetes mellitus. Open Heart. 2017;4(2):e000647.
260. Demer LL, Tintut Y. Vascular Calcification: Pathobiology of a Multifaceted Disease. Circulation. 2001;104(16):1881-3.
261. Wilkinson FL, Liu Y, Rucka AK, Jeziorska M, Hoyland JA, Heagerty AM, et al. Contribution of VCAF-positive cells to neovascularization and calcification in atherosclerotic plaque development. J Pathol. 2007;211(3):362-9.
262. Hosaka N, Mizobuchi M, Ogata H, Kumata C, Kondo F, Koiwa F, et al. Elastin degradation accelerates phosphate-induced mineralization of vascular smooth muscle cells. Calcif Tissue Int. 2009;85(6):523-9.
263. Georgakopoulou EA, Tsimaratou K, Evangelou K, Fernandez Marcos PJ, Zoumpourlis V, Trougakos IP, et al. Specific lipofuscin staining as a novel biomarker to detect replicative and stress-induced senescence. A method applicable in cryo-preserved and archival tissues. Aging. 2013;5(1):37-50.
264. Shi SR, Chaiwun B, Young L, Cote RJ, Taylor CR. Antigen retrieval technique utilizing citrate buffer or urea solution for immunohistochemical demonstration of androgen receptor in formalin-fixed paraffin sections. J Histochem Cytochem. 1993;41(11):1599-604.
265. Klaude M, Eriksson S, Nygren J, Ahnstrom G. The comet assay: mechanisms and technical considerations. Mutat Res. 1996;363(2):89-96.
266. Morgan RG, Ives SJ, Lesniewski LA, Cawthon RM, Andtbacka RHI, Noyes RD, et al. Age-related telomere uncapping is associated with cellular senescence and inflammation independent of telomere shortening in human arteries. Am J Physiol Heart Circ Physiol. 2013;305(2):H251-8.

267. Pauly RR, Passaniti A, Bilato C, Monticone R, Cheng L, Papadopoulos N, et al. Migration of cultured vascular smooth muscle cells through a basement membrane barrier requires type IV collagenase activity and is inhibited by cellular differentiation. Circ Res. 1994;75(1):41-54.
268. Faries PL, Rohan DI, Takahara H, Wyers MC, Contreras MA, Quist WC, et al. Human vascular smooth muscle cells of diabetic origin exhibit increased proliferation, adhesion, and migration. J Vasc Surg. 2001;33(3):601-7.
269. Miranda KM, Espey MG, Wink DA. A rapid, simple spectrophotometric method for simultaneous detection of nitrate and nitrite. Nitric Oxide. 2001;5(1):62-71.
270. James Pritchett VSA, Emma Harvey, Katherine Martin, Jessica Llewellyn, Philip Ireland, Alexander Nicolaides, Martin J. Humphries, Nicoletta Bobola, Neil A. Hanley, Karen Piper Hanley. PLOS ONE: Epimorphin Alters the Inhibitory Effects of SOX9 on Mmp13 in Activated Hepatic Stellate Cells. PLoS One. 2014.
271. Pozarowski P, Darzynkiewicz Z. Analysis of cell cycle by flow cytometry. Methods Mol Biol. 2004;281:301-11.
272. Al-Nozha MM, Ismail HM, Al Nozha OM. Coronary artery disease and diabetes mellitus. Journal of Taibah University Medical Sciences. 2016;11(4):330-8.
273. Bin Zhou YL, Kaveh Hajifathalian, James Bentham. Worldwide trends in diabetes since 1980: a pooled analysis of 751 population-based studies with 4·4 million participants - The Lancet. 2018.
274. Alves RD, Eijken M, van de Peppel J, van Leeuwen JP. Calcifying vascular smooth muscle cells and osteoblasts: independent cell types exhibiting extracellular matrix and biomineralization-related mimicries. BMC Genomics. 2014;15:965.
275. Wu M, Rementer C, Giachelli CM. Vascular Calcification: an Update on Mechanisms and Challenges in Treatment. Calcif Tissue Int. 2013;93(4):365-73.
276. Karwowski W, Naumnik B, Szczepanski M, Mysliwiec M. The mechanism of vascular calcification - a systematic review. Med Sci Monit. 2012;18(1):Ra1-11.
277. Andrews J, Psaltis, P., Bartolo, B., Nicolls, S., Puri, R. Coronary arterial calcification: A review of mechanisms, promoters and imaging. Trends in Cardiovascular Medicine. 2018;4.
278. Coscas R, Bensussan M, Jacob MP, Louedec L, Massy Z, Sadoine J, et al. Free DNA precipitates calcium phosphate apatite crystals in the arterial wall in vivo. Atherosclerosis. 2017;259:60-7.
279. Lara MJ, Ros E, Sierra M, Dorronsoro C, Aguilar J. Composition and genesis of calcium deposits in atheroma plaques. Ultrastruct Pathol. 2014;38(3):167-77.
280. Louvet L, Bazin D, Büchel J, Steppan S, Passlick-Deetjen J, Massy ZA. Characterisation of Calcium Phosphate Crystals on Calcified Human Aortic Vascular Smooth Muscle Cells and Potential Role of Magnesium. PLoS One. 2015;10(1).
281. Afonso P, Auclair M, Boccara F, Vantyghem MC, Katlama C, Capeau J, et al. LMNA mutations resulting in lipodystrophy and HIV protease inhibitors trigger vascular smooth muscle cell senescence and calcification: Role of ZMPSTE24 downregulation. Atherosclerosis. 2016;245:200-11.
282. Lin X, Zhan JK, Zhong JY, Wang YJ, Wang Y, Li S, et al. lncRNA-ES3/miR-34c-5p/BMF axis is involved in regulating high-glucose-induced calcification/senescence of VSMCs. Aging (Albany NY). 2019;11(2):523-35.
283. van Deursen JM. The role of senescent cells in ageing. Nature. 2014;509(7501):439-46.

284. Uryga AK, Bennett MR. Ageing induced vascular smooth muscle cell senescence in atherosclerosis. J Physiol. 2016;594(8):2115-24.
285. Regulsk M. Understanding Diabetic Induction of Cellular Senescence: A Concise Review. Wounds. 2019;30(4):96-101.
286. Kim DY, Kim EJ, Jang WG. Piperine induces osteoblast differentiation through AMPK-dependent Runx2 expression. Biochem Biophys Res Commun. 2018;495(1):1497-502.
287. Gao P, Han P, Jiang D, Yang S, Cui Q, Li Z. Effects of the donor age on proliferation, senescence and osteogenic capacity of human urine-derived stem cells. Cytotechnology. 2017;69(5):751-63.
288. Byon CH, Chen Y. Molecular Mechanisms of Vascular Calcification in Chronic Kidney Disease: The Link between Bone and the Vasculature. Curr Osteoporos Rep. 2015;13(4):206-15.
289. Yan J, Stringer SE, Hamilton A, Charlton-Menys V, Gotting C, Muller B, et al. Decorin GAG synthesis and TGF-beta signaling mediate Ox-LDL-induced mineralization of human vascular smooth muscle cells. Arterioscler Thromb Vasc Biol. 2011;31(3):608-15.
290. Zhang H, Zhao X, Zhang Z, Chen W, Zhang X. An Immunohistochemistry Study of Sox9, Runx2, and Osterix Expression in the Mandibular Cartilages of Newborn Mouse. Biomed Res Int. 2013;2013.
291. Shao JS, Cheng SL, Pingsterhaus JM, Charlton-Kachigian N, Loewy AP, Towler DA. Msx2 promotes cardiovascular calcification by activating paracrine Wnt signals. J Clin Invest. 2005;115(5):1210-20.
292. Zhou N, Li Q, Lin X, Hu N, Liao JY, Lin LB, et al. BMP2 induces chondrogenic differentiation, osteogenic differentiation and endochondral ossification in stem cells. Cell Tissue Res. 2016;366(1):101-11.
293. Mehta A, Patel J, Al Rifai M, Ayers CR, Neeland IJ, Kanaya AM, et al. Inflammation and coronary artery calcification in South Asians: The Mediators of Atherosclerosis in South Asians Living in America (MASALA) study. Atherosclerosis. 2018;270:49-56.
294. Lowery JW, deCaestecker MP. BMP signaling in vacular development and disease. Cytokine Growth Factor Rev. 2010;21(4):287-98.
295. Giachelli CM. The Emerging Role of Phosphate in Vascular Calcification. Kidney Int. 2009;75(9):890-7.
296. Li X, Giachelli CM. Sodium-dependent phosphate cotransporters and vascular calcification. Curr Opin Nephrol Hypertens. 2007;16(4):325-8.
297. Albanese I, Khan K, Barratt B, Al-Kindi H, Schwertani A. Atherosclerotic Calcification: Wnt Is the Hint. 2018.
298. Weng JJ, Su Y. Nuclear matrix-targeting of the osteogenic factor Runx2 is essential for its recognition and activation of the alkaline phosphatase gene. Biochim Biophys Acta. 2013;1830(3):2839-52.
299. Takarada T, Hinoi E, Nakazato R, Ochi H, Xu C, Tsuchikane A, et al. An analysis of skeletal development in osteoblast-specific and chondrocyte-specific runt-related transcription factor-2 (Runx2) knockout mice. J Bone Miner Res. 2013;28(10):2064-9.
300. Lin ME, Chen T, Leaf EM, Speer MY, Giachelli CM. Runx2 Expression in Smooth Muscle Cells Is Required for Arterial Medial Calcification in Mice. Am J Pathol. 2015;185(7):1958-69.
301. Zainabadi K, Liu CJ, Guarente L. SIRT1 is a Positive Regulator of the Master Osteoblast Transcription Factor, RUNX2. PLoS One. 2017.

302. Shimoyama Y, Mitsuda Y, Tsuruta Y, Suzuki K, Hamajima N, Niwa T. SIRTUIN 1 gene polymorphisms are associated with cholesterol metabolism and coronary artery calcification in Japanese hemodialysis patients. J Ren Nutr. 2012;22(1):114-9.
303. Figarska SM, Vonk JM, Boezen HM. SIRT1 polymorphism, long-term survival and glucose tolerance in the general population. PLoS One. 2013;8(3):e58636.
304. Zhang P, Li Y, Du Y, Li G, Wang L, Zhou F. Resveratrol Ameliorated Vascular Calcification by Regulating Sirt-1 and Nrf2. Transplant Proc. 2016;48(10):3378-86.
305. North BJ, Verdin E. Sirtuins: Sir2-related NAD-dependent protein deacetylases. Genome Biol. 52004. p. 224.
306. Millar SA, Patel H, Anderson SI, England TJ, O'Sullivan SE. Osteocalcin, Vascular Calcification, and Atherosclerosis: A Systematic Review and Meta-analysis. Front Endocrinol (Lausanne). 2017;8:183.
307. Liu TM, Lee EH. Transcriptional Regulatory Cascades in Runx2-Dependent Bone Development. Tissue Eng Part B Rev. 2013;19(3):254-63.
308. Andrade MC, Carmo LS, Farias-Silva E, Liberman M. Msx2 is required for vascular smooth muscle cells osteoblastic differentiation but not calcification in insulin-resistant ob/ob mice. Atherosclerosis. 2017;265:14-21.
309. Camici GG, Steffel J, Akhmedov A, Schafer N, Baldinger J, Schulz U, et al. Dimethyl sulfoxide inhibits tissue factor expression, thrombus formation, and vascular smooth muscle cell activation: a potential treatment strategy for drug-eluting stents. Circulation. 2006;114(14):1512-21.
310. Ducy P, Karsenty G. Two distinct osteoblast-specific cis-acting elements control expression of a mouse osteocalcin gene. Mol Cell Biol. 1995;15(4):1858-69.
311. Voelkl J, Lang F, Eckardt KU, Amann K, Kuro-o M, Pasch A, et al. Signaling pathways involved in vascular smooth muscle cell calcification during hyperphosphatemia. Cell Mol Life Sci. 2019;76(11):2077-91.
312. Mackenzie NC, MacRae VE. The role of cellular senescence during vascular calcification: a key paradigm in aging research. Curr Aging Sci. 2011;4(2):128-36.
313. Ivanov GS, Ivanova T, Kurash J, Ivanov A, Chuikov S, Gizatullin F, et al. Methylation-Acetylation Interplay Activates p53 in Response to DNA Damage ▿ . Mol Cell Biol. 2007;27(19):6756-69.
314. Razi S, Cogger VC, Kennerson M, Benson VL, McMahon AC, Blyth FM, et al. SIRT1 Polymorphisms and Serum-Induced SIRT1 Protein Expression in Aging and Frailty: The CHAMP Study. J Gerontol A Biol Sci Med Sci. 2017;72(7):870-6.
315. Sierra OL, Towler DA. Runx2 Trans-Activation Mediated by the Msx2-Interacting Nuclear Target Requires Homeodomain Interacting Protein Kinase-3. Mol Endocrinol. 2010;24(7):1478-97.
316. Jonason J, Xiao G, Zhang M, Xing L, Chen D. Post-translational Regulation of Runx2 in Bone and Cartilage. J Dent Res. 2009;88(8):693-703.
317. Li Q, Zhao H, Xia S, Wei H, Chen F, Jin P. RUNX2 promotes epithelial differentiation of ADSCs and burn wound healing via targeting E-cadherin. Oncotarget. 2018;9(2):2646-59.
318. Speer MY, Li X, Hiremath PG, Giachelli CM. Runx2/Cbfa1, but not loss of Myocardin, is Required for Smooth Muscle Cell Lineage Reprogramming toward Osteochondrogenesis. J Cell Biochem. 2010;110(4):935-47.
319. Akech J, Wixted JJ, Bedard K, van der Deen M, Hussain S, Guise TA, et al. Runx2 Association with Progression of Prostate Cancer in Patients: Mechanisms Mediating Bone Osteolysis and Osteoblastic Metastatic Lesions. Oncogene. 2010;29(6):811-21.

320. Napierala D, Garcia-Rojas X, Sam K, Wakui K, Chen C, Mendoza-Londono R, et al. Mutations and promoter SNPs in RUNX2, a transcriptional regulator of bone formation. Mol Genet Metab. 2005;86(1-2):257-68.
321. Giachelli CM, Speer MY, Li X, Rajachar RM, Yang H. Regulation of vascular calcification: roles of phosphate and osteopontin. Circ Res. 2005;96(7):717-22.
322. Paloian NJ, Leaf EM, Giachelli CM. Osteopontin protects against high phosphate-induced nephrocalcinosis and vascular calcification. Kidney Int. 2016;89(5):1027-36.
323. Steitz SA, Speer MY, McKee MD, Liaw L, Almeida M, Yang H, et al. Osteopontin Inhibits Mineral Deposition and Promotes Regression of Ectopic Calcification. Am J Pathol. 2002;161(6):2035-46.
324. Hayakawa T, Iwai M, Aoki S, Takimoto K, Maruyama M, Maruyama W, et al. SIRT1 suppresses the senescence-associated secretory phenotype through epigenetic gene regulation. PLoS One. 2015;10(1):e0116480.
325. Kitada M, Ogura Y, Koya D. The protective role of Sirt1 in vascular tissue: its relationship to vascular aging and atherosclerosis. Aging (Albany NY). 2016;8(10):2290-307.
326. Ye X, Li M, Hou T, Gao T, Zhu W, Yang Y. Sirtuins in glucose and lipid metabolism. Oncotarget. 2017;8(1):1845-59.
327. Yu J, Auwerx J. The role of sirtuins in the control of metabolic homeostasis. Ann N Y Acad Sci. 2009;1173(0 1):E10-9.
328. Sada K, Nishikawa T, Kukidome D, Yoshinaga T, Kajihara N, Sonoda K, et al. Hyperglycemia Induces Cellular Hypoxia through Production of Mitochondrial ROS Followed by Suppression of Aquaporin-1. PLoS One. 2016;11(7).
329. Williamson JR, Chang K, Frangos M, Hasan KS, Ido Y, Kawamura T, et al. Hyperglycemic pseudohypoxia and diabetic complications. Diabetes. 1993;42(6):801-13.
330. Jing H, Su X, Gao B, Shuai Y, Chen J, Deng Z, et al. Epigenetic inhibition of Wnt pathway suppresses osteogenic differentiation of BMSCs during osteoporosis. Cell Death Dis. 2018;9(2).
331. Herranz D, Serrano M. Sirt1: recent lessons from mouse models. Nat Rev Cancer. 2010;10(12):819-23.
332. Banks AS, Kon N, Knight C, Matsumoto M, Gutiérrez-Juárez R, Rossetti L, et al. SirT1 gain-of-function increases energy efficiency and prevents diabetes in mice. Cell Metab. 2008;8(4):333-41.
333. Madi HA, Riches K, Warburton P, O'Regan DJ, Turner NA, Porter KE. Inherent differences in morphology, proliferation, and migration in saphenous vein smooth muscle cells cultured from nondiabetic and Type 2 diabetic patients. Am J Physiol Cell Physiol. 2009;297(5):C1307-17.
334. Gao P, Xu TT, Lu J, Li L, Xu J, Hao DL, et al. Overexpression of SIRT1 in vascular smooth muscle cells attenuates angiotensin II-induced vascular remodeling and hypertension in mice. J Mol Med (Berl). 2014;92(4):347-57.
335. Stultz CM, Edelman ER. A Structural Model that Explains the Effects of Hyperglycemia on Collagenolysis. Biophys J. 2003;85(4):2198-204.
336. Maeda M, Hayashi T, Mizuno N, Hattori Y, Kuzuya M. Intermittent High Glucose Implements Stress-Induced Senescence in Human Vascular Endothelial Cells: Role of Superoxide Production by NADPH Oxidase. PLoS One. 2015;10(4).
337. Zhou S, Li MT, Jia YY, Liu JJ, Wang Q, Tian Z, et al. Regulation of Cell Cycle Regulators by SIRT1 Contributes to Resveratrol-Mediated Prevention of Pulmonary Arterial Hypertension. Biomed Res Int. 2015;2015.

338. Jung-Hynes B, Ahmad N. Role of p53 in the anti-proliferative effects of Sirt1 inhibition in prostate cancer cells. Cell Cycle. 2009;8(10):1478-83.
339. Troyano N, Nogal MD, Mora I, Diaz-Naves M, Lopez-Carrillo N, Sosa P, et al. Hyperphosphatemia induces cellular senescence in human aorta smooth muscle cells through integrin linked kinase (ILK) up-regulation. Mech Ageing Dev. 2015;152:43-55.
340. Kilbey A, Blyth K, Wotton S, Terry A, Jenkins A, Bell M, et al. Runx2 disruption promotes immortalization and confers resistance to oncogene-induced senescence in primary murine fibroblasts. Cancer Res. 2007;67(23):11263-71.
341. Grootaert MOJ, Moulis M, Roth L, Martinet W, Vindis C, Bennett MR, et al. Vascular smooth muscle cell death, autophagy and senescence in atherosclerosis. Cardiovasc Res. 2018;114(4):622-34.
342. Rufini A, Tucci P, Celardo I, Melino G. Senescence and aging: the critical roles of p53. Oncogene. 2013;32(43):5129.
343. Reed SM, Quelle DE. p53 Acetylation: Regulation and Consequences. Cancers (Basel). 2015;7(1):30-69.
344. Yang H, Yan B, Liao D, Huang S, Qiu Y. Acetylation of HDAC1 and degradation of SIRT1 form a positive feedback loop to regulate p53 acetylation during heat-shock stress. Cell Death & Disease. 2015;6(5).
345. Shi X, Pi L, Zhou S, Li X, Min F, Wang S, et al. Activation of Sirtuin 1 Attenuates High Glucose-Induced Neuronal Apoptosis by Deacetylating p53. Front Endocrinol (Lausanne). 2018;9:274.
346. Barlev NA, Liu L, Chehab NH, Mansfield K, Harris KG, Halazonetis TD, et al. Acetylation of p53 activates transcription through recruitment of coactivators/histone acetyltransferases. Mol Cell. 2001;8(6):1243-54.
347. Kong Y, Sharma RB, Nwosu BU, Alonso LC. Islet biology, the CDKN2A/B locus and type 2 diabetes risk. Diabetologia. 2016;59(8):1579-93.
348. Wang W, Pan K, Chen Y, Huang C, Zhang X. The acetylation of transcription factor HBP1 by p300/CBP enhances p16INK4A expression. Nucleic Acids Res. 2012;40(3):981-95.
349. Michael Pittilo R. Cigarette smoking, endothelial injury and cardiovascular disease. Int J Exp Pathol. 2000;81(4):219-30.
350. Lee JE, Cooke JP. The role of nicotine in the pathogenesis of atherosclerosis. Atherosclerosis. 2011;215(2):281-3.
351. Lacolley P, Regnault V, Avolio AP. Smooth muscle cell and arterial aging: basic and clinical aspects. Cardiovasc Res. 2018;114(4):513-28.
352. Muto A, Fitzgerald TN, Pimiento JM, Maloney S, Teso D, Paszkowiak JJ, et al. Smooth Muscle Cell Signal Transduction: Implications of vascular biology for vascular surgeons. J Vasc Surg. 2007;45(6S):15-24.
353. Hu P, Lai D, Lu P, Gao J, He H. ERK and Akt signaling pathways are involved in advanced glycation end product-induced autophagy in rat vascular smooth muscle cells. Int J Mol Med. 2012;29(4):613-8.
354. Kruger D. Neo-intimal hyperplasia, diabetes and endovascular injury. Cardiovasc J Afr. 2012;23(9):507-11.
355. Park SH, Marso SP, Zhou Z, Foroudi F, Topol EJ, Lincoff AM. Neointimal hyperplasia after arterial injury is increased in a rat model of non-insulin-dependent diabetes mellitus. Circulation. 2001;104(7):815-9.
356. Raines EW, Ross R. Biology of atherosclerotic plaque formation: possible role of growth factors in lesion development and the potential impact of soy. J Nutr. 1995;125(3 Suppl):624s-30s.

357. Fatkhullina AR, Peshkova IO, Koltsova EK. The Role of Cytokines in the Development of Atherosclerosis. Biochemistry (Mosc). 2016;81(11):1358-70.
358. Ramji DP, Davies TS. Cytokines in atherosclerosis: Key players in all stages of disease and promising therapeutic targets. Cytokine Growth Factor Rev. 2015;26(6):673-85.
359. Demer LL, Tintut Y. Inflammatory, metabolic, and genetic mechanisms of vascular calcification. Arterioscler Thromb Vasc Biol. 2014;34(4):715-23.
360. Biros E, Karan M, Golledge J. Genetic Variation and Atherosclerosis. Curr Genomics. 2008;9(1):29-42.
361. Louis SF, Zahradka P. Vascular smooth muscle cell motility: From migration to invasion. Exp Clin Cardiol. 2010;15(4):e75-85.
362. Gerthoffer WT. Mechanisms of vascular smooth muscle cell migration. Circ Res. 2007;100(5):607-21.
363. Tajsic T, Morrell NW. Smooth muscle cell hypertrophy, proliferation, migration and apoptosis in pulmonary hypertension. Compr Physiol. 2011;1(1):295-317.
364. Wilson JL, Rupasinghe C, Usheva A, Warburton R, Kaplan C, Taylor L, et al. Modulating the dysregulated migration of pulmonary arterial hypertensive smooth muscle cells with motif mimicking cell permeable peptides. Curr Top Pept Protein Res. 2015;16:1-17.
365. Doran AC, Meller N, McNamara CA. Role of smooth muscle cells in the initiation and early progression of atherosclerosis. Arterioscler Thromb Vasc Biol. 2008;28(5):812-9.
366. Stehbens S, Wittmann T. Targeting and transport: How microtubules control focal adhesion dynamics. J Cell Biol. 2012;198(4):481-9.
367. Huttenlocher A, Horwitz AR. Integrins in Cell Migration. 2011.
368. Tang DD, Gerlach BD. The roles and regulation of the actin cytoskeleton, intermediate filaments and microtubules in smooth muscle cell migration. Respir Res. 2017;18.
369. Bradbury J. Move along there: focal adhesions and cell mortility. Journal of Cell Science. 2003;116.
370. Kim DH, Wirtz D. Focal adhesion size uniquely predicts cell migration. FASEB J. 2013;27(4):1351-61.
371. Ilic D, Kovacic B, Johkura K, Schlaepfer DD, Tomasevic N, Han Q, et al. FAK promotes organization of fibronectin matrix and fibrillar adhesions. J Cell Sci. 2004;117(Pt 2):177-87.
372. Ge JJ, Zhao ZW, Zhou ZC, Wu S, Zhang R, Pan FM, et al. p38 MAPK inhibitor, CBS3830 limits vascular remodelling in arterialised vein grafts. Heart Lung Circ. 2013;22(9):751-8.
373. Wang Z, Niu Q, Peng X, Li M, Liu Y, Liu J, et al. Mitofusin 2 ameliorates aortic remodeling by suppressing ras/raf/ERK pathway and regulating mitochondrial function in vascular smooth muscle cells. Int J Cardiol. 2015;178:165-7.
374. Ma X, Yao J, Yue Y, Du S, Qin H, Hou J, et al. Rapamycin reduced pulmonary vascular remodelling by inhibiting cell proliferation via Akt/mTOR signalling pathway down-regulation in the carotid artery-jugular vein shunt pulmonary hypertension rat model. Interact Cardiovasc Thorac Surg. 2017;25(2):206-11.
375. Yu H, Littlewood T, Bennett M. Akt isoforms in vascular disease. Vascul Pharmacol. 2015;71:57-64.
376. Algire C, Moiseeva O, Deschenes-Simard X, Amrein L, Petruccelli L, Birman E, et al. Metformin reduces endogenous reactive oxygen species and associated DNA damage. Cancer Prev Res (Phila). 2012;5(4):536-43.

377. Rice S, Pellatt L, Ramanathan K, Whitehead SA, Mason HD. Metformin inhibits aromatase via an ERK (extracellular signal-regulated kinase) - mediated pathway. Endocrinology. 2009;150(10):4794-801.
378. Marycz K, Tomaszewski KA, Kornicka K, Henry BM, Wroński S, Tarasiuk J, et al. Metformin Decreases Reactive Oxygen Species, Enhances Osteogenic Properties of Adipose-Derived Multipotent Mesenchymal Stem Cells In Vitro, and Increases Bone Density In Vivo. Oxid Med Cell Longev. 2016;2016.
379. Luna V, Casauban L, Sajan MP, Gomez-Daspet J, Powe JL, Miura A, et al. Metformin improves atypical protein kinase C activation by insulin and phosphatidylinositol-3,4,5-(PO4)3 in muscle of diabetic subjects. Diabetologia. 2006;49(2):375-82.
380. Hui X, Zhang M, Gu P, Li K, Gao Y, Wu D, et al. Adipocyte SIRT1 controls systemic insulin sensitivity by modulating macrophages in adipose tissue. EMBO Rep. 2017;18(4):645-57.
381. Qiang L, Wang H, Farmer SR. Adiponectin secretion is regulated by SIRT1 and the endoplasmic reticulum oxidoreductase Ero1-L alpha. Mol Cell Biol. 2007;27(13):4698-707.
382. Luu L, Dai FF, Prentice KJ, Huang X, Hardy AB, Hansen JB, et al. The loss of Sirt1 in mouse pancreatic beta cells impairs insulin secretion by disrupting glucose sensing. Diabetologia. 2013;56(9):2010-20.
383. Kitada M, Koya D. SIRT1 in Type 2 Diabetes: Mechanisms and Therapeutic Potential. Diabetes Metab J. 2013;37(5):315-25.
384. Wang K, Deng X, Shen Z, Jia Y, Ding R, Li R, et al. High glucose promotes vascular smooth muscle cell proliferation by upregulating proto-oncogene serine/threonine-protein kinase Pim-1 expression. Oncotarget. 82017. p. 88320-31.
385. Maile L, Capps, B., Ling, Y., Xi, G., Clemmons, D.,. Hyperglycemia Alters the Responsiveness of Smooth Muscle Cells to Insulin-Like Growth Factor-I. Endocrinology. 2007;148(5):2435-43.
386. Napoli C, Paolisso G, Casamassimi A, Al-Omran M, Barbieri M, Sommese L, et al. Effects of nitric oxide on cell proliferation: novel insights. J Am Coll Cardiol. 2013;62(2):89-95.
387. Katakami N. Mechanism of Development of Atherosclerosis and Cardiovascular Disease in Diabetes Mellitus. J Atheroscler Thromb. 2018;25(1):27-39.
388. Chait A, Bornfeldt KE. Diabetes and atherosclerosis: is there a role for hyperglycemia? J Lipid Res. 2009;50(Suppl):S335-9.
389. Rondas D, Tomas A, Halban PA. Focal Adhesion Remodeling Is Crucial for Glucose-Stimulated Insulin Secretion and Involves Activation of Focal Adhesion Kinase and Paxillin. Diabetes. 2011;60(4):1146-57.
390. Dieter Rondas AT, Martinho Soto-Ribeiro, Bernhard Wehrle-Haller Phillippe Halba. Novel mechanistic linkbetween focal adhesion remodeling and glucose-stimulated insulin growth. Journal of Biological Chemistry. 2012;287:2423-36.
391. Saunders RM, Holt MR, Jennings L, Sutton DH, Barsukov IL, Bobkov A, et al. Role of vinculin in regulating focal adhesion turnover. Eur J Cell Biol. 2006;85(6):487-500.
392. Wood CK, Turner CE, Jackson P, Critchley DR. Characterisation of the paxillin-binding site and the C-terminal focal adhesion targeting sequence in vinculin. J Cell Sci. 1994;107 (Pt 2):709-17.
393. Pasapera AM, Schneider IC, Rericha E, Schlaepfer DD, Waterman CM. Myosin II activity regulates vinculin recruitment to focal adhesions through FAK-mediated paxillin phosphorylation. J Cell Biol. 2010;188(6):877-90.

394. Deramaudt TB, Dujardin D, Noulet F, Martin S, Vauchelles R, Takeda K, et al. Altering FAK-paxillin interactions reduces adhesion, migration and invasion processes. PLoS One. 2014;9(3):e92059.
395. Luk CT, Shi SY, Cai EP, Sivasubramaniyam T, Krishnamurthy M, Brunt JJ, et al. FAK signalling controls insulin sensitivity through regulation of adipocyte survival. Nat Commun. 2017;8.
396. Golubovskaya VM, Cance WG. FAK and p53 Protein Interactions. Anticancer Agents Med Chem. 2011;11(7):617-9.
397. Tanimura S, Takeda, K. ERK signalling as a regulator of cell motility. The Journal of Biochemistry. 2017;162(3):145-54.
398. Begum N, Song Y, Rienzie J, Ragolia L. Vascular smooth muscle cell growth and insulin regulation of mitogen-activated protein kinase in hypertension. Am J Physiol. 1998;275(1):C42-9.
399. Gogg S, Smith, U., Jansson, P.,. Increased MAPK Activation and Impaired Insulin Signaling in Subcutaneous Microvascular Endothelial Cells in Type 2 Diabetes: The Role of Endothelin-1. Diabetes. 2009;58(10).
400. Cizek SM, Bedri S, Talusan P, Silva N, Lee H, Stone JR. Risk Factors for Atherosclerosis and the Development of Pre-Atherosclerotic Intimal Hyperplasia. Cardiovasc Pathol. 2007;16(6):344-50.
401. Hao H, Ropraz P, Verin V, Camenzind E, Geinoz A, Pepper MS, et al. Heterogeneity of smooth muscle cell populations cultured from pig coronary artery. Arterioscler Thromb Vasc Biol. 2002;22(7):1093-9.
402. Goikuria H, Freijo Mdel M, Vega Manrique R, Sastre M, Elizagaray E, Lorenzo A, et al. Characterization of Carotid Smooth Muscle Cells during Phenotypic Transition. Cells. 2018;7(3).
403. Yu PK, Yu DY, Cringle SJ, Su EN. Endothelial F-actin cytoskeleton in the retinal vasculature of normal and diabetic rats. Curr Eye Res. 2005;30(4):279-90.
404. Espitia O, Chatelais M, Steenman M, Charrier C, Maurel B, Georges S, et al. Implication of molecular vascular smooth muscle cell heterogeneity among arterial beds in arterial calcification. PLoS One. 2018;13(1):e0191976.
405. Lawes CM, Parag V, Bennett DA, Suh I, Lam TH, Whitlock G, et al. Blood glucose and risk of cardiovascular disease in the Asia Pacific region. Diabetes Care. 2004;27(12):2836-42.
406. Coutinho M, Gerstein HC, Wang Y, Yusuf S. The relationship between glucose and incident cardiovascular events. A metaregression analysis of published data from 20 studies of 95,783 individuals followed for 12.4 years. Diabetes Care. 1999;22(2):233-40.
407. Kizub IV, Pavlova OO, Johnson CD, Soloviev AI, Zholos AV. Rho kinase and protein kinase C involvement in vascular smooth muscle myofilament calcium sensitization in arteries from diabetic rats. Br J Pharmacol. 2010;159(8):1724-31.
408. Fleischhacker E, Esenabhalu VE, Spitaler M, Holzmann S, Skrabal F, Koidl B, et al. Human diabetes is associated with hyperreactivity of vascular smooth muscle cells due to altered subcellular Ca2+ distribution. Diabetes. 1999;48(6):1323-30.
409. Guo Z, Su W, Allen S, Pang H, Daugherty A, Smart E, et al. COX-2 up-regulation and vascular smooth muscle contractile hyperreactivity in spontaneous diabetic db/db mice. Cardiovasc Res. 2005;67(4):723-35.
410. Hien TT, Turczyńska KM, Dahan D, Ekman M, Grossi M, Sjögren J, et al. Elevated Glucose Levels Promote Contractile and Cytoskeletal Gene Expression in Vascular Smooth Muscle via Rho/Protein Kinase C and Actin Polymerization*. J Biol Chem. 2016;291(7):3552-68.

411. Kaneto H, Katakami N, Matsuhisa M, Matsuoka TA. Role of reactive oxygen species in the progression of type 2 diabetes and atherosclerosis. Mediators Inflamm. 2010;2010:453892.
412. Yoder MC. Human Endothelial Progenitor Cells. Cold Spring Harb Perspect Med. 2012;2(7).
413. Hamed S, Brenner B, Roguin A. Nitric oxide: a key factor behind the dysfunctionality of endothelial progenitor cells in diabetes mellitus type-2. Cardiovasc Res. 2011;91(1):9-15.
414. Reddy MA, Das S, Zhuo C, Jin W, Wang M, Lanting L, et al. Regulation of Vascular Smooth Muscle Cell Dysfunction under Diabetic Conditions by miR-504. Arterioscler Thromb Vasc Biol. 2016;36(5):864-73.
415. Cao L, Arany P, Kim J, Rivera-Feliciano J, Wang YS, He Z, et al. Modulating Notch Signaling to Enhance Neovascularization and Reperfusion in Diabetic Mice. Biomaterials. 2010;31(34):9048-56.
416. Boucher J, Gridley T, Liaw L. Molecular Pathways of Notch Signaling in Vascular Smooth Muscle Cells. Front Physiol. 2012;3.
417. Xu Z, Sun J, Tong Q, Lin Q, Qian L, Park Y, et al. The Role of ERK1/2 in the Development of Diabetic Cardiomyopathy. Int J Mol Sci. 2016;17(12).
418. Huang X, Liu G, Guo J, Su Z. The PI3K/AKT pathway in obesity and type 2 diabetes. Int J Biol Sci. 2018;14(11):1483-96.
419. K Hayashi HS, Y Chimori, K Kimura, Y Yamanaka, K Sobue. Differentiated Phenotype of Smooth Muscle Cells Depends on Signaling Pathways through Insulin-like Growth Factors and Phosphatidylinositol 3-Kinase. Journal of Biological Chemistry. 1998;273:28860-7.
420. Lee JH, Ragolia L. AKT Phosphorylation Is Essential For Insulin-induced Relaxation of Rat Vascular Smooth Muscle Cells. Am J Physiol Cell Physiol. 2006;291(6):C1355-65.
421. Hwang CY, Lee C, Kwon KS. Extracellular Signal-Regulated Kinase 2-Dependent Phosphorylation Induces Cytoplasmic Localization and Degradation of p21Cip1. Mol Cell Biol. 2009;29(12):3379-89.
422. Lu Z, Hunter T. Ubiquitylation and proteasomal degradation of the p21Cip1, p27Kip1 and p57Kip2 CDK inhibitors. Cell Cycle. 2010;9(12):2342-52.
423. Ozaki KI, Awazu M, Tamiya M, Iwasaki Y, Harada A, Kugisaki S, et al. Targeting the ERK signaling pathway as a potential treatment for insulin resistance and type 2 diabetes. Am J Physiol Endocrinol Metab. 2016;310(8):E643-e51.
424. Liu L, Zhou M, Lang H, Zhou Y, Mi M. Dihydromyricetin enhances glucose uptake by inhibition of MEK/ERK pathway and consequent down-regulation of phosphorylation of PPARgamma in 3T3-L1 cells. J Cell Mol Med. 2018;22(2):1247-56.
425. Zhao Y, Adjei AA. The clinical development of MEK inhibitors. Nat Rev Clin Oncol. 2014;11(7):385-400.
426. Hosogai N, Fukuhara A, Oshima K, Miyata Y, Tanaka S, Segawa K, et al. Adipose tissue hypoxia in obesity and its impact on adipocytokine dysregulation. Diabetes. 2007;56(4):901-11.
427. Chiachen Chen Y-CC, Michael Lan, Mary Breslin. Leptin stimulates ovarian cancer cell growth and inhibits apoptosis by increasing cyclin D1 and Mel-1 expression via the activaation of the MEK/ERK1/2 and PI3K/Akt signalling pathways. Int J Oncol. 2016;49(2):847.
428. Hanly EK, Tuli NY, Bednarczyk RB, Suriano R, Geliebter J, Moscatello AL, et al. Hyperactive ERK and persistent mTOR signaling characterize vemurafenib resistance in papillary thyroid cancer cells. Oncotarget. 2016;7(8):8676-87.

429. Kohno M, Pouyssegur J. Targeting the ERK signaling pathway in cancer therapy. Ann Med. 2006;38(3):200-11.
430. Adnan Al-Ayoubi AT, Hui Zheng Wayne Sakati Scott T. Eblen. ERK activation and nuclear signalling induced by the loss of cell/matrix adhesion stimulates anchorage-independent growth of ovarian cancer cells. Journal of Cellular Biochemistry. 2008;105:875-84.
431. Wang CC, Gurevich I, Draznin B. Insulin affects vascular smooth muscle cell phenotype and migration via distinct signaling pathways. Diabetes. 2003;52(10):2562-9.
432. Malabanan KP, Sheahan AV, Khachigian LM. Platelet-derived growth factor-BB mediates cell migration through induction of activating transcription factor 4 and tenascin-C. Am J Pathol. 2012;180(6):2590-7.
433. Mitchell SJ, Martin-Montalvo A, Mercken EM, Palacios HH, Ward TM, Abulwerdi G, et al. The SIRT1 activator SRT1720 extends lifespan and improves health of mice fed a standard diet. Cell Rep. 2014;6(5):836-43.
434. Zhang Y, Thai K, Jin T, Woo M, Gilbert RE. SIRT1 activation attenuates α cell hyperplasia, hyperglucagonaemia and hyperglycaemia in STZ-diabetic mice. Scientific Reports. 2018;8(1):13972.
435. Lin JN, Lin VC, Rau KM, Shieh PC, Kuo DH, Shieh JC, et al. Resveratrol modulates tumor cell proliferation and protein translation via SIRT1-dependent AMPK activation. J Agric Food Chem. 2010;58(3):1584-92.
436. Li B, Hu Y, Li X, Jin G, Chen X, Chen G, et al. Sirt1 Antisense Long Noncoding RNA Promotes Cardiomyocyte Proliferation by Enhancing the Stability of Sirt1. J Am Heart Assoc. 2018;7(21):e009700.
437. Kang X, Yang W, Wang R, Xie T, Li H, Feng D, et al. Sirtuin-1 (SIRT1) stimulates growth-plate chondrogenesis by attenuating the PERK-eIF-2alpha-CHOP pathway in the unfolded protein response. J Biol Chem. 2018;293(22):8614-25.
438. Mebratu Y, Tesfaigzi Y. How ERK1/2 Activation Controls Cell Proliferation and Cell Death Is Subcellular Localization the Answer? Cell Cycle. 2009;8(8):1168-75.
439. Aplin AE, Stewart SA, Assoian RK, Juliano R. Integrin-Mediated Adhesion Regulates ERK Nuclear Translocation and Phosphorylation of Elk-1. J Cell Biol. 2001;153(2):273-82.
440. Chuderland D, Seger R. Calcium regulates ERK signaling by modulating its protein-protein interactions. Commun Integr Biol. 2008;1(1):4-5.
441. Tatsukawa Y, Kiyosue T, Arita M. Mechanical stretch increases intracellular calcium concentration in cultured ventricular cells from neonatal rats. Heart Vessels. 1997;12(3):128-35.
442. Joumaa V, Herzog W. Does Calcium Sensitivity Increase after Active Stretch in Skinned Muscle Fibres? Biophysical Journal. 2014;106(2):765a.
443. Danciu TE, Adam RM, Naruse K, Freeman MR, Hauschka PV. Calcium regulates the PI3K-Akt pathway in stretched osteoblasts. FEBS Lett. 2003;536(1-3):193-7.
444. Cecchinato V, Chiaramonte R, Nizzardo M, Cristofaro B, Basile A, Sherbet GV, et al. Resveratrol-induced apoptosis in human T-cell acute lymphoblastic leukaemia MOLT-4 cells. Biochem Pharmacol. 2007;74(11):1568-74.
445. Ning J, Xi G, Clemmons DR. Suppression of AMPK Activation via S485 Phosphorylation by IGF-I during Hyperglycemia Is Mediated by AKT Activation in Vascular Smooth Muscle Cells. Endocrinology. 2011;152(8):3143-54.

446. Sharma N, Arias EB, Bhat AD, Sequea DA, Ho S, Croff KK, et al. Mechanisms for increased insulin-stimulated Akt phosphorylation and glucose uptake in fast- and slow-twitch skeletal muscles of calorie-restricted rats. Am J Physiol Endocrinol Metab. 2011;300(6):E966-78.
447. Wang S, Basson MD. Akt directly regulates focal adhesion kinase through association and serine phosphorylation: implication for pressure-induced colon cancer metastasis. Am J Physiol Cell Physiol. 3002011. p. C657-70.
448. Tang BL. Sirt1 and cell migration. Cell Adh Migr. 2010;4(2):163-5.
449. Schnoor M, Stradal TE, Rottner K. Cortactin: Cell Functions of A Multifaceted Actin-Binding Protein. Trends Cell Biol. 2018;28(2):79-98.
450. Wilking MJ, Ahmad N. The Role of SIRT1 in Cancer: The Saga Continues. Am J Pathol. 2015;185(1):26-8.
451. Yuan H, Su L, Chen WY. The emerging and diverse roles of sirtuins in cancer: a clinical perspective. Onco Targets Ther. 2013;6:1399-416.
452. Longo VD, Fontana L. Calorie restriction and cancer prevention: metabolic and molecular mechanisms. Trends Pharmacol Sci. 2010;31(2):89-98.
453. Zhang Y, Zhang M, Dong H, Yong S, Li X, Olashaw N, et al. Deacetylation of cortactin by SIRT1 promotes cell migration. Oncogene. 2009;28(3):445-60.
454. Bosch-Presegué L, Vaquero A. The Dual Role of Sirtuins in Cancer. Genes Cancer. 2011;2(6):648-62.
455. Bachir A, Horwitz AR, Nelson WJ, Bianchini JM. Cell Adhesions: Actin-Based Modules that Mediate Cell-Extracellular Matrix and Cell-Cell Interactions. Cold Spring Harb Perspect Biol. 2017;9(7).
456. Geiger B, Bershadsky A, Pankov R, Yamada KM. Transmembrane crosstalk between the extracellular matrix--cytoskeleton crosstalk. Nat Rev Mol Cell Biol. 2001;2(11):793-805.
457. Xu W, Baribault H, Adamson ED. Vinculin knockout results in heart and brain defects during embryonic development. Development. 1998;125(2):327-37.
458. Volberg T, Geiger B, Kam Z, Pankov R, Simcha I, Sabanay H, et al. Focal adhesion formation by F9 embryonal carcinoma cells after vinculin gene disruption. J Cell Sci. 1995;108 (Pt 6):2253-60.
459. Coll JL, Ben-Ze'ev A, Ezzell RM, Rodriguez Fernandez JL, Baribault H, Oshima RG, et al. Targeted disruption of vinculin genes in F9 and embryonic stem cells changes cell morphology, adhesion, and locomotion. Proc Natl Acad Sci U S A. 1995;92(20):9161-5.
460. Peng X, Nelson ES, Maiers JL, DeMali KA. New Insights into Vinculin Function and Regulation. Int Rev Cell Mol Biol. 2011;287:191-231.
461. Yeo RW, Yang K, Li G, Lim SK. High glucose predisposes gene expression and ERK phosphorylation to apoptosis and impaired glucose-stimulated insulin secretion via the cytoskeleton. PLoS One. 2012;7(9):e44988.
462. López-Colomé AM, Lee-Rivera I, Benavides-Hidalgo R, López E. Paxillin: a crossroad in pathological cell migration. J Hematol Oncol. 2017;10.
463. Hu Y-L, Lu S, Szeto KW, Wang Y, Lasheras JC, Chien S. Focal adhesion kinase leads paxillin in focal adhesion assembly at lamellipodial protrusion of migrating endothelial cells. 2013.
464. Zhao Y, Scott A, Zhang P, Hao Y, Feng X, Somasundaram S, et al. Regulation of paxillin-p130-PI3K-AKT signaling axis by Src and PTPRT impacts colon tumorigenesis. Oncotarget. 2017;8(30):48782-93.
465. Zhao Y, Zhang X, Guda K, Lawrence E, Sun Q, Watanabe T, et al. Identification and functional characterization of paxillin as a target of protein tyrosine phosphatase receptor T. Proc Natl Acad Sci U S A. 2010;107(6):2592-7.

466. Mogford AMJ. Control of smooth muscle cell proliferation and phenotype by intergrin signaling through focal adhesion kinase. Biochemical and Biophysical Research Communications. 2000;272:298-392.
467. Yu H, Gao M, Ma Y, Wang L, Shen Y, Liu X. Inhibition of cell migration by focal adhesion kinase: Time-dependent difference in integrin-induced signaling between endothelial and hepatoblastoma cells. Int J Mol Med. 2018;41(5):2573-88.
468. Brown MC, Cary LA, Jamieson JS, Cooper JA, Turner CE. Src and FAK Kinases Cooperate to Phosphorylate Paxillin Kinase Linker, Stimulate Its Focal Adhesion Localization, and Regulate Cell Spreading and Protrusiveness. Mol Biol Cell. 2005;16(9):4316-28.
469. Zhao X, Guan JL. Focal adhesion kinase and its signaling pathways in cell migration and angiogenesis. Adv Drug Deliv Rev. 2011;63(8):610-5.
470. Kalwat MA, Thurmond DC. Signaling mechanisms of glucose-induced F-actin remodeling in pancreatic islet β cells. Exp Mol Med. 2013;45(8):e37-.
471. Buhrmann C, Shayan P, Goel A, Shakibaei M. Resveratrol Regulates Colorectal Cancer Cell Invasion by Modulation of Focal Adhesion Molecules. Nutrients. 2017;9(10).
472. Koene RJ, Prizment AE, Blaes A, Konety SH. Shared Risk Factors in Cardiovascular Disease and Cancer. Circulation. 2016;133(11):1104-14.
473. Giovannucci E, Harlan DM, Archer MC, Bergenstal RM, Gapstur SM, Habel LA, et al. Diabetes and Cancer: A consensus report. Diabetes Care. 2010;33(7):1674-85.
474. Collins KK. The Diabetes-Cancer Link. Diabetes Spectr. 2014;27(4):276-80.
475. Dubois F, Alpha K, Turner CE. Paxillin regulates cell polarization and anterograde vesicle trafficking during cell migration. Mol Biol Cell. 2017;28(26):3815-31.
476. Yan LJ. Redox imbalance stress in diabetes mellitus: Role of the polyol pathway. Animal Model Exp Med. 2018;1(1):7-13.
477. Srinivasan B, Taub N, Khunti K, Davies M. Diabetes: glycaemic control in type 2. BMJ Clin Evid. 2008;2008.
478. Demer LL, Tintut Y. Vascular calcification: pathobiology of a multifaceted disease. Circulation. 2008;117(22):2938-48.
479. Leopold JA. Vascular Calcification: Mechanisms of Vascular Smooth Muscle Cell Calcification. Trends Cardiovasc Med. 2015;25(4):267-74.
480. Burton DG, Matsubara H, Ikeda K. Pathophysiology of vascular calcification: Pivotal role of cellular senescence in vascular smooth muscle cells. Exp Gerontol. 2010;45(11):819-24.
481. Yamada S, Tatsumoto N, Tokumoto M, Noguchi H, Ooboshi H, Kitazono T, et al. Phosphate binders prevent phosphate-induced cellular senescence of vascular smooth muscle cells and vascular calcification in a modified, adenine-based uremic rat model. Calcif Tissue Int. 2015;96(4):347-58.
482. Williams GJ, Lees-Miller SP, Tainer JA. Mre11-Rad50-Nbs1 conformations and the control of sensing, signaling, and effector responses at DNA double-strand breaks. DNA Repair (Amst). 2010;9(12):1299-306.
483. C TVaG. Multiple facets of histone variant H2AX: a DNA double-strand-break marker with several biological functions. Nucleic Acids Research. 2015;43(5):2489-98.
484. Syed A, Tainer JA. The MRE11-RAD50-NBS1 Complex Conducts the Orchestration of Damage Signaling and Outcomes to Stress in DNA Replication and Repair. Annu Rev Biochem. 2018;87:263-94.

485. Kuo LJ, Yang LX. Gamma-H2AX - a novel biomarker for DNA double-strand breaks. In Vivo. 2008;22(3):305-9.
486. Chowdhury D, Keogh MC, Ishii H, Peterson CL, Buratowski S, Lieberman J. gamma-H2AX dephosphorylation by protein phosphatase 2A facilitates DNA double-strand break repair. Mol Cell. 2005;20(5):801-9.
487. Wang W, Sun W, Cheng Y, Xu Z, Cai L. Role of sirtuin-1 in diabetic nephropathy. J Mol Med (Berl). 2019;97(3):291-309.
488. Ren X, Chen N, Chen Y, Liu W, Hu Y. TRB3 stimulates SIRT1 degradation and induces insulin resistance by lipotoxicity via COP1. Experimental Cell Research. 2019.
489. Chen D, Pacal M, Wenzel P, Knoepfler PS, Leone G, Bremner R. Division and apoptosis in the E2f-deficient retina. Nature. 2009;462(7275):925.
490. Seung-Hyun Song M-OL, Ji-Seon Lee, Je-Sok Oh, Sung-Uk Cho and Hyuk-Jin Cha. Sirt1 Promotes DNA Damage Repair and Cellular Survival. 2011.
491. Yuan Z, Zhang X, Sengupta N, Lane WS, Seto E. SIRT1 regulates the function of the Nijmegen breakage syndrome protein. Mol Cell. 2007;27(1):149-62.
492. Guarente L. Overcoming ATM Deficiency by Activating the NAD(+)/SIRT1 Axis. Cell Metab. 2016;24(4):526-8.
493. Maréchal A, Zou L. DNA Damage Sensing by the ATM and ATR Kinases. Cold Spring Harb Perspect Biol. 2013;5(9).
494. Giglia-Mari G, Zotter A, Vermeulen W. DNA Damage Response. Cold Spring Harb Perspect Biol. 2011;3(1).
495. Orimo M, Minamino T, Miyauchi H, Tateno K, Okada S, Moriya J, et al. Protective role of SIRT1 in diabetic vascular dysfunction. Arterioscler Thromb Vasc Biol. 2009;29(6):889-94.
496. Herskovits A, Guarente L. SIRT1 in neurodevelopment and brain senescence. Neuron. 2014;81(3):471-83.
497. Gorenne I, Kumar S, Gray K, Figg N, Yu H, Mercer J, et al. Vascular smooth muscle cell sirtuin 1 protects against DNA damage and inhibits atherosclerosis. Circulation. 2013;127(3):386-96.
498. Gray K, Kumar S, Figg N, Harrison J, Baker L, Mercer J, et al. Effects of DNA damage in smooth muscle cells in atherosclerosis. Circ Res. 2015;116(5):816-26.
499. Garcia-Vizcaino EM, Liarte S, Alonso-Romero JL, Nicolas FJ. Sirt1 interaction with active Smad2 modulates transforming growth factor-beta regulated transcription. Cell Commun Signal. 2017;15(1):50.
500. Wang T, Yang B, Ji R, Xu W, Mai K, Ai Q. Omega-3 polyunsaturated fatty acids alleviate hepatic steatosis-induced inflammation through Sirt1-mediated nuclear translocation of NF-kappaB p65 subunit in hepatocytes of large yellow croaker (Larmichthys crocea). Fish Shellfish Immunol. 2017;71:76-82.
501. Choi SE, Kwon S, Seok S, Xiao Z, Lee KW, Kang Y, et al. Obesity-Linked Phosphorylation of SIRT1 by Casein Kinase 2 Inhibits Its Nuclear Localization and Promotes Fatty Liver. Mol Cell Biol. 2017;37(15).
502. Sun Y, Xu Y, Roy K, Price BD. DNA Damage-Induced Acetylation of Lysine 3016 of ATM Activates ATM Kinase Activity ▿ †. Mol Cell Biol. 272007. p. 8502-9.
503. Peng L, Ling H, Yuan Z, Fang B, Bloom G, Fukasawa K, et al. SIRT1 negatively regulates the activities, functions, and protein levels of hMOF and TIP60. Mol Cell Biol. 2012;32(14):2823-36.
504. Ikura M, Furuya K, Matsuda S, Matsuda R, Shima H, Adachi J, et al. Acetylation of Histone H2AX at Lys 5 by the TIP60 Histone Acetyltransferase Complex Is Essential for the Dynamic Binding of NBS1 to Damaged Chromatin. Molecular and Cellular Biology. 2015.

505. Cheng HL, Mostoslavsky R, Saito S, Manis JP, Gu Y, Patel P, et al. Developmental defects and p53 hyperacetylation in Sir2 homolog (SIRT1)-deficient mice. Proc Natl Acad Sci U S A. 2003;100(19):10794-9.
506. Kijas AW, Lim YC, Bolderson E, Cerosaletti K, Gatei M, Jakob B, et al. ATM-dependent phosphorylation of MRE11 controls extent of resection during homology directed repair by signalling through Exonuclease 1. Nucleic Acids Res. 2015;43(17):8352-67.
507. Kish A, DiRuggiero J. Rad50 Is Not Essential for the Mre11-Dependent Repair of DNA Double-Strand Breaks in Halobacterium sp. Strain NRC-1. Journal of Bacteriology. 2008.
508. Yuan Z, Seto E. A functional link between SIRT1 deacetylase and NBS1 in DNA damage response. Cell Cycle. 2007;6(23):2869-71.
509. Yamaguchi H, Woods NT, Piluso LG, Lee HH, Chen J, Bhalla KN, et al. p53 Acetylation Is Crucial for Its Transcription-independent Proapoptotic Functions. J Biol Chem. 2009;284(17):11171-83.
510. Tang Y, Zhao W, Chen Y, Zhao Y, Gu W. Acetylation is indispensable for p53 activation. Cell. 2008;133(4):612-26.
511. Keelan PC, Bielak LF, Ashai K, Jamjoum LS, Denktas AE, Rumberger JA, et al. Long-term prognostic value of coronary calcification detected by electron-beam computed tomography in patients undergoing coronary angiography. Circulation. 2001;104(4):412-7.
512. Wayhs R, Zelinger A, Raggi P. High coronary artery calcium scores pose an extremely elevated risk for hard events. J Am Coll Cardiol. 2002;39(2):225-30.
513. Uryga A, Gray K, Bennett M. DNA Damage and Repair in Vascular Disease. Annu Rev Physiol. 2016;78:45-66.
514. Dobbin MM, Madabhushi R, Pan L, Chen Y, Kim D, Gao J, et al. SIRT1 collaborates with ATM and HDAC1 to maintain genomic stability in neurons. Nat Neurosci. 2013;16(8):1008-15.
515. Sanchis P, Ho, C., Liu, Y., Beltran, L., Ahmad, S., Jacob, A., Furmanik, M., Laycock, J., Long, D., Shroff, R., Shanahan, C.,. Arterial "inflammaging" drives vascular calcification in children on dialysis. Kidney International. 2019;95(4).
516. Spin JM, Maegdefessel L, Tsao PS. Vascular smooth muscle cell phenotypic plasticity: focus on chromatin remodelling. Cardiovasc Res. 2012;95(2):147-55.
517. Marzi SJ, Leung SK, Ribarska T, Hannon E, Smith AR, Pishva E, et al. A histone acetylome-wide association study of Alzheimer's disease identifies disease-associated H3K27ac differences in the entorhinal cortex. Nat Neurosci. 2018;21(11):1618-27.
518. Hannon E, Marzi SJ, Schalkwyk LS, Mill J. Genetic risk variants for brain disorders are enriched in cortical H3K27ac domains. Mol Brain. 2019;12(1):7.
519. Mumbach MR, Satpathy AT, Boyle EA, Dai C, Gowen BG, Cho SW, et al. Enhancer connectome in primary human cells identifies target genes of disease-associated DNA elements. Nat Genet. 2017;49(11):1602-12.
520. Ross R. Atherosclerosis--an inflammatory disease. N Engl J Med. 1999;340(2):115-26.
521. Marx SO, Totary-Jain H, Marks AR. Vascular Smooth Muscle Cell Proliferation in Restenosis. Circ Cardiovasc Interv. 2011;4(1).
522. Ross R, Glomset JA. Atherosclerosis and the Arterial Smooth Muscle Cell. Science. 1973;180(4093):1332-9.
523. Sata M, Saiura A, Kunisato A, Tojo A, Okada S, Tokuhisa T, et al. Hematopoietic stem cells differentiate into vascular cells that participate in the pathogenesis of atherosclerosis. Nat Med. 2002;8(4):403-9.

524. Caplice NM, Bunch TJ, Stalboerger PG, Wang S, Simper D, Miller DV, et al. Smooth muscle cells in human coronary atherosclerosis can originate from cells administered at marrow transplantation. Proc Natl Acad Sci U S A. 2003;100(8):4754-9.
525. Ionita MG, Arslan F, de Kleijn DP, Pasterkamp G. Endogenous inflammatory molecules engage Toll-like receptors in cardiovascular disease. J Innate Immun. 2010;2(4):307-15.
526. Liu SQ, Tieche C, Alkema PK. Neointima formation on vascular elastic laminae and collagen matrices scaffolds implanted in the rat aortae. Biomaterials. 2004;25(10):1869-82.
527. Brassart B, Fuchs P, Huet E, Alix AJ, Wallach J, Tamburro AM, et al. Conformational dependence of collagenase (matrix metalloproteinase-1) up-regulation by elastin peptides in cultured fibroblasts. J Biol Chem. 2001;276(7):5222-7.
528. Swirski FK, Nahrendorf M. Leukocyte behavior in atherosclerosis, myocardial infarction, and heart failure. Science. 2013;339(6116):161-6.
529. Tang D, Wu, D., Hirao, A., Lahti, J., Liu, L., Mazza, B., Kidd, V., Mak, T., Ingram, A.,. ERK Activation mediates cell cycle arrest and apoptosis after DNA damage independently of p53. Journal of Biological Chemistry. 2002;227:12710-7.
530. Blaser MC, Aikawa E. Roles and Regulation of Extracellular Vesicles in Cardiovascular Mineral Metabolism. Front Cardiovasc Med. 2018;5:187.
531. Kadota T, Fujita, Y., Yoshioka, Y., Araya, J., Kuwano, K., Ochiya, T.,. Emerging role of extracellular vesicles as a senescence-associated secretory phenotype: Insights into the pathophysiology of lung disease. Molecular Aspects of Medicine. 2018;60:92-103.
532. Budnik B, Levy E, Harmange G, Slavov N. SCoPE-MS: mass spectrometry of single mammalian cells quantifies proteome heterogeneity during cell differentiation. Genome Biology. 2018;19(1):161.
533. Moiseeva EP. Adhesion receptors of vascular smooth muscle cells and their functions. Cardiovasc Res. 2001;52(3):372-86.
534. Karnik SK, Brooke BS, Bayes-Genis A, Sorensen L, Wythe JD, Schwartz RS, et al. A critical role for elastin signaling in vascular morphogenesis and disease. Development. 2003;130(2):411-23.
535. Kowluru R, Santos, JM, Zhong, Q. SIRT1, a negative regulator of matrix metalloprotienase-9 in diabetic retinopathy. Investigative Ophthalmology and Vision Science. 2014;55(9).
536. Qu L, Yu Y, Qiu L, Yang D, Yan L, Guo J, et al. Sirtuin 1 regulates matrix metalloproteinase-13 expression induced by Porphyromonas endodontalis lipopolysaccharide via targeting nuclear factor-kappaB in osteoblasts. J Oral Microbiol. 2017;9(1):1317578.
537. Bustamante S, Jayasena, T., Richani, D., Gilchrist, R., Wu, L., Sinclair, D., Sachdev, P.,Braidy, N. Quantifying the cellular NAD+ metabolome using a tandem liquid chromatography mass spectrometry approach | SpringerLink. Metabolomics. 2018;14(15).
538. Wagner TC, Scott MD. Single extraction method for the spectrophotometric quantification of oxidized and reduced pyridine nucleotides in erythrocytes. Anal Biochem. 1994;222(2):417-26.
539. Veskoukls A, Margaritelis, N., Kyparos, A>, Paschalis, V., Nikolaidis, M.,. Spectrophotometric assays for measuring redox biomarkers in blood and tissues: the NADPH network. Redox Report. 2017;23(1):47-56.